Petrogenetic evolution of Uralian-Alaskan-type mafic- ultramafic complexes in the southern and middle Urals, Russia

Dissertation

zur Erlangung des Grades

“Doktor der Naturwissenschaften”

im Promotionsfach Geologie/Paläontologie

am Fachbereich Chemie, Pharmazie und Geowissenschaften

der Johannes Gutenberg-Universität in Mainz

vorgelegt von

Joachim Krause

geb. in Darmstadt

Mainz, 2008

Erklärung:

Ich versichere hiermit, die vorliegende Arbeit selbständig verfasst und alle benutzten Hilfsmittel und Quellen in der Arbeit angegeben zu haben. Diese Arbeit wurde an keiner anderen Fakultät als Dissertation eingereicht.

Mainz, August 2008

Summary

The PhD thesis at hand consists of three parts and describes the petrogenetic evolution of Uralian-Alaskan-type mafic ultramafic complexes in the Ural Mountains, Russia. Uralian-Alaskan-type mafic-ultramafic complexes are recognized as a distinct class of intrusions. Characteristic petrologic features are the concentric zonation of a central dunite body grading outward into wehrlite, clinopyroxenite and gabbro, the absence of orthopyroxene and frequently occurring platinum group element (PGE) mineralization. In addition, the presence of ferric iron-rich spinel discriminates Uralian-Alaskan-type complexes from most other mafic ultramafic rock assemblages. The studied Uralian-Alaskan-type complexes (Nizhnii Tagil, Kytlym and Svetley Bor) belong to the southern part of a 900 km long, N–S-trending chain of similar intrusions between the Main Uralian Fault to the west and the Serov-Mauk Fault to the east.

The first chapter of this thesis studies the evolution of the ultramafic rocks tracing the compositional variations of rock forming and accessory minerals. The comparison of the chemical composition of olivine, clinopyroxene and chromian spinel from the Urals with data from other localities indicates that they are unique intrusions having a characteristic spinel and clinopyroxene chemistry. Laser ablation-ICPMS (LA-ICPMS) analyses of trace element concentrations in clinopyroxene are used to calculate the composition of their parental melt which is characterized by enriched LREE (0.5-5.2 prim. mantle) and other highly incompatible elements (U, Th, Ba, Rb) relative to the HREE (0.25-2.0 prim. mantle). A subduction-related geotectonic setting is indicated by a positive anomaly for Sr and negative anomalies for Ti, Zr and Hf. The mineral compositions monitor the evolution of the parental magmas and decipher differences between the studied complexes. In addition, the observed variation in LREE/HREE (for example La/Lu = 2-24) can be best explained with the model of an episodically replenished and erupted open magma chamber system with the extensive fractionation of olivine, spinel and clinopyroxene. The data also show that ankaramites in a subduction-related geotectonic setting could represent parental magmas of Uralian-Alaskan-type complexes.

The second chapter of the thesis discusses the chemical variation of major and trace elements in rock-forming minerals of the mafic rocks. Electron microprobe and LA-ICPMS analyses are used to quantitatively describe the petrogenetic relationship

between the different gabbroic lithologies and their genetic link to the ultramafic rocks. The composition of clinopyroxene identifies the presence of melts with different trace element abundances on the scale of a thin section and suggests the presence of open system crustal magma chambers. Even on a regional scale the large variation of trace element concentrations and ratios in clinopyroxene (e.g. La/Lu = 3-55) is best explained by the interaction of at least two fundamentally different magma types at various stages of fractionation. This requires the existence of a complex magma chamber system fed with multiple pulses of magmas from at least two different coeval sources in a subduction-related environment. One source produces silica saturated Island arc tholeiitic melts. The second source produces silica undersaturated, ultra-calcic, alkaline melts. Taken these data collectively, the mixing of the two different parental magmas is the dominant petrogenetic process explaining the observed chemical variations. The results further imply that this is an intrinsic feature of Uralian-Alaskan-type complexes and probably of many similar mafic-ultramafic complexes world-wide.

In the third chapter of this thesis the major element composition of homogeneous and exsolved spinel is used as a petrogenetic indicator. Homogeneous chromian spinel in dunites and wehrlites monitors the fractionation during the early stages of the magma chamber and the onset of clinopyroxene fractionation as well as the reaction of spinel with interstitial liquid. Exsolved spinel is present in mafic and ultramafic rocks from all three studied complexes. Its composition lies along a solvus curve which defines an equilibrium temperature of 600°C, given that spinel coexists with olivine. This temperature is considered to be close to the temperature of the host rocks into which the studied Uralian-Alaskan-type complexes intruded. The similarity of the exsolution temperatures in the different complexes over a distance of several hundred kilometres implies a regional tectonic event that terminated the exsolution process. This event is potentially associated with the final exhumation of the Uralian-Alaskan-type complexes along the Main Uralian Fault and the Serov-Mauk Fault in the Uralian fold belt.

Zusammenfassung

Die vorliegende Dissertation besteht aus drei Kapiteln und beschreibt die petrogenetische Entwicklung von Uralian-Alaskan-type mafisch-ultramafischen Komplexen im Ural in Russland. Uralian-Alaskan-type Komplexe werden als eigene Gruppe mafisch-ultramafischer Intrusionen angesehen. Eine konzentrische Struktur mit einem Kern aus Dunit, der von einer Abfolge aus Wehrlit, Klinopyroxenit und Gabbro umgeben ist, die Abwesenheit von Orthopyroxen, ein hoher Gehalt an Fe^{3+} in Spinell und das Auftreten von Platin-Gruppen-Element Mineralisation (PGE) unterscheiden Uralian-Alaskan-type Komplexe von anderen ultramafischen Intrusionen. Die drei beprobten Komplexe (Nizhnii Tagil, Svetley Bor und Kytlym) bilden den südlichen Teil einer Nord-Süd streichenden, 900 km langen Kette zwischen der Haupt-Ural-Störung im Westen und der Serov-Mauk-Störung im Osten.

Im ersten Kapitel wird die Entwicklung der ultramafischen Gesteine aus der Variation der chemischen Zusammensetzung der akzessorischen und gesteinsbildenden Minerale abgeleitet. Anhand der chemischen Zusammensetzung von Olivin, Klinopyroxen und Chromspinell lassen sich die Intrusionen im Ural von anderen Vorkommen weltweit unterscheiden. Aus den mittels Laser-Ablations-ICPMS (LA-ICPMS) gemessenen Spurenelement-Konzentrationen in Klinopyroxen lässt sich die Zusammensetzung der koexistierenden Schmelze ableiten. Dabei zeigt sich, dass leichte Seltene Erden (LREE = 0.5-5.2-fach primitiver Mantel) sowie hoch inkompatible Elemente (U, Th, Ba, Rb) gegenüber schweren Seltenen Erden (HREE = 0.25-5.2-fach primitiver Mantel) angereichert sind. Darüber hinaus deuten eine positive Anomalie in Sr und negative Anomalien in Ti, Zr und Hf auf eine Entstehung an einem konvergierenden Plattenrand hin. In der Zusammensetzung der Minerale spiegelt sich auch die Entwicklung der koexistierenden Schmelzen, sowie Unterschiede zwischen den Intrusionen wieder. Die beobachteten chemischen Variationen (z.B. La/Lu = 2-24 in Klinopyroxen) lassen sich am besten mit dem Modell eines offenen Magmakammer-Systems erklären in dem es wiederholt zur Intrusion primitiver Schmelzen, gefolgt von fraktionierender Kristallisation und der Eruption von Teilschmelzen kommt. Die Ergebnisse zeigen auch, dass Ankaramite mögliche Stamm-Magmen für Uralian-Alaskan-type Komplexe sind.

Im Mittelpunkt des zweiten Abschnittes stehen Variationen der Haupt- und Spurenelement-Konzentrationen in den gesteinsbildenden Mineralen der mafischen Gesteine. Mit Hilfe der Elektronenstrahl-Mikrosonde und von LA-ICPMS werden die petrogenetischen Beziehungen verschiedener mafischer Gesteine und deren Bezug zu den ultramafischen Gesteinen quantitativ beschrieben. Die variable Zusammensetzung von Klinopyroxen impliziert das Vorhandensein von Magmen mit einer unterschiedlichen Spurenelement-Systematik innerhalb eines Dünnschliffes und die Existenz von offenen Magmakammer-Systemen. Auch die auf regionale Ebene beobachteten Variationen von Spurenelement-Gehalten und -Verhältnissen (z.B. La/Lu = 3-55) lässt sich am besten durch das Zusammenspiel von mindestens zwei vollkommen unterschiedlichen Magmen mit variablem Fraktionierungsgrad beschreiben. Dies erfordert ein komplexes System von Magmakammern, gespeist durch multiple Intrusion von koexistierenden Schmelzen aus zwei unterschiedlichen, subduktionsbezogenen Quellen. Aus einer Quelle kommen Silizium-gesättigte Inselbogen-Tholeiite. Silizium untersättigte, calziumreiche, alkaline Schmelzen kommen aus der zweiten Quelle. Die Studie zeigt, dass die Mischung von Magmen aus unterschiedlichen Quellen, auch in ähnlichen Intrusionen weltweit, der dominierende Prozess ist, um die beobachteten chemischen Variationen zu erklären.

Im dritten Kapitel wird die Zusammensetzung homogener und entmischter Spinelle als Indikator petrogenetischer Prozesse benutzt. Die chemische Zusammensetzung homogener Chromspinelle in Duniten und Wehrliten gibt die frühen Stadien der Fraktionierung in der Magmakammer ebenso wie den Beginn der Kristallisation von Klinopyroxen und die Reaktion von Spinell mit Schmelze im Porenraum wieder. Entmischte Spinelle treten in mafischen und ultramafischen Gesteinen aller drei beprobten Komplexe auf. Die Zusammensetzung folgt einer Solvuskurve für Spinell der bei 600°C mit Olivin im Gleichgewicht steht. Es wird angenommen, dass diese Temperatur der Umgebungstemperatur im Intrusionsniveau der Uralian-Alaskan-type Komplexe entspricht. Die Ähnlichkeit der Entmischungstemperaturen in Spinellen verschiedener Komplexe über eine Distanz von einigen hundert Kilometern legt nahe, dass ein regional-tektonisches Ereignis die thermische Äquilibrierung der Spinelle verhinderte. Dieses ist vermutlich mit der finalen Exhumierung der Uralian-Alaskan-type Komplexe entlang der Haupt-Ural-Störung und der Serov-Mauk-Störung verbunden.

Table of Contents

Chapter 3 Chemical composition and petrogenetic significance of spinel from Uralian-Alaskan-type Mafic-Ultramafic Complexes

Preface

Uralian-Alaskan-type mafic to ultramafic complexes form a narrow, 900 km long, N-S-trending chain in the northern and central parts of the Ural orogenic belt. Characteristic features like their concentric lithologic zonation, the absence of orthopyroxene in the ultramafic rocks and platinum group element (PGE) mineralization, which is the source for economic PGE placer deposits, discriminate Uralian-Alaskan-type complexes from other mafic-ultramafic intrusions. The genesis, structure and the geotectonic setting of the Uralian-Alaskan-type complexes in the Ural Mountains have been controversially discussed during the last decades. Genetic models include metasomatic, metamorphic and magmatic processes in order to explain the special rock assemblage and structure. Island arc and supra subduction zone environments and a diapiric mantle upwelling related to extensional tectonics along the edge of the east European Craton have been postulated as geological setting.

The aim of the PhD thesis at hand is to constrain the petrogenetic evolution of three Uralian-Alaskan-type complexes. Based on the detailed analysis of variations in major and trace element concentrations and ratios in rock forming and accessory minerals from mineral grain to regional scale, magma mixing has been found to be the most important petrogenetic process to explain the observed chemical variations. The compositional variation in minerals from the ultramafic rocks can be explained with the successive fractionation of olivine, spinel and clinopyroxene in an open magma chamber system. However, the observed chemical variation in minerals especially clinopyroxene from the mafic rocks requires the presence of a complex magma chamber system fed with multiple pulses of magma from at least two different coeval sources in a subduction-related environment. One source produces silica saturated Island arc tholeiitic melts. The second source produces silica undersaturated, ultra-calcic, alkaline melts. The presence of exsolved spinel that equilibrated at temperatures close to 600°C in various lithologies in all three studied Uralian-Alaskan-type complexes indicates that this temperature represents the thermal conditions in the intrusion level. After formation and thermal equilibration of the cumulates, a regional tectonic event probably related to the final exhumation of the Uralian-Alaskan-type complexes in the Uralian fold belt terminated a further equilibration.

Chapter 1 entitled “Accessory and Rock Forming Minerals monitoring the Evolution of Zoned Mafic-Ultramafic Complexes in the Central Ural Mountains” is largely identical with the manuscript which was published under the same title in LITHOS in April 2007 (vol. 95, 19-42). Co-authors are G. Brügmann (Institute of Geosciences, University of Mainz, Germany) and E. Pushkarev (Institute of Geology and Geochemistry, Russian Academy of Sciences, Yekaterinburg, Russia). Data interpretation and preparation of the manuscript were done by J. Krause.

Chapter 2 entitled “Evolution of mafic rocks of Uralian-Alaskan-type Complexes: Implications for Subduction Zone Magmatism” is under consideration to be submitted for publication in the near future. Co-authors are G. Brügmann (Institute of Geosciences, University of Mainz, Germany) and E. Pushkarev (Institute of Geology and Geochemistry, Russian Academy of Sciences, Yekaterinburg, Russia). Some of the whole rock analyses were done by E. Pushkarev, who also provided additional samples. Data interpretation and preparation of the manuscript were done by J. Krause.

Chapter 3 entitled “Chemical composition and petrogenetic significance of spinel from Uralian-Alaskan-type Mafic-Ultramafic Complexes” is under consideration to be submitted for publication in the near future. Co-authors are G. Brügmann (Institute of Geosciences, University of Mainz, Germany) and E. Pushkarev (Institute of Geology and Geochemistry, Russian Academy of Sciences, Yekaterinburg, Russia). E. Pushkarev, also provided additional samples. Data interpretation and preparation of the manuscript were done by J. Krause.

Chapter 1

Accessory and Rock Forming Minerals monitoring the Evolution of Zoned Mafic-Ultramafic Complexes in the Central Ural Mountains

Joachim Krause, Gerhard E. Brügmann and Evgeny V. Pushkarev

Abstract

This study describes major and trace element compositions of accessory and rock forming minerals from three Uralian-Alaskan-type complexes in the Ural Mountains (Kytlym, Svetley Bor, Nizhnii Tagil) for the purpose of constraining the origin, evolution and composition of their parental melts. The mafic-ultramafic complexes in the Urals are aligned along a narrow, 900 km long belt. They consist of a central dunite body grading outward into clinopyroxenite and gabbro lithologies. Several of these dunite bodies have chromitites with platinum group element mineralization.

High Fo contents in olivine (Fo 92-93) and high Cr/(Cr+Al) in spinel (0.67-0.84) suggest a MgO-rich (>15 wt.%) and Al_2O_3-poor ultramafic parental magma. During its early stages the magma crystallized dominantly olivine, spinel and clinopyroxene forming cumulates of dunite, wehrlite and clinopyroxenite. This stage is monitored by a common decrease in the MgO content in olivine (Fo 93-86) and the Cr/(Cr+Al) value of coexisting accessory chromite (0.81-0.70). Subsequently, at subsolidus conditions, the chromite equilibrated with the surrounding silicates producing Fe-rich spinel while Al-rich spinel exsolved chromian picotite and chromian titanomagnetite. This generated the wide compositional ranges typical for spinel from Uralian-Alaskan type complexes world wide.

Laser ablation analyses (LA-ICPMS) reveal that clinopyroxene from dunites and clinopyroxenite from all three complexes have similar REE patterns with an enrichment of LREE (0.5-5.2 prim. mantle) and other highly incompatible elements (U, Th, Ba, Rb) relative to the HREE (0.25-2.0 prim. mantle). This large concentration range implies the

extensive crystallization of olivine and clinopyroxene together with spinel from a continuously replenished, tapped and crystallizing magma chamber. Final crystallization of the melt in the pore spaces of the cooling cumulate pile explains the large variation in REE concentrations on the scale of a thin section, the REE-rich rims on zoned clinopyroxene phenocrysts (e.g. La_{Rim}/La_{Core}~2), and the formation of interstitial clinopyroxene with similar REE enrichment.

Trace element patterns of the parental melt inferred from clinopyroxene analyses show negative anomalies for Ti, Zr, Hf, and a positive anomaly for Sr. These imply a subduction related geotectonic setting for the Uralian zoned mafic-ultramafic complexes. Ankaramites share many petrological and geochemical features with these complexes and could represent the parental melts of this class of mafic-ultramafic intrusions.

Diopside from chromitites and cross cutting diopside veins in dunite has similar trace element patterns with LREE/HREE ratios (e.g. La/Lu=5-60) much higher than those in diopside from all other lithologies. We suggest that the chromitites formed at high temperatures (800-900°C) during the waning stages of solidification as a result of the interaction of an incompatible element-rich melt or fluid with the dunite cumulates.

Keywords: Uralian-Alaskan-type complex, Ural Mountains, spinel, chromitite, parental melt, ankaramites.

1 Introduction

Uralian-Alaskan-type zoned mafic-ultramafic complexes are a class of intrusions which are distinct with regard to their tectonic setting, internal structure and petrology (Taylor and Noble, 1960; Noble and Taylor, 1960; Himmelberg et al., 1986; Himmelberg and Loney, 1995). The complexes are known from convergent margin settings, for example the Ural Mountains (Noble and Taylor, 1960; Taylor, 1967), the Cordillera of Alaska and British Columbia (Himmelberg et al., 1986; Himmelberg and Loney, 1995; Findlay, 1969; Clark, 1980; Nixon et al., 1990), and on Northern Kamchatka, Russia (Batanova and Astrakhantsev, 1992; Batanova and Astrakhantsev, 1994). The intrusions are distributed along narrow belts often several hundreds of kilometres long. Their classical distinctive geologic and petrographic feature is a zonal distribution of mafic and ultramafic rocks.

Often a central dunite body grades outward into wehrlite, clinopyroxenite and gabbroic lithologies. Many of these complexes host a mineralization of platinum group minerals (PGM) locally of economic importance.

In the Ural Mountains 15 Uralian-Alaskan-type mafic-ultramafic complexes define a linear belt along the 60-th meridian, which is about 900 km long (Fig. 1a). Due to the occurrence of economic platinum deposits associated with these complexes this chain is called the “Ural platinum belt” (UPB). This is a narrow belt in the middle and southern part of the Tagil-Magnitogorsk zone consisting of island arc related volcanic rocks and plutons in tectonic contact with ophiolite fragments and different types of mafic to ultramafic intrusive complexes.

For the Uralian-Alaskan type complexes of the UPB important geological and geochemical features such as the age and mechanism of emplacement or the composition and evolution of their parental melts are poorly understood. In addition the origin of the chromitites, sources for PGM placer deposits, is not well known.

The composition of minerals, rock forming and accessory phases, is controlled by parameters such as pressure, temperature and the composition of the parental magma. This is why the chemical composition of minerals, such as chromian spinel, give important information regarding the degree of partial melting in the mantle or the evolution of mantle melts during their rise to the surface (e.g. Hill and Roeder, 1974; Sack and Ghiorso, 1991a; Sack and Ghiorso, 1991b; Van der Veen and Maaskant, 1995). The compositional variations of chromian spinel can be further used to discriminate among different tectonic settings (e.g. Irvine, 1967; Roeder, 1994; Cookenboo et al., 1997; Zhou et al., 1997; Lee, 1999; Barnes and Roeder, 2001). However, one has to keep in mind that the composition of chromian spinel can be easily re-equilibrated at subsolidus conditions.

Trace element concentrations, for example those of the REE, play a key role in monitoring the fractionation of silicate melts. In particular in cumulate rocks, where there is no direct access to the melt composition, the trace element distribution in minerals provides powerful clues to the origin and evolution of the parental melts. For example, melt compositions can be calculated with experimentally determined mineral–melt partition coefficients and calculated trace element patterns can be compared with those

of natural samples from different tectonic environments (e.g. Mc Kenzie and O`Nions, 1991; Hart and Dunn, 1993; Ionov et al., 1997; Bédard et al., 2001; Ionov et al., 2002).

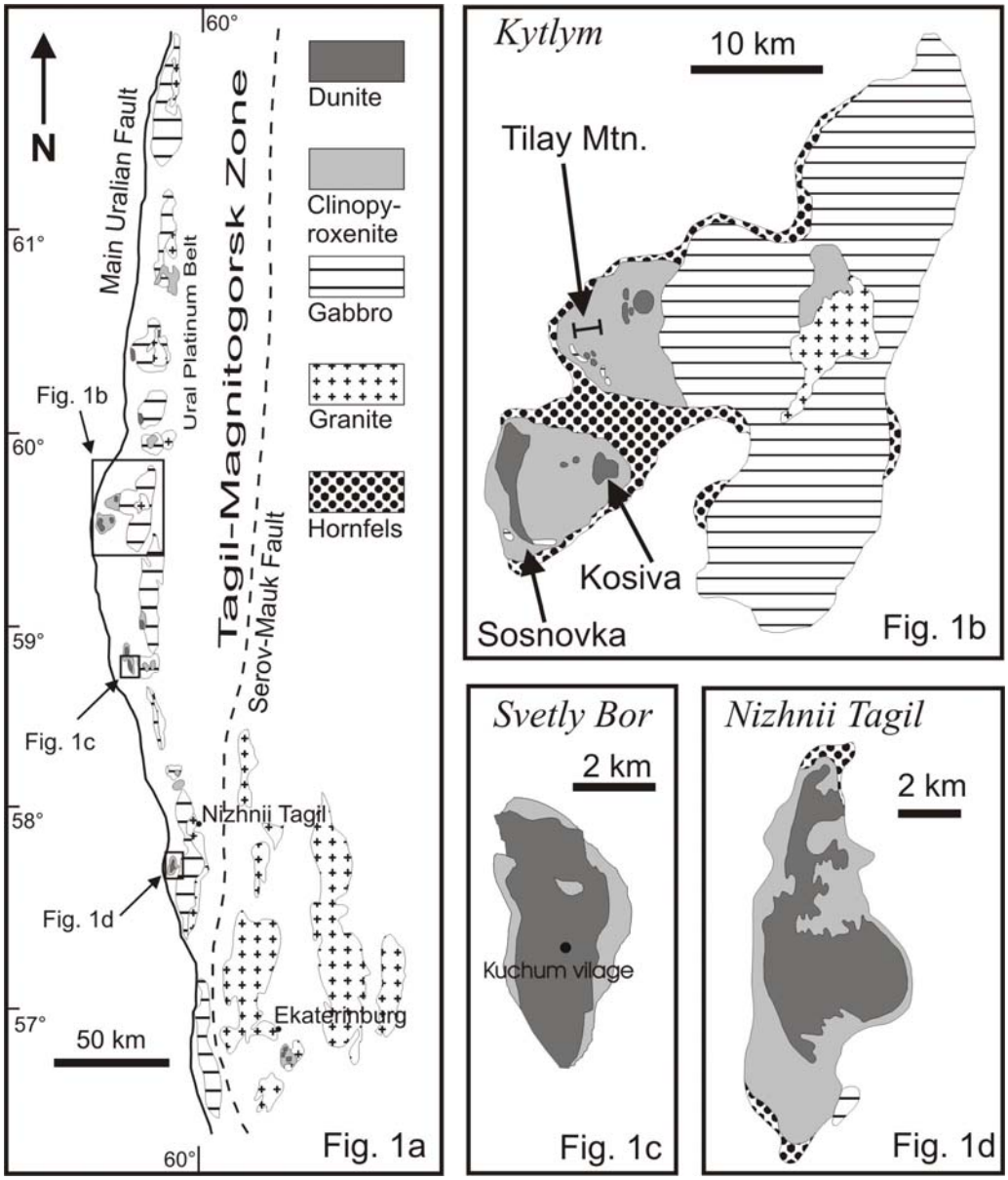

Fig. 1: Geological maps of the Ural platinum belt (a) and the studied Uralian-Alaskan type complexes (b-d). Modified after Chashukhin et al. (2002) and Garuti et al. (1997).

In this study we present new major and trace element data from rocks and minerals from three Uralian-Alaskan-type complexes in the middle and southern Urals. The comparison of the chemical composition of olivine and chromian spinel from the Urals

with data from other localities indicates that they are unique intrusions having a characteristic spinel chemistry. Laser-ICPMS analyses of trace element concentrations in clinopyroxene are used to calculate the melt composition. The mineral compositions monitor the evolution of the parental magmas and decipher differences between the complexes. The data also show that ankaramites could be the parental magmas of Uralian-Alaskan-type complexes.

2 Samples and Analytical Methods

2.1 Sample description

For this study dunites, chromitites, wehrlites, clinopyroxenites, hornblendites and gabbros were sampled from three Uralian-Alaskan-type complexes of the UPB. The Nizhnii Tagil complex is dominated by dunite of different grain sizes and textures containing chromitites in places (Fig. 1d) (Chashukhin et al., 2002; Savelieva et al., 2002). The dunites are overlain by clinopyroxenites with, in places, a few meters of wehrlite at the contact. Gabbro occurs only in a small body at the south-eastern rim of the complex.

In the dunitic core of the Svetley Bor complex no chromitites have been found (Fig. 1c). This core is surrounded by clinopyroxenite that locally contains hornblendites. Gabbroic rocks are not exposed in this complex (Garuti et al., 1997).

The Kytlym complex is the largest of the studied complexes (Fig. 1b). Several dunite bodies (Sosnovka, Kosiva Mountain, Tilay Mountain) are surrounded by clinopyroxenite. Some of the dunite bodies contain chromitites. Several smaller and at least two larger gabbro massifs are also present (Garuti et al., 1997; Savelieva et al., 1999; Savelieva et al., 2002; Chashukhin et al., 2002). In places tectonically induced interlayering between different lithologies can be observed. Lithological contacts are sharp and a foliation is often visible.

Dunites consist of 97-99 % olivine, and up to 2 % of accessory chromite. Interstitial clinopyroxene is present in most of the samples as an accessory component. Amphibole was found in one, strongly serpentinizised sample. The degree of serpentinization is variable (5-50 %) and often is extensive if the rocks are foliated. Dunites from each

complex are crosscut by millimetre to centimetre wide, coarse grained (up to 1 cm grain size) clinopyroxenite veins consisting of pure, green diopside. Dykes of hornblendite, cm to dm wide, occur in the dunite bodies of the Svetley Bor and the Sosnovka dunite (Kytlym).

Chromitites occur as lenses several millimetres to decimetres in size and consist of more than 80 % chromite. Relictic olivine and clinopyroxene as well as serpentine, talc, chlorite and other retrograde minerals are present along chromite grain boundaries as well as crosscutting cracks in the chromitite. Sulphides such as pentlandite and platinum group minerals such as isoferroplatinum and tetraferroplatinum occur as idiomorphic grains either included in the chromite or along grain boundaries. Most of the chromitites are surrounded by a millimetre thick green serpentine rim at the contact to the dunite. According to Chachukhin et al. (2002) the occurrence of chromitite lenses and schlieren is accompanied by a recrystallization of olivine in the neighbouring dunite.

The clinopyroxenites consist of 90 to 99 % clinopyroxene with minor amounts of olivine and hornblende. Spinel, apatite, titanite and sulphides are accessory phases. The textures vary from equigranular to porphyric. A wehrlite zone several centimetres to metres wide is often present at the contact between the clinopyroxenite and the dunite. An interlayering of clinopyroxenite with hornblendite occurs in several places in Svetley Bor. Here clinopyroxene and hornblende coexist along 0.5 to 1cm thick bands with equilibrated grain boundaries. This could signify the interaction of a fluid or melt phase with pre-existing clinopyroxenite.

In the Kosiva Mountain area of Kytlym and in Svetley Bor hornblendites form centimetres to decimetres wide dykes crosscutting dunites and clinopyroxenites. However massive bodies of hornblendite to hornblendite-pyroxenites can also be found. Clinopyroxene, in places partially replaced by hornblende, often forms idiomorphic phenocrysts in a hornblende-rich matrix, which also contains accessory phases such as sulphides, spinel, titanite, ilmenite and apatite.

The gabbros consist of 30 to 70 % clinopyroxene phenocrysts in a matrix of olivine, phlogopite, plagioclase (bytownite), and pseudoleucite (nepehline- K-feldspar intergrowth). In places with a higher feldspar content the gabbros are often strongly foliated with a protomylonitic texture and sharp tectonic contacts to the clinopyroxenites.

2.2 Major element analysis

After removing weathered crusts, the samples were powdered in an agate mill for XRF analysis. Polished thin sections 35 and 150 µm thick were used for the microprobe and Laser-ICPMS measurements. The XRF analyses were conducted with a Philips MagiXPRO spectrometer at the University of Mainz. Minerals were analysed with the Jeol JXA8200 microprobe of the Max-Planck-Institute for Chemistry and the Jeol JXA 8900RL microprobe at the Institute of Geosciences of the University of Mainz. We used natural minerals and oxides (Si, Ti, Al, Fe, Mg, Mn, Ca, Na, K, Cr, Zn) and pure element standards (V, Co) for calibration. Silicate minerals were measured with an acceleration voltage of 15 or 20 kV and a probe current of 12 or 20 nA. For the spinel analysis voltages and currents of 20 kV and 12 or 20 nA were used. Element maps were obtained with a 20 kV and 20 nA electron beam.

2.3 Trace element analysis

A New Wave UP213 laser system with a wavelength of 213 nm for the ablation was used to determine the trace element concentrations in clinopyroxene and hornblende. Applying a frequency of 10 Hz and energies between 2 and 12 J/cm² produced ablation pits with diameters of 80 and 120 µm. Helium was used as the carrier gas. The ablated material was analyzed with a ThermoFinnigan Element2 sectorfield ICPMS in the low resolution mode and a measuring time of 20 s on the background and 80 to 100 s on the sample. NIST612, KL2G and GOR132 were used as standard materials. The analytical procedure is described in more detail by Jochum et al. (in submission).

3 Results

Due to the large number of analysis (34 whole rock analyses, 584 olivine, 1326 spinel, 892 clinopyroxene with microprobe and 289 trace element analyses of clinopyroxene) only selected analyses can be here presented in Tables 1-4. The entire dataset can be found in the online version.

3.1 Major element composition of whole rocks

The major element composition for selected samples is shown in Tab. 1. There are systematic trends among the major element oxides, e.g. Al_2O_3, CaO, and TiO_2 with MgO, which are controlled by the lithology of the samples (Fig. 2).

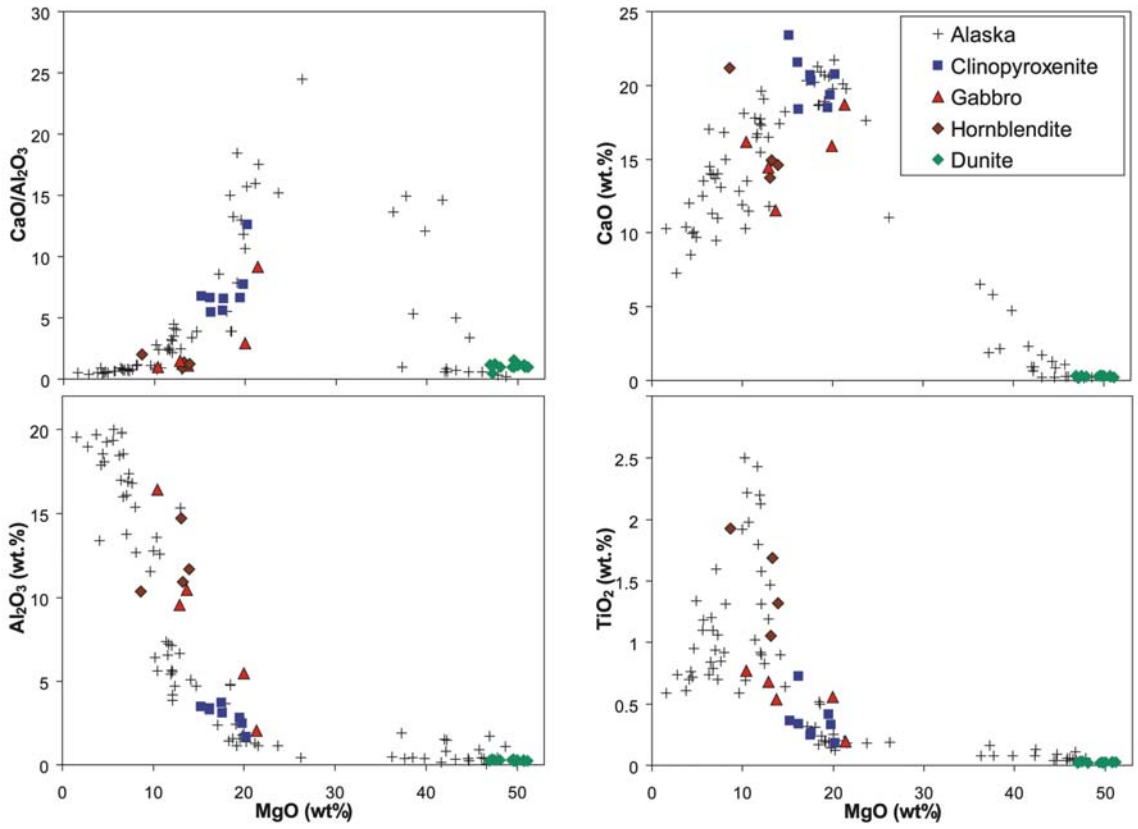

Fig. 2: Correlation diagrams for major oxides of rocks from Uralian-Alaskan-type complexes in the UPB. Comparison with other occurrences in the Cordillera of Alaska and W-Canada (Wyllie, 1967; Findlay, 1969; Himmelberg and Loney, 1995).

The Al_2O_3 content rises from less than 1 wt.% in the dunites and 1.6-3.3 wt.% in the clinopyroxenites to values between 2.0 wt.% and 16.4 wt.% in the hornblendites and gabbros. Most dunites also have low CaO concentrations of less than 1 wt.%, whereas the clinopyroxenites contain the highest CaO concentrations of all rock types (15.5-23.4 wt.%). The CaO decreases slightly in the gabbro (11.5-20.0 wt.%) and the hornblendite (13.7-21.2 wt.%). The TiO_2 content is lowest in the dunites (0.02-0.04 wt.%), but increases in the clinopyroxenite (0.18-0.72 wt.%) and the gabbro (0.19-0.77 wt.%), and reaches a maximum in the hornblendite (1.05-1.92 wt.%).

Tab. 1: Whole rock major and trace element contents of selected samples from Uralian-Alaskan-type complexes in the Urals. Fe_2O_3* = Total iron content, NT = Nizhnii Tagil, KT = Kytlym, SB = Svetley Bor, Du = Dunite, Wh = Wehrlite, Cp = Clinopyroxenite, Gb = Gabbro, Hb = Hornblendite, b.d. = below limit of detection.

Sample	NT1	NT3	NT8	NT12	NT13	NT14	SB18	SB22	SB23	SB30	KT32	KT37
Lithology	Du	Du	Gb	Du	Cp	Wh	Du	Cp	Cp	Hb	Du	Du
SiO_2 (wt.%)	34.95	36.14	47.64	34.74	46.29	44.98	37.45	51.04	50.87	35.5	37.96	37.85
TiO_2	0.02	0.02	0.53	0.02	0.41	0.31	0.02	0.36	0.18	1.88	0.03	0.02
Al_2O_3	0.19	0.21	10.3	0.2	2.75	1.96	0.25	3.42	1.62	10.14	0.26	0.27
Fe_2O_3*	8.55	8.38	10.6	6.58	12.32	12	9.08	6.22	5.55	20.91	11.66	10.95
MnO	0.17	0.16	0.19	0.12	0.18	0.2	0.16	0.11	0.12	0.23	0.22	0.19
MgO	43.05	44.42	13.5	43.67	19.18	20.92	45.78	15.06	19.9	8.44	45.23	45.33
CaO	0.3	0.3	11.38	0.19	18.19	15.39	0.25	23.16	20.4	20.69	0.32	0.26
Na_2O	b.d.	b.d.	2.15	b.d.	0.16	0.03	b.d.	0.15	0.06	0.33	b.d.	b.d.
K_2O	b.d.	b.d.	2.86	b.d.	0.01	0.01	b.d.	0.01	0.02	0.15	b.d.	b.d.
P_2O_5	b.d.	b.d.	0.34	b.d.	b.d.	b.d.	b.d.	b.d.	b.d.	1.49	b.d.	b.d.
Cr_2O_3	0.27	0.39	0.09	0.39	0.14	0.17	0.63	0.06	0.19	0.01	0.57	0.35
NiO	0.15	0.12	0.03	0.21	0.03	0.03	0.19	0.01	0.03	0.01	0.15	0.16
LOI	13.42	10.23	0.54	14.54	0.59	4.67	6.6	0.31	1.32	0.41	4.46	5.32
Total	101.02	100.33	100.15	100.60	100.24	100.67	100.36	99.90	100.26	100.19	100.79	100.66
CaO/Al_2O_3	1.58	1.43	1.10	0.95	6.61	7.85	1.00	6.77	12.59	2.04	1.23	0.96
Rb (ppm)	2	3	55	2	3	2	4	3	1	5	3	3
Sr	6	3	982	4	174	98	7	56	95	200	4	4
Ba	16	23	619	15	22	14	20	26	34	b.d.	20	23
Sc	3	4	38	3	89	65	3	135	88	76	2	1
V	5	6	244	4	179	121	9	188	69	662	9	12
Co	126	121	55	111	69	85	131	31	46	60	147	147
Cu	b.d.	b.d.	94	b.d.	6	4	b.d.	6	3	17	b.d.	b.d.
Zn	45	44	76	34	51	54	48	22	27	98	68	61
Ga	1	b.d.	13	1	5	5	1	5	3	18	2	1
Y	3	3	14	3	7	6	2	9	6	26	4	3
Nb	1	2	5	2	2	1	1	2	2	1	2	2
Zr	17	17	54	18	24	20	17	22	20	73	17	17
U	1	0.6	2.2	b.d.	1.1	1.1	0.1	b.d.	b.d.	2.4	b.d.	0.5
Th	b.d.	0	3.1	b.d.	b.d.	b.d.	b.d.	b.d.	b.d.	b.d.	b.d.	b.d.
Pb	2	2	12	3	b.d.	1	3	4	b.d.	1	4	4

Sample	KT39	KT44	KT46	KT49
Lithology	Cp	Gb	Gb	Cp
SiO_2 (wt.%)	48.72	45.14	46.65	50.17
TiO_2	0.33	0.55	0.67	0.26
Al_2O_3	2.47	5.42	9.39	3.05
Fe_2O_3*	9.1	12.82	12.52	7.69
MnO	0.16	0.21	0.21	0.15
MgO	19.61	19.76	12.68	17.3
CaO	19.16	15.71	14.22	19.94
Na_2O	0.13	0.4	1.79	0.23
K_2O	0.01	0.05	1.26	0.03
P_2O_5	b.d.	0.01	0.24	b.d.
Cr_2O_3	0.32	0.17	0.08	0.22
NiO	0.02	0.04	0.02	0.02
LOI	0.44	0.06	0.12	1.23
Total	100.47	100.33	99.85	100.29
CaO/Al_2O_3	7.76	2.90	1.51	6.54

	KT39	KT44	KT46	KT49
	Cp	Gb	Gb	Cp
Rb (ppm)	2	4	21	2
Sr	80	294	898	76
Ba	20	16	185	58
Sc	78	63	45	89
V	132	229	280	154
Co	57	74	56	53
Cu	7	11	77	10
Zn	42	72	86	36
Ga	5	11	12	5
Y	8	14	14	7
Nb	2	b.d.	2	3
Zr	23	39	55	21
U	0.6	0.7	1.8	b.d.
Th	b.d.	b.d.	b.d.	b.d.
Pb	2	2	6	3

A typical feature of all lithologies is the high CaO/Al_20_3 ratio. It varies from 0.5 – 1.6 in the dunite, 0.9-2 in the hornblendite and 0.9-2.8 in the gabbros to 3.6-12.6 in the clinopyroxenites and is therefore significantly higher than that observed in most mantle melts and upper mantle peridotites.

3.2 Mineral chemistry

3.2.1 Chemical composition of Olivine

Olivine is present in all rock types and Table 2 summarizes its chemical composition in selected samples. In dunites, olivine shows a rather large compositional variation as the Forsterite (Fo) content ranges from 86-94 (Fig. 3). It is important to note that the forsterite content of olivine in the vicinity of the chromitite is high (Fo_{90-93}), but the highest Fo contents (Fo_{93-96}) are observed in olivine inclusions in spinel from the chromitites (Fig. 3). Olivine in the other rock types has lower Fo values decreasing systematically from Fo_{84-86} in the hornblendites, Fo_{80-83} in the clinopyroxenites to Fo_{74-84} in the gabbros.

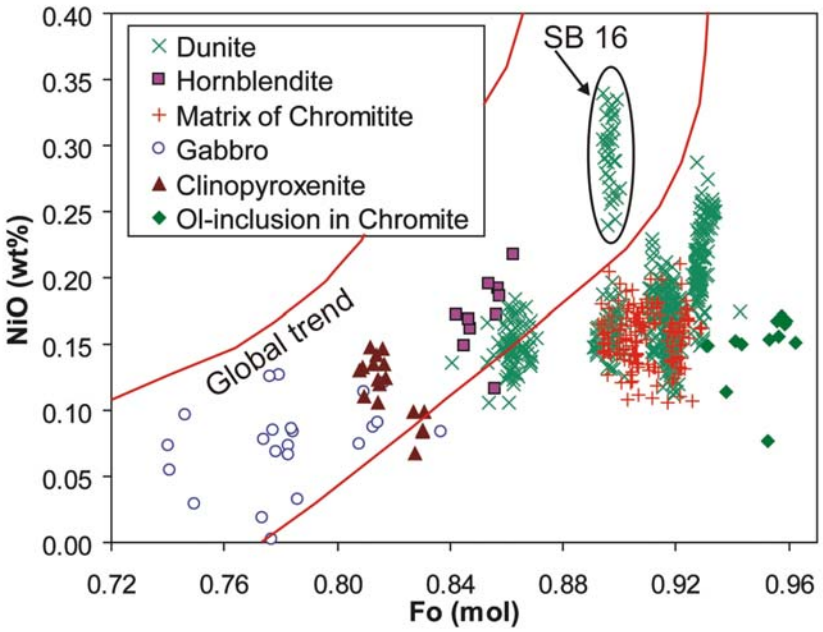

Fig. 3: Chemical composition of olivine in different lithologies from the Uralian-Alaskan-type complexes in the Tagil Magnitogorsk zone of the Ural Mountains. Fo-rich samples (except sample SB16) have low Ni contents if compared with the global trend. Literature data are from the GEOROC-database (http://georoc.mpch-mainz.gwdg.de/georoc/)

Tab. 2: Olivine compositions of selected samples from Uralian-Alaskan-type intrusions. FeO* = Total iron content, NT = Nizhnii Tagil, KT = Kytlym, SB = Svetley Bor, Du = Dunite, Ch = Chromitite, Ch* = inclusion in Spinel, Wh = Wehrlite, Cp = Clinopyroxenite, Gb = Gabbro, Hb = Hornblendite, b.d. = below limit of detection.

Sample	NT1-42	NT2-58	NT3-38	NT4-177	NT5-103	NT5-177	NT6-75	NT7-13	NT8-91	NT9a-43
Locality	NT	NT	NT	NT	NT	NT	NT	NT	NT	NT
Lithology	Du	Du	Du	Du	Ch*	Ch	Du	Du	Gb	Gb
SiO_2 (wt.%)	41.28	40.62	40.74	40.74	41.04	40.39	40.28	40.64	38.55	38.36
TiO_2	0.01	0.02	0.02	0.02	0.03	0.02	0.04	0.00	0.03	0.00
Al_2O_3	0.00	0.00	0.00	0.01	0.03	0.00	0.04	0.01	0.05	0.02
FeO*	8.71	7.76	8.11	7.15	4.33	7.44	7.49	6.92	20.74	20.94
MnO	0.17	0.17	0.18	0.15	0.06	0.18	0.20	0.11	0.65	0.65
MgO	49.86	50.63	50.62	51.29	53.41	50.88	50.91	51.81	39.74	41.33
CaO	0.25	0.28	0.33	0.28	0.24	0.27	0.20	0.24	0.04	0.06
Cr_2O_3	0.00	0.01	0.00	0.01	0.46	0.00	1.04	0.01	0.01	0.00
NiO	0.18	0.15	0.14	0.20	0.16	0.17	0.16	0.22	0.02	0.07
Total	100.46	99.65	100.21	99.84	99.74	99.35	100.43	99.99	99.83	101.43
Fo (mol)	0.91	0.92	0.92	0.93	0.96	0.92	0.92	0.93	0.77	0.78

Sample	NT12-132	NT13-112	NT15-121	SB16-73	SB18-47	KT31G-19	KT31G-69	KT32-118	KT33-129	KT33-177
Locality	NT	NT	NT	SB	SB	KT	KT	KT	KT	KT
Lithology	Du	Wh	Du	Du	Du	Ch*	Ch	Du	Ch	Ch*
SiO_2 (wt.%)	40.74	39.23	40.64	39.85	40.22	40.73	40.84	39.99	40.91	41.04
TiO_2	0.02	0.02	0.02	0.00	0.01	0.00	0.00	0.02	0.01	0.01
Al_2O_3	0.02	0.00	0.02	0.00	0.00	0.02	0.00	0.00	0.00	0.00
FeO*	6.68	16.28	6.83	10.17	8.38	5.64	8.43	10.35	9.30	6.73
MnO	0.15	0.38	0.18	0.20	0.17	0.09	0.16	0.25	0.23	0.17
MgO	51.74	43.63	51.68	49.82	50.95	52.57	50.06	48.81	49.30	51.23
CaO	0.19	0.04	0.20	0.05	0.07	0.16	0.24	0.30	0.19	0.18
Cr_2O_3	0.00	0.02	0.04	0.03	0.00	0.55	0.05	0.02	0.04	0.56
NiO	0.25	0.10	0.24	0.32	0.21	0.15	0.18	0.16	0.15	0.15
Total	99.84	99.73	99.88	100.44	100.02	99.90	99.96	100.01	100.17	100.08
Fo (mol)	0.93	0.83	0.93	0.90	0.92	0.94	0.91	0.89	0.90	0.93

Sample	KT35-25	KT36-272	KT36-311	KT37-190	KT38-32	KT40-343	KT42-194	NT46-171	KT49-191	KT51-256
Locality	KT	KT	KT	KT	KT	KT	KT	NT	KT	KT
Lithology	Hb	Ch*	Ch	Du	Du	Du	Du	Gb	Cp	Cp
SiO_2 (wt.%)	39.48	41.64	41.17	40.13	39.88	40.35	40.36	37.88	38.39	38.67
TiO_2	0.00	0.05	0.02	0.03	0.00	0.02	0.03	0.00	0.00	0.00
Al_2O_3	0.00	0.00	0.00	0.00	0.00	0.00	0.00	0.02	0.00	0.00
FeO*	13.06	4.72	9.50	10.29	13.26	8.28	8.29	23.34	16.91	17.62
MnO	0.24	0.09	0.17	0.22	0.30	0.15	0.16	0.69	0.40	0.33
MgO	47.27	53.17	49.54	49.19	46.35	50.46	50.56	39.14	44.62	43.47
CaO	0.03	0.05	0.08	0.05	0.04	0.26	0.33	0.02	0.03	0.00
Cr_2O_3	0.00	0.64	0.03	0.03	0.02	0.05	0.01	0.00	0.01	0.00
NiO	0.15	0.08	0.11	0.14	0.13	0.18	0.17	0.03	0.12	0.12
Total	100.22	100.46	100.66	100.13	99.98	99.74	100.02	101.12	100.53	100.21
Fo (mol)	0.87	0.95	0.90	0.89	0.86	0.92	0.92	0.75	0.82	0.81

Nickel in olivine shows a systematic positive correlation with the Fo content (Fig. 3). This variation follows the lower limit of a global field defined by olivine which crystallized from different mantle-derived magma types. However, Fo-rich olivine ($Fo_{<89}$), especially inclusions of olivine in chromitite, have relatively low and rather constant Ni concentrations and many are outside of this field (Fig. 3).

3.2.2 Chemical composition of Spinel

Spinel is present as an accessory phase in all rock types and as the main component in the chromitites. This mineral displays a wide compositional range with regard to its major components, Mg, Fe^{2+}, Cr, Fe^{3+}, Al and Ti (Tab. 3; Fig. 4, 5).

The accessory spinel in the dunites follows characteristic trends, which in most cases can even be observed in one single thin section (Fig. 4a, 5a). These trends divide the spinel population into three different groups. In Figure 4a the trend starts at a composition of $Al_{13}Cr_{63}Fe^{3+}_{24}$ and evolves in group I due to the exchange of Cr and Fe^{3+} towards $Al_{13}Cr_{50}Fe^{3+}_{37}$. At this point Al is replaced with Fe^{3+} towards a composition of $Al_0Cr_{51}Fe^{3+}_{49}$ (group II spinel Fig. 4a). Subsequently Cr is substituted in group III with Fe^{3+} until the spinel composition reaches the miscibility gap ($Al_0Cr_{35}Fe^{3+}_{65}$) or forms pure magnetite, which can be sometimes observed as rims around chromite grains Fig. 4a-c). The TiO_2 content (not shown) rises from 0.4 to 0.8 wt.% in group I and II spinel until Al is substituted with Cr and Fe^{3+}, when it decreases to 0.05 wt.% in group III spinel. Similarly $Fe^{2+}/(Mg+Fe^{2+})$ and $Fe^{3+}/(Cr+Al+Fe^{3+})$ increase from 0.55 to 0.85 and 0.15 to 0.55, respectively in group I and II (Fig. 5a). In Al-free spinel (group III) $Fe^{2+}/(Mg+Fe^{2+})$ remains fairly constant close to 0.9, but $Fe^{3+}/(Cr+Al+Fe^{3+})$ increases to 1 (Fig. 5a,d). The Cr/(Cr+Al) is constant around 0.8 in group I. However, the replacement of Al with Fe^{3+} in group II causes an increase in Cr/(Cr+Al) to about 1.

There is also a systematic chemical difference between spinel from different complexes. For example, accessory spinel from Nizhnii Tagil tends to have lower TiO_2 and Al_2O_3-concentrations and higher Cr/(Cr+Al) values than those of Kytlym and Sevtley Bor (Fig. 4, Fig. 5e-f, Tab. 3).

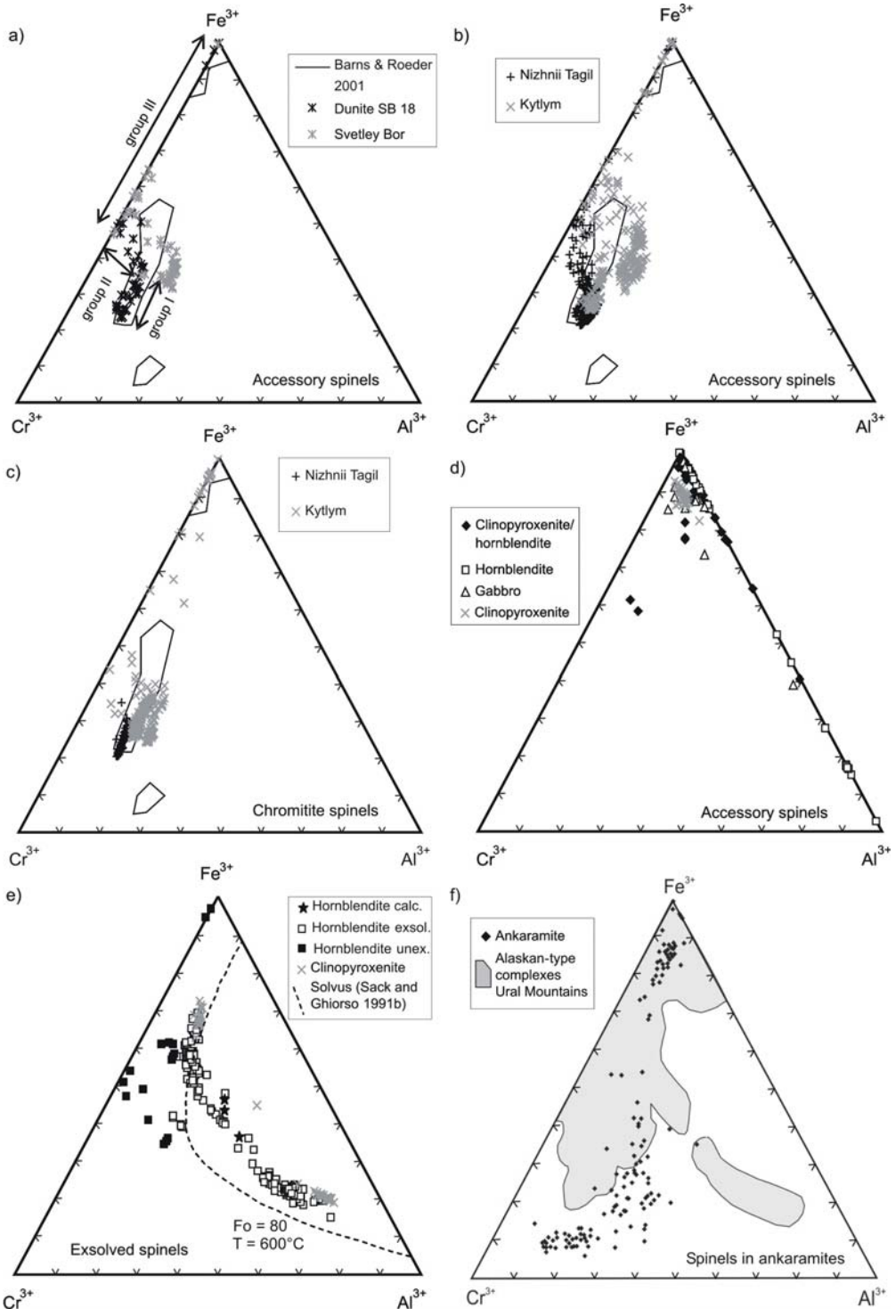

Fig. 4: Distribution of trivalent cations in spinel from Uralian-Alaskan-type complexes and ankaramites. These include: a) accessory spinel Svetley Bor, b) accessory spinel Kytlym and Nizhnii Tagil, c) spinel from chromitite, d) accessory spinel from clinopyroxenite, hornblendite and gabbro, e) exsolved spinel calc. = calculated spinel composition before exsolution, and f) comparison with spinel from ankaramites (Mossman et al., 2000; Nono et al., 1994; Barsdell and Smith, 1989; Barsdell, 1988). Compositional fields for Uralian-Alaskan-type complexes are from Barns and Roeder (2001). The solvus curve for spinel in e) was calculated for 600°C and Fo_{90} olivine by Sack and Ghiorso (1991b).

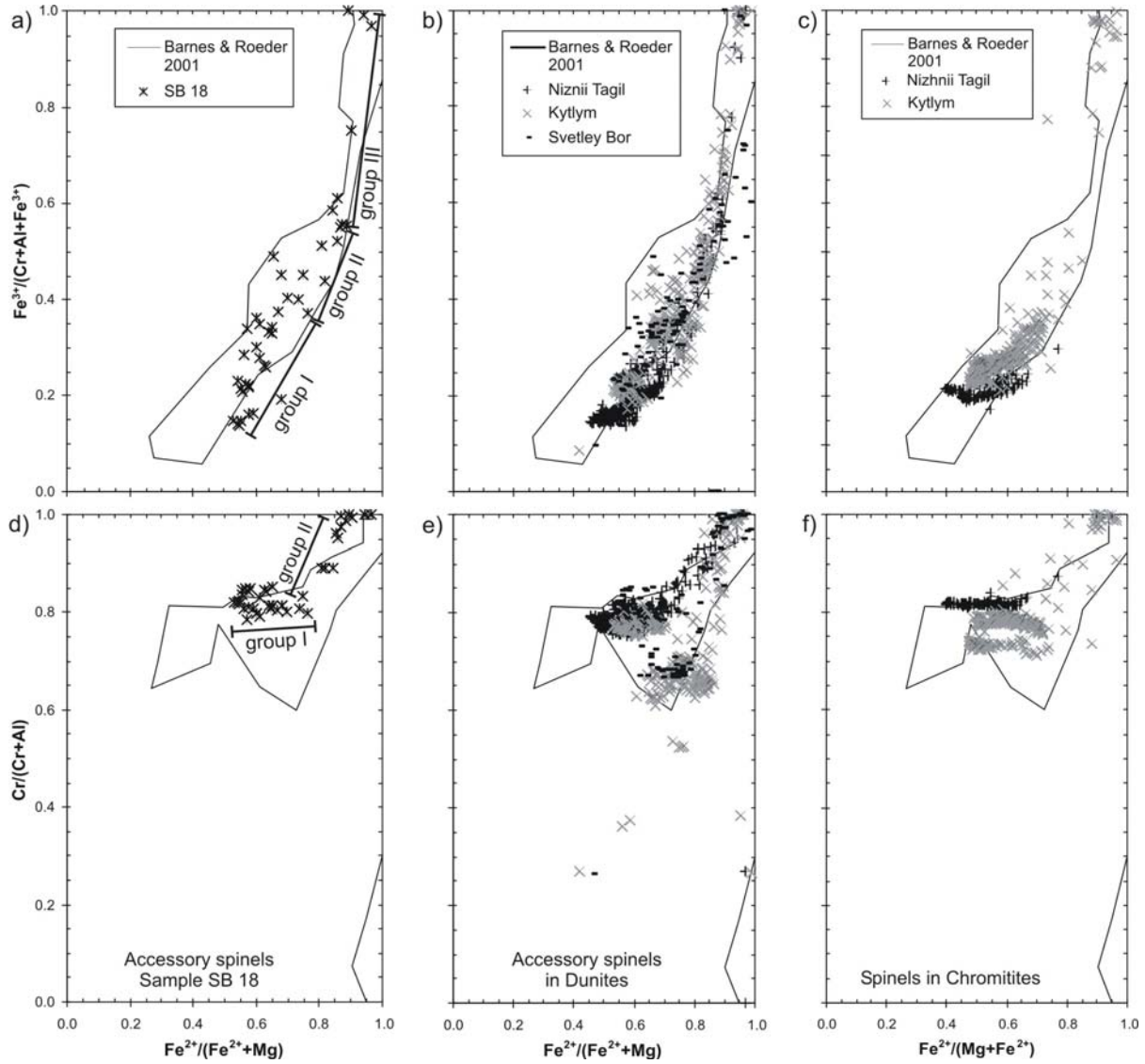

Fig. 5: Variation of $Fe^{2+}/(Fe^{2+}+Mg)$, $Fe^{3+}/(Cr+Al+Fe^{3+})$ and Cr/(Cr+Al) in spinel from Uralian-Alaskan-type intrusions. a, d) accessory spinel in sample SB18, b ,e) accessory spinel in dunite, c, f) spinel in chromitite.

The chemical composition of spinel in the chromitites is considerably less variable than that of accessory spinel in the dunites. We only observe Cr-rich spinel (Fig. 4c) and their chemical variations are similar to those observed for accessory spinel belonging to group I. In Kytlym some of the spinels have magnetite-rich compositions. Like the accessory spinel in the dunites, the chromitite spinel from Nizhnii Tagil has higher Cr/(Cr+Al) values and lower TiO_2 contents than that from Kytlym (Fig. 4c, Fig. 5f, Tab. 3). The cataclastic deformation of spinel observed in some chromitites has no influence on their chemical composition.

Tab. 3: Spinel compositions of selected samples from Uralian-Alaskan-type intrusions. FeO_m = measured iron content, FeO_{calc} and Fe_2O_{3calc} = Calculated assuming stichiometry, NT = Nizhnii Tagil, KT = Kytlym, SB = Svetley Bor, Du = Dunite, Ch = Chromitite, Cp = Clinopyroxenite, Gb = Gabbro, Hb = Hornblendite, ex = exsolved spinel, orig = composition before exsolution calculated from area analysis, b.d. = below limit of detection.

Sample	NT2-29	NT5-106	NT12-111	SB18-49	SB20-28	SB30-231	KT31G-65	KT31F-232	KT32-128
Locality	NT	NT	NT	SB	SB	SB	KT	KT	KT
Lithology	Du	Ch	Du	Du	Cp	Hb	Ch	Ch	Du
TiO_2 (wt.%)	0.54	0.45	0.45	0.52	0.89	0.73	0.77	0.69	0.70
Al_2O_3	8.65	7.15	7.78	6.04	4.09	63.94	7.71	7.53	7.47
FeO_m	33.95	30.12	31.18	50.10	70.09	16.10	40.85	39.68	43.44
MnO	0.47	0.36	0.52	0.62	0.59	0.45	0.43	0.40	0.55
MgO	8.54	11.83	8.15	4.39	0.37	10.33	7.79	8.29	6.51
Cr_2O_3	46.54	48.90	50.25	35.58	17.71	0.10	41.09	41.53	38.73
NiO	0.06	0.07	0.07	0.15	0.11	0.05	0.11	0.12	0.12
V_2O_3	0.01	b.d.	0.02	0.04	0.20	b.d.	0.03	0.03	0.02
ZnO	0.16	b.d.	0.23	0.27	0.12	3.66	0.08	0.07	0.18
CoO	0.08	b.d.	0.12	0.12	0.03	0.19	0.08	0.05	0.10
Total	98.99	98.87	98.77	97.83	94.19	95.54	98.95	98.38	97.79
Cr/(Cr+Al)	0.78	0.82	0.81	0.80	0.74	<0.01	0.78	0.79	0.78
$Fe^{3+}/(Cr+Al+Fe^{3+})$	0.20	0.21	0.16	0.37	0.63	<0.01	0.28	0.28	0.31
$Fe^{2+}/(Mg+Fe^{2+})$	0.57	0.42	0.58	0.76	0.98	0.47	0.61	0.58	0.66
FeO_{calc}	20.17	15.00	20.31	25.90	31.12	16.10	21.70	20.80	23.12
Fe_2O_{3calc}	15.56	16.80	12.37	27.90	43.31	<0.01	21.75	21.69	23.47

Sample	KT35-4b	KT35-4a	KT 35-4 calc	KT35-1a	KT35-1b	KT35-1core	KT 35-1 calc	KT51-272	KT51-280
Locality	KT	KT	KT	KT	KT	KT	KT	KT	KT
Lithology	Hb	Hb	Hb	Hb	Hb	Hb	Hb	Cp	Cp
TiO_2 (wt.%)	4.80	0.45	3.78	4.46	0.60	2.55	2.60	0.09	2.06
Al_2O_3	5.92	37.53	13.31	7.25	33.78	15.31	17.91	46.56	3.75
FeO_m	67.62	30.11	58.86	60.80	30.94	53.00	49.47	26.11	76.40
MnO	0.47	0.31	0.43	0.53	0.33	0.42	0.43	0.21	0.29
MgO	3.31	11.33	5.19	3.56	10.74	5.33	6.27	11.25	1.12
Cr_2O_3	16.52	18.90	17.08	19.76	23.19	20.76	21.16	14.32	9.62
NiO	0.25	0.17	0.23	0.24	0.11	0.19	0.19	0.12	0.16
V_2O_3	0.46	0.16	0.39	0.32	0.13	0.26	0.24	0.03	0.26
ZnO	0.06	0.43	0.15	0.10	0.48	0.18	0.24	1.36	0.11
CoO	0.13	0.11	0.12	0.12	0.12	0.13	0.12	0.12	0.04
Total	99.56	99.56	99.56	97.18	100.42	98.14	98.65	100.18	93.82
Cr/(Cr+Al)	0.65	0.25	0.46	0.65	0.32	0.48	0.44	0.17	0.63
$Fe^{3+}/(Cr+Al+Fe^{3+})$	0.60	0.12	0.46	0.51	0.13	0.38	0.33	0.06	0.76
$Fe^{2+}/(Mg+Fe^{2+})$	0.85	0.50	0.76	0.83	0.52	0.75	0.71	0.51	0.94
FeO_{calc}	32.26	20.29	29.47	30.73	21.00	27.85	26.91	20.77	31.24
Fe_2O_{3calc}	39.30	10.91	32.67	33.41	11.05	27.95	25.07	5.93	50.18

Spinel from clinopyroxenites, hornblendites and gabbros generally has low Cr_2O_3 contents, up to 18 wt.% in clinopyroxenites and less than 4 wt.% in hornblendites and gabbros (Tab. 3). Thus, most of the spinel has a magnetite-rich composition (Fig. 4d). In hornblendites (SB30, SB29b) some spinels are hercynites and have elevated ZnO contents (up to 3.6 wt.%).

3.2.3 Major and trace element concentrations in clinopyroxene

Clinopyroxene is present in all rock types. In dunites it mainly appears as a xenomorphic interstitial phase. It occurs as an idiomorphic to hypidiomorphic cumulate phase in clinopyroxenites, hornblendites and gabbros, where exsolutions of titanomagnetite often form a visible zonation. Clinopyroxene is also present in the chromitites as interstitial phase and as inclusions in spinel. Its composition is similar to that of interstitial grains occurring in the dunites. In Svetley Bor and Nizhnii Tagil veins of green, idiomorphic clinopyroxene crosscut some of the dunites. Almost all clinopyroxenes are diopsides, but some augite is found in the clinopyroxenites and the dunite (Fig. 6 Tab. 4).

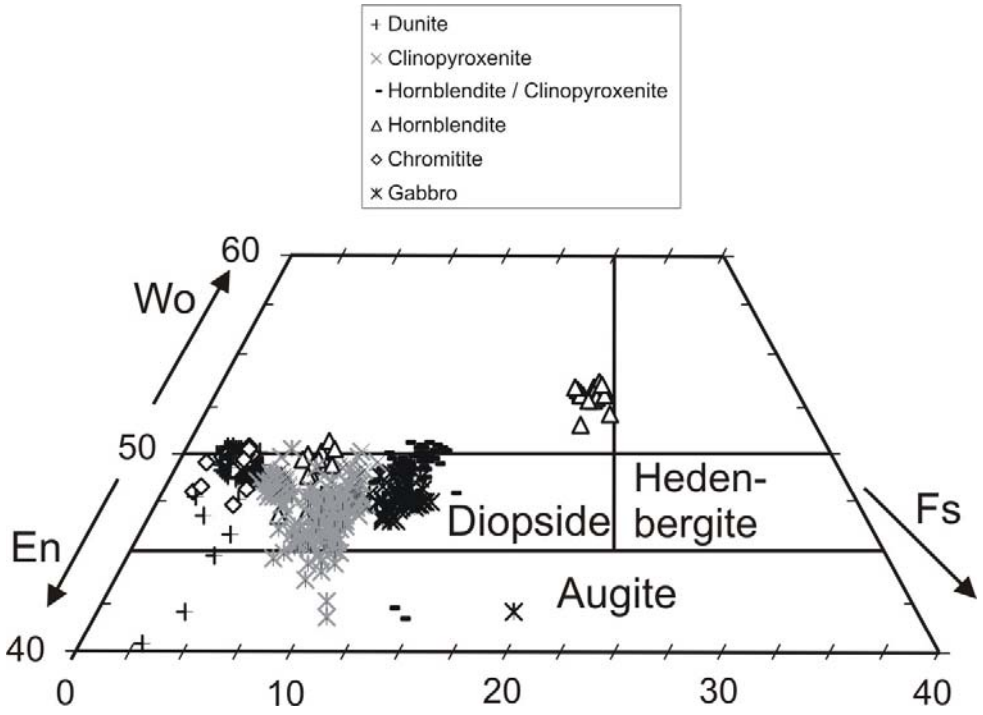

Fig. 6: Classification of clinopyroxene from Uralian-Alaskan-type complexes.

Tab. 4: Clinopyroxene compositions of selected samples from Uralian-Alaskan-type intrusions. FeO* = all iron measured as FeO, NT = Nizhnii Tagil, KT = Kytlym, SB = Svetley Bor, Du = Dunite, Vn = Diopside vein in dunite, Wh = Wehrlite, Ch = Chromitite, Cp = Clinopyroxenite, Hb = Hornblendite, M = matrix, C = core of phenocryst, R = rim of phenocryst, b.d. = below limit of detection, n.m. = not measured.

Sample	NT1-69	NT6-14	NT12-114	NT13-115	SB16-64	SB22-88	KT31F-249	KT33-132	KT37-148	KT38-69
Location	NT	NT	NT	NT	SB	SB	KT	KT	KT	KT
Lithology	Du	Vn	Du	Cp	Vn	Cp	Ch	Ch	Du	Wh
Position	M	M	M	M	M	M	M	M	M	M
SiO_2 (wt.%)	54.03	54.58	54.06	52.22	53.40	50.88	53.08	54.38	54.64	53.93
TiO_2	0.10	0.09	0.09	0.32	0.18	0.33	0.11	0.05	0.09	0.23
Cr_2O_3	0.33	0.81	0.39	0.03	0.53	0.07	0.17	0.35	0.14	0.45
Al_2O_3	0.80	0.93	0.72	2.57	1.46	3.43	0.52	0.81	0.41	1.57
FeO*	2.26	1.84	1.39	5.62	2.37	5.46	1.39	1.85	1.49	3.42
MnO	0.04	0.04	0.05	0.14	0.07	0.10	0.02	0.02	0.05	0.11
MgO	17.60	16.93	17.42	15.17	17.14	15.34	17.56	16.85	17.30	16.39
CaO	25.29	24.28	25.31	23.48	24.60	23.31	25.32	25.25	25.37	23.58
K_2O	0.01	0.01	b.d.	0.01	0.01	0.02	b.d.	b.d.	b.d.	0.01
Na_2O	0.24	0.47	0.36	0.33	0.30	0.27	0.07	0.21	0.07	0.29
Total	100.70	100.04	99.82	99.93	100.08	99.20	98.27	99.83	99.59	100.03
Mg/(Fe+Mg)	0.93	0.94	0.96	0.83	0.93	0.83	0.96	0.94	0.95	0.90
Ba (ppm)	1.8	4.6	b.d.	0.1	0.2	0.1	1.8	1.3	2.0	1.5
Th	0.003	0.046	0.003	0.014	0.020	0.008	0.002	0.017	0.026	0.007
U	0.005	0.018	b.d	0.002	0.012	0.004	b.d	0.007	0.004	0.004
La	0.07	1.45	0.17	1.58	1.04	0.40	0.06	1.07	0.42	0.46
Ce	0.19	3.72	0.42	5.05	3.34	1.67	0.22	2.85	1.53	1.81
Sr	24	191	26	214	140	57	8	102	40	65
Pr	0.03	0.61	0.07	0.97	0.75	0.43	0.04	0.44	0.35	0.40
Nd	0.2	3.1	0.4	5.3	4.1	2.8	0.2	2.1	1.9	2.5
Hf	0.10	0.15	0.10	0.45	0.16	0.30	0.07	0.12	0.90	0.21
Sm	0.14	0.90	0.29	1.76	1.24	1.08	0.08	0.58	0.72	0.85
Zr	1.7	3.4	1.5	9.3	2.8	5.2	0.9	3.2	13.6	3.6
Eu	0.07	0.32	0.17	0.56	0.41	0.37	0.03	0.19	0.22	0.29
Ti	474	685	448	1775	973	1913	294	462	1293	981
Gd	0.37	0.97	0.66	1.88	1.20	1.24	0.15	0.69	0.92	0.88
Tb	0.09	0.13	0.13	0.25	0.14	0.20	0.03	0.10	0.20	0.13
Dy	0.54	0.71	0.66	1.37	0.73	1.18	0.21	0.55	1.38	0.80
Ho	0.08	0.12	0.12	0.25	0.14	0.23	0.04	0.09	0.26	0.16
Er	0.20	0.26	0.28	0.63	0.33	0.60	0.09	0.19	0.83	0.41
Tm	0.02	0.03	0.03	0.09	0.04	0.08	0.01	0.02	0.08	0.06
Yb	0.16	0.20	0.16	0.48	0.25	0.48	0.07	0.14	0.58	0.43
Lu	0.02	0.03	0.03	0.08	0.04	0.06	0.01	0.02	0.07	0.07

Tab. 4: (cont.)

Sample	KT49-110	KT51-245	KT51-247	KT51-251		KT49-110	KT51-245	KT51-247	KT51-251
Location	KT	KT	KT	KT		KT	KT	KT	KT
Lithology	Cp	Cp	Cp	Cp		Cp	Cp	Cp	Cp
Position	M	C	R	M		M	C	R	M
SiO_2 (wt.%)	51.63	52.83	51.72	51.45	Sr (ppm)	79	43	47	48
TiO_2	0.28	0.12	0.23	0.29	Pr	0.62	0.24	0.41	0.56
Cr_2O_3	0.14	0.48	0.52	0.39	Nd	3.7	1.4	2.4	3.4
Al_2O_3	2.33	1.26	1.95	2.65	Hf	0.25	0.05	0.10	0.28
FeO*	4.54	4.27	4.86	5.08	Sm	1.22	0.42	0.77	1.15
MnO	0.13	0.09	0.13	0.19	Zr	5.0	1.2	2.8	5.9
MgO	16.14	17.41	16.46	16.00	Eu	0.41	0.16	0.27	0.38
CaO	23.89	22.36	22.71	22.35	Ti	1571	647	893	1418
K_2O	0.01	0.01	b.d.	b.d.	Gd	1.32	0.52	0.90	1.33
Na_2O	0.16	0.20	0.22	0.25	Tb	0.19	0.07	0.13	0.21
Total	99.25	99.06	98.86	98.69	Dy	1.04	0.43	0.78	1.26
Mg/(Fe+Mg)	0.86	0.88	0.86	0.85	Ho	0.19	0.09	0.17	0.25
Ba (ppm)	1.5	b.d.	b.d.	b.d.	Er	0.50	0.22	0.43	0.67
Th	0.018	0.007	0.011	0.018	Tm	0.06	0.03	0.06	0.08
U	0.007	0.002	0.003	0.004	Yb	0.42	0.21	0.37	0.57
La	0.77	0.41	0.60	0.80	Lu	0.05	0.03	0.06	0.09
Ce	2.78	1.33	2.14	2.88					

The clinopyroxene shows chemical variations which are controlled by the host lithology. For example, a negative correlation between Al_2O_3 and Mg/(Mg+Fe) is displayed in Fig. 7a where clinopyroxene from dunites has the lowest contents of Al_2O_3, MnO and TiO_2 but they systematically increase towards clinopyroxenite, gabbro and hornblendite, while SiO_2 contents systematically decrease (not shown). Clinopyroxene in one hornblendite from Svetley Bor (SB30) has Al_2O_3 contents up to 12.3 wt. %. This requires an extensive incorporation of the Tschermak component and explains the high proportion of the wollastonite component (>50; Fig. 6).

A positive correlation of the middle and heavy REE contents with Al_2O_3, FeO, and TiO_2 and a negative one with Mg/(Mg+Fe) can be observed for all lithologies. The distribution of the middle and heavy REE is similar to that of Al_2O_3 in that, for example, Lu concentrations increase from dunite to clinopyroxenite (Fig 7b). For Nb, U, Th and Sr no clear correlation with the major elements and the REEs is seen.

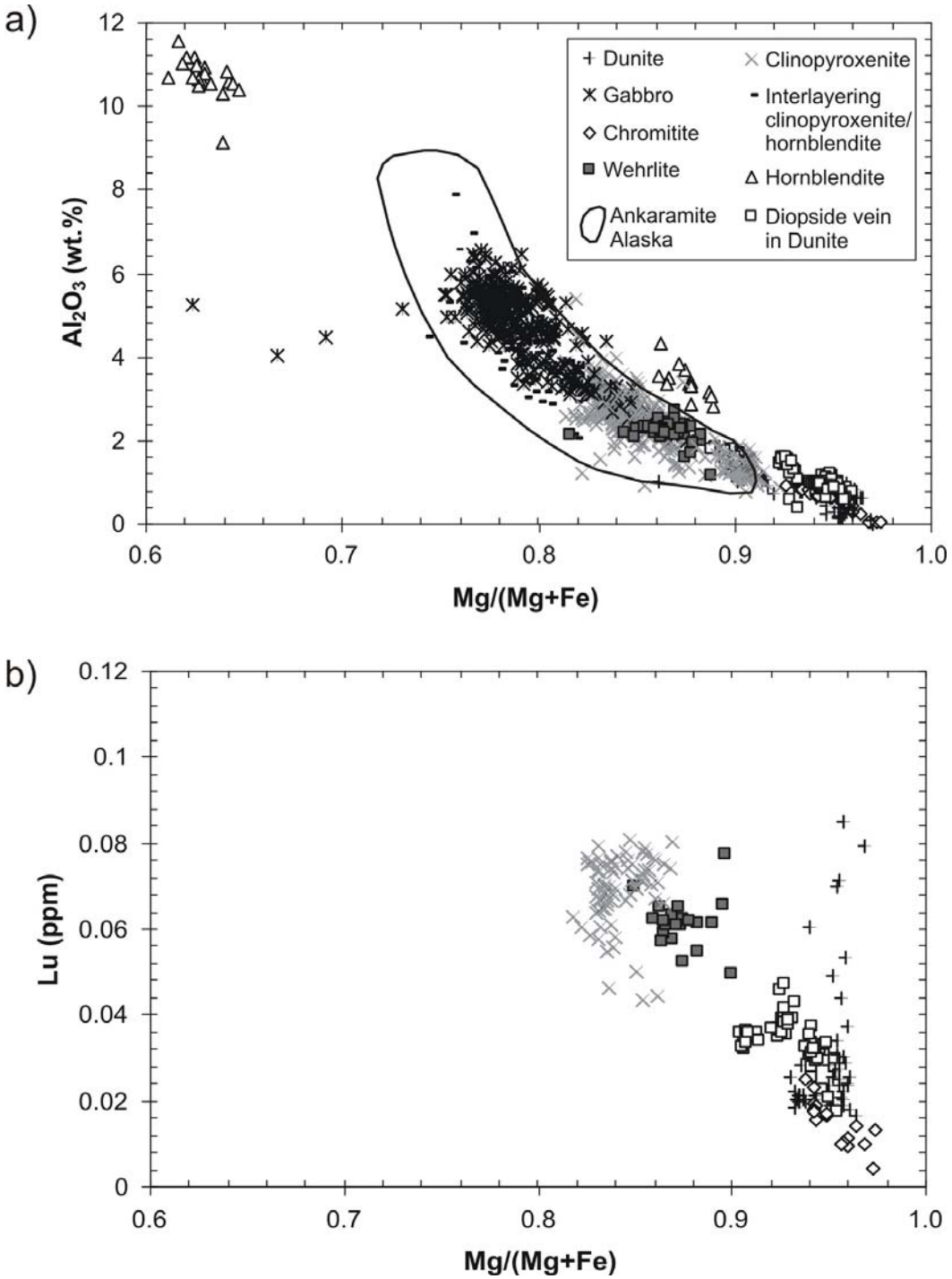

Fig. 7: a) Al_2O_3 content and the Mg/(Mg+Fe) in clinopyroxene from Uralian-Alaskan-type intrusions. Data for Ankaramites are from (Irvine, 1973). The systematic decrease of Mg# and the decrease of Al_2O_3 monitors the evolution of the parental melt. b) Lu content decreases with increasing Mg/(Mg+Fe) in clinopyroxene.

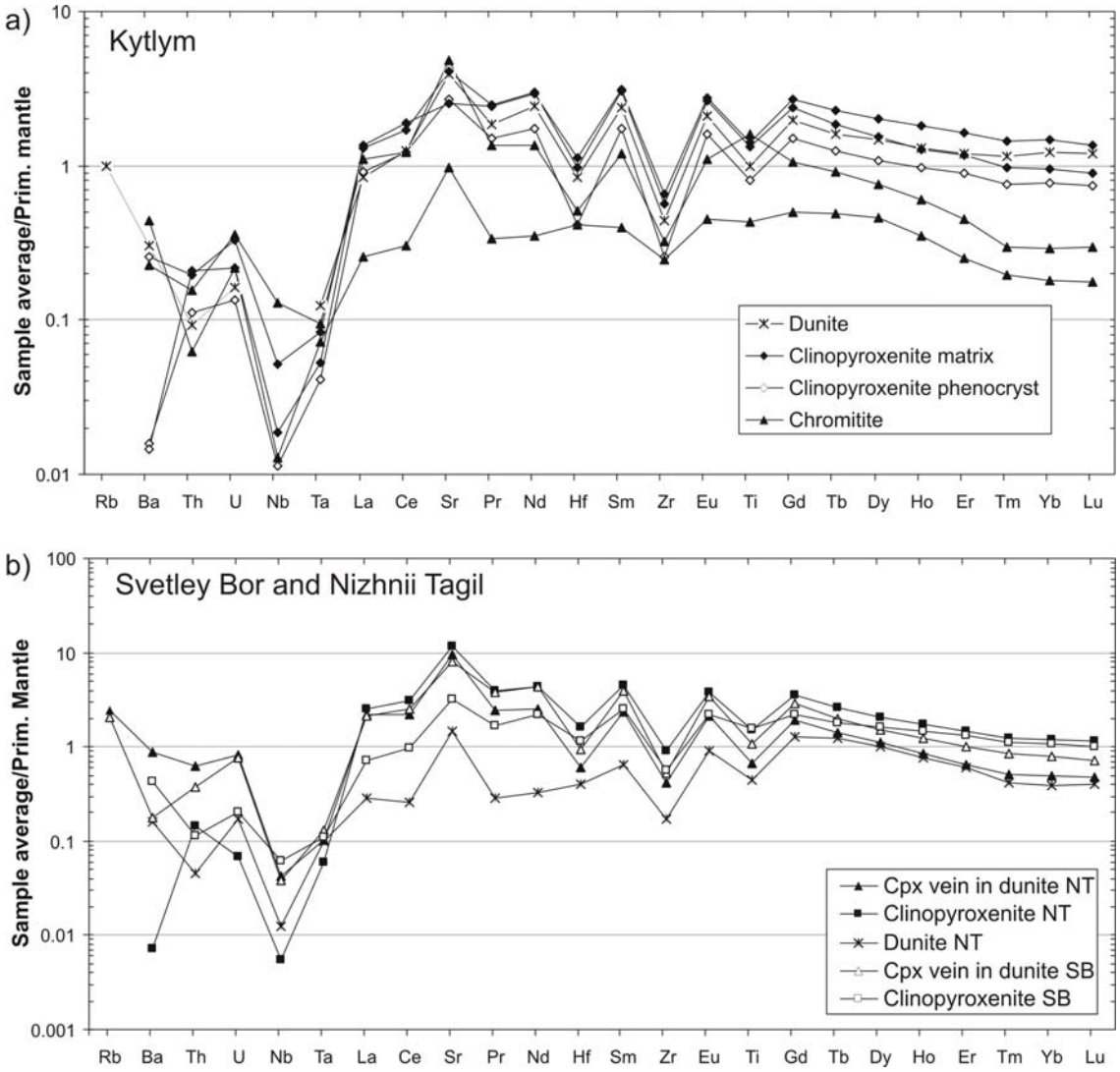

Fig. 8: Average trace element concentrations in diopside for a) Kytlym, b) Svetley Bor (SB) and Nizhnii Tagil (NT). Primitive mantle data are from Hofmann (1988).

The REE patterns (primitive mantle normalized) for all diopside, irrespective of rock type and sample location, have a convex shape with a maximum enrichment of MREE (Fig. 8). However, the concentrations of different grains within a single sample could vary by a factor of 2-6, and the total spread is about one and a half orders of magnitude. All samples show a linear correlation among the middle and heavy REE (Fig. 9a). However, correlations with highly incompatible elements (La) are poor, as demonstrated by variable La/Lu ratios in Fig. 9b.

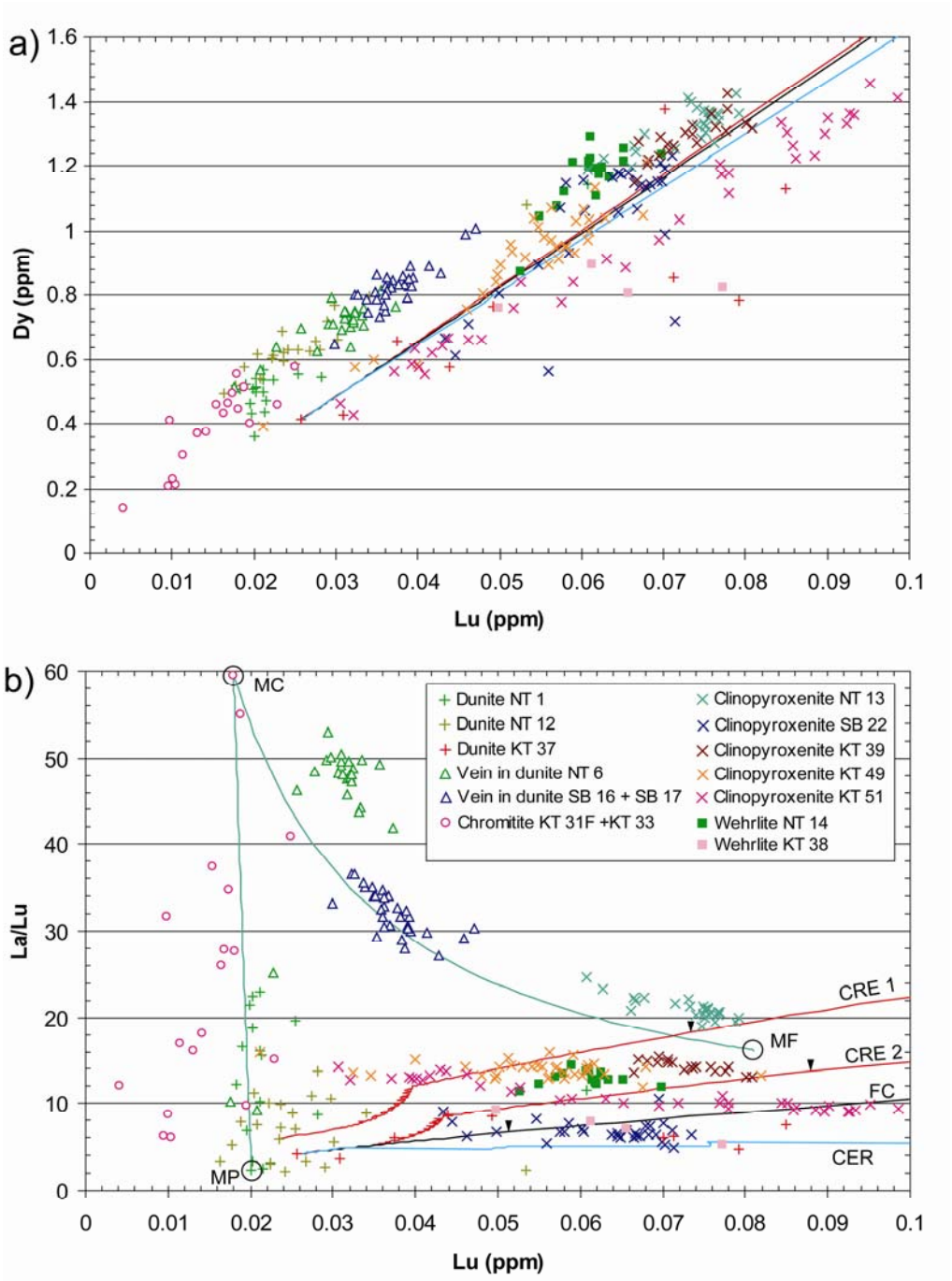

Fig. 9: REE variation in clinopyroxene from dunites, clinopyroxenites and chromitites from Uralian-Alaskan-type complexes in the Urals. These include a) diagram of Lu vs. Dy. b) diagram of Lu vs. La/Lu. Models calculated for two types of periodically tapped and replenished magma chambers are shown.

CER model (blue dotted line): 5 cycles of 40% crystallization, 30% tapping, 30% recharge.

CRE model (red dashed lines): 10 cycles of 40% crystallization, 10%recharged, 10% erupted. The last cycle is followed by fractional crystallization of the residual melt. Tick marks indicate the clinopyroxene composition after 70% fractional crystallization. MC, MF, MP represent end members of mixing lines (green solid lines) which explain the chemical variation in clinopyroxene from chromitite and diopside veins in dunites. For details see text.

Many extended mantle normalized trace element patterns of clinopyroxene run virtually parallel, regardless of the rock type. The lowest trace element concentrations are measured on interstitial grains in dunites, diopside veins crosscutting dunite and in chromitites. The concentrations increase systematically in the clinopyroxenites (Fig. 8). Most of the clinopyroxene grains show positive anomalies for Sr and negative anomalies for Th, U, Nb, Ta, Hf, Zr and Ti (Fig. 8).

4 Discussion

Major element composition and mineralogical observations reveal a successive crystallisation of olivine + chromite forming dunite, olivine + chromite + clinopyroxene forming wehrlite, clinopyroxene + chromian magnetite forming clinopyroxenite and clinopyroxene + spinel + plagioclase + phlogopite ± k- feldspar ± nepheline to forming gabbro. The major element composition and trends in whole rock samples closely follow published data from British Columbia and Canada (Fig. 2) (Wyllie, 1967; Findlay, 1969; Himmelberg and Loney, 1995). The high CaO/Al_2O_3 ratios in all rock types and their alkaline affinity are well established features for all Uralian-Alaskan-type complexes.

Himmelberg and Loney (1995) observed well defined negative correlations between decreasing MgO and the increase of incompatible elements, such as Al_2O_3, in both whole rocks and minerals. Therefore, these authors suggested that MgO and Al_2O_3 represent good tracers of fractionation processes in the parental magmas of Uralian-Alaskan-type complexes in Alaska. However, this study observes remarkably large variations in the spinel composition and the concentrations of incompatible trace elements in clinopyroxene even on the scale of a single thin section. These characteristics cannot simply be primary features. The concentration of an element in minerals as well as the mineral composition in cumulate rocks can potentially be changed by several late processes including modification due to interaction with late interstitial or percolating melts and fluids and subsolidus equilibration with neighbouring grains.

4.1 *Subsolidus equilibration of spinel*

The chemical composition of spinel from the Uralian complexes is similar to those from Uralian-Alaskan type complexes world wide (Fig. 4, 5; Barnes and Roeder, 2001). These complexes are characterized by a complex and multifaceted spinel chemistry.

In a clinopyroxenite (KT 51) from Tilay mountain (Kytlym) and an olivine- and clinopyroxene-rich hornblendite dyke (KT35) intruding the dunite from Kosiva mountain (Kytlym) exsolved spinel can be found (Fig. 4e), which coexist with olivine (Fo_{80}). Spinel in the clinopyroxenite from Tilay mountain (Kytlym) exsolved a picotitic phase at $Al_{65}Cr_{14}Fe^{3+}_{21}$ and a chromian titanomagnetite at $Al_{12}Cr_{21}Fe^{3+}_{67}$ with 2.5 wt.% TiO_2 (Fig. 4e, Tab. 3). Figure 10 shows element maps of two exsolved spinel grains from sample KT35. In the first grain the Al-rich and Fe-Ti-poor spinel phases occur as blebs in a matrix of Al-poor and Fe-rich spinel (Fig. 10a). Both phases do not indicate any zonation. The centre of the other grain from the same sample is zoned and separated by sharp boundaries from the rim of the grain which predominantly consists of an Al- and Mg-rich chromian spinel with low Fe and Ti concentrations (Fig. 10a). This spinel exsolved into a chromian picotite $Al_{57}Cr_{23}Fe^{3+}_{20}$ and a chromian titanomagnetite $Al_{12}Cr_{30}Fe^{3+}_{58}$ with 3-7 wt.% TiO_2. The centre of this grain is zoned, because the Cr content decreases from the core towards the phase boundary. The Cr content is a little higher in the Al-rich spinel (Fig. 10b). On the bais of an area analysis of the element maps, the initial spinel composition is $Al_{29}Cr_{25}Fe^{3+}_{46}$ for the first grain and $Al_{35}Cr_{28}Fe^{3+}_{37}$ for the second grain (Tab. 3). These compositions are very similar but they are enriched in Al_2O_2 and TiO_2 (2.4-4.8 wt.%) compared to unexsolved spinel in the same sample (Fig. 4e). Similar spinel exsolutions have been observed in the Uktus massif, another Uralian- Alaskan- type complex in the Ural (Garuti et al. 2003), and in the Iwanai-dake peridotite complex in Japan (Tamura and Arai 2005).

However, the compositions of the exsolved spinels do not follow the solvus calculated for chromite coexisting at 600°C with an olivine of Fo_{80}, because most of them are too Al-rich (Fig. 4e; Sack and Ghiorso, 1991b). Estimates of solvus curves at higher or lower temperatures do not improve the fit. Chashukhin et al. (2002) demonstrated that the Ti content of spinel strongly influences the temperature estimates and that the commonly used olivine-spinel thermometers underestimate equilibrium temperatures. Thus, the

high content of TiO_2 in this spinel potentially explains the difference between the observed and calculated spinel compositions in Figure 4e.

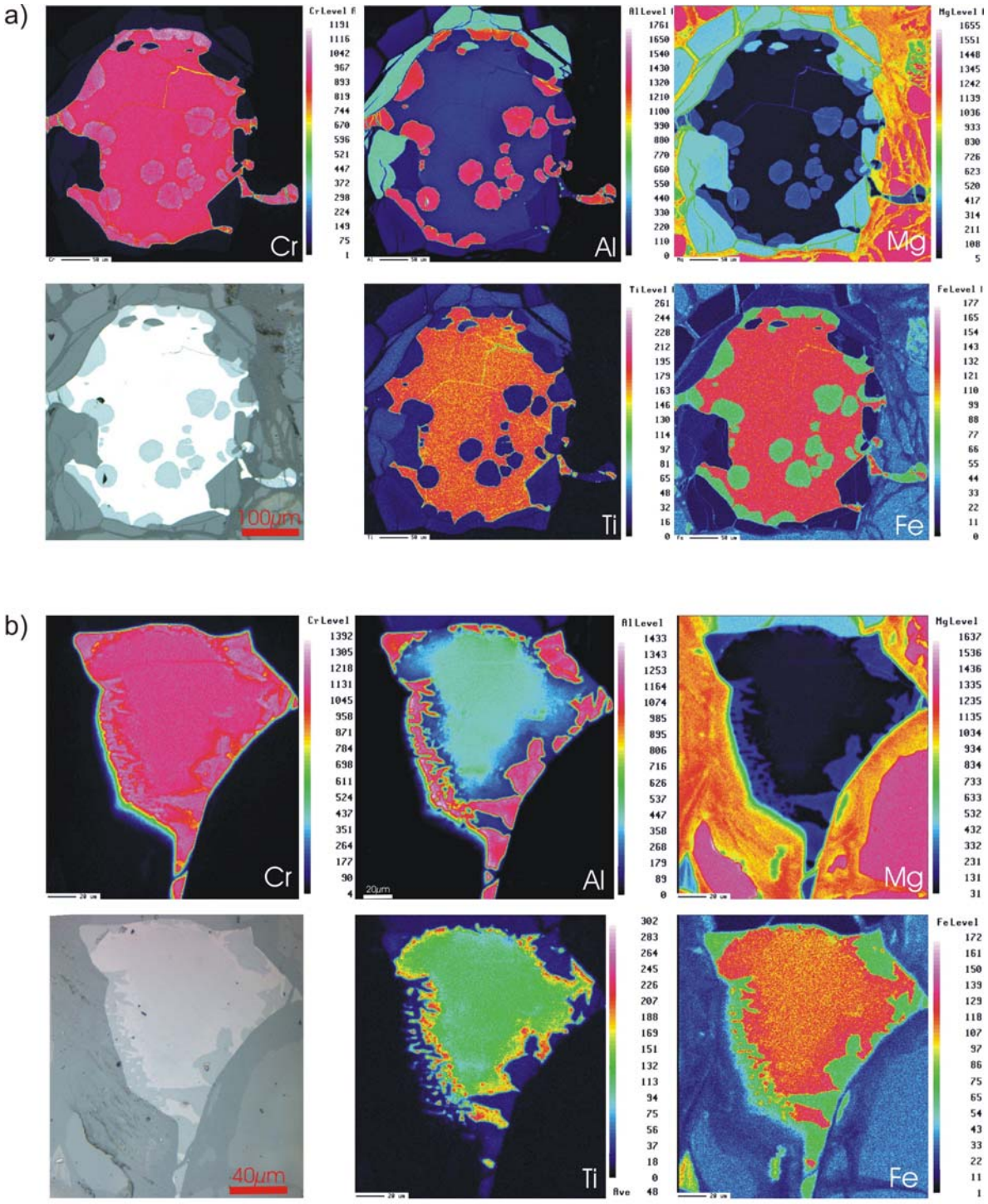

Fig. 10: Element maps for Al, Fe, Mg, Ti, and Cr and the reflected light image of two exsolved spinel grains from an ol-cpx-hornblendite dike crosscutting a dunite (Kytlym complex). (a) shows an entirely equilibrated spinel grain. (b) shows a spinel grain with a zoned core.

The variation seen in group III spinel from dunites can be entirely ascribed to subsolidus reactions (Fig. 4a, b, c). It is partly the result of the expansion of the solvus of ternary spinel towards Cr-Fe^{3+}-rich compositions with decreasing temperature. In addition, some of the Fe-rich spinel (magnetite) probably is an alteration product formed during the serpentinization of the rocks (Fig. 4, 5).

Group II spinel displays a rather unusual evolution from Cr-Al-rich to Al-poor spinel (Fig. 4a, b). In addition, the Al-depletion is accompanied by a coherent increase of Fe^{2+} and Fe^{3+} (Fig. 5). This cannot represent a primary crystallization trend, because this process should produce a decrease in Cr, but not affect Al_2O_3 to any significant degree. Expansion of the ternary spinel solvus towards Fe-Cr-spinel at temperatures below 600°C is also an unlikely explanation. This exsolution would produce a spinel with similar Al_2O_3 contents and not decreasing Al_2O_3 contents as observed here (Sack and Ghiorso, 1991a; Sack and Ghiorso, 1991b). Equilibration with surrounding diopside under subsolidus conditions may influence the composition of chromian spinel. If this is the case, clinopyroxene could gather the Al_2O_3 from the spinel leaving behind Al-poor chromites.

4.2 Olivine and chromian spinel as monitors of the evolution of the parental magma

The compositional variation observed in group I spinel from dunites, where $Fe^{2+}/(Mg+Fe^{2+})$ and Fe^{3+} coherently increase while Cr/(Cr+Al) decreases (Fig. 4, 5), is consistent with the crystallization of Fo-rich olivine and chromian spinel from a MgO-rich melt (Roeder 1994). Interestingly, spinel from different complexes follows different trends due to variable Cr/(Cr+Al). For example accessory spinel and spinel from chromitites from Kytlym have systematically higher Cr/(Cr+Al) than those from Nizhnii Tagil (Fig. 5e, f). The diverse Cr/(Cr+Al) are due to variable Al_2O_3 content in the spinel, and this is probably a fingerprint of the Al_2O_3 content of the parental melt.

Olivine also shows a substantial compositional variation as the Fo-content ranges from 74 to 96 mol% (Fig. 3, Tab. 2). The highest Fo-content ($>Fo_{93}$) occurs in olivine inclusions in chromite (Fig. 3) together with unusually high Cr_2O_3 contents of up to 0.85

wt.%. In dunite-chromite cumulates from layered intrusions and ophiolite complexes and particularly in inclusions of olivine in chromite, the Fo-content increases with increasing proportions of chromite due to subsolidus exchange of Fe-Mg (e.g. Jackson, 1969; Lehmann, 1983; Melcher et al., 1997). A vacancy coupled subsolidus substitution of Cr^{3+} between spinel and olivine could explain the high Cr concentration for olivine inclusions in chromite (Lehmann, 1983). At lower Fo contents (Fo<93), however, the combined decrease in Ni and Fo content in olivine from dunite, clinopyroxenite and gabbro monitors the crystallization of the parental melts.

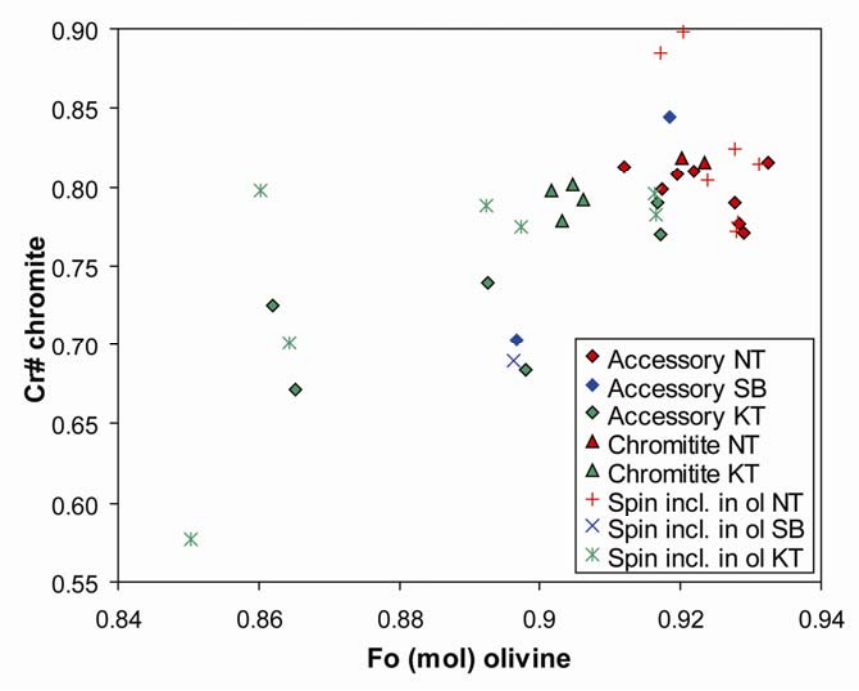

Fig. 11: The mean Fo component in olivine and Cr/(Cr+Al) in spinel monitor the early evolution of the parental magma from the Uralian-Alaskan-type complexes. SB = Svetley Bor, NT = Nizhnii Tagil, KT = Kytlym.

Figure 11 shows the variation of the average forsterite content in olivine and the average Cr/(Cr+Al) for group I spinel in each sample. These samples define a positive correlation as expected during the joint fractional crystallization of olivine and chromite (Roeder, 1994). This variation is narrow in Nizhnii Tagil and restricted to the primitive part of the trend with high Cr/(Cr+Al) in spinel and high Fo contents in olivine (Cr/(Cr+Al)>0.76, $>Fo_{91}$). Dunites from Kytlym show a much larger variation, but the most primitive samples overlap with those from Nizhnii Tagil. The greater heterogeneity at Kytlym

reflects the larger extent of fractional crystallization of the parental magma. The crystallization of spinel with high Cr/(Cr+Al) (~0.80) and low Al_2O_3 contents and MgO-rich olivine (Fo_{92-93}) indicates that the parental magma of the Uralian-Alaskan type complexes was of ultramafic composition with a high MgO (>15 wt.%) and a low Al_2O_3 content.

Spinel in clinopyroxenite, gabbro and hornblende-bearing lithologies has variable Al_2O_3 contents, and is very Ti-Fe-rich, but Cr-poor (Fig. 4d). This has to be anticipated for gabbroic and hornblende-rich rocks considering the evolved nature of their parental melts.

4.3 Clinopyroxene a monitor of the evolution of the parental magma in Uralian-Alaskan-type complexes

One distinctive feature of the parental magma of Uralian-Alaskan-type complexes is the early and prevailing crystallization of clinopyroxene. It is present in all lithologies and, hence, the mineral is an ideal tracer for the evolution of the magma. Indeed the clinopyroxene composition monitors the course of crystallization by its systematic decrease of the Mg/(Mg+Fe) with increasing Al_2O_3, TiO_2, Mn or REE content from dunite, clinopyroxenite, and gabbro towards hornblendite (Fig. 7). The strong decrease of Cr/(Cr+Al) in spinel from clinopyroxenite and gabbro (Tab. 3) can also be attributed to the crystallisation of diopside (Irvine, 1967). Fractional crystallization appears to be the dominant process controlling this chemical variation. However, several observations suggest that a more detailed and complex model is needed in order to explain, in particular, the trace element distribution in the clinopyroxene.

4.3.1 Zonation of clinopyroxene – reaction with interstitial liquid

Clinopyroxene phenocrysts in some clinopyroxenite and gabbro samples (KT51, SB22, KT46) are zoned with regard to major and trace elements (Fig. 12). Although the differences for major elements are rather small, the cores of phenocrysts often have lower Al_2O_3, FeO, and higher SiO_2 contents then their rims (Fig. 12a). However, there are large variations in incompatible trace elements. For example the rim can be enriched

in REE by a factor of 1.5-2.5 compared to the core (Fig. 12b). In contrast concentrations of compatible elements, such as Cr, are higher in the core (Fig. 12a).

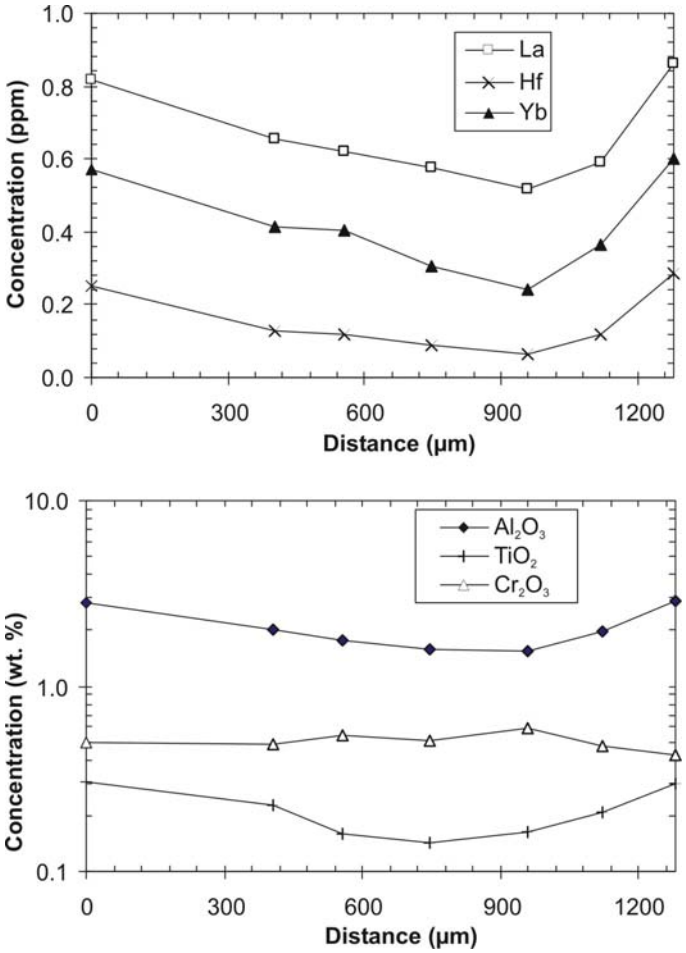

Fig 12: Concentration profiles for a) major and b) trace elements in a diopside phenochryst from clinopyroxenite KT51.

This zonation could reflect a magma mixing process. The crystal core formed in a magma chamber with relatively primitive liquid, rich in Cr but low in Al_2O_3, TiO_2, and REE whereas the rim crystallized after the addition of a more fractionated melt.

Different La/Lu ratios in the core (La/Lu~13) and rim (La/Lu~10) of the phenocrysts from sample KT51 also suggest the existence of two different magmas. Interestingly, the chemical composition of interstitial clinopyroxene is similar to that of the phenocryst-rims (Tab. 4, KT51). This suggests that the interstitial clinopyroxene and the REE-rich clinopyroxene rims crystallized from fractionated residual melt in the pore space of the solidifying cumulate. This process may also explain the large variation of the REE

concentration in clinopyroxene from a single lithology or even a single sample. For example, the Dy and Lu contents in clinopyroxene from dunites or clinopyroxenites can vary by more than a factor of 3 in one thin section (Fig. 9a).

4.3.2 Clinopyroxene as monitor of the evolution of the parental magma

Presuming simple fractional crystallization the increased enrichment in REE concentrations in clinopyroxene from dunites compared to clinopyroxene from clinopyroxenites necessitates the parental magma to have been already more than 70% crystallized (F.C. in Fig. 9b). Such high degrees of crystallization are unrealistic. Even a crystal mush containing just 50% crystals would essentially behave like a solid due its high viscosity, and crystal separation would not be possible. Fractional crystallization of clinopyroxene also cannot explain the large fractionation of LREE from HREE that we observe overall in clinopyroxene from dunites and clinopyroxenites (La/Lu: 2-23; Fig. 9; Tab. 4). A pronounced enrichment and fractionation of REE can be achieved in a crystallizing and periodically tapped and replenished magma chamber (Shaw, 2006). Concentrations of compatible elements would become buffered at a certain level in such an open system magma chamber, due to the replenishment of more primitive magma (Shaw, 2006). This could explain the rather low and constant NiO content in the MgO-rich olivine (Fo>86; NiO ~0.15 wt.%) from most dunites if compared to the trend defined by mantle-derived magmas (Fig. 3).

Two model calculations in Figure 9b show the REE evolution of crystallizing clinopyroxene during such a process. The replenishing magma is assumed to have the same composition as the initial magma. In order to maximize the fractionation of LREE and HREE clinopyroxene is the only crystallizing phase (clinopyroxene/liquid partition coefficients are from Ionov et al. (1997).

In the one model (CER), 40% fractional crystallization is first followed by erupting 30% of the mass and the residual melt is mixed with the replenishing melt (30 % of the initial magma mass). In the second model (CRE1, CER2) the cycle also starts with 40 percent of fractional crystallization. However, the residual liquid is replenished with 10 % of the initial magma mass. Subsequently both magmas are mixed and 10 % of the mass is

erupted. The difference between these models is that CER is dominated by replenishment of the magma, whereas CRE is controlled by the crystallization process. The CER model is characterized by a strong increase in the incompatible elements but little fractionation in the La/Lu ratio (Fig. 9b). Such a magma chamber system could explain the large Lu increase in some dunites and clinopyroxenites (SB22, KT37). However, most samples from Kytlym and Nizhnii Tagil display an increase in La/Lu as crystallization proceeds from dunite to clinopyroxenite (Fig. 9b). This is reflected in the CRE chamber in which cumulates display a continuous increase in REE accompanied by an enrichment of LREE relative to HREE (Fig. 9b). However, even such a model cannot explain the overall La/Lu variation in the dunite and clinopyroxenite cumulates of Kytlym. This necessitates the presence of parental magmas with different La/Lu ratios (model CRE1 and CRE2 in Fig. 9b).

It is appreciated that the proposed models are rather simplistic and represent only a few solutions out of numerous possibilities. The calculations can be tuned by adjusting the amount of fractional crystallization in between replenishment events and/or the amount of removed/added magma in order to better model specific details of the relationship between samples as well as between different intrusions. In fact it is reasonable to assume that during the life time of a magma chamber both CER and CRE processes will occur. This would explain most of the chemical variations we observe in the clinopyroxene.

An alternative explanation for the variable La/Lu ratios could be that parental magmas from different intrusions formed by variable degrees of partial melting. However, given that the magmas are MgO-rich (MgO>15 wt.%), the degree of partial melting would be rather high (>10%), and hence, a strong fractionation of HREE from LREE is unlikely. Other possibilities would then have to be invoked, such as heterogeneous mantle sources variably enriched in highly incompatible elements or contamination of the parental magma with continental crust. Evaluation of such hypothesis is beyond the scope of this study.

4.4 Implications for the formation of the chromitites

Chromitites occur as massive, but isolated lenses or schlieren in the dunites. The composition of the spinel in the dunite mirrors that in the chromitites. For example, the difference in Cr/(Cr+Al) observed between accessory spinel from dunites in Kytlym and Nizhnii Tagil is conserved in the associated chromitites (Fig. 11). This indicates that the formation of chromitites is due to the mobilization and re-precipitation of Cr in the dunite, probably during the final stages of crystallization. Recent studies comparing spinel compositions in chromitite with those in dunite and analyzing platinum-group minerals suggested that the chromitites formed by the interaction of a fluid with the dunite at temperatures of about 800-900°C (Chashukhin et al., 2002; Garuti et al., 1997; Garuti et al., 2003).

One intriguing observation is the extreme variation in the La/Lu ratio at rather low Lu concentrations in diopside from chromitites (KT31F, KT33; Fig. 9b). The diopside is strongly enriched in LREE compared to MREE and HREE resulting e.g. in high La/Lu of 20-60 compared to 5-15 in diopside from dunite and clinopyroxenite. Likewise, MREE are enriched relative to HREE (Fig. 9a). Some interstitial diopside from dunite samples close to chromitites (NT1, NT12) follow the same trends in Figure 9. This suggests that the process, which formed the chromitite also crystallized or re-equilibrated the interstitial diopside in the neighbouring dunite.

The high La/Lu ratio at low and rather constant Lu concentrations cannot be explained by any crystallization process. Rather the steep trend built up by clinopyroxene from the chromitites and some dunites indicates a mixing relationship (MP-MC, Fig. 9b). One end member is represented by diopside with low REE contents and low La/Lu ratios. Its trace element pattern is similar to clinopyroxene which crystallized from the MgO-rich parental melt (Fig. 9b). The second end member is characterized by similar Lu concentrations but it has a La/Lu ratio greater than or equal to 60 (Fig. 9b). The origin of this component is enigmatic. Its chemical features are not preserved in any other rock type and there appears to be no reasonable igneous hypothesis relating its composition to the parental melt or even to that of extreme fractionation products in interstitial spaces. However, one might speculate that it represents a hydrous fluid enriched in LREE which developed during the final crystallization of the pore liquid.

Diopside from clinopyroxenite veins in dunite (NT6, SB16, SB17) also have high La/Lu ratios comparable to those from chromitites. Again, clinopyroxene within a single sample displays variable La/Lu ratios and, typically, they define non-linear trends between La/Lu and Lu concentrations. This can also be observed in some clinopyroxenites (e.g. sample NT13, Fig. 9b). Such trends are characteristic of mixing relationships. This diopside can then be interpreted to represent the crystallization product from a mixture of the LREE-enriched “fluid” component (MC) and a fractionation product, maybe the residual interstitial liquid, of the parental ultramafic melt (MF, Fig. 9b). Therefore, we believe that there is a close genetic relationship between the diopside veins in dunite and the chromitites. These observations strengthen our earlier suggestion that the formation of the chromitites is a late stage magmatic process and thus an integral part of the evolution of the parental magma forming Uralian-Alaskan-type complexes.

4.5 Trace element composition of the parental melt

Trace element abundances for the parental melt were calculated by dividing the average trace element content of the clinopyroxene in each sample by the diopside/liquid partition coefficient given by Ionov et al. (1997). Figure 13 shows that trace element patterns for the parental melts are parallel regardless from which of the different main lithologies or even complexes they are calculated. The dunites from Kytlym (KT37) and Nizhnii Tagil (NT1) are derived from the most primitive parental melts having rather low REE concentrations of 1-10 times primitive mantle. The trace element concentrations in the parental melts systematically increase with increasing incompatibility but they also show pronounced negative anomalies for the HFSE.

The similarity of the trace elements in concentrations and patterns in all studied complexes implies that they were derived from parental melts with similar compositions and that these melts formed in source materials with similar trace element characteristics.

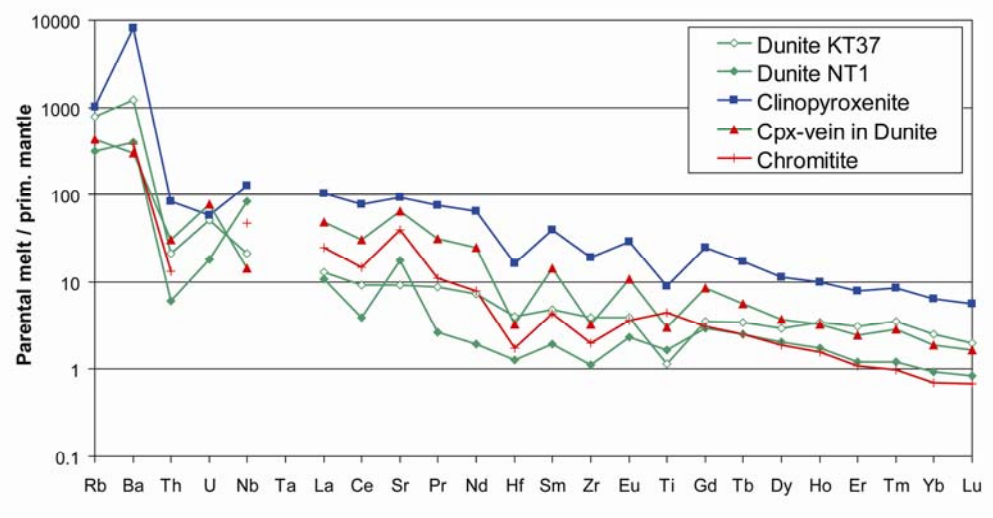

Fig. 13: Parental melt compositions calculated from trace element abundances in clinopyroxene. Partition coefficients are from Ionov et al. (1997).

4.6 Geotectonic setting

From major and trace element variations in minerals and whole rocks, a subduction related island arc setting has been assumed for the Uralian Platinum belt (Ivanov and Shmelev, 1996; Chashukhin et al., 2002; Garuti et al., 2003) and for other belts of Uralian-Alaskan-type intrusions in Alaska/British Columbia and Kamchatka (e.g. Himmelberg and Loney, 1995; Batanova el al., 2005)

The trace element composition of the parental melts from the Uralian complexes are characterized by positive Sr and negative anomalies of the HFSE (Fig. 13). This supports the idea that these rocks have a subduction related origin. Clinopyroxene compositions can also be used to discriminate between different geotectonic settings. Figure 14 shows the percentage of tetrahedral sites occupied by Al vs. the TiO_2 content (Loucks, 1990). Our data are in good agreement with clinopyroxene compositions from other occurrences in the Ural Mountains and with Uralian-Alaskan-type complexes world wide. They clearly follow the trend defined by volcanic rocks and cumulates from island arc magmas (Loucks, 1990; Himmelberg and Loney, 1995) which is significantly steeper than that observed for plutonic and volcanic rocks related to continental rifts or large igneous provinces. At low Al^{IV} and TiO_2 concentrations, the island-arc and MORB-trends are similar. However the enriched trace element pattern in the parental magma from the Ural Mountains clearly distinguishes them from MORB-magmas.

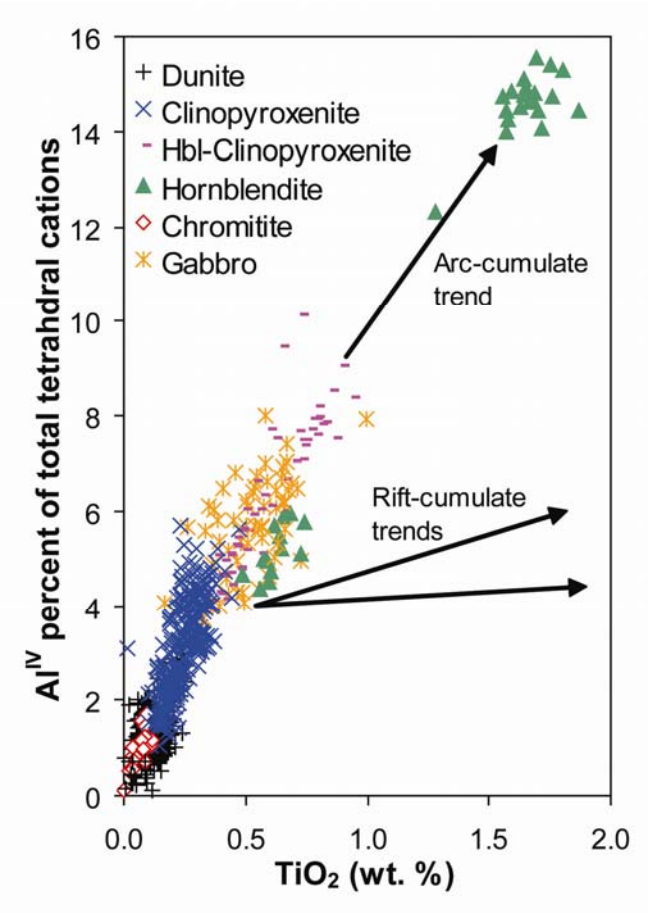

Fig. 14: Al^{IV} (in percent of total tetrahedral cations) vs. TiO_2 content in clinopyroxene. Trends are shown for cumulates and volcanic rocks from different tectonic settings. Data is from Loucks (1990).

4.7 Parental magmas of Uralian-Alaskan-type complexes: Comparison with Ankaramites

The trace element composition for melts determined in this study is similar to that calculated by Batanova et al. (2005) using melt inclusion data from the Galmoenan Uralian- Alaskan- type complex in Kamchatka. The coincidence with whole rock data from zoned mafic-ultramafic complexes in Alaska and British Columbia (Himmelberg and Loney, 1995), indicates that this class of intrusions formed under similar physico-chemical conditions and in mantle sources with comparable compositional fingerprints. However, the petrological affiliation of Uralian-Alaskan-type complexes to specific mantle-derived melts is not well established.

Irvine (1973) proposed that there is a genetic relationship between ankaramitic dykes in British Columbia and the ultramafic Uralian-Alaskan-type intrusions of the Cordillera of Alaska and British Columbia. Ankaramites are known from different geotectonic settings e.g. ocean islands (Frey et al., 1991; Tronnes et al., 1999; Woodhead, 1996) and island-arcs (Mossman et al., 2000; Barsdell and Smith, 1989; Barsdell, 1988; Thirwall et al., 1994). They represent a class of clinopyroxene-rich, mafic-ultramafic volcanic rocks that share many chemical and mineralogical features with Uralian-Alaskan-type mafic to ultramafic intrusions. These volcanic rocks are characterized by the early crystallization of olivine, spinel and clinopyroxene. Therefore, the subvolcanic emplacement and crystallization of such melts should result in the formation of dunitic, wehrlitic and clinopyroxenic cumulates containing accessory spinel, as observed in Uralian-Alaskan-type intrusions.

The chemical composition of chromian spinel phenocrysts in ankaramites from different localities (Vanuatu Arc, Pacific Ocean, Greenhills complex, New Zealand, Cameroon) (Mossman et al., 2000; Nono et al., 1994; Barsdell and Smith, 1989; Barsdell, 1988) is similar to that for spinel from the studied complexes in the Ural Mountains (Fig. 4f). Some ankaramites appear to be derived from more primitive melts as their spinel is richer in Cr than observed for the Uralian complexes.

Trace element patterns from subduction-related ankaramites from Vanuatu in the Pacific Ocean (Barsdell, 1988) and the Lesser Antilles (Thirwall et al., 1994) are in good agreement with our calculated melt compositions (Fig. 15). They share the negative anomalies for Hf, Zr and Ti, the positive Sr anomaly, and the LREE-enrichment relative to the HREE.

These features are also observed in ankaramites intruding the Nurali Massive, which is located close to the Uralian-Alaskan-type complexes in the Tagil-Magnitogorsk zone (Spadea et al., 2002). These authors suggested that they are related to island arc magmatism in the Magnitogorsk arc. Age, geochemical and spatial relationships may even imply a genetic link between these ankaramites and the Uralian-Alaskan-type complexes of the UPB. Hence in summarizing these observations we agree with the suggestion by Irvine (1973) that ankaramites could represent the parental magmas of Uralian-Alaskan-type complexes.

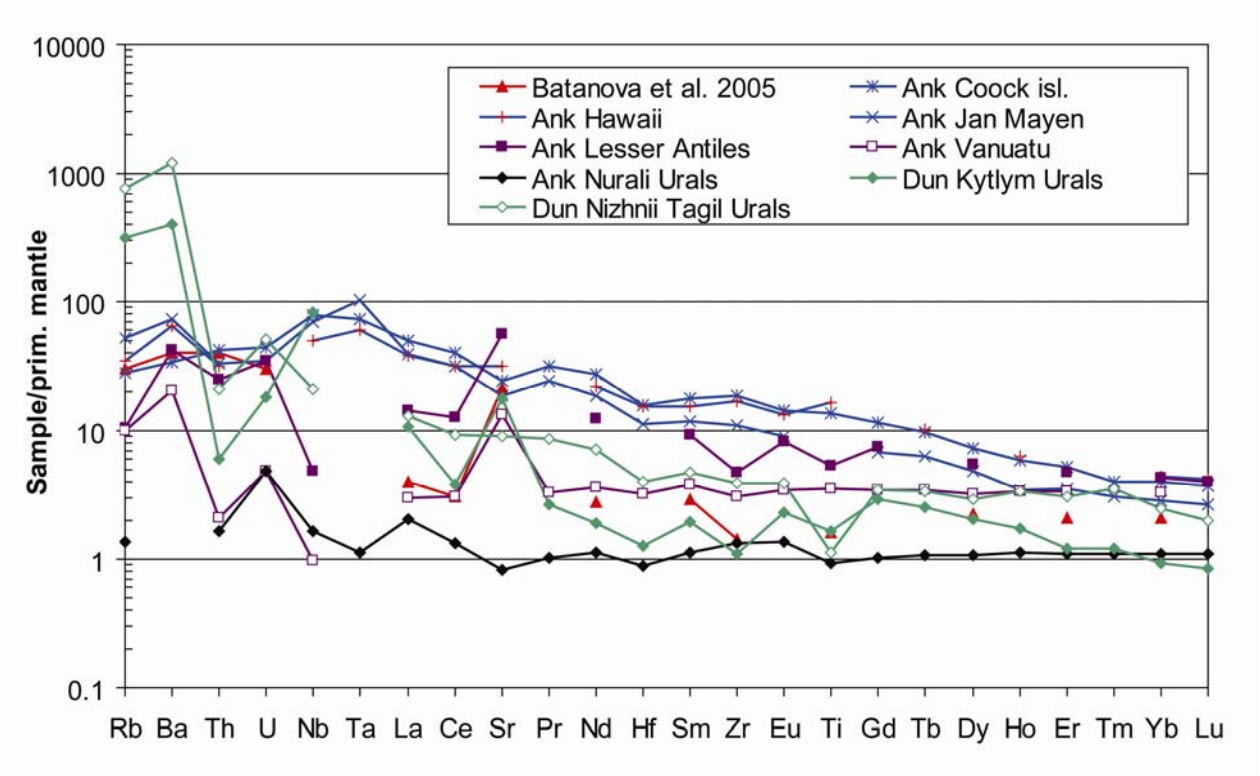

Fig. 15: Comparison of trace element abundances in Ankaramites (Ank) from different locations compared with those from the parental melt as proposed by Batanova et al. (2005) and calculated in this study from clinopyroxene from the most primitive dunite (Dun) in Nizhnii Tagil and Kytlym. For references see text.

5 Conclusions

This study describes Uralian-Alaskan-type complexes from the Ural Platinum Belt in the Ural Mountains. It constrains the composition of the parental magma by monitoring the evolution of the complexes using mainly major and trace element abundances of spinel, olvine and clinopyroxene.

The complexes in the Ural Mountains share many distinct structural, petrological and geochemical features described from other examples world wide. The Uralian complexes are interpreted to represent cumulates from an ankaramitic ultramafic melt which successively crystallized olivine + chromite, olivine + chromite + clinopyroxene, clinopyroxene + chromian magnetite, and eventually clinopyroxene + spinel + plagioclase + phlogopite ± K- feldspar ± nepheline resulting in dunites, wehrlites, clinopyroxenites and gabbros, respectively.

The early stages of crystallization are monitored by a decreasing Fo content in the olivine and a decreasing Cr/(Cr+Al) in the coexisting chromite. The high Fo content of olivine (Fo>90) and the high Cr/(Cr+Al) in the spinel (Cr/(Cr+Al)~080) imply a parental magma rich in MgO (>15 wt.%) but poor in Al_2O_3. The positive anomaly in Sr, negative anomalies in HFSE, and the high ratio of the tetrahedrally coordinated Al to the TiO_2 content in clinopyroxene indicate that these rocks crystallized from magmas forming at destructive plate margins. Irvine (1973) proposed a genetic relationship between Uralian-Alaskan-type complexes and ankaramites. The good agreement between the major and trace element composition of accessory and rock forming minerals from Uralian-Alaskan-type complexes in the Urals with those of subduction-related ankaramites from different localities world wide support Irvine's suggestion.

Nevertheless, the compositions of minerals in different complexes from the Ural Mountains display small but significant differences in the parental melt compositions. For example, spinel and olivine from Kytlym tend to be more Al_2O_3 and fayalite rich, respectively, than those from Nizhnii Tagil. In addition, clinopyroxene from different complexes and lithologies could display large variations in their LREE/HREE ratios. Different stages of evolution of the parental magma at the time of emplacement can explain these differences. However, this could also be due to crustal contamination processes, or caused by different degrees of partial melting in a heterogeneous mantle source.

The dominance of dunite and clinopyroxenite in the complexes necessitates an extensive and prolonged crystallization of olivine and clinopyroxene. This could be achieved during the crystallization of a continuously erupted and replenished magma chamber. Such a model is also required in order to explain the strong enrichment of incompatible trace elements as the crystallization of olivine and clinopyroxene proceeds.

Clinopyroxenites and gabbros have zoned clinopyroxene phenocrysts which probably indicate magmatic reactions between a high-temperature clinopyroxene and a crystallizing interstitial liquid during the later stages of the evolution of the cumulate pile. The local replacement of clinopyroxene with hornblende in the clinopyroxenites from Svetley Bor also demonstrates the presence of a hydrous melt or fluid during the final stages of solidification.

Diopside from chromitites and cross cutting diopside veins in dunite share similar trace element patterns with LREE/HREE ratios higher than those in diopside from all other lithologies. It implies the involvement of a fluid or melt during the formation of the chromitites, which is more enriched in highly incompatible elements than the parental magma. The chromitites likely formed at high temperatures (800-900°C) during the waning stages of crystallization. However, there is little information on the mechanism responsible for the mobilization of Cr and PGE in the dunites or their ultimate concentration in the chromitite lenses.

Ongoing investigations of the Os isotope systematics and the distribution of the platinum group elements would provide additional constraints on the formation of the PGE-rich chromitite bodies. It could also strengthen the proposed genetic relationships between the different lithologies as well as between ankaramites and Uralian-Alaskan-type complexes.

Acknowledgement

We thank N. Groschopf, K Herwig, B. Stoll and B. Schulz-Dobrick for assistance during the LA-ICPMS and Microprobe analyses. D. Harlov and an anonymous reviewer are thanked for their helpful suggestions that significantly improved the manuscript. This Study was funded by grant GK392 of the Graduiertenkolleg 'Stoffbestand und Entwicklung von Kruste und Mantel' at the University of Mainz to J. Krause.

References

Barnes, S.J., Roeder, P.L., 2001. The range of spinel compositions in terrestrial mafic and ultramafic rocks. Journal of Petrology, 42 (12), 2279-2302.

Barsdell, M., 1989. Petrology and petrogenesis of Clinopyroxene-rich tholeiitic lavas, Merelava volcano, Vanuatu. Journal of Petrology, 29 (5), 927-964.

Barsdell, M., Smith, I.E.M., 1989. Petrology of recrystallized ultramafic xenoliths from Merelava volcano, Vanuatu. Contributions to Mineralogy and Petrology, 102, 230-241.

Batanova, V.G., Astrakhantsev, O.V., 1992. Tectonic position and origins of the zoned mafic-ultramafic plutons in the Northern Olyutor Zone, Koryak Highlands. Geotectonics 26 (2), 153-165.

Batanova, V.G., Astrakhantsev, O.V., 1994. Island-arc mafic-ultramafic plutonic complexes of northern Kamchatka. In: Ishiwatari, A., Malpas, J., Ishizuka, H., (eds.) Proceedings of the 29th International Geological Congress, Part D, Circum-Pacific-ophiolites VSP, 129-143.

Batanova, V.G., Pertsev, A.N., Kamenetsky, V.S., Ariskin, A.A., Mochalov, A.G., Sobolev, A.V., 2005. Crustal evolution of island-arc ultramafic magma: Galmoenan pyroxenites-dunite plutonic complex, Koryak Highland (Far East Russia). Journal of Petrology, 46, 1345-1366.

Bédard, J. H., 2001. Parental magmas of the Nain Plutonic Suite anorthosites and mafic cumulates: a trace element modelling approach. Contributions to Mineralogy and Petrology, 141, 747-771.

Chashchukhin, I.S., Votyakov, S.L., Pushkarev, E.V., Anikina, E., 2002. Oxithermobarometry of ultramafic rocks from the Ural Platinum Belt. Geochemistry International, 40 (8), 762-778.

Clark, T., 1980. Petrology of the Turnagain ultramafic complex, northwestern British Columbia. Canadian Journal of Earth Sciences, 17, 744-757.

Cookenboo, H.O., Bustin, R.M., Wilks, K.R., 1997. Detrial chromian spinel compositions used to reconstruct the tectonic setting or provenance: Implications for orogeny in the Canadian Cordillera. Journal of Sedimentary Research, 67 (1), 116-123.

Findlay, D.C., 1969. Origin of the Tulameen ultramafic-gabbro complex, southern British Columbia. Canadian Journal of Earth Sciences 6, 399-425.

Frey, F.A., Garcia, M.O., Wise, W.S., Kennedy, A.K., Gurriet, P., Albarède, F., 1991. The evolution of Mauna Kea volcano, Hawaii: Petrogenesis of tholeiitic and alkalic basalts. Journal of Geopysical Research, B96, 14347-14375.

Garuti, G., Fershtater, G., Bea, F., Montero, P., Pushkarev, E.V., Zaccarini, F., 1997. Platinum-group elements as petrological indicators in mafic-ultramafic intrusions

of the central and southern Urals: preliminary results. Tectonophysics, 276, 181-194.

Garuti, G., Pushkarev, E.V., Zaccarini, F., Cabella, R., Anikina, E., 2003. Chromite composition and platinum-group mineral assemblage in the Uktus Uralian-Alaskan-type complex (Central Urals, Russia). Mineralium Deposita, 38, 312-326.

Hart, S.R., Dunn, T. 1993. Experimental cpx/melt partitioning of 24 trace elements. Contributions to Mineralogy and Petrology, 113, 1-8.

Hill, R., Roeder, P., 1974. The crystallization of spinel from basaltic liquid as a function of oxygen fugacity. Journal of Geology, 82, 709-729.

Himmelberg, R.G., Loney, R.A., 1995. Characteristics and petrogenesis of Alaskan-Type ultramafic-mafic intrusions, southeastern Alaska. US Geological Survey Professional Papers 1564, 1-47.

Himmelberg, R.G., Loney, R.A., Craig, J.T., 1986. Petrogenesis of the ultramafic complex at the Blashke Islands, southeastern Alaska. US Geological Survey Bulletin 1662, 1-14.

Hofmann, A.W., 1988. Chemical differentiation on the earth: The relationship between mantle, continental crust, and oceanic crust. Earth and Planetary Science Letters, 90, 297-314.

Ionov, D.A., Bodinier, J.-L., Mukasa, S.B., Zanetti, A., 2002. Mechanisms and sources of mantle metasomatism: Major and trace element compositions of peridotite xenoliths from Spitzbergen in the context of numerical modelling. Journal of Petrology, 43 (12), 2219-2259.

Ionov, D.A., Griffin, W.L., O`Reilly, S.Y., 1997. Volatile-bearing minerals and lithophile trace elements in the upper mantle. Chemical Geology, 141, 153-184.

Irvine, T.N., 1967. Chromian spinel as a petrogenetic indicator; Part 2, Petrologic applications. Canadian Journal of Earth Sciences, 7, 71-103.

Irvine, T.N., 1973. Bridget Cove volcanics, Juneau Area, Alaska : Possible parental magma of Alaskan-type ultramafic complexes. Carnegie Institution Washington Yearbook, 72, 478-491.

Ivanov, K.S., Shmelev, V.R., 1996. Urals Platinum Belt – Magamtic trace of an early Paleozoic subduction zone. Dokl. Ross. Akad. Nauk., 347 (5), 649-652.

Jackson, E.D., 1969. Chemical variation in coexisting chromite and olivine in chromitite zones of the Stillwater Complex. In: Wilson, H.D.B., (ed) Magmatic ore deposits a symposium, Economic Geology, Monograph 4, 41-71

Jochum, K.P., Stoll, B., Herwig, K., Amini, M. submitted. Trace element and isotope analysis of geo- and cosmochemical samples by laser ablation sector field ICPMS. In: Douthitt, C.B. (ed.). High resolution ICP-MS,

Lee, Y.L., 1999. Geotectonic significance of detrial chromian spinel: a review. Geosciences Journal, 3 (1), 23-29.

Lehmann, J., 1983. Diffusion between olivine and spinel: application to geothermometry. Earth and Planetary Science Letters, 64, 123-138.

Loucks, R.B., 1990. Discrimination of ophiolitic from nonophiolitic ultramafic-mafic allochthons in orogenic belts by the Al/Ti ratio in Clinopyroxene. Geology, 18, 346-349.

McKenzie, D., O`Nions, R.K., 1991. Partial melt distributions from inversion of rare earth element concentrations. Journal of Petrology, 32 (5), 1021-1091.

Melcher, F., Grum, W., Simon, G., Thalhammer, T., Stumpfl, E., 1997. Petrogenesis of the ophiolitic giant chromitite deposits of Kempirsai, Kazahkstan: a study of solid and fluid inclusions in chromite. Journal of Petrology, 40 (10), 1419-1458.

Mossman, D.J., Coombs, D.S., Kawachi, Y., Reay, A., 2000. High-Mg Arc-ankaramitic dikes, Greenhills complex, Southland, New Zealand. The Canadian Mineralogist, 38, 191-216.

Nixon, G.T., Hammack, J.L., Connelly, J.N., Case, G., Paterson, W.P.E., 1990. Geology and noble metal geochemistry of the Polaris ultramafic complex, north-central British Columbia In: Geologic fieldwork 1989: British Columbia Ministry of Energy, Mines and Petroleum resources, 1988 (1), 307-404.

Noble, J.A., Taylor, H.P., 1960. Correlation of the ultramafic complexes of southeastern Alaska with those of North America and the World. 21st International Geological Congress in Copenhagen 1960, Report part 13, 188-197.

Nono, A., Déruelle, B., Demaiffe, D., Kambou, R., 1994. Journal of Volcanology and Geothermal Research, 60, 147-178.

Roeder, P.L., 1994. Chromite: From the fiery rain of chondrules to the Kilauea Iki lava lake. The Canadian Mineralogist, 32, 729-746.

Sack, R.O., Ghiorso, M.S., 1991a. Chromite as a petrogenetic indicator. In: Lindsley (ed.). Oxide minerals petrogenetic and magnetic significance, Reviews in Mineralogy, 25, 323-353.

Sack, R.O., Ghiorso, M.S., 1991b. Chromian spinel as petrogenetic indicators: Thermodynamics and petrological applications. American Mineralogist, 76, 827-847.

Savelieva, G.N., Sharaskin, A.Y., Saveliev, A.A., Spadea, P., Pertsev, A.N., Babarina, I.I., 2002. Ophiolites and zoned mafic-ultramafic massifs of the Urals: A comparative analysis and some tectonic implications. In: Browen, D., Juhlin, C., Puchkov, V. (eds.). Mountain building in the Uralides: Pangea to the present. Geophysical Monograph 132, 135-153.

Savelieva, G.N., Pertsev, A.N., Astrakhantsev, O.V., Denisova, E.A., Boudier, F., Bosch, D., Puchkova, A.V., 1999. Kytlym pluton, north Urals: Structure and emplacement history. Geotectonics, 33 (2), 119-142.

Shaw, D.M., 2006. Trace elements in magmas A theoretical treatment. Cambridge University Press. 1-243.

Spadea, P., D'Antonio, M., Kosarev, A., Gorozhanina, Y., Brown, D., 2002. Arc-continent collision in the southern Urals: Petrogenetic aspects of the forearc-arc complex. In: Browen, D., Juhlin, C., Puchkov, V. (eds.). Mountainbuilding in the Uralides: Pangea to the present. Geophysical Monograph 132, 101-134.

Tamura, A., Arai, S., 2005. Unmixed spinel in chromitite from the Iwanai-Dake peridotite complex, Hokkaido, Japan: A reaction between peridotite and highly oxidized magma in the mantle wedge. American Mineralogist, 90, 473-480.

Taylor, H.P., 1967. The zoned ultramafic complexes of souteastern Alaska, part 4.III. In: Wyllie, P. J., (ed.) Ultramafic and related rocks. New York John Wiley, 96-118.

Taylor, H.P., Noble, J.A., 1960. Origin of the ultramafic complexes in southeastern Alaska. 21st International Geological Congress in Copenhagen 1960, Report part 13, 175-187.

Thirlwall, M.F., Smith, T.E., Graham, A.M., Theodorou, N., Hollings, P., Davidson, J.P., Arculus, R.J. 1994. High field strength element anomalies in arc lavas: Source or process? Journal of Petrology, 35, 819-838.

Tronnes, R.G., Planke, S., Sundvoll, B., Imsland, P., 1999. Recent volcanic rocks from Jan Mayen: Low-degree melt fractions of enriched notheast Atlantic mantle. Journal of Geophysical Research, 104 (B4), 7153-7168.

Van der Veen, A.H., Maaskant, P., 1995. Chromian spinel mineralogy of the Staré Ransko gabbro-peridotite, Czech Republic, and its implications for sulfide mineralization. Mineralium Deposita, 30, 397-407.

Woodhead, J.D., 1996. Extreme HIMU in an oceanic setting: The geochemistry of Mangaia Island (Polynesia), and temporal evolution of the Cook-Austral Hot Spot. Journal of Volcanology and Geothermal Research, 72, 1-19.

Wyllie, P. J., 1967. Ultramafic and related rocks. New York John Wiley, 1-464.

Zhou, M.-F., Lightfoot, P.C., Keays, R.R., Moore, M.L., Morrison, G.G., 1997. Petrogenetic significance of chromian spinels from the Sudbury Igneous Complex, Ontario, Canada. Canadian Journal of Earth Sciences, 34, 1405-1419.

Chapter 2

Evolution of mafic rocks of Uralian-Alaskan-type Complexes: Implications for Subduction Zone Magmatism

Joachim Krause, Gerhard E. Brügmann and Evgeny V. Pushkarev

Abstract

The present study describes variations in the major and trace element composition of rock forming minerals in various gabbros and tilaites (feldspar-bearing clinopyroxenites) from two Uralian-Alaskan-type complexes in the Ural Mountains (Kytlym and Nizhnii Tagil). The objective is to monitor the petrogenetic processes forming these cumulates in order to understand the origin and the composition of their parental melts. The results of the study provide new insights into the interaction of fundamentally different magma chamber systems forming Uralian-Alaskan-type magmatic complexes at destructive plate margins.

The distinctive geologic and petrographic feature of classical Uralian-Alaskan-type zoned mafic-ultramafic complexes is a zonal distribution of orthopyroxene-free mafic and ultramafic rocks with a central dunite body that grades outward into clinopyroxenite and mafic lithologies, the latter consisting of gabbroic and tilaitic cumulates. The tilaites have clinopyroxene phenocrysts in a matrix of olivine, clinopyroxene and spinel ± phlogopite ± amphibole. Based on additional minerals and their spatial distribution three types of tilaites can be distinguished. The nepheline tilaites are silica undersaturated and contain in the matrix plagioclase$_{An28-48}$, K-feldspar$_{Or47-98}$ and nepheline. They are only observed in Nizhnii Tagil and the south western part of the Kytlym Complex. The second type, the bytownite tilaites are silica saturated, contain up to 15% plagioclase$_{An56-89}$ and in places orthopyroxene as matrix phases. They coexist with the nepheline tilaites in Nizhnii Tagil and south west Kytlym. The third group of tilaites at the Tilay Mountain massif in the

central part of the Kytlym complex also consists of bytownite tilaites, but they do not coexist with nepheline tilaites and have distinct mineral and trace element compositions.
Gabbro-norites and melano gabbros in the eastern part of the Kytlym complex contain 15-35% plagioclase$_{An85-97}$ and a significant amount orthopyroxene and amphibole. They are not genetically related to the mafic-ultramafic association in the western part of the Kytlym complex and therefore called external gabbros.
Clinopyroxene cores of nepheline and coexisting bytownite tilaites in Nizhnii Tagil and the western part of the Kytlym Complex have high LREE/HREE (e.g. La/Lu 30-55) and Sr contents (195-470 ppm), if compared to the bytownite tilaites from Tilay Mountain (La/Lu = 5.5-16; Sr = 26-77 ppm). Clinopyroxene from the external gabbros has the lowest La/Lu (2.9-6.8) and low Sr contents (27-104 ppm). Positive anomalies of Ba and Sr and negative ones for the HFSE in clinopyroxenes imply that they crystallized from melts that formed in a subduction related geotectonic setting.
The nepheline tilaite is the most fractionated product of a suite of parental melts generated by different degrees of partial melting that also formed the ultramafic cumulates. Its mineral assemblage and its composition characterize this melt as silica undersaturated, with an alkaline affinity, low Al_2O_3 and high LREE/HREE, Sr, MgO and CaO ($CaO/Al_2O_3 > 1$). According to experimental results these kinds of melts can be generated from a wehrlitic, amphibole-bearing upper mantle source at 1 GPa and T > 1190°C. A second suite of melts is parental to the external gabbros and found to be silica saturated, having low LREE/HREE, Sr and $CaO/Al_2O_3 < 1$ at high Al_2O_3 and shows affinities to island arc tholeiites. Such melts can be formed in the mantle wedge above a subduction zone at 2-4 GPa and 1200-1400°C. The cores of most clinopyroxenes of the Bytownite gabbros lie on a mixing line between the silica under-saturated nepheline tilaite and the silica-saturated external gabbro. Hence, the continuous increase of La/Lu from silica-saturated to silica-undersaturated mafic rocks traces predominantly the mixing of two distinctively different parental magmas.
Strikingly, the LREE/HREE in most clinopyroxenes from all lithologies decreases from the core towards the rim with increasing HREE concentration – i.e. with increasing fractionation. This can not be explained by fractional crystallization of clinopyroxene and feldspar, but by adding and mixing of fractionated melts of arc tholeiitic composition to a residing melt in a magma chamber.

Magma mixing processes can be observed on the scale of a single thin section. Clinopyroxene cores, rich in inclusions have La/Lu of 13-16, whereas other clinopyroxene cores within the same thin section are poor in inclusions and have low La/Lu of 5-8 at similar Lu concentrations (0.15-0.2 ppm). Just outside of the core, both phenocryst types have intermediate and similar La/Lu of 9-11 and Lu (0.27-0.32ppm). From there the La/Lu decreases towards the rim, which has the same composition as the matrix grains (La/Lu = 7-9, Lu = 0.35-0.52ppm). The different core compositions indicate the coeval presence of the two different parental magmas. After mixing of these magmas the clinopyroxene cores were overgrown by clinopyroxene crystallizing from the hybrid magma. The addition of more fractionated tholeiitic magma explains the low La/Lu of the clinopyroxene rims and in the matrix grains.

The present study highlights the critical role of magma mixing which dominates the petrogenetic evolution of gabbroic and tilaitic rocks and what can be recognized on regional down to thin section scale. The mixing of parental magmas and their different fractionation products which are derived from two different sources is necessary in order to explain the observed variations in the composition of Uralian-Alaskan-type complexes. We propose that the coeval occurrence of magmas derived from different source compositions is a characteristic feature of this type of intrusions and might play an important role in magmatic systems at destructive plate margins worldwide.

Keywords: Magma Mixing, Alaskan-type complexes, Clinopyroxene, Trace elements, Magmatism in island arcs, Laser-ICPMS.

1 Introduction

High resolution analytical methods like electron microprobe analysis (EMPA), secondary ion mass spectrometry (SIMS) and laser ablation inductively coupled plasma mass spectrometry (LA-ICPMS) allow the detailed study of variations of major and trace element abundances in rock forming minerals (e.g. Maclennan et al., 2003; Rankenburg et al., 2004; Gioncada et al., 2005; Francalanci et al., 2005; Monjoie et al., 2005; Batanova et al., 2005; Guo et al., 2007; Hidalgo et al., 2007; Krause et al., 2007). These techniques provide a powerful tool to monitor the petrologic evolution of igneous rocks, and to identify petrogenetic processes such as magma mixing and mingling or crystal

fractionation, as well as a postmagmatic, low-temperature overprint. The advantage of these methods, if compared to analytical data from whole rock samples, is the spatial and temporal resolution that offers a direct link between mineralogical - geochemical observations and petrogenetic processes.

Uralian-Alaskan-type complexes or zoned mafic-ultramafic complexes are recognized as a distinctive class of mafic-ultramafic intrusions with respect to their tectonic setting, internal structure, petrology and geochemistry (e.g. Taylor and Noble, 1960; Noble and Taylor, 1960; Irvine, 1963; Irvine, 1967; Findlay, 1969; Efimov, 1977; Himmelberg et al., 1986; Hammack et al., 1991; Himmelberg and Loney, 1995; Pertsev et al, 2002; Batanova et al., 2005; Krause et al., 2007). These complexes are described from convergent margin settings, for example the Cordillera of Alaska and British Columbia (e.g. Taylor and Noble, 1960; Irvine, 1963; Irvine, 1967; Findlay, 1969; Clark, 1980; Himmelberg et al., 1986; Nixon et al., 1990; Hammack et al., 1991; Himmelberg and Loney, 1995), on Northern Kamchatka, Russia (e.g. Astrakhantsev et al., 1991; Batanova and Astrakhantsev, 1992; Kepezhinskas et al., 1993a-b; Batanova and Astrakhantsev, 1994; Sidorov et al., 2004; Batanova et al., 2005) and in the Ural Mountains, Russia (e.g. Levinson and Lessing, 1900; Wyssotzky, 1913; Duparc and Tikhonowitch, 1920; Noble and Taylor, 1960; Efimov and Efimova, 1967; Taylor, 1967; Efimov, 1977; Ivanov and Shmelev, 1996; Savelieva et al., 1996; Pertsev et al., 2000; Krause et al., 2007). Uralian-Alaskan-type complexes have been also found in Colombia (Tistl et al., 1994), Venezuela (Murray, 1972), Ontario, Canada (Pettigrew and Hattori, 2006), New South Wales, Australia (Slansky et al., 1991; Andrew et al., 1995) and Egypt (Helmy and El Mahallawi, 2003). In addition ultramafic dunite-clinopyroxenite complexes are described from within-plate geological settings in the Aldan Shield, Siberia, where they intrude the platform cover (e.g. Efimov and Tavrin, 1978; Malitch, 1999).

In convergent margin settings like in the Cordillera of Alaska and British Columbia, on Kamchatka and in the Ural Mountains the intrusions are aligned along narrow belts, several hundreds of kilometers long. Their classical geologic and petrographic characteristic is the zonal distribution of mafic and ultramafic rocks, where often a central dunite body grades outward into wehrlite, clinopyroxenite and gabbroic

lithologies and the almost complete absence of orthopyroxene-bearing rocks. Some of these complexes host a chromite-PGE mineralization.

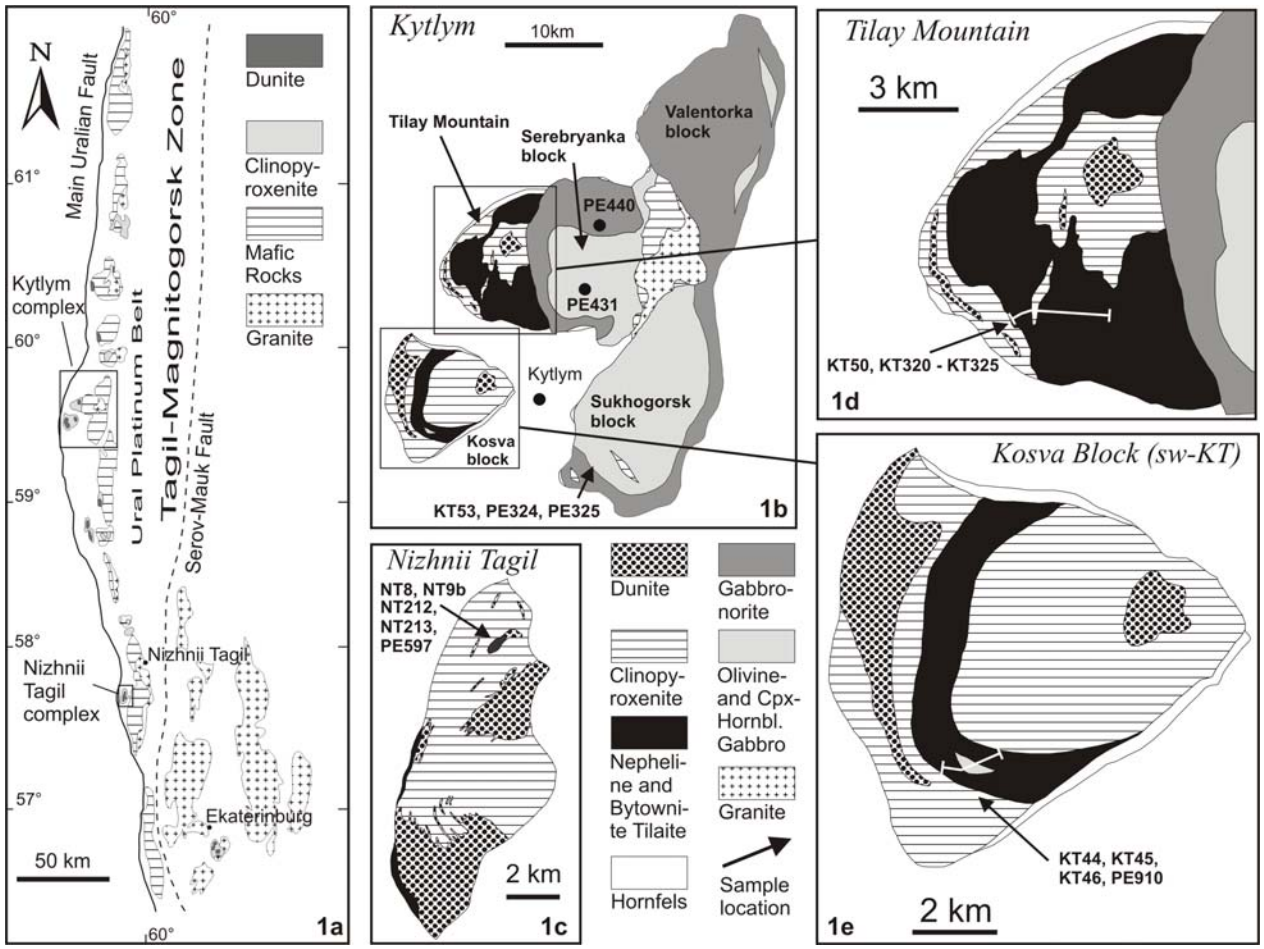

Fig. 1: Geological maps of the Ural platinum belt (a) and the studied Uralian-Alaskan type complexes of Kytlym (b, d, e) and Nizhnii Tagil (c). Modified after Savelieva et al. (2002) and Garuti et al. (1997).

In the Ural Mountains 15 Uralian-Alaskan-type mafic-ultramafic complexes define a 900 km long linear belt along the 60-th meridian (Fig. 1a), called the “Ural platinum belt” (UPB). This belt is situated eastward of Main Uralian Fault (MUF), traced by serpentinite ophiolite melange, which traces the paleosubduction zone of the Tagil island-arc system (Ivanov and Shmelev, 1996). Directly westward from the MUF, the Precambrian sedimentary and volcanic formations of the East-European platform occur. Ordovician and Silurian island-arc basic volcanic rocks of the Tagil zone rim the massifs from east and partly from south and north. Many of the ultramafic and mafic bodies have a narrow rim of high temperature hornfels. Efimov and Efimova (1967) suggested that these

contact metamorphosed rocks represent lower-crustal mafic rocks, perhaps granulites that are not related to the arc-volcanics. The mafic-ultramafic complexes together with their narrow rims of hornfels have low temperature tectonic contacts with the surrounding island-arc rocks.

Genesis and structure of the Uralian-Alaskan-type complexes in the UPB have been controversially discussed during the last decades. Genetic models propose metasomatic (Vorobeva et al., 1962), metamorphic (Efimov et al., 1993), and magmatic processes (e.g. Ivanov and Shmelev, 1996; Fershtater et al., 1999; Savelieva et al., 1999; Pertsev et al., 2000) in order to explain the special rock assemblage. There is also a debate on the geological setting, because island arc (Ivanov and Shmelev, 1996; Krause et al., 2007) and supra subduction zone environments (e.g. Fershtater et al., 1999) as well as a diapiric mantle upwelling related to extensional tectonics along the edge of the east European Craton (Efimov et al., 1993; Savelieva et al., 1999; Savelieva et al., 2002) have been postulated.

For this study we sampled mafic rocks from two Uralian-Alaskan-type complexes, Nizhnii Tagil and Kytlym (Fig. 1). The Nizhny Tagil complex mainly comprises a dunite core, bounded by a narrow rim of clinopyroxenite (Fig. 1c). This dunite body covers an area of 30 km^2 and is the largest in a Uralian-Alaskan-type complex in the Ural Mountains. Wehrlite forms in places narrow rims between dunite and clinopyroxenite. Mafic rocks are found in the northern part of the complex along the Zotikha and Chauzh rivers within clinopyroxenite.

The Kytlym Complex is a large, composite intrusive complex of mafic and ultramafic rocks (Fig. 1b). At its western side occur the Kosva and Tilay-Konjak ultramafic blocks, consisting of dunite, clinopyroxenite and mafic rocks (Figs. 1e, d). The eastern part of the Kytlym complex (Valentorka, Serebryanka and Sukhogorsk blocks) is made up of gabbro norite, olivine- and clinopyroxene- hornblende gabbros surrounding several schollen of clinopyroxenite and a younger plagiogranite body (Fig. 1b). Based on petrological and structural observations, especially the presence of orthopyroxene-bearing gabbros in the eastern part of the Kytlym complex, it is believed that eastern and western massifs are not genetically related (Efimov and Efimova, 1967; Efimov et al., 1993; Savelieva et al., 1999; Savelieva et al., 2002).

Some clinopyroxene-rich ultramafic rocks in Nizhnii Tagil and the western parts of the Kytlym Complex contain varying amounts of feldspar grading into a melano gabbro. Similar rocks have been described also from Uralian-Alaskan-type complexes in Alaska and British Columbia (Findlay, 1969; Himmelberg et al., 1986; Hammack et al., 1991; Himmelberg and Loney, 1995) and Kamchatka (e.g. Astrakhantsev et al., 1991; Kepezhinskas et al., 1993a-b; Batanova et al., 2005) and were named as “tilaites” by Dupark and Tikhonowitch (1920). Since the modal feldspar content of these rocks is in general below 15% we will apply the term tilaite to clinopyroxene-rich, porphyric, in places layered rocks, that contain feldspar in the matrix. The term gabbro will be used only for rocks that contain more than 15% feldspar and in addition at least 10% of orthopyroxene and/or hornblende. Here feldspar often forms phenocrysts with a grain size similar to that of the mafic phases.

Based on their mineralogical composition and their spatial distribution three types of mafic rocks can be distinguished:

1) *Nepheline tilaite* is exposed in Nizhnii Tagil and in the Kosiva massif in southwest Kytlym (Fig. 1). Its characteristic feature is the occurrence of interstitial nepheline and K-feldspar along with plagioclase and the absence of orthopyroxene. Such lithologies were described also from the Tulameen complex, British Columbia, Canada (Findley, 1969) and the Galmoenan complex, Kamchatka, Russia (Astrakhantsev et al., 1991; Batanova et al., 2005)

2) *Bytownite tilaite* coexsists with the nepheline tilaite in Nizhnii Tagil and the southwest of Kytlym. They contain up to 10 % of plagioclase of predominantly bytownitic composition and in a few cases orthopyroxene and amphibole. Bytownite tilaites also comprise a large part of the Tilay Mountain massif (Kytlym) where they do not coexist with nepheline tilaites. Based on this observation – and on chemical differences as we shall see later - we subdivided the bytownite tilaites into two groups. The bytownite tilaites of the first group coexist with nepheline tilaite (Nizhnii Tagil and southwest Kytlym), the second group are the ones at Tilay Mountain (Kytlym).

3) Gabbros of the eastern part of the Kytlym complex (Fig. 1b) are regarded to be in an external position (Efimov and Efimiova, 1967). They are divided into three

general groups, gabbronorite, olivine gabbro and amphibole-clinopyroxene gabbro, and form separate massifs with their own internal structures (Efimov and Efimova, 1967). They differ in their chemical and mineralogical composition from the tilaites and might have been formed from a different parental melt. We will refer to them as *external gabbros*. They commonly have a substantial amount of hornblende and/or orthopyroxene and up to 35% plagioclase forming hornblende gabbros and gabbronorites.

The petrogenetic evolution of the Uralian-Alaskan-type complexes in the UPB especially for the larger and more complex massifs like Kytlym is still not well understood. The present study gives a systematical overview on the trace element geochemistry in rock forming minerals from mafic rocks of the Uralian-Alaskan-type complexes of the UPB using LA-ICPMS especially alongside detailed profiles across clinopyroxene phenocrysts. Previously, few data about the trace element distribution in clinopyroxene, plagioclase, apatite, amphibole and orthopyroxene were obtained by XRF and ICP-MS (Efimov et al., 1989; Pushkarev et al., 1996; Anikina et al., 2006).

Applying electron microprobe and LA-ICPMS our study focuses on the petrogenetic relationship between the different gabbroic lithologies and their genetic link to the ultramafic rocks. On thin section to regional scale, we will show that the diversity of rocks can be explained by the interaction of two fundamentally different magma types. We believe that this is an integrated feature of Uralian-Alaskan-type complexes world-wide.

2 Samples and Analytical Methods

2.1 Sample description

Nepheline tilaites were sampled at the northernmost gabbroic lens in Nizhnii Tagil (Fig. 1c) and at the western part of the Sosnofka massif (Kytlym, Fig. 1e). They have a porphyric texture with clinopyroxene phenocrysts 3-12 mm in diameter in a matrix of olivine + clinopyroxene + phlogopite + plagioclase + K-feldspar + nepheline. Accessory phases are spinel and apatite.

Bytownite tilaites were sampled from the same outcrops as the nepheline tilaites. Additionally samples of bytownite tilaites were taken at their type locality the Tilay Mountain, where they form a large massif (Fig. 1d). Porphyric textures dominate, however, layering and protomylonitic textures can be observed towards the western margin of the massifs. A strongly deformed bytownite tilaite with protomylonitic textures and dynamically recrystallized clinopyroxene and olivine was sampled in Nizhnii Tagil (NT212, NT213). Clinopyroxene forms phenocrysts 3-15 mm in diameter. Olivine also forms large hypidiomorphic phenocrysts in some of the samples from Tilay Mountain (Kytlym). Orthopyroxene phenocrysts occur in one sample from the same area (KT325). The phenocrysts are surrounded by a fine grained matrix of clinopyroxene + olivine + plagioclase + spinel ± orthopyroxene ± hornblende ± phlogopite. Accessory phases are apatite and spinel in places with intergrowths of ilmenite.

External gabbro samples are from three massifs in the eastern part of the Kytlym mafic-ultramafic complex: gabbronorite from Valentorka block, amphibole-clinopyroxene gabbro from Serebryanka block and olivine gabbro from Sukhogorsk block (Fig. 1b). They have a banded or granular texture and clinopyroxene or hornblende, less commonly also orthopyroxene, form crystals up to 10 mm in size. These are surrounded by coarse grained aggregates of plagioclase which are in size similar to the mafic minerals. These phases also occur in the interstitial pore spaces together with apatite and spinel often intergrown with ilmenite (Chapter 3).

2.2 Major element analysis

After removing weathered crusts, the samples were powdered in an agate mill for XRF analysis, which were made with a Philips MagiXPRO spectrometer at the University of Mainz. Additional analyses were made on 5 g of sample pressed to tablets with an XRF spectrometer (SRM-25) in the Institute of Geology and Geochemistry, Ural Division of RAS (Yekaterinburg, Russia).

Polished thin sections, 150 µm thick, were used for the microprobe and Laser-ICPMS measurements. Major elements of minerals were analyzed with the Jeol JXA8200 microprobe at the Max-Planck-Institute for Chemistry and the Jeol JXA8900RL microprobe at the Institute of Geosciences of the University of Mainz. We used natural

minerals and oxides (Si, Ti, Al, Fe, Mg, Mn, Ca, Na, K, Cr, Zn, Sr) and pure element standards (V, Co) for calibration. Silicate minerals were measured with an acceleration voltage of 15 or 20 kV, a probe current of 12 or 20 nA, a beam diameter of 1 or 2 µm and counting times between 20 and 80 s on the peak and 10-40 s on the background.

2.3 Element mapping

Element maps of Cpx were obtained with the Jeol JXA 8900RL microprobe at the Institute of Geosciences of the University of Mainz at 20 kV and 15 nA with a beam diameter of 5 µm. Cr, Na, Al, Fe and Ti were measured with WDS spectrometers, Ca, Mg and Si with an EDS Spectrometer at counting times between 120 and 155 ms. The step size varied between 5 and 7µm.

2.4 Trace element analysis

For the determination of trace element concentrations in the whole rock samples 40 mg of sample powder were molten to a homogeneous glass on an Iridium strip under an Ar atmosphere following the procedure described by Stoll et al. (2008).

A New Wave UP193 laser system with a wavelength of 193 nm for the ablation was used to determine the trace element concentrations in clinopyroxene, nepheline, feldspars and whole rock glasses. Application of a frequency of 10 Hz and energies between 2 and 8 J/cm² produced ablation pits with diameters between 50 and 80 µm. A spot size of 120 µm was used for the glasses. Helium was used as a carrier gas. The ablated material was analyzed with a ThermoFinnigan Element2 sectorfield ICPMS in the low resolution mode and a counting time of 20 s on the background and 80 to 100 s on the sample. NIST612, KL2-G and GOR132-G glasses were used as standard materials and ^{43}Ca and ^{29}Si as internal reference isotopes. The detection limit varies between 0.2-2 ppb for REE, U, Th, Hf and Ta, between 2-20 ppb for Ba, Pb, Nb, Zr and Y, and between 100-200 ppb for Rb and Sr. In this study we only consider concentration data which are at least ten times above the limit of detection. According to Jochum et al. (2006) the accuracy is better than 3% and the total analytical uncertainty is less than 5%. The analytical procedure is described in detail by Jochum et al. (2006, 2007).

In addition, homogeneous powder (50-100 mg) was dissolved in acids under standard procedure using high pressure or microwave technique (Puschkarev pers. com. 2008). The analyses were carried out on solutions using ICPMS, an ELLAN-9000 instrument at the Institute of Geology and Geochemistry, Ural Division of RAS, Yekaterinburg, Russia, and an ELLAN-500 instrument at the Granada University, Spain.

3 Results

Given the large number of analysis (28 whole rock XRF analyses; microprobe data of 232 olivine, 441 feldspar, 78 nepheline, 1301 pyroxene; LA-ICPMS data of 16 whole rock samples, 319 feldspar, 43 nepheline and 757 clinopyroxene) only a representative subset is given in Tables 1-4. The entire dataset can be found in the electronic attachments.

3.1 Major and trace element composition of whole rocks

The different groups of tilaitic and gabbroic rocks can be well discerned by their major and trace element composition (Tab. 1; Figs. 2 and 3). Tilaites have lower contents in Al_2O_3 (4.1-12.2 wt.%), higher contents in SiO_2 (42-50.4 wt.%) and K_2O (0.05-2.86 wt.%) and higher CaO/Al_2O_3 (1.05-2.9) and Mg/(Mg+Fe) (0.67-0.80) than the external gabbros from the Valentorka, Serebryanka and Sukhogorsk blocks in E Kytlym (CaO/Al_2O_3 = 0.59-0.98; Al_2O_3 = 16.0-25.9 wt.%; SiO_2 = 40.6-43.3 wt.%; K_2O < 0.07 wt.%; Mg/(Mg+Fe) = 0.52-0.68). In turn the nepheline tilaites have higher contents in Na_2O (> 1.22 wt.%) and K_2O (>0.71 wt.%) and lower Mg/(Mg+Fe) of 0.68-0.75 than the bytownite tilaites, which have, with the exception of one sample, 0.22-0.87 wt.% Na_2O, 0.05-0.5 wt.% K_2O and their Mg/(Mg+Fe) varies between = 0.75-0.80 (Fig. 2).

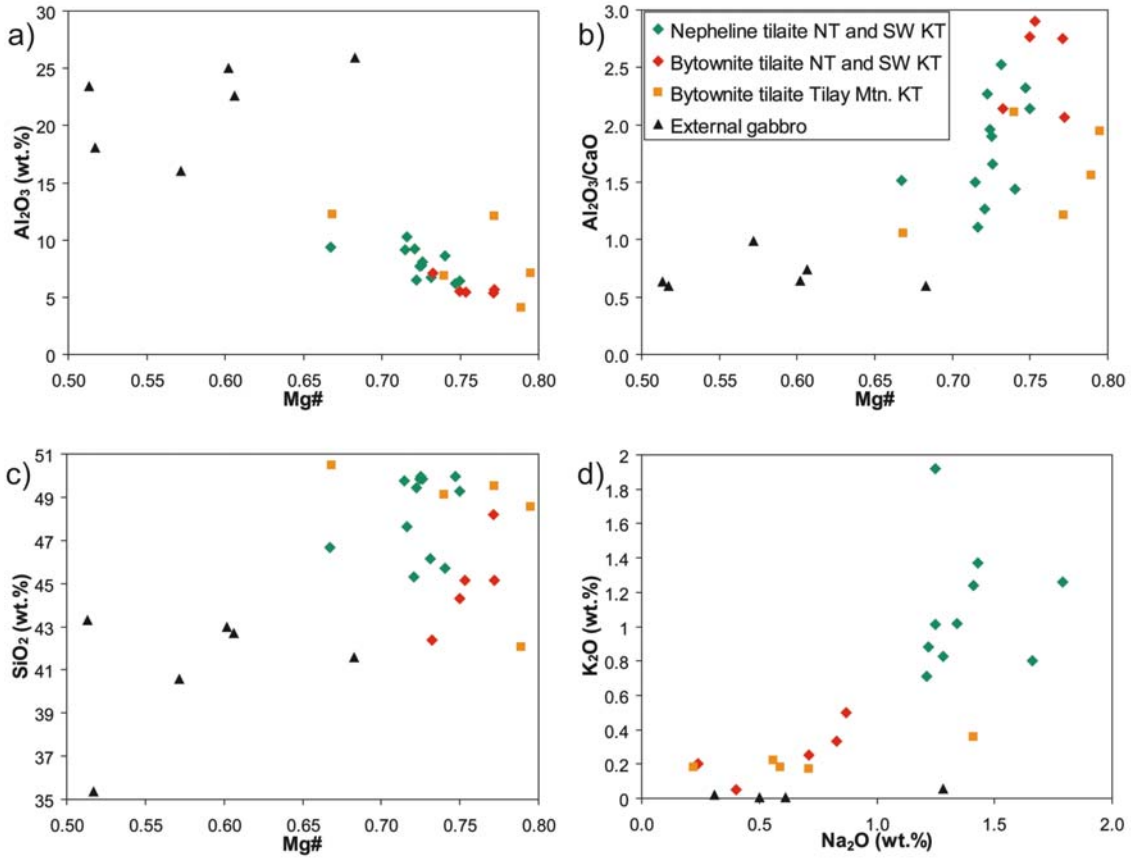

Fig. 2: Correlation diagrams of major elements vs. Mg# (Mg/(Mg+Fe)) (a-c) and of alkali elements (d) in mafic rocks from Uralian-Alaskan-type complexes in the UPB.

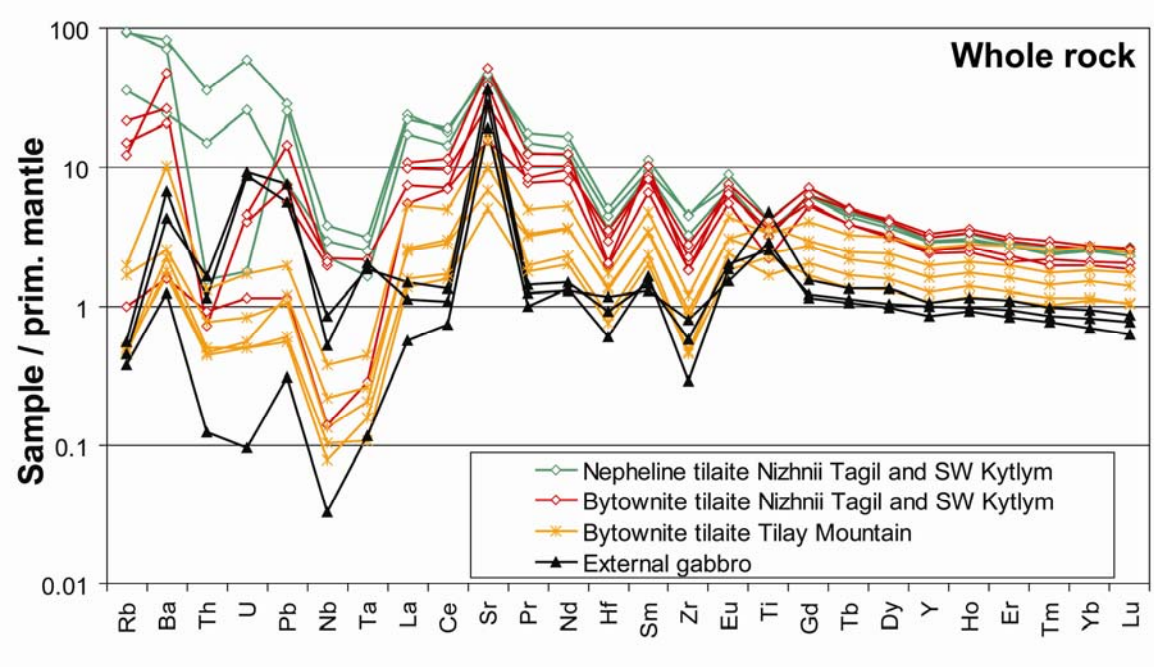

Fig. 3: Whole rock trace element abundances in mafic rocks of Uralian-Alaskan-type complexes in the UPB. Data are normalized to the primitive mantle of Hofmann, (1988).

Tab. 1: Whole rock composition of selected samples from Uralian-Alaskan-type complexes. Fe_2O_3* = all iron measured as Fe_2O_3. NT = Nizhnii Tagil, SW KT = southwest Kytlym, Til KT = Tilay Mountain, Kytlym, SH E-KT = External gabbro (Sukhogorsk Block), b.d. = below limit of detection.

Sample	NT 8	KT 46	TG 212	KT 44	KT 320	KT 325	KT 53	PE 325
Locality	NT	SW KT	NT	SW KT	Til KT	Til KT	SH E-KT	SH E-KT
Lithology	NeTi	NeTi	ByTi	ByTi	ByTi	ByTi	ExGb	ExGb
SiO_2 (wt.%)	47.64	46.65	42.37	45.14	49.12	50.47	40.56	42.96
TiO_2	0.53	0.67	0.75	0.55	0.61	0.57	0.75	0.35
Al_2O_3	10.30	9.39	7.07	5.42	6.86	12.24	16.00	25.02
Fe_2O_3*	10.60	12.52	13.61	12.82	10.97	10.32	15.05	7.76
MnO	0.19	0.21	0.21	0.21	0.23	0.23	0.14	0.10
MgO	13.50	12.68	18.81	19.76	15.76	10.49	10.14	5.92
CaO	11.38	14.22	15.11	15.71	14.47	12.89	15.74	16.04
Na_2O	2.15	1.79	0.71	0.40	0.59	1.41	0.31	0.61
K_2O	2.86	1.26	0.25	0.05	0.18	0.36	0.02	0.01
P_2O_5	0.34	0.24	0.38	0.01	b.d.	0.09	b.d.	0.01
LOI	0.54	0.12	0.75	0.06	b.d.	b.d.	0.98	0.55
Total	100.03	99.75	100.02	100.13	98.79	99.07	99.69	99.32
CaO/Al_2O_3	1.10	1.51	2.14	2.90	2.11	1.05	0.98	0.64
Mg#	0.72	0.67	0.73	0.75	0.74	0.67	0.57	0.60
Rb (ppm)	49.60	19.12	6.56	0.53	0.24	1.06	0.20	0.29
Ba	493.7	147.1	285.9	9.6	11.0	61.6	7.4	40.6
Th	2.930	1.220	b.d.	0.074	0.037	0.106	0.010	0.093
U	1.205	0.525	b.d.	0.023	0.011	0.035	0.002	0.178
Pb	5.014	1.318	0.982	0.201	0.209	0.342	0.054	0.979
Nb	2.343	1.823	1.221	0.086	0.135	0.233	0.020	0.524
Ta	0.110	0.087	b.d.	0.010	0.009	0.015	0.004	0.065
La	14.61	13.60	6.66	3.39	1.52	3.24	0.35	0.91
Ce	28.66	30.80	18.38	11.21	4.56	7.99	1.17	2.16
Sr	936.1	842.1	928.6	282.7	123.7	286.7	351.0	663.5
Pr	3.66	4.27	3.02	2.04	0.77	1.21	0.24	0.34
Nd	16.22	19.91	15.01	11.53	4.25	6.32	1.60	1.76
Hf	1.21	1.34	0.55	0.95	0.37	0.45	0.16	0.25
Sm	3.62	4.40	3.96	3.15	1.33	1.85	0.63	0.57
Zr	44.63	43.68	17.68	22.05	9.13	11.45	2.83	5.59
Eu	1.06	1.31	1.11	0.93	0.45	0.63	0.27	0.29
Gd	3.19	3.64	3.62	2.84	1.52	2.07	0.78	0.62
Tb	0.41	0.44	0.48	0.37	0.23	0.30	0.13	0.11
Dy	2.34	2.46	2.71	2.07	1.52	1.99	0.85	0.66
Y	11.26	11.68	13.18	9.90	7.71	10.28	4.16	3.91
Ho	0.42	0.44	0.51	0.38	0.30	0.39	0.16	0.14
Er	1.13	1.13	1.30	0.97	0.82	1.12	0.45	0.39
Tm	0.16	0.15	0.19	0.13	0.11	0.16	0.06	0.05
Yb	1.05	1.03	1.13	0.81	0.76	1.09	0.39	0.34
Lu	0.16	0.15	0.17	0.12	0.11	0.16	0.06	0.05

The mantle normalized trace element pattern of all tilaites and gabbros shows a typical arc related signature (e.g. Kelemen et al., 2003) with a positive anomaly for Ba, Sr (Sr/Sr* = 2.0-54.0) and negative anomalies for Nb, Ta and the HFSE (Fig. 3; Tab. 1). The highest trace element concentrations are observed in nepheline and bytownite tilaites from Nizhnii Tagil and SW-Kytlym. The concentrations in most bytownite tilaites from the Tilay Mountain (Kytlym) are lower but they are higher than those of the external gabbros (Fig. 3). The nepheline tilaites show a continuous enrichment of the LREE over the HREE (Fig. 3). All other mafic rocks show an increase of the mantle normalized concentrations from the HREE to the MREE (until Nd), but from there on the LREE pattern is flat or decreases slightly (Fig. 3). The nepheline tilaites have the highest La/Lu of 62-93 but bytownite tilaites from the same outcrop have lower La/Lu (28-40). Bytownite tilaites from Tilay Mountain and the external gabbros from the Valentorka, Serebryanka and Sukhogorsk blocks have the lowest La/Lu (6-23). Thus, the mafic rocks display a fan-shape trace element distribution, but whereas the HREE and MREE vary by just a factor of 10, highly incompatible elements have a concentration range of more than 2 orders of magnitude. End members of this range are external gabbros and nepheline tilaites suggesting different parental melts.

3.2 Mineral chemistry

3.2.1 Major and trace element concentrations in ortho- and clinopyroxene

Clinopyroxene is the major constituent in all mafic rocks from the Uralian-Alaskan-type complexes forming phenocrysts up to 15 mm in diameter and smaller grains in the matrix. In places a dynamic recrystallization is present (e.g. Efimov, 1977; Fershtater and Pushkarev, 1992; Savelieva et al., 1999; Pertsev et al., 2000; Savelieva et al., 2002). Only two of our samples (bytownite tilaites from Nizhnii Tagil NT212, NT213) show this feature, although undulose extinction is common in clinopyroxene. Clinopyroxene phenocrysts often have numerous exsolutions of Ti-magnetite, which define an oscillatory zoning like that described for clinopyroxene from the ultramafic rocks of the Uralian Alaskan-type complexes (Fershtater and Pushkarev, 1992; Savelieva et al., 1999; Ivanov et al., 2000; Krause et al., 2007). The innermost core of the clinopyroxene phenocrysts contains dominantly inclusions of spinel and olivine.

Phlogopite, Apatite and plagioclase inclusions are here less abundant and often restricted to the marginal parts of the phenocrysts.

Orthopyroxene was found in minor amounts in some bytownite tilaite samples primarily at Tilay Mountain, where it forms hypidiomorphic to xenomorphic grains in the matrix. Phenocrysts of orthopyroxene were observed in one bytownite tilaite (KT325). In some samples of the external gabbro orthopyroxene represents a major constituent, and it forms hypidiomorphic phenocrysts with a diameter of up to 10 mm or small xenomorphic grains in the matrix. Exsolutions of fine lamellas of orthopyroxene in clinopyroxene are confined to some samples in the external gabbros.

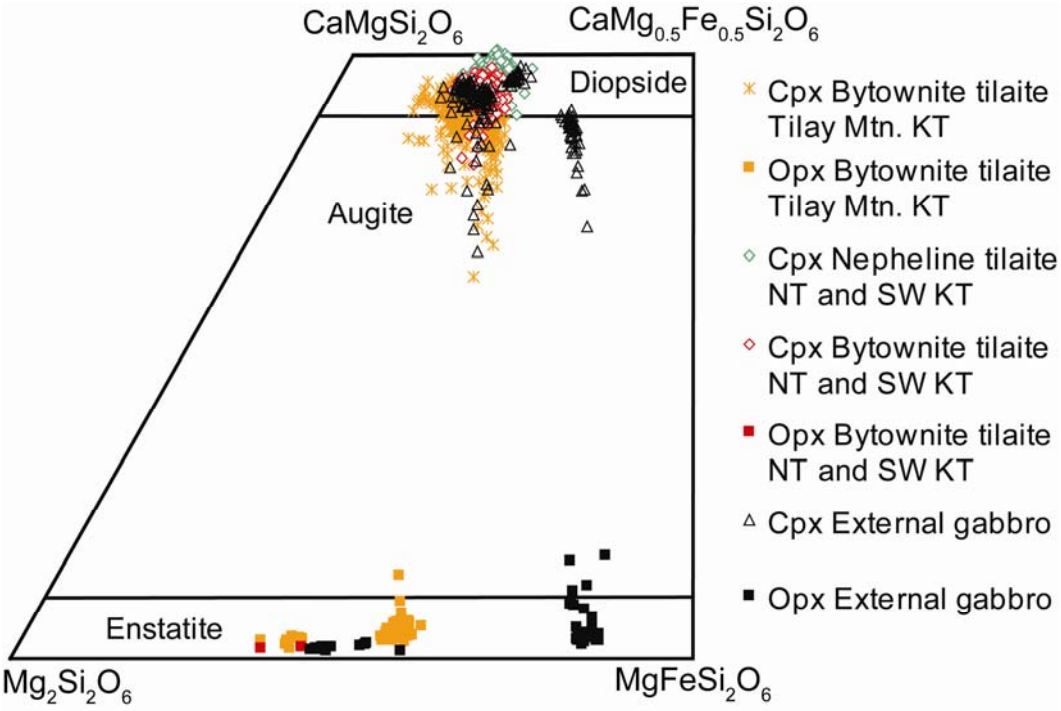

Fig. 4: Classification and composition of ortho- and clinopyroxenes in mafic rocks from Uralian-Alaskan-type complexes in the UPB.

Representative compositions of ortho- and clinopyroxene are summarized in Tab. 2. Most of the clinopyroxene in the nepheline and bytownite tilaites in Nizhnii Tagil and SW-Kytlym is diopside, rarely augite. In the tilaites from Tilay Mountain and in the external gabbros augite becomes more abundant. Orthopyroxene always has an enstatite composition (Fig. 4). Nevertheless, the pyroxenes show large variations in major and trace element concentrations.

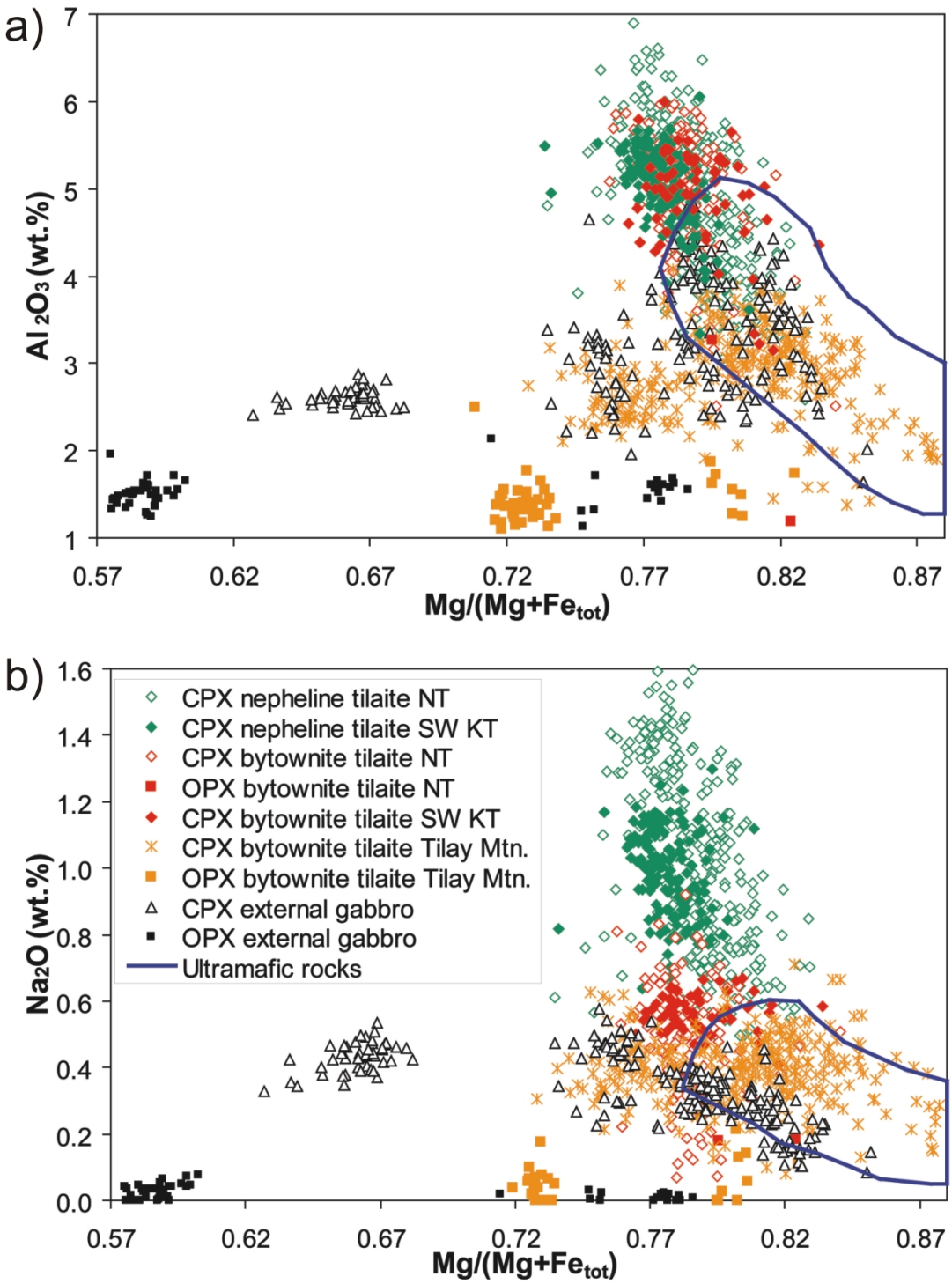

Fig. 5: Variation of major element composition of clino- and orthopyroxenes from Uralian-Alaskan-type intrusions. (a) Al_2O_3 vs. Mg/(Mg+Fe). Tilaites from Nizhnii Tagil and southwest Kytlym continue the trend observed in the ultramafic rocks (field outlined in blue). Clinopyroxene from the external gabbro and the bytownite tilaites at Tilay Mountain shoes a decreasing Al_2O_3 with increasing fractionation. (b) Variation of Na_2O with the Mg/(Mg+Fe). Data for the ultramafic rocks are from Krause et al. (2007).

The Mg# ($Mg/(Mg+Fe_{tot}$) of clinopyroxene in the bytownite and nepheline tilaites from Nizhnii Tagil and SW-Kytlym (Mg# = 0.74-0.82) show a negative correlation with the Al_2O_3 content (2.5-6.5 wt.%, Fig. 5a). This extends and overlaps with the trend observed in clinopyroxene from the ultramafic rocks (Krause et al., 2007). Clinopyroxene in the Bytownite tilaites from Tilay Mountain (Mg# = 0.72-0.88) and the external gabbro (Mg# = 0.63-85) follow a different trend indicating a larger Mg# range, but the Al_2O_3 content remains rather stable (2-4 wt.%; Fig. 5a). Orthopyroxene has typically low Al_2O_3 contents (1.1-2.4 wt.%) over a wide range of Mg# (0.57-0.82).

Clinopyroxene from the different lithologies also shows distinct variations in the Na_2O-content (Fig. 5b). In the bytownite and nepheline tilaites from Nizhnii Tagil and southwest Kytlym the Na_2O content in clinopyroxene varies considerably. Interestingly clinopyroxene in both tilaite types coexisting in southwest Kytlym have a more restricted variation in Na_2O (bytownite tilaite 0.5-0.7 wt.%, nepheline tilaite 0.6-1.3 wt.%), if compared to Nizhnii Tagil (bytownite tilaite 0.1-0.9 wt.%, nepheline tilaite 0.5-1.6 wt.% Na_2O). Clinopyroxene in the tilaites from Tilay Mountain has lower Na_2O concentrations (0.1-0.7 wt.%) similar to that in the external gabbro (0.1-0.5 wt.%).

Clinopyroxene from all samples share negative anomalies in HFSE, Nb and Ta (Fig. 6). This has also been observed in clinopyroxene from the ultramafic rocks (Krause et al., 2007) and suggests an arc related geotectonic setting for these complexes. The positive Sr anomaly described in clinopyroxene in ultramafic rocks (Krause et al., 2007) is only present in the core of large phenocrysts. The rims of these grains and small interstitial grains develop a negative Sr anomaly due to the onset of feldspar crystallization. This process is corroborated by the development of a negative Eu anomaly towards the rim of the large clinopyroxene phenocrysts and in interstitial grains.

Tab. 2: Clinopyroxene compositions of selected samples from mafic rocks in Uralian-Alaskan-type complexes. FeO* = all iron measured as FeO. NT = Nizhnii Tagil, SW KT = southwest Kytlym, Til KT = Tilay Mountain, Kytlym, E-KT = External gabbro. C = core, I = intermediate, R = rim, M = Matrix, a and b denote Type A and B, b.d. = below limit of detection.

Sample	04NT8-191	04NT8-195	04NT8-204	KT46-1	KT46-6	KT46-9	NT212-1	NT212-5	NT212-58	NT212-37
Locality	NT	NT	NT	SW KT	SW KT	SW KT	NT	NT	NT	NT
Lithologie	NeTi	NeTi	NeTi	NeTi	NeTi	NeTi	ByTi	ByTi	ByTi	ByTi
Position	C	R	M	R	C	M	R	C	M	M
Mineral	Cpx	Cpx	Cpx	Cpx	Cpx	Cpx	Cpx	Cpx	Cpx	Opx
SiO_2 (wt.%)	50.81	50.34	50.33	50.26	50.10	49.39	50.79	50.41	50.51	53.98
TiO_2	0.45	0.40	0.47	0.70	0.65	0.65	0.51	0.54	0.46	0.12
Cr_2O_3	0.06	0.10	0.22	0.08	0.04	0.05	0.07	0.07	0.16	0.03
Al_2O_3	6.52	5.98	4.77	5.26	4.54	4.72	5.17	4.35	4.98	3.29
FeO*	6.90	6.49	6.28	6.93	6.80	7.06	7.39	7.02	6.67	13.22
MnO	0.21	0.16	0.13	0.16	0.16	0.17	0.22	0.28	0.25	0.56
MgO	12.71	13.15	14.08	13.62	14.25	13.89	14.41	14.04	13.98	28.82
CaO	21.54	22.41	23.02	22.63	22.64	22.27	21.68	22.68	22.08	0.48
Na_2O	1.44	1.04	0.56	0.89	0.59	1.02	0.45	0.37	0.28	0.18
Total	100.64	100.08	99.87	100.54	99.76	99.30	100.70	99.75	99.35	100.68
Mg/(Mg+Fe)	0.767	0.783	0.800	0.778	0.789	0.772	0.777	0.781	0.789	0.795
Ba (ppm)	b.d.	b.d.	0.93	b.d.	0.29	0.34	b.d.	b.d.	b.d.	
Th	4.223	1.125	0.193	0.393	0.121	0.771	0.008	0.010	0.009	
U	1.038	0.496	0.080	0.175	0.036	0.249	b.d.	b.d.	b.d.	
Pb	1.32	1.30	0.66	0.63	0.29	0.73	0.10	0.13	0.12	
Nb	1.10	0.29	b.d.	0.37	0.11	0.92	b.d.	b.d.	b.d.	
Ta	0.20	0.03	b.d.	0.04	0.01	0.13	b.d.	0.02	b.d.	
La	16.67	8.31	5.39	12.18	7.71	14.83	5.65	5.91	6.01	
Ce	52.61	25.00	16.60	38.77	26.21	47.40	18.66	19.15	19.44	
Sr	116.1	368.6	355.1	187.3	228.3	163.2	260.8	251.4	284.1	
Pr	8.10	4.09	2.81	6.50	4.82	7.63	3.27	3.23	3.39	
Nd	36.34	20.08	14.07	31.79	25.43	35.56	16.66	16.58	17.74	
Hf	5.69	1.65	0.98	2.55	1.69	4.93	1.12	1.22	0.91	
Sm	8.95	5.40	3.78	7.56	6.38	8.36	4.53	4.55	4.88	
Zr	231.2	41.6	24.5	80.2	46.2	170.1	26.1	31.0	21.3	
Eu	2.25	1.65	1.21	2.08	1.88	2.27	1.39	1.35	1.40	
Gd	8.38	5.24	3.72	6.58	5.61	7.32	4.50	4.54	4.91	
Tb	1.14	0.69	0.51	0.83	0.70	0.94	0.61	0.60	0.69	
Dy	6.31	3.71	2.71	4.51	3.68	5.24	3.38	3.17	3.78	
Y	31.2	16.6	12.6	21.1	16.3	24.6	16.1	14.9	18.0	
Ho	1.20	0.68	0.51	0.79	0.65	0.96	0.61	0.56	0.67	
Er	3.39	1.79	1.33	2.10	1.60	2.54	1.71	1.53	1.80	
Tm	0.49	0.24	0.18	0.29	0.22	0.37	0.22	0.19	0.23	
Yb	3.23	1.56	1.08	1.85	1.43	2.43	1.47	1.27	1.52	
Lu	0.48	0.23	0.17	0.26	0.21	0.37	0.20	0.19	0.25	

Tab. 2: (cont.)

Sample	KT 325-4	KT 325-10	KT325-184	KT325-186	KT325-190	KT325-123	KT325-126	KT325-129	KT 325-8	KT 322-87
Locality	Til KT	Til KT	Til KT	Til KT	Til KT	Til KT	Til KT	Til KT	Til KT	Til KT
Lithologie	ByTi	ByTi	ByTi	ByTi	ByTi	ByTi	ByTi	ByTi	ByTi	ByTi
Position	Ma	Mb	Ra	Ia	Ca	Rb	Ib	Cb	M	M
Mineral	Cpx	Cpx	Cpx	Cpx	Cpx	Cpx	Cpx	Cpx	Opx	Opx
SiO_2 (wt.%)	51.66	50.78	51.80	50.82	51.21	51.29	50.09	51.38	53.54	54.82
TiO_2	0.36	0.41	0.36	0.41	0.24	0.44	0.44	0.37	0.16	0.06
Cr_2O_3	0.12	0.01	0.03	0.17	0.37	0.09	0.16	0.19	0.02	b.d.
Al_2O_3	2.34	2.29	2.37	2.88	2.71	2.55	3.45	2.88	1.41	1.27
FeO*	7.67	8.84	8.23	9.29	7.61	8.82	7.83	8.56	17.38	13.06
MnO	0.28	0.29	0.28	0.29	0.17	0.28	0.36	0.28	0.50	0.34
MgO	15.04	14.71	15.00	15.07	14.87	15.65	14.72	15.86	25.97	29.72
CaO	22.05	21.10	21.60	19.43	21.44	20.18	21.94	20.54	1.46	0.53
Na_2O	0.46	0.62	0.35	0.33	0.35	0.33	0.41	0.33	0.04	b.d.
Total	99.96	99.05	100.02	98.70	98.97	99.63	99.39	100.37	100.53	99.84
Mg/(Mg+Fe)	0.778	0.748	0.765	0.743	0.777	0.760	0.770	0.768	0.727	0.802
Ba (ppm)	0.24	b.d.	b.d.	0.42	b.d.	b.d.	6.08	1.57		
Th	0.068	0.119	0.082	0.117	0.139	0.092	0.123	0.047		
U	0.018	0.027	0.023	0.035	0.046	0.020	0.034	0.020		
Pb	0.14	0.10	0.14	0.20	0.46	0.13	0.18	0.16		
Nb	b.d.	b.d.	0.43	0.66	7.38	0.41	1.10	0.35		
Ta	0.01	b.d.	b.d.	b.d.	0.03	b.d.	b.d.	b.d.		
La	3.96	3.38	3.41	3.34	2.48	3.44	2.97	1.12		
Ce	15.01	12.37	12.83	11.80	7.76	13.03	10.48	3.86		
Sr	30.7	29.9	31.9	38.7	44.0	33.1	30.3	32.9		
Pr	3.00	2.53	2.56	2.18	1.40	2.62	1.95	0.78		
Nd	16.67	14.46	14.03	11.35	7.50	14.52	10.38	4.51		
Hf	1.46	1.47	1.15	0.60	0.67	1.43	0.73	0.35		
Sm	5.13	4.73	4.60	3.56	2.43	4.79	3.30	1.67		
Zr	37.7	33.6	27.4	16.9	15.6	32.2	20.4	7.0		
Eu	1.37	1.20	1.16	1.01	0.76	1.18	0.96	0.59		
Gd	6.08	5.72	5.31	4.07	2.69	5.57	3.96	2.13		
Tb	0.96	0.92	0.81	0.64	0.39	0.86	0.61	0.35		
Dy	5.82	5.56	4.96	3.87	2.28	5.16	3.65	2.09		
Y	28.0	28.8	25.7	18.6	11.7	25.8	17.6	11.3		
Ho	1.21	1.15	1.05	0.81	0.46	1.09	0.78	0.45		
Er	3.35	3.26	2.91	2.26	1.27	3.05	2.10	1.24		
Tm	0.48	0.46	0.41	0.32	0.18	0.43	0.31	0.17		
Yb	3.01	2.91	2.63	2.06	1.13	2.72	1.91	1.11		
Lu	0.45	0.45	0.39	0.30	0.16	0.40	0.29	0.17		

Tab. 2: (cont.)

Sample	KT44-334	KT44-338	04KT53-240	04KT53-282	PE324-305	PE 325-76	PE440-9	PE440-18	PE440-63	PE440-6
Locality	SW KT	SW KT	E KT	E KT	E KT	E KT	E KT	E KT	E KT	E KT
Lithologie	ByTi	ByTi	ExGb	ExGb	ExGb	ExGb	ExGb	ExGb	ExGb	ExGb
Position	C	R	M	C	M	M	C	C	C	M
Mineral	Cpx	Cpx	Cpx	Cpx	Opx	Opx	Cpx	Cpx	Cpx	Opx
SiO_2 (wt.%)	50.45	48.74	53.45	51.32	54.08	52.14	51.53	51.13	51.00	50.36
TiO_2	0.41	0.69	0.19	0.52	0.07	0.09	0.34	0.34	0.33	0.18
Cr_2O_3	0.37	0.16	0.01	b.d.	0.03	b.d.	0.05	0.03	b.d.	0.01
Al_2O_3	3.34	5.30	1.64	3.45	1.44	1.70	2.62	2.59	2.61	1.97
FeO*	6.41	6.45	5.14	5.85	14.83	16.26	11.05	12.07	12.12	24.22
MnO	0.16	0.14	0.20	0.20	0.37	0.47	0.44	0.45	0.37	0.71
MgO	15.30	14.40	16.36	15.23	29.32	27.69	12.69	12.97	12.98	18.66
CaO	22.55	22.29	23.46	23.13	0.48	1.18	21.41	20.17	20.02	4.13
Na_2O	0.47	0.55	0.08	0.16	b.d.	b.d.	0.47	0.43	0.38	0.04
Total	99.47	98.70	100.53	99.86	100.61	99.54	100.61	100.18	99.80	100.32
Mg/(Mg+Fe)	0.810	0.799	0.850	0.823	0.779	0.752	0.672	0.657	0.656	0.579
Ba (ppm)	b.d.	b.d.	b.d.	0.66			b.d.	b.d.	b.d.	
Th	0.062	0.134	0.005	0.007			0.148	0.132	0.142	
U	0.025	0.043	0.002	b.d.			0.046	0.041	0.059	
Pb	0.16	0.18	0.08	0.04			0.18	0.15	0.18	
Nb	b.d.	0.11	b.d.	b.d.			b.d.	b.d.	b.d.	
Ta	b.d.	0.01	b.d.	b.d.			0.02	0.01	b.d.	
La	3.10	5.53	0.25	0.41			3.68	3.50	3.64	
Ce	10.10	19.11	1.09	2.10			16.70	15.62	17.17	
Sr	165.4	166.5	26.9	36.6			33.4	31.0	33.6	
Pr	1.86	3.62	0.24	0.52			3.59	3.39	3.64	
Nd	10.09	19.99	1.51	3.51			21.59	20.52	21.33	
Hf	0.67	1.68	0.20	0.43			2.16	2.29	2.05	
Sm	2.86	5.52	0.52	1.60			7.37	7.14	7.28	
Zr	13.7	38.1	3.2	7.8			60.3	61.3	56.3	
Eu	0.82	1.61	0.25	0.56			1.25	1.12	1.23	
Gd	2.68	5.35	0.63	2.16			9.02	8.71	8.45	
Tb	0.33	0.67	0.11	0.34			1.42	1.38	1.33	
Dy	1.68	3.55	0.62	2.11			8.81	8.59	8.33	
Y	7.6	16.5	3.3	9.9			46.6	46.4	41.3	
Ho	0.32	0.68	0.15	0.45			1.82	1.76	1.68	
Er	0.82	1.70	0.40	1.19			5.35	5.16	4.81	
Tm	0.11	0.24	0.05	0.16			0.73	0.72	0.68	
Yb	0.66	1.36	0.35	0.92			4.95	4.61	4.37	
Lu	0.09	0.21	0.06	0.14			0.73	0.71	0.66	

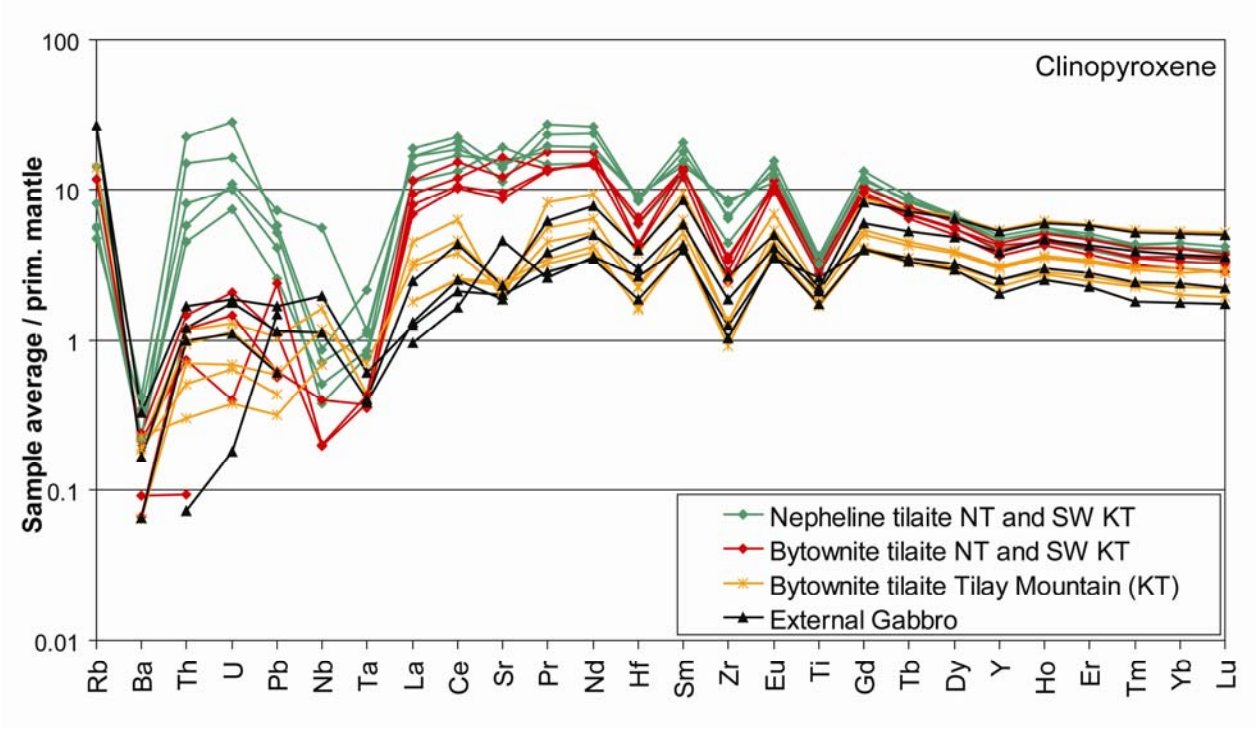

Fig. 6: Sample-averaged trace element concentrations in clinopyroxene from mafic rocks from Uralian-Alaskan-type complexes. Data are normalized to the primitive mantle of Hofmann (1988). Note the variations of the trace element compositions between the samples from different lithological groups and the rather constant HREE abundances if compared to the LREE.

Clinopyroxene from nepheline tilaites has the most evolved composition because it is enriched in U, Th, Pb and LREE compared to other lithologies Fig. 6). As a result they have the highest LREE/HREE, for example La/Lu of 20-55 (Fig. 7a). Clinopyroxene in bytownite and nepheline tilaites from the same sample location have similar REE patterns. However, the bytownite tilaites tend to have lower LREE/HREE (La/Lu 17-35; Fig. 7), and remarkably, up to one order of magnitude lower U, Th and Pb concentrations (Fig. 6). Clinopyroxene in the tilaites from Tilay Mountain and from the external gabbro have the lowest Th, U, Pb, and (L)REE concentrations and the lowest LREE/HREE, for example La/Lu of 3-17 (Fig. 6, 7a). MREE/HREE in clinopyroxene, for example Gd/Lu, shows variations similar to those observed for LREE/HREE (Fig. 7b).

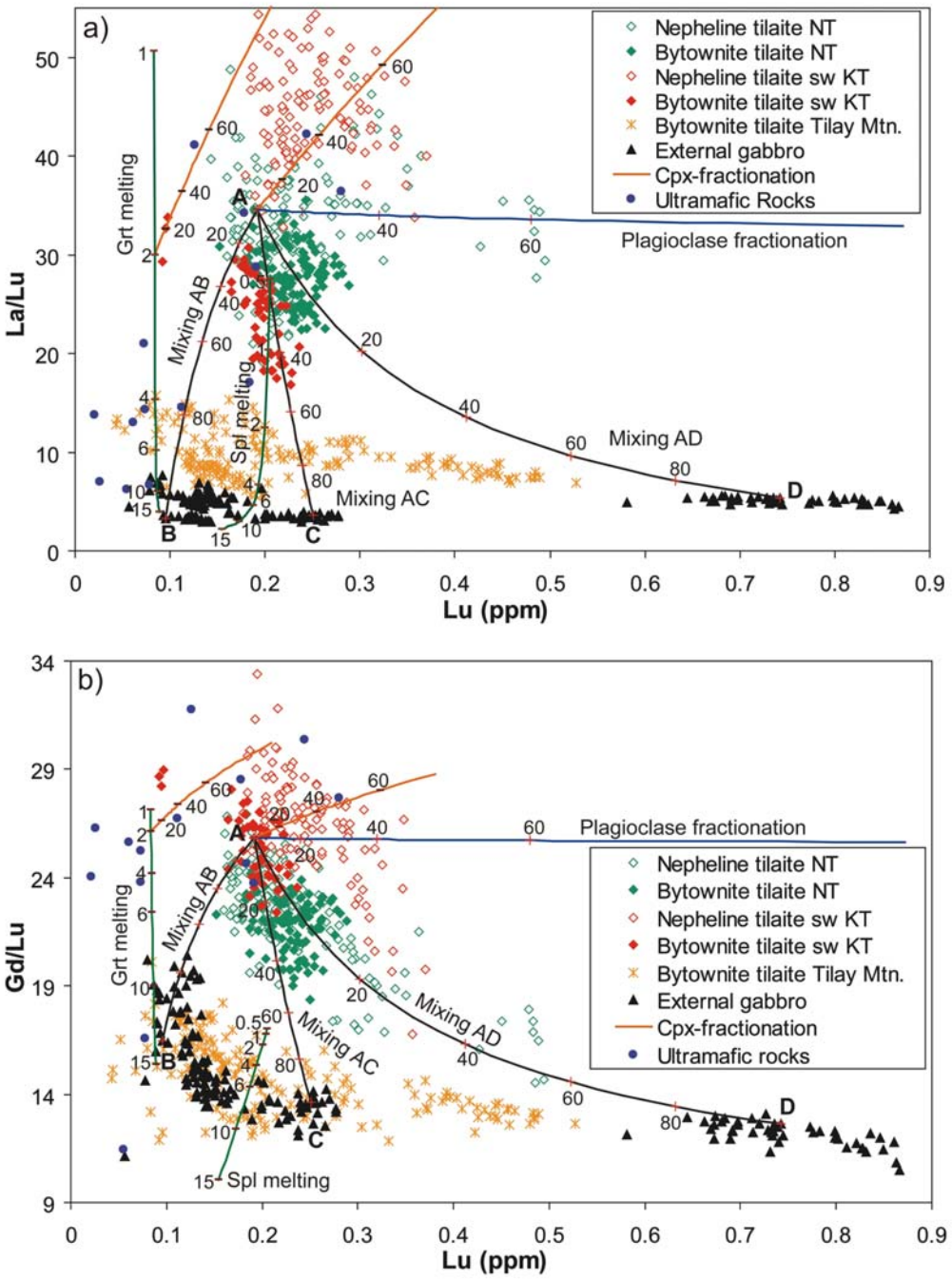

Fig. 7: Variation diagrams for trace element ratios and concentrations in clinopyroxene from mafic rocks. (a) Variation of Lu and La/Lu. Fractionation trends are shown for clinopyroxene (orange lines) and plagioclase (blue line). Ticks represent the degree of fractionation (%). Green lines represent the composition of the first clinopyroxene in equilibrium with a melt produced by garnet field melting and spinel field melting (after Salters and Stracke (2004)). Ticks represent the degree (%) of partial melting. The mantle source is assumed to be enriched in LREE (La = 1.91* primitive mantle, Gd = 1.33 *primitive mantle, Lu = primitive mantle after Hofmann (1988). Black lines represent the composition of the first clinopyroxene fractionated from a mixture of Alaskan type magma (A) with tholeiitic melt at various degrees of fractionation (B, C, D; ticks represent the fraction (%) of the components B, C, D). (b) Variation of Lu and Gd/Lu; lines are defined as in a). Partition coefficients for Cpx/melt are from Ionov et al. (1997).

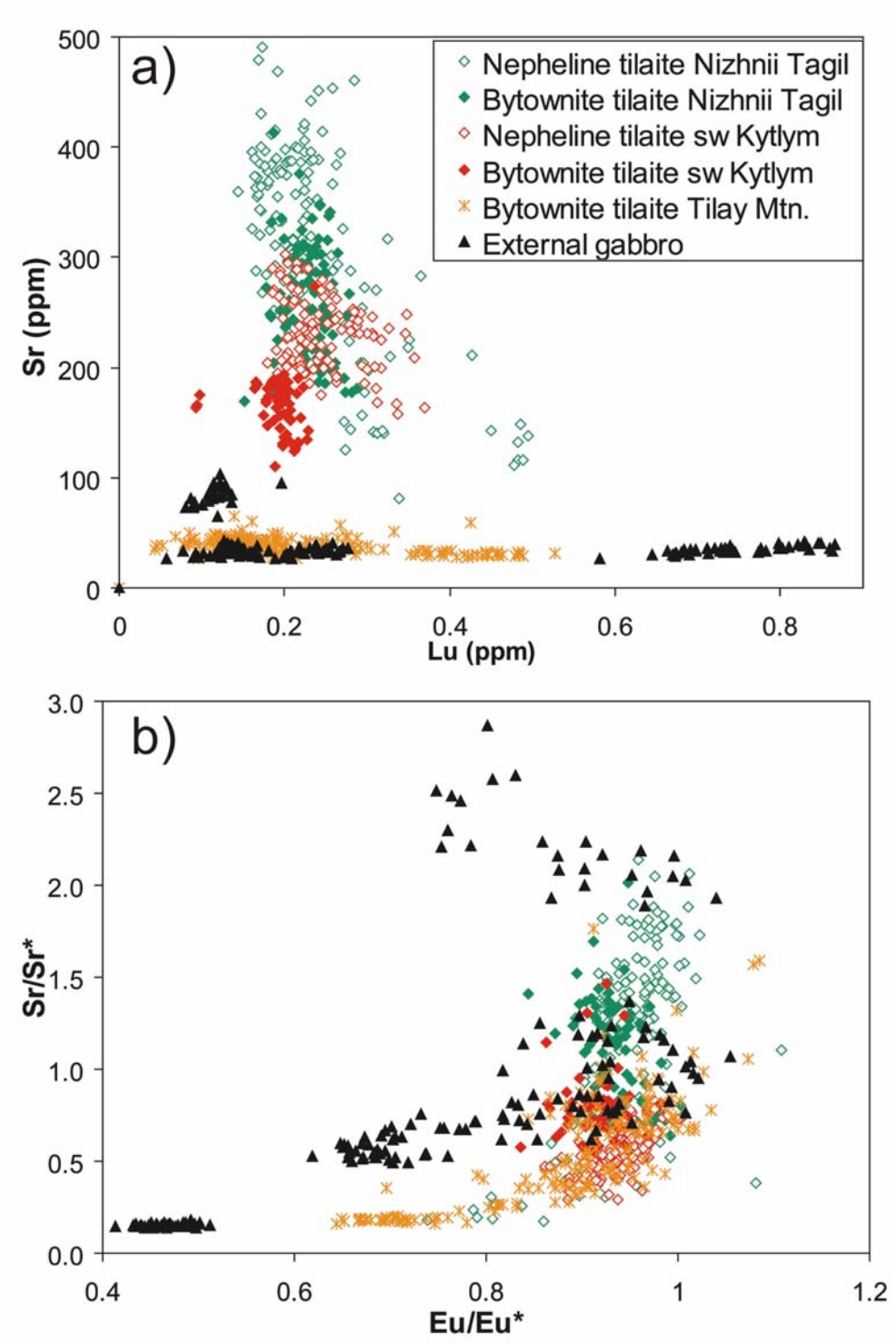

Fig. 8: (a) Variation of Lu and Sr concentrations in clinopyroxene from mafic rocks. (b) Variation of Eu_N/Eu^* and Sr_N/Sr^* in the mafic rocks ($Eu^* = (Sm_N^2+Gd_N^2)^{0.5}$, $Sr^* = (Ce_N^2+Pr_N^2)^{0.5}$). Note the large variation in the Sr contents similar to the LREE among the different lithologies.

At least two different compositional fields can be defined using the REE abundances, because clinopyroxenes from the external gabbro of the Valentorka, Serebryanka and Sukhogorsk blocks in E Kytlym and from Tilay Mountain have much lower Gd/Lu and La/Lu than the remaining tilaites (Fig. 7). The low concentrations of HREE and the large variation of Gd/Lu signify fractionation of HREE, and suggest the involvement of garnet during magma formation. In all lithologies Lu concentrations vary by more than a factor of two and La/Lu and Gd/Lu generally decreases with increasing Lu. These variations cannot be reasonably explained by simple fractional crystallization of plagioclase and/or clinopyroxene (Figs. 7a, b)

Similarly, Sr contents of clinopyroxene vary widely, both among and within the different lithologies (Fig 8a). In the nepheline tilaites clinopyroxene has the highest Sr concentrations of 80-490 ppm. The variable Sr concentrations monitor a rapid decrease of Sr in the parental melt, due to the crystallization of feldspar and nepheline. Clinopyroxenes from the external gabbro of the Sukhogorskaya Association and from Tilay Mountain have distinctively lower Sr concentrations (<100 pmm) over a large range of fractionation (Fig. 8a). The low Eu_N/Eu^* (1.04-0.4) supports the presence of plagioclase either simultaneously or even prior to the crystallization of clinopyroxene (Fig. 8b).

The variation in the trace elements delimits two major, compositionally different groups. Moreover chemical differences between the nepheline tilaites in Nizhnii Tagil and southwest Kytlym also indicate regional variations in the composition of the parental melt. For example, clinopyroxene in nepheline tilaite from Nizhnii Tagil has lower LREE/HREE and MREE/HREE and shows a wide variation in Sr, Sr/Sr* and Eu/Eu* at similar Lu concentrations and Mg#, if compared with clinopyroxene in nepheline tilaite from southwest Kytlym (Figs. 7 and 8, Tab. 2).

Variations of the Cpx composition on the scale of a thin section

Single grains of clinopyroxene phenocrysts in all rock types show strong compositional variations in major and trace elements, which is interpreted to be of magmatic origin. The zoning is also recognizable as concentric zones with variable amounts of Ti-

magnetite exsolutions. Thus, geochemical and petrographic observations identified clinopyroxenes with different concentric zonation patterns and different distributions of mineral inclusions on the scale of a single thin section (Fig. 9).

In a bytownite tilaite from Tilay Mountain (KT325) grain 1 has an innermost core with many inclusions of spinel, some olivine (Fo=66-68) and phlogopite but no orthopyroxene is enclosed. It is rich in Cr and poor in Fe and Al (Fig. 9a, c). This core is concentrically surrounded by an area with high Al and Fe and lower Cr contents and fewer inclusions of spinel, olivine, orthopyroxene and plagioclase. The rim has only few inclusions of olivine, orthopyroxene and plagioclase at low concentrations of Cr and Al and high concentrations of Fe.

Clinopyroxene grain 2 has an inner zone containing rarely inclusions of orthopyroxene and olivine (Fo=70) It has low to intermediate contents of Cr, Al and Fe and is surrounded by a rim with few inclusions of olivine, orthopyroxene and plagioclase and even lower concentrations of Cr and Al and elevated Fe contents (Fig. 9b, d).

Trace element profiles for both clinopyroxene grains show similar parallel patterns for all REE and HFSE, as concentrations increase from the core towards the rim (Fig. 9e, f). However, the LREE/HREE variation, for example La/Lu, differs: in grain type 1 La/Lu is high in the core decreasing towards the rim, whereas it is low in the core of grain type 2 and increases towards the rim. Similarly, U and Th concentration are correlated, but their distribution differs among the two grain sections and follows that of La/Lu. The diverse trace element characteristics in the core of the clinopyroxenes imply that the cores crystallized from different parental melts. Interestingly, type 1 clinopyroxene has no inclusions of orthopyroxene in the core. It also has high Sr concentrations and La/Lu ratios similar to clinopyroxenes in the ultramafic rocks (Krause et al., 2007), whereas the type 2 clinopyroxene shows a strong affinity to the external gabbro (Figs. 7, 8, 9).

The rims of both clinopyroxene phenocryst types have very similar trace element and major element abundances as well as La/Lu ratios. These are also indistinguishable from the composition of clinopyroxene grains in the matrix. This observation suggests that both the rim of the clinopyroxene phenocrysts and the matrix clinopyroxenes crystallized from one common melt.

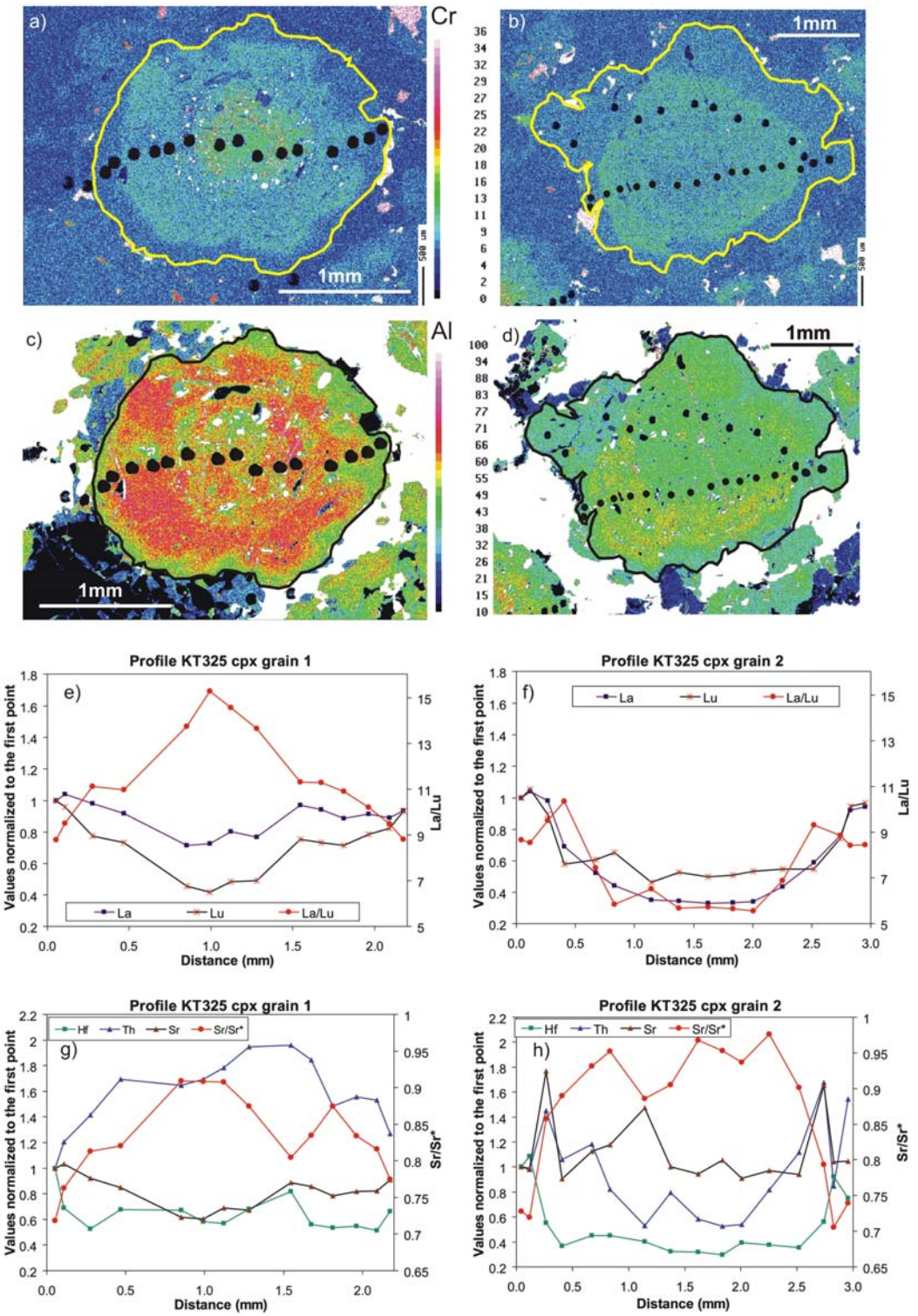

Fig. 9: Chemical zoning in clinopyroxene phenocrysts on thin section scale. X-ray element concentration maps show the Cr (a, b) and Al (c, d) distribution in two phenocrysts in a bytownite tilaite from Tilay Mountain, Kytlym (sample KT325). Black dots represent the LA-ICPMS- spots. Profiles for La, Lu and La/Lu (e, f) and for Hf, U, Sr and Sr/Sr* (g, h); Sr* = $(Ce_N^2+Pr_N^2)^{0.5}$. Concentrations in the profiles are normalized to the concentration at the first point of the profile. Note the presence of clinopyroxene cores with different major and trace elements compositions within the same sample.

Eu_N/Eu^* and Sr_N/Sr^* decrease from the core towards the rim in both clinopyroxene types and reflect decreasing Sr and Eu concentrations in the parental magma due to the crystallization of plagioclase (Figs. 9g, h). In the core of both grains Eu_N/Eu^* is close to unity, which indicates that plagioclase is not at the liquidus during the early stages of clinopyroxene crystallization.

Whereas these grains display continuous geochemical variations indicating a continuous change of the magma composition, clinopyroxene grains from sample NT-8 (nepheline tilaite, Nizhnii Tagil) show sudden changes of trace element concentrations and ratios (Fig. 10c). The narrow centre, characterized by high REE and Th, La/Lu but low Sr and Sr/Sr*, is surrounded by a ca. 1mm wide zone with significantly lower REE, Th, La/Lu but high Sr and Sr/Sr* (Fig. 10). Towards the rim REE, HFSE, U concentrations and La/Lu increase again, whereas Sr and Sr/Sr* decrease. These features suggest that this grain crystallized from at least three different, discrete magma batches.

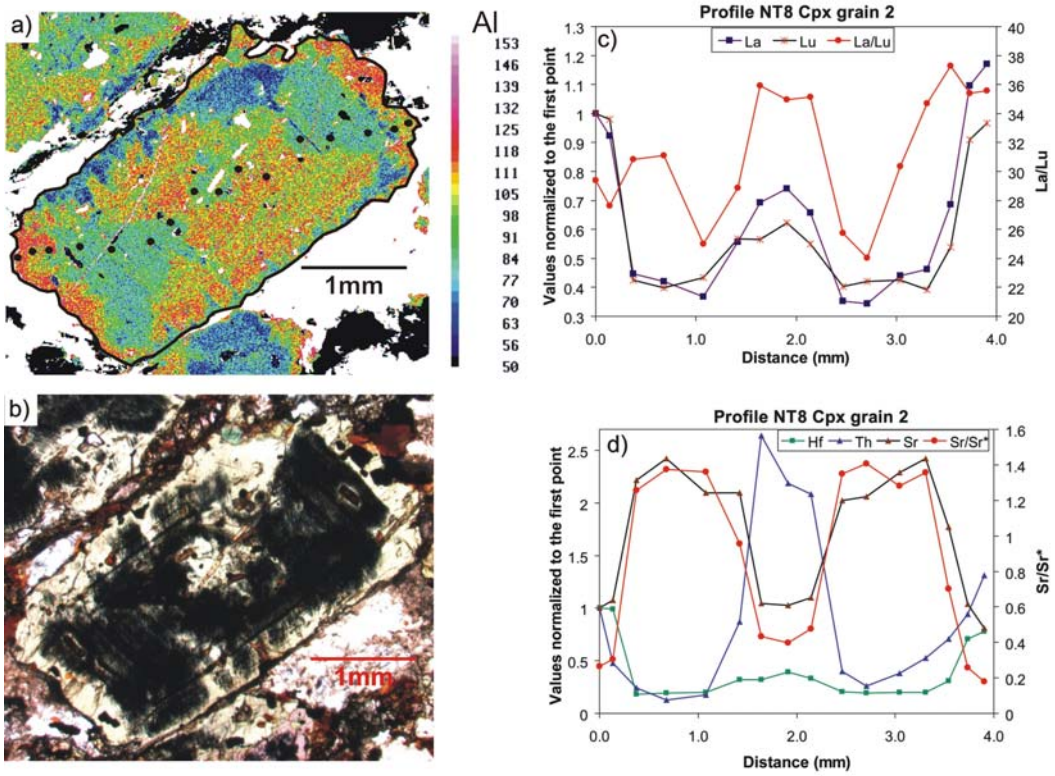

Fig. 10: Complex chemical zoning in a clinopyroxene phenocryst in a nepheline tilaite from Nizhnii Tagil (NT8). X-ray element concentration map for Al (a) and transmitted light image (b) show an hour glass zonation. Black dots represent the LA-ICPMS spots. Profiles for La, Lu and La/Lu (c) and Hf, U, Sr and Sr/Sr* (d); $Sr^* = (Ce_N^2+Pr_N^2)^{0.5}$. Concentrations in the profiles are normalized to the concentration at the first point of the profile. Note the presence of numerous Ti-magnetite exsolutions and the sudden compositional changes in the clinopyroxene reflecting the magmatic zonation.

3.2.2 Chemical composition of olivine

Olivine is present as xenomorphic to hypidiomorphic interstitial grains in all samples except the most fractionated external gabbros. In many samples olivine also occurs as idiomorphic to hypidiomorphic, often prismatic inclusion in clinopyroxene. Large hypidiomorphic olivine phenocrysts are restricted to the bytownite tilaites from Tilay Mountain (Kytlym). The forsterite (Fo) content in these olivines is variable (Fo 66-87), but is more homogeneous in the other lithologies (nepheline tilaite Nizhnii Tagil: Fo 75-84; nepheline tilaite southwest Kytlym: Fo 73-82; bytownite tilaite Nizhnii Tagil: Fo 77-80; bytownite tilaite southwest Kytlym: Fo 75-81; external gabbro: Fo: 68-78) (Fig. 11; Tab. 3).

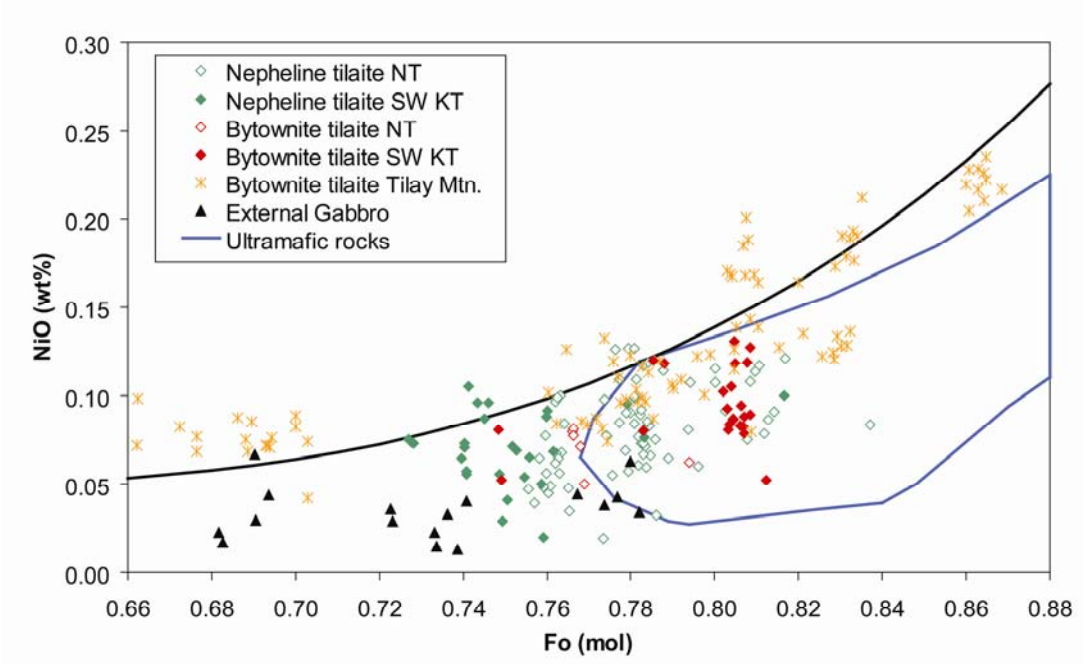

Fig. 11: Variation of NiO and Mg/(Mg+Fe) in olivine from mafic rocks of the Uralian- Alaskan-type complexes in the UPB. Data for ultramafic rocks are from Krause et al. (2007). The global trend is a regression line (black) based on olivine of destructive plate margins; data are taken from the GEOROC-database (http://georoc.mpch-mainz.gwdg.de/georoc/). Note that most of the olivines in Uralian-Alaskan-type complexes of the UPB lie below this trend.

Olivine enclosed in clinopyroxene phenocrysts often has higher Fo contents than interstitial olivine (Tab. 3). The NiO content in olivine of tilaites from Nizhnii Tagil and SW Kytlym varies between 0.03 and 0.14 wt.%. Olivine in the external gabbro has the lowest NiO contents >0.07 wt.%. In olivine from tilaites at Tilay Mountain, NiO increases

systematically from 0.08 wt.% at low Fo contents to 0.24 wt.% at high Fo contents (Fig. 11). Olivine with Fo >85 is enclosed in the core of large clinopyroxene (Tab. 3). While the composition of olivine in the tilaites from Tilay Mountain closely matches the trend calculated for olivines from convergent margin settings, olivine in tilaites from Nizhnii Tagil and SW Kytlym has systematically lower NiO at a given Fo and extends the trend observed in the ultramafic rocks (Krause et al., 2007; Fig. 11). The decrease in NiO with decreasing Fo is consistent with crystal fractionation in a cooling magma (Fig. 11).

Tab. 3: Olivine composition of selected samples from Uralian-Alaskan-type complexes FeO* = all iron measured as FeO. NT = Nizhnii Tagil, SW KT = southwest Kytlym, Til KT = Tilay Mountain, Kytlym, E-KT = External gabbro. IC = inclusion in clinopyroxene, M = Matrix, b.d. = below limit of detection.

Sample	04NT8-190	04NT8-223	KT46-66	KT46-68	PE-910-1-182 b	PE-910-1-211	NT 213-62	KT44-247	KT44-300	KT45b-215
Locality	NT	NT	SW KT	SW KT	SW KT	SW KT	NT	SW KT	SW KT	SW KT
Lithology	NeTi	NeTi	NeTi	NeTi	NeTi	NeTi	ByTi	ByTi	ByTi	ByTi
Position	M	IC	IC	IC	M	IC	M	IC	M	M
SiO_2 (wt.%)	38.29	39.90	38.49	38.31	38.64	39.44	38.97	38.97	38.79	38.44
TiO_2	b.d.	b.d.	b.d.	b.d.	b.d.	b.d.	b.d.	b.d.	b.d.	b.d.
Cr_2O_3	0.02	0.02	0.03	0.02	0.01	0.01	0.01	0.07	0.04	0.02
Al_2O_3	0.04	b.d.	b.d.	b.d.	b.d.	b.d.	0.05	b.d.	b.d.	b.d.
FeO*	23.91	16.96	22.65	24.97	22.20	19.96	21.41	20.24	18.22	23.40
MnO	0.61	0.51	0.53	0.56	0.58	0.61	0.51	0.35	0.35	0.41
MgO	37.34	42.75	38.15	36.19	39.15	40.44	40.18	39.75	41.82	37.89
CaO	0.03	0.14	0.09	0.07	0.03	0.07	0.04	0.05	0.03	0.03
NiO	0.08	0.08	0.07	0.08	0.05	0.08	0.07	0.08	0.13	0.08
Total	100.45	100.42	100.12	100.28	100.70	100.65	101.30	99.56	99.42	100.30
Mg/(Mg+Fe)	0.736	0.818	0.750	0.721	0.759	0.783	0.770	0.778	0.804	0.743

Sample	04KT50-140	04KT50-167	KT50-518	KT 320-95	KT321-50	KT324-183	KT325-233	04KT53-268	PE324-272	PE 325-90
Locality	Til KT	Til KT	Til KT	Til KT	Til KT	Til KT	Til KT	E KT	E KT	E KT
Lithology	ByTi	ByTi	ByTi	ByTi	ByTi	ByTi	ByTi	ExGb	ExGb	ExGb
Position	M	IC	IC	M	M	M	M	M	M	M
SiO_2 (wt.%)	38.79	39.70	39.01	37.96	38.17	39.35	37.54	38.07	37.67	37.29
TiO_2	b.d.	b.d.	b.d.	b.d.	b.d.	b.d.	b.d.	b.d.	b.d.	0.04
Cr_2O_3	b.d.	0.01	0.01	b.d.	b.d.	b.d.	b.d.	b.d.	b.d.	b.d.
Al_2O_3	b.d.	0.04	b.d.	b.d.	b.d.	b.d.	b.d.	b.d.	b.d.	b.d.
FeO*	18.74	13.37	15.64	22.41	21.41	18.07	26.63	22.58	24.86	28.54
MnO	0.31	0.19	0.26	0.45	0.38	0.42	0.41	0.39	0.39	0.46
MgO	42.89	47.59	44.49	39.87	39.02	42.80	35.33	40.08	38.84	34.26
CaO	0.03	0.06	0.02	0.03	0.04	b.d.	0.11	0.02	b.d.	0.07
NiO	0.17	0.22	0.21	0.10	0.13	0.14	0.04	0.04	0.02	b.d.
Total	100.93	101.18	99.65	101.05	99.15	100.78	100.07	101.18	101.79	100.66
Mg/(Mg+Fe)	0.803	0.864	0.835	0.760	0.765	0.809	0.703	0.760	0.736	0.682

3.2.3 Chemical composition of feldspar and nepheline

The mineralogy and chemistry of the feldspars most effectively discriminate the different lithologies (Fig. 12). Representative feldspar and nepheline analyses can be found in Tab. 4. Alongside with an intermediate plagioclase (An = 28-48 mol.%; Or = 0-10 mol.%) the nepheline tilaites contain K-feldspar (An = 0-8 mol.%; Or 47-98 mol.%) and nepheline with a low kalsilite component in a fine grained symplectitic intergrowth around the plagioclase (Fig. 12a, b). These intergrowths of nepheline and K-feldspar are described in previous studies as “pseudoleucite” and have been interpreted as breakdown products of leucite forming K-feldspar and nepheline (e.g. Bowen, 1928) However Gittins et al. (1980) suggested confining the use of the term pseudoleucite to intergrowths of nepheline and K-feldspar which display the crystal morphology of leucite.

In the nepheline tilaites from Nizhnii Tagil nepheline + K-feldspar in symplectitic intergrowth seem to replace plagioclase and thus can not be called pseudoleucite. These intergrowths also do not show the crystal morphology of leucite. In addition the low kalsilite component in the nepheline (17.7 – 22.8 wt.%) from the nepheline tilaites precludes an equilibrium or a reaction relationship with leucite (Fig. 12b). Besides the intergrowths with K-feldspar nepheline is also present in larger hypidiomorpic grains in the nepheline tilaites from Nizhnii Tagil and southwest Kytlym.

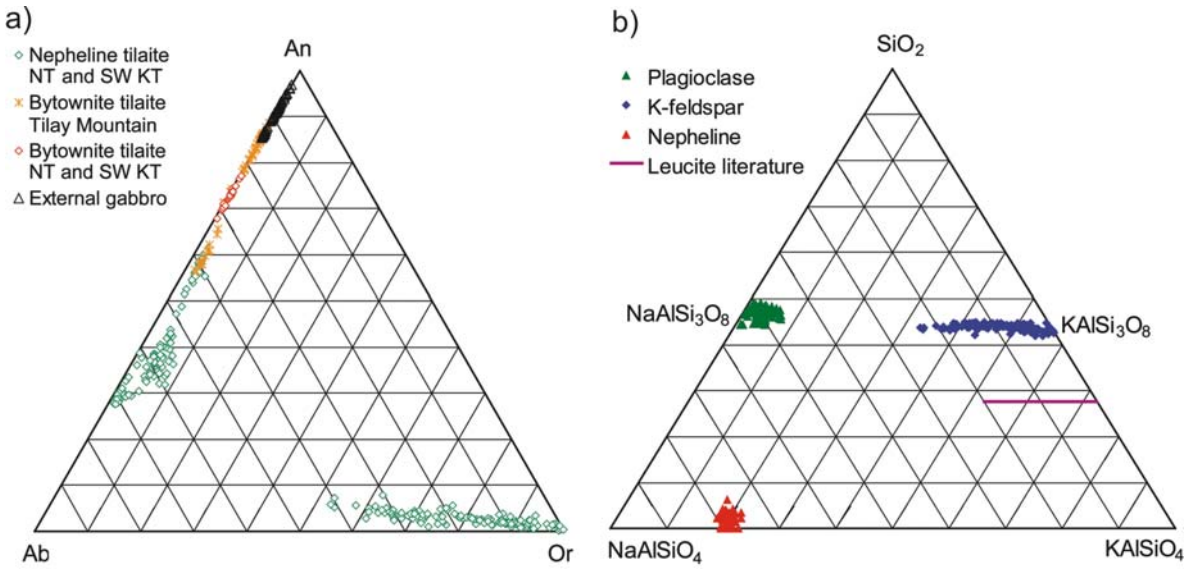

Fig. 12: An-Ab-Or variation diagram (a) and compositions of feldspars and nepheline from the mafic rocks in the quartz-nepheline-kalsilite space (b). The composition of leucite is taken from Deer et al. (1992). Note that due to the low K_2O in nepheline the intergrowth of nepheline + K-feldspar in some nepheline tilaites can not be explained as a replacement product of leucite.

Tab. 4: Major and trace elements in selected feldspar and nepheline in Uralian-Alaskan-type complexes. FeO* = all iron measured as FeO. NT = Nizhnii Tagil, SW KT = southwest Kytlym, Til KT = Tilay Mountain, Kytlym, E-KT = External gabbro. Ne = nepheline, K-fs = K-feldspar, Plg = plagioclase, b.d. = below limit of detection.

Sample	NT8-353	NT9b-11	PE 597-502	KT46-304	NT8-65	NT9b-29	PE 597-468	PE 910-454	NT8-325	NT9b-54
Locality	NT	NT	NT	SW KT	NT	NT	NT	SW KT	NT	NT
Lithology	NeTi	NeTi	NeTi	NeTi	NeTi	NeTi	NeTi	NeTi	NeTi	NeTi
Mineral	Ne	Ne	Ne	Ne	K-fs	K-fs	K-fs	K-fs	Plg	Plg
SiO_2 (wt.%)	42.56	43.82	42.47	43.53	63.57	64.79	64.10	60.96	59.81	60.17
Al_2O_3	33.09	33.40	34.31	32.96	19.66	19.04	19.75	21.31	24.81	24.60
FeO*	0.07	0.06	0.12	0.25	0.04	0.01	0.03	0.40	0.06	b.d.
MgO	0.01	b.d.	1.28	0.02	b.d.	b.d.	0.72	2.64	0.01	b.d.
CaO	2.59	1.40	5.99	1.67	0.91	0.43	12.27	11.12	5.85	5.70
K_2O	5.47	5.02	15.25	5.00	10.98	12.64	2.42	2.20	0.22	0.24
Na_2O	15.20	15.89	0.00	15.30	3.32	2.40	0.52	0.68	7.58	7.64
Total	98.99	99.65	99.46	98.73	98.91	99.59	100.24	0.00	98.38	98.45
An	-	-	-	-	7	2	4	2	29	29
Or	-	-	-	-	49	76	74	57	1	1
Rb (ppm)	44.21	75.26	82.47	54.04	143.31	167.11	163.94	143.46	12.09	b.d.
Ba	505.83	164.78	537.14	b.d.	2294.84	1244.70	2128.45	366.58	279.66	139.72
Th	b.d.	b.d.	b.d.	0.3930	0.0132	b.d.	b.d.	0.0055	0.0040	0.0100
U	b.d.	b.d.	b.d.	0.1671	b.d.	b.d.	0.0066	0.0192	0.0079	b.d.
Pb	9.87	3.57	5.80	0.35	44.61	36.58	28.15	12.02	16.63	12.83
La	2.26	1.25	0.63	3.08	5.60	2.88	2.38	1.39	13.61	5.55
Ce	1.81	1.16	0.47	6.08	4.07	2.16	1.52	2.20	14.00	7.52
Sr	1018.2	532.5	689.4	121.4	3613.6	3069.4	2864.6	1921.3	3229.7	2788.2
Pr	0.091	0.076	0.019	0.542	0.185	0.086	0.071	0.181	0.872	0.521
Nd	0.241	0.181	0.033	1.689	0.350	0.160	0.111	0.540	1.906	1.362
Sm	0.020	0.020	0.028	0.074	0.055	b.d.	b.d.	0.058	0.106	0.085
Eu	0.085	0.076	0.078	0.028	0.539	0.351	0.356	0.308	0.419	0.392
Ti	27.5	30.0	39.7	28.8	152.0	129.5	119.5	34.8	101.5	109.4
Gd	b.d.	b.d.	b.d.	0.149	b.d.	b.d.	b.d.	0.038	0.048	0.074
Tb	b.d.	b.d.	b.d.	0.028	b.d.	b.d.	b.d.	b.d.	b.d.	b.d.

Bytownite tilaites in Nizhnii Tagil and southwest Kytlym contain plagioclase with a narrow compositional range (An = 68-77 mol.%; Or <1 mol.%; Fig. 12a). Plagioclase in the bytownite tilaites from Tilay Mountain have higher An contents (An = 71-89 mol.%), except one sample (KT325 An = 56-80 mol.%). Plagioclase from the external gabbro of the Valentorka, Serebryanka and Sukhogorsk blocks in E-Kytlym has the highest An contents (85-97 mol.%; Fig. 12a).

Mantle normalized patterns of the trace element concentrations in K-Feldspar, plagioclase and nepheline (sample average, Fig. 13) show positive anomalies for Rb, Ba, Pb, Sr and Eu, negative anomalies for Th and U and a continuous decrease from the LREE to the MREE. These are well established common features for these minerals (e.g. Masuda et al., 1972; Nagasawa, 1973; Masuda et al., 1976; Bindeman and Bailey,

Tab. 4: (cont.)

Sample	PE 910-508	KT46-123	KT44-264	KT50-187	KT321-47	KT325-249	KT322-162	KT53-275	PE325-83	PE431-183
Locality	SW KT	SW KT	SW KT	Til KT	Til KT	Til KT	Til KT	E KT	E KT	E KT
Lithology	NeTi	NeTi	ByTi	ByTi	ByTi	ByTi	ByTi	ExGb	ExGb	ExGb
Mineral	Plg	Plg	Plg	Plg	Plg	Plg	Plg	Plg	Plg	Plg
SiO_2 (wt.%)	57.58	58.32	49.83	46.55	47.18	53.49	47.79	44.03	46.25	45.27
Al_2O_3	25.92	26.27	33.01	33.49	32.85	28.57	34.12	35.59	33.74	34.59
FeO*	0.06	0.18	0.38	0.28	0.20	0.27	0.35	0.36	0.39	0.335
MgO	7.64	b.d.	0.03	0.01	b.d.	0.03	b.d.	b.d.	0.01	0.014
CaO	1.26	7.46	15.04	17.29	17.25	11.98	14.05	19.59	17.46	18.17
K_2O	6.07	1.16	0.03	0.02	0.04	0.46	b.d.	0.01	0.03	0.036
Na_2O	0.52	6.31	2.86	1.61	1.88	4.53	3.13	0.42	1.55	1.132
Total	99.58	99.75	101.21	99.27	99.42	99.34	99.47	100.03	99.49	99.547
An	38	38	74	86	83	59	71	96	86	90
Or	7	4	0	0	0	1	0	0	0	0
Rb (ppm)	9.25	b.d.	b.d.	b.d.	b.d.	b.d.	b.d.	b.d.	b.d.	b.d.
Ba	841.45	562.42	72.58	47.06	42.92	195.29	44.58	11.09	70.47	15.83
Th	b.d.	b.d.	b.d.	b.d.	b.d.	b.d.	b.d.	b.d.	b.d.	b.d.
U	b.d.	b.d.	b.d.	b.d.	b.d.	b.d.	b.d.	b.d.	b.d.	b.d.
Pb	15.26	13.13	2.25	0.44	0.43	1.90	0.64	0.19	1.06	1.37
La	11.76	11.87	5.52	1.66	1.52	3.89	1.25	0.25	1.18	0.61
Ce	12.54	13.82	6.94	2.68	1.98	5.42	1.49	0.42	2.09	0.97
Sr	4645.2	3556.9	3868.4	922.8	1218.3	1105.4	955.6	813.6	1059.6	2074.4
Pr	0.951	0.952	0.682	0.274	0.189	0.499	0.164	0.038	0.216	0.110
Nd	2.460	2.124	1.986	1.037	0.692	1.575	0.531	0.156	0.707	0.351
Sm	0.198	0.238	0.185	0.180	0.064	0.191	b.d.	0.011	0.092	0.059
Eu	0.686	0.610	0.467	0.254	0.270	0.694	0.167	0.153	0.312	0.174
Ti	202.6	232.5	48.8	216.2	22.0	150.2	36.6	b.d.	39.8	14.8
Gd	0.124	0.076	0.039	0.301	0.047	0.101	b.d.	b.d.	0.123	b.d.
Tb	b.d.	b.d.	b.d.	0.032	b.d.	0.009	b.d.	b.d.	b.d.	b.d.

1999; Yokoyama et al., 2003; Kimura et al., 2003; Tepley et al., 2006). Plagioclase has 2-5 times higher concentrations of LREE and Sr than coexisting K-feldspar and nepheline. All coexisting feldspartoids have similar contents in Th, U, Pb and the MREE. K-feldspar has up to one order of magnitude higher concentrations in Rb and Ba (Fig. 13a), if compared with the coexisting Plagioclase (Fig. 13a, b). Trace element patterns of plagioclase in the bytownite tilaites and the external gabbros are parallel to the patterns of the nepheline gabbros for the MREE (Fig. 13b). Analogue to the observations in clinopyroxene, the Plagioclase in the mafic rocks has a fan-shape trace element distribution. Plagioclase in the bytownite tilaites and the external gabbros has systematically lower Ba, Pb and LREE, if compared to plagioclase in the nepheline tilaites (Fig. 13 b).

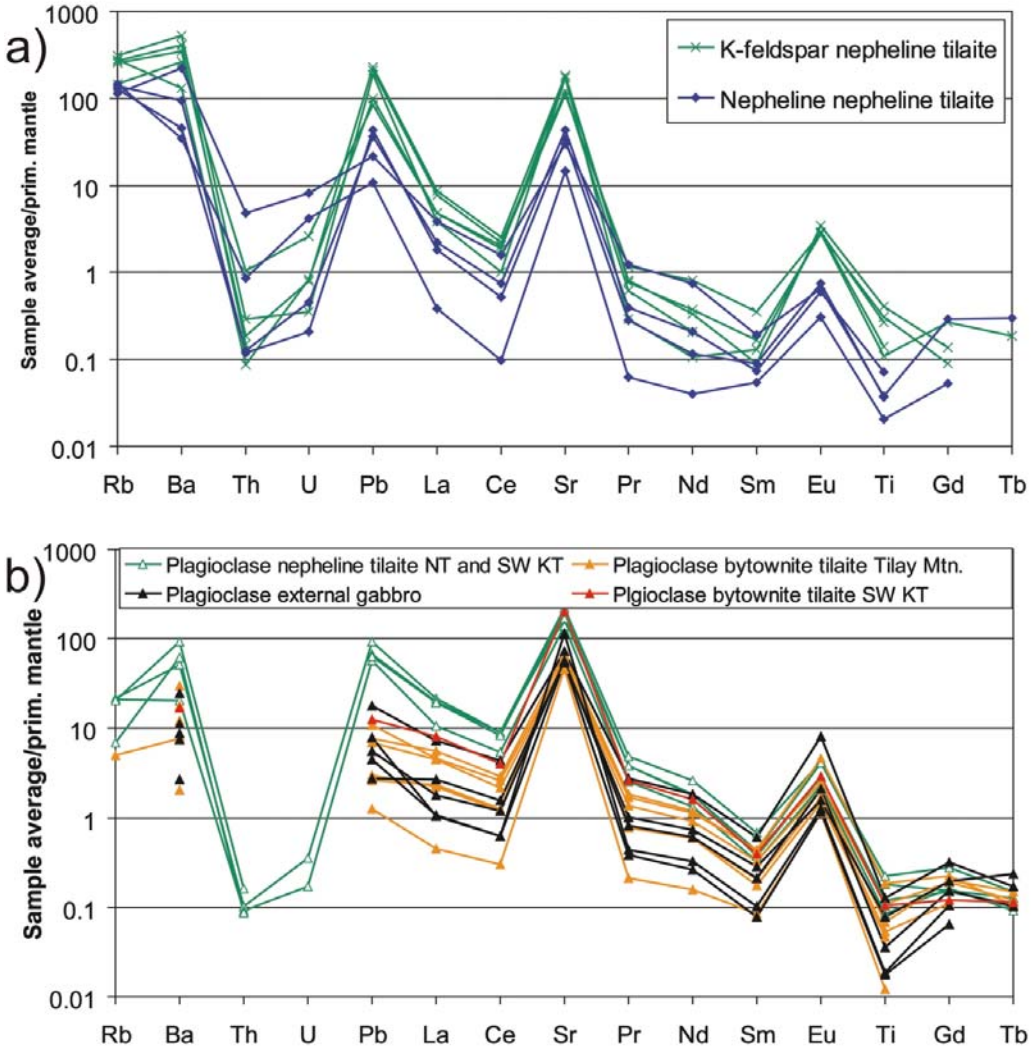

Fig. 13: Trace element concentrations (sample averages) in K-feldspar and nepheline (a) and plagioclase (b) from the mafic rocks in the UPB normalized to the primitive mantle of Hofmann (1988).

4 Discussion

Textural and structural observations in the ultramafic and mafic rocks of the Kytlym and in Nizhnii Tagil complexes indicate that they represent cumulates (Fershtater et al, 1999; Savelieva et al., 1999; Pertsev et al., 2000; Savelieva et al., 2002). The cumulative origin of mafic and ultramafic rocks in Uralian-Alaskan-type complexes has also been proposed for other intrusions of this type in the Ural Mountains and world wide (e.g. Irvine, 1967; Astrkahantsev et al., 1991; Hammack et al., 1992; Himmelberg and Loney, 1995; Ivanov and Shmelev, 1996; Batanova et al., 2005; Krause et al., 2007). The

positive anomalies for Ba, Sr and Eu in the whole rock samples from the external gabbros infer a cumulative origin for these rocks by the accumulation of plagioclase as well (Fig. 3).

Trace element concentrations, for example those of REE, play a key role in monitoring the fractionation of silicate melts. In particular in cumulate rocks, where there is no direct access to the melt composition, the trace element distribution in minerals provides a powerful tool to get information on the origin and evolution of parental melts. This can be done, for example, by calculating melt compositions using mineral–melt partition coefficients which are either experimentally determined or measured on natural samples assuming equilibrium. This approach also reveals the cumulate nature of the tilaitic and gabbroic rocks. The ratio of trace element concentrations of the melt calculated from the clinopyroxene abundances and measured in the whole rock varies greatly from 8 to more than 100. This implies that the whole rocks have either lost most of the liquid portion or that the liquid composition became diluted by the accumulation of minerals containing low amounts of incompatible trace elements. However, the compositional variations of the rock forming minerals reflect their derivation from magmas representing different degrees of partial melting and indicate a complex igneous plumbing system conveying at least two fundamentally different magma series.

4.1 Estimation of parental magma compositions

On a regional scale, the large variation of La/Lu among different complexes suggests that they are derived from parental melts representing different degrees of partial melting (Figs. 7, 14). Figures 7 and 14 show the composition of the first clinopyroxene crystallizing in equilibrium with a melt generated with melting models after Salters and Stracke (2004) presuming a garnet- or spinel-bearing mantle composition. The source is assumed to have Lu abundances of the primitive mantle after Hofmann (1988) and twice the amount of La. Partition coefficients for clinopyroxene/melt are from Ionov et al. (1997); partition coefficients for plagioclase/melt were calculated from average plagioclase coexisting with clinopyroxene (Tab. 5).

Tab. 5: Partition coefficients for clinopyroxene/melt and plagioclase/melt used for the calculation of the trace element concentration of parental melts and fractionation trends. Coefficients for clinopyroxene are from Ionov et al. (1997). Values for plagioclase were calculated from plagioclase NT9b-58 and clinopyroxene NT9b-340 assuming equilibrium.

	Ba	Th	U	Pb	La	Ce	Sr	Pr	Nd	Hf	Sm	Zr
Cpx/melt	0.0006	0.012	0.01	0.0087	0.044	0.084	0.124	0.124	0.173	0.29	0.28	0.164
Plg/melt	-	-	-	-	0.031	0.026	1.143	0.017	0.012	-	0.0074	-

	Eu	Ti	Gd	Tb	Dy	Y	Ho	Er	Tm	Yb	Lu
Cpx/melt	0.31	0.36	0.34	0.36	0.41	0.44	0.38	0.41	0.3	0.41	0.43
Plg/melt	0.059	-	0.0046	0.0009	-	-	-	-	-	-	-

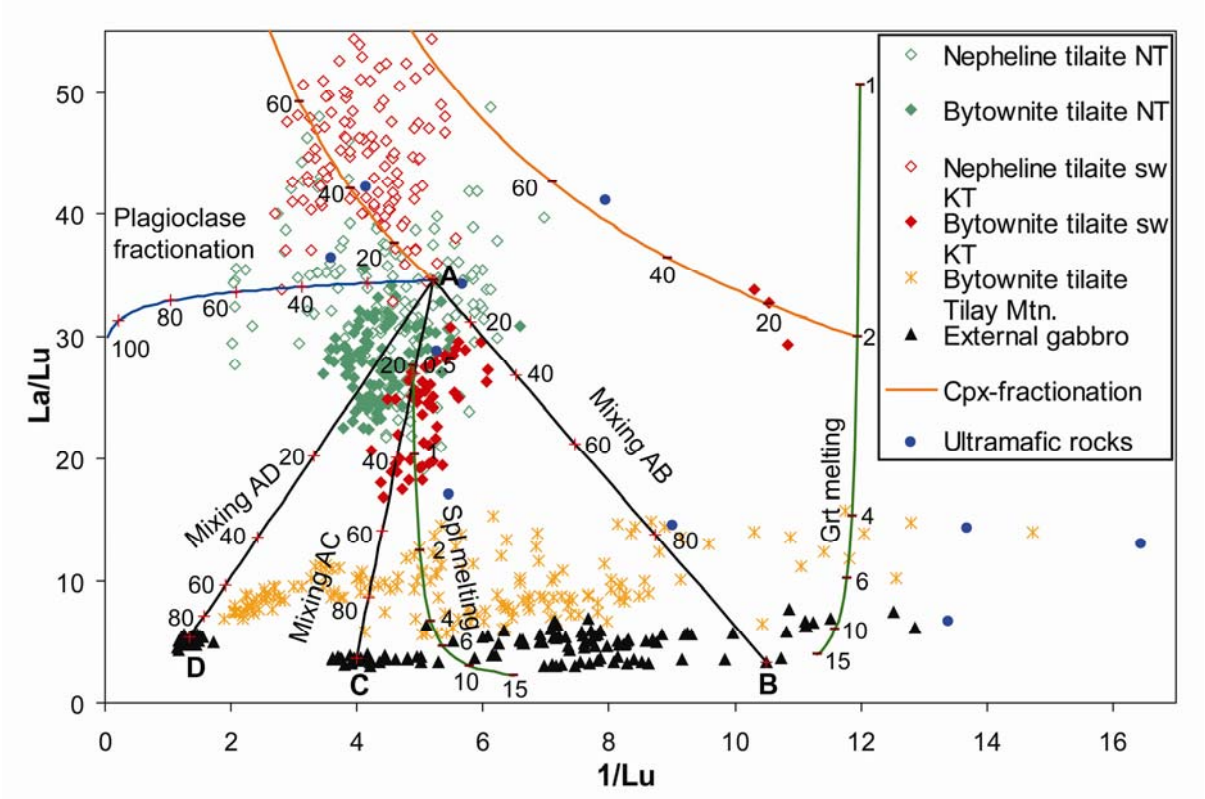

Fig.14: Model calculations describing the petrogenetic processes explaining the observed variation of 1/Lu and La/Lu of clinopyroxenes in mafic rocks from Uralian-Alaskan-type complexes in the Urals. Fractionation trends are shown for clinopyroxene (orange lines) and plagioclase (blue line). Green lines represent the composition of clinopyroxene in equilibrium with a melt produced by garnet field melting and spinel field melting (after Salters and Stracke, 2004). Ticks represent % degree of partial melting. The mantle source is assumed to be enriched in LREE (La = 1.91* primitive mantle, Gd = 1.33 *primitive mantle, Lu = primitive mantle after Hofmann (1988). Black lines represent the composition of clinopyroxene crystallized from a mixture of Alaskan-type magma (A) with a tholeiitic melt at various degrees of fractionation (B, C, D). Partition coefficients for Cpx/melt are from Ionov et al. (1997). Note that the trends observed in most of the groups can not be explained by a simple petrogenetic process and that magma mixing is the dominating process causing the observed chemical variation.

In particular the high Gd/Lu and the rather low Lu concentrations (<10-times primitive mantle) suggest the involvement of garnet during the partial melting process. A garnet melting model explains that the parental melts of the gabbroic samples – calculated from the composition of the most primitive clinopyroxene cores - have rather constant Yb or Lu concentrations (variation of Lu by a factor of 2.5), but have highly variable La concentrations which vary by more than a factor of 10 (Fig 15).

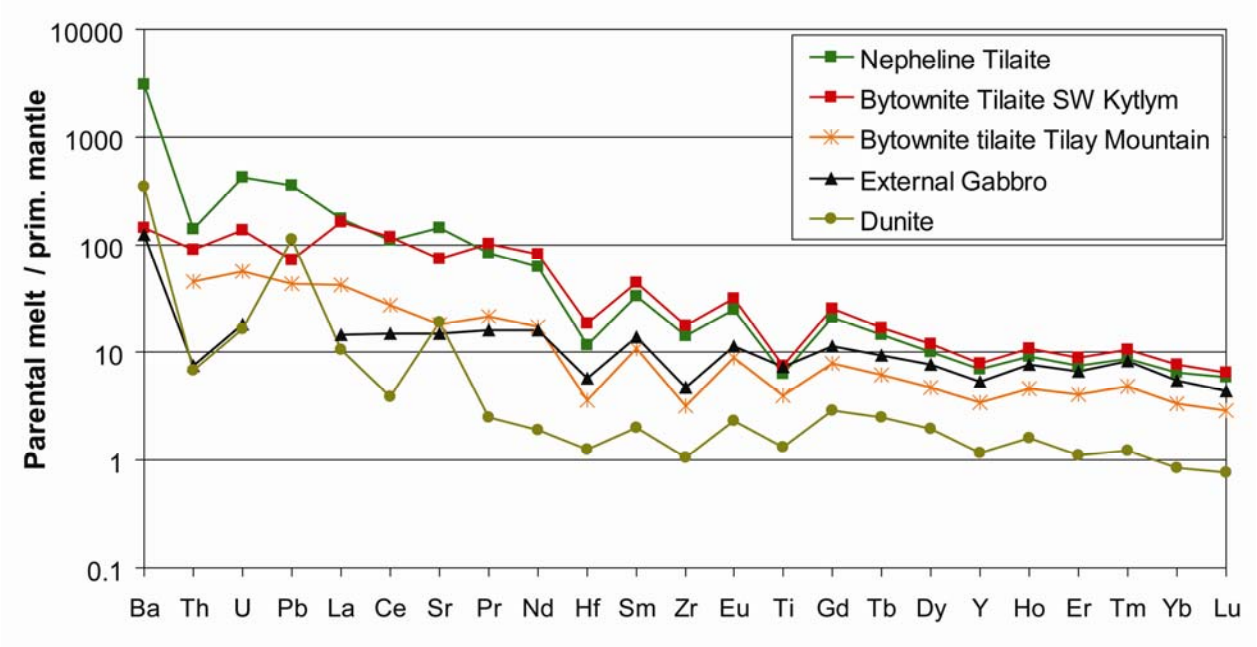

Fig. 15: Mantle normalized trace element concentrations in the parental melt coexisting with the cores of clinopyroxene from mafic rocks and interstitial clinopyroxene in a dunite. Partition coefficients for Cpx/melt are from Ionov et al. (1997). Note the parallel patterns in dunite and nepheline tilaite.

The most primitive clinopyroxenes of the external gabbro and some bytownite tilaites closely lie along a garnet melting trend and suggest melt fractions of 2-15% (Figs. 7, 14). However, due to their higher Lu concentrations the parental melts of the remaining tilaites can only be derived by partial melting in a garnet-bearing sources more enriched in REE. Alternatively, these tilaites melts are fractionation products of more primitive liquids lying along the melting curve and represent lower degrees of partial melting (2-4%; Fig. 7, 14). However, extremely large quantities of clinopyroxene crystallization (>60%; Fig. 7) are necessary until one attains the observed tilaite melt composition. Partial melting at lower pressure in the spinel field would be prone with similar shortcomings (Fig. 7, 14) and in addition would necessitate mantle compositions with

extreme REE depletion. For example, Lu abundances must be less than 0.3-times primitive mantle in order to explain the low Lu contents in the parental magmas of external gabbros and tilaites (Fig. 7, 14). Thus, no single model can explain the trace element variation in the parental magmas of the Uralian Alaskan-type complexes. These model calculations imply that the parental magmas forming the different complexes are probably derived by polybaric melting processes involving variable degrees of partial melting. They also suggest that they formed in mantle source having different trace element compositions. Even major element variability is likely considering the different chemical and mineralogical compositions of the tilaites and the external gabbros (Figs. 2, 3). Two end-member compositions can be inferred from the trace element abundances and they point out that these rocks do not have a common ancestor.

Composition A represents a melt that formed the cores of the clinopyroxene phenocrysts in the tilaites of Nizhnii Tagil and southwest Kytlym (Figs. 7, 8). They have high La/Lu of 30-35 at about 0.15 ppm Lu and high Sr and Na_2O concentrations (150-450 ppm, 0.5-1.2 wt.% respectively; Figs. 5, 7 and 8). The parental melt in equilibrium with these clinopyroxene cores (e.g. nepheline tilaite NT8) has a high LREE/HREE (e.g. La/Lu = 30.2), and high contents in incompatible elements like Ba, Th, U, Pb and Sr (Fig. 15). The presence of nepheline and the absence of orthopyroxene indicate that this melt is silica undersaturated. Furthermore the high content in Na and K in the whole rock (Fig. 2c) and the elevated Na contents in clinopyroxene and plagioclase (Figs. 5b, 11a) indicate the alkaline nature of this melt. The major and trace element composition of the cores of clinopyroxenes in the nepheline tilaites are very similar to those of the clinopyroxenes in the most evolved ultramafic rocks (Figs. 5 and 7a, b; Krause et al., 2007). Therefore, composition A represents the silica undersaturated, alkaline parental melt of the Uralian-Alaskan-type complexes in the Ural Mountains which during its evolution, likely along the line of a RFC process (Krause et al., 2007), formed the ultramafic cumulates prior to the emplacement of the tilaites (Fig. 7). Based on the chemical composition of minerals in the ultramafic rocks this parental melt has initially high CaO, MgO and low Al_2O_3 contents (Krause et al., 2007) and the nepheline tilaite represents its most fractionated crystallization product (Alaskan-type magma). Positive anomalies for Ba and Sr and negative anomalies for the HFSE indicate that this melt was formed in a subduction related geotectonic setting.

The presence of another parental melt composition is implied by the composition of the clinopyroxene cores of the external gabbro (composition B, Figs. 7, 8, 15). These clinopyroxene cores have a low La/Lu (3.5-7) at Lu ≈ 0.1 ppm and low contents in Sr and Na_2O (26-43 ppm and 0.1-0.4 wt.% respectively, Figs. 5b and 7a, b). The parental melt in equilibrium with these clinopyroxene cores (KT53) has a flat REE pattern with a low LREE/HREE (e.g. La/Lu = 3.2) and one order of magnitude lower concentrations in incompatible elements like Ba, Th, U and the LREE, if compared with the nepheline tilaite (Fig. 15). Nevertheless, this melt composition displays typical subduction related features such as low TiO_2 and HFSE concentrations. The occurrence of orthopyroxene in these gabbros and the significantly different composition of olivine, clinopyroxene and feldspar compared to those of the tilaites of Nizhnii Tagil and southwest Kytlym also reflect the different major element composition of this melt. It requires silica saturation and high Al_2O_3 content due to the presence of orthopyroxene and the dominance of plagioclase. These mineralogical and chemical features resemble those of island arc tholeiites and volcanic rocks described from the Tagil-zone in the Ural Mountains (Spadea et al., 2002). Tholeiitic melts with a higher degree of fractionation or from a source with higher HREE contents can be parental to the clinopyroxenes with a low La/Lu at higher Lu contents in some external gabbros (C and D in Figs. 7 and 14).

All the remaining measured clinopyroxenes, and therefore their host magmas, have compositions that are intermediate with regard to these end member components in terms of their mineralogy and trace element abundances. This suggests that they represent fractionation products of these parental magmas and/or crystallization products of hybrid melts formed by mixing of the end member melts.

4.2 Evolution of Alaskan-type parental magma: Magma mixing dominates fractional crystallization

In order to explain major and trace element variations in olivine and clinopyroxene from the ultramafic rocks of Alaskan-type complexes in the UPB (Nizhnii Tagil and Kytlym), Krause et al. (2007) proposed a model of a magma chamber which continuously crystallizes olivine, spinel and clinopyroxene, becomes repeatedly replenished with primitive magma and emptied by magma eruption (RFC). At this stage of magma

differentiation spinel, olivine, and clinopyroxene are crystallizing, but only clinopyroxene has significant contents of REE. The process provides a reasonable explanation for the large variation of incompatible trace elements observed in the clinopyroxenes of the ultramafic rocks. A similar process has been proposed by Batanova et al. (2005) to model the evolution of Alaskan-type complexes on Kamchatka.

Savelieva et al. (1999), Pertsev et al. (2000) and Savelieva et al. (2002) suggested a co-genetic relationship of the tilaites from Nizhnii Tagil and SW-Kytlym with the ultramafic rocks. Interestingly, clinopyroxenes from the most evolved ultramafic rocks (highest Lu concentration in Cpx) have compositions which are very similar to those which crystallized from the least evolved tilaites (lowest Lu concentration in the phenocryst cores; Fig. 7). Indeed, the similar clinopyroxene composition suggests that the amount of residual or interstitial liquid is the principal difference between clinopyroxenite and tilaite cumulates. Thus, the broad regional major and trace element variations observed in clinopyroxene support and strengthen the idea that ultramafic and tilaite cumulates in Uralian-Alaskan-type complexes are derived from coeval parental melts representing different degrees of partial melting. These melts subsequently crystallized in distinct open system magma chambers olivine plus spinel, followed by olivine plus clinopyroxene plus spinel, clinopyroxene plus spinel, and eventually clinopyroxene plus feldspar.

However, several features of the REE distribution in clinopyroxenes from the tilaites and gabbros, on a regional scale and on the scale of a thin section, cannot be explained by an RFC process assuming dominantly clinopyroxene crystallization and replenishment with primitive melt. For example, most of the lithologies show a decrease of the La/Lu with increasing Lu (Fig. 7a). This trend is most obvious in the bytownite tilaites from Tilay Mountain and Nizhnii Tagil and is defined by the core-rim evolution of clinopyroxenes and the composition of interstitial clinopyroxenes (Fig. 7a). For example, the bytownite tilaites from Nizhnii Tagil KT212, KT 213 display two parallel trends where clinopyroxene cores have Lu concentrations of about 0.21 ppm but different La/Lu of 28.5 and 31.5. As the Lu concentration increase to about 0.27 ppm La/Lu decreases in both populations to 22.6 and 26.9, respectively. A similar observation is obvious for the bytownite tilaites from Tilay Mountain.

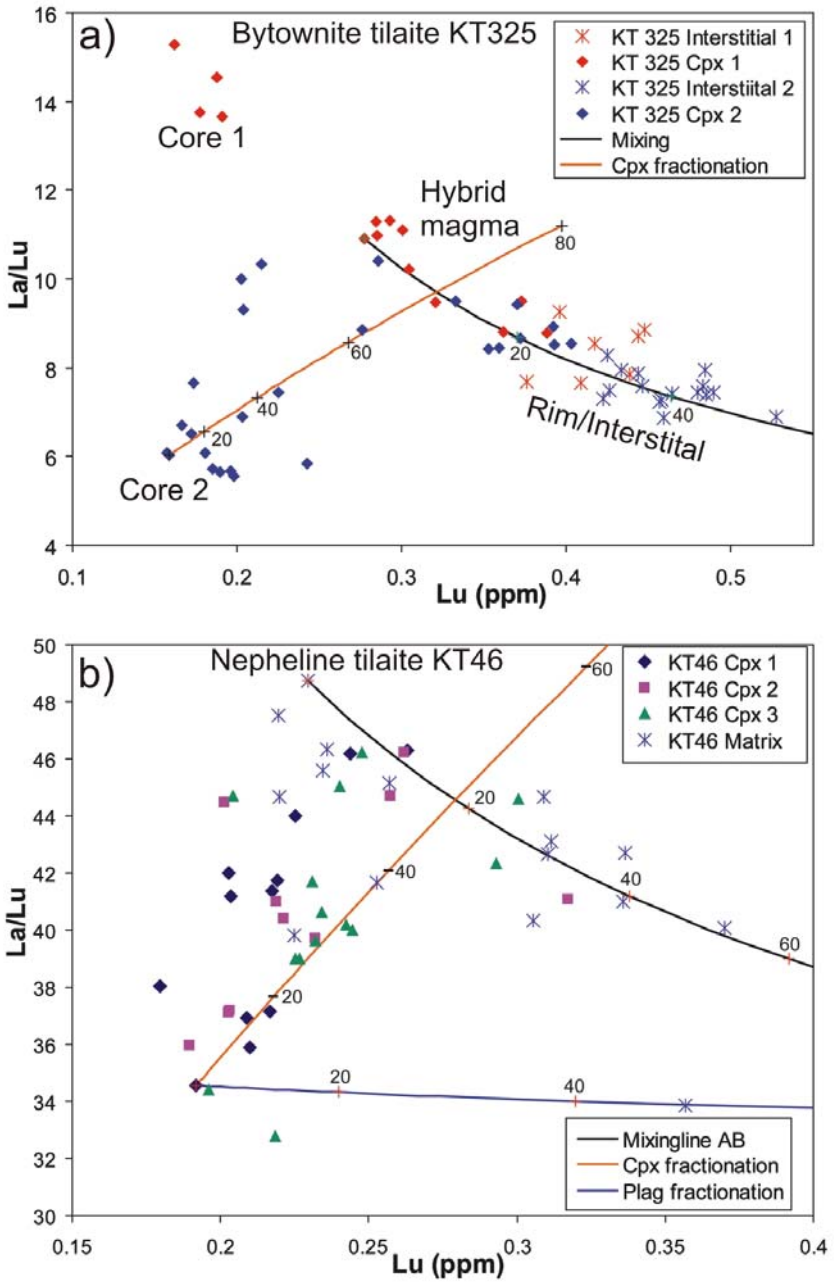

Fig. 16: Variation of the La/Lu vs. Lu concentration on the scale of a thin section for selected samples. (a) in a bytownite tilaite (sample KT325) from Tilay Mountain the cores of two phenocrysts have different La/Lu at similar Lu indicating their formation from different parental melts. Red line indicates fractionation of clinopyroxene. After the mixing clinopyroxene continue to crystallize from the hybrid magma. In order to explain the decreasing La/Lu with increasing Lu, addition of a hybrid magma with a fractionated tholeiitic composition (D in Figs. 7 a, b and 14) is necessary (black line).
(b) for a multiple zoned clinopyroxene in nepheline tilaite the rapid increase of the La/Lu can not be explained by the fractionation of clinopyroxene (red line) or plagioclase (blue line). The decreasing La/Lu with increasing Lu at Lu > 0.22 ppm follows a mixing line (black) with a melt that is in equilibrium with clinopyroxene having low La/Lu = 36 and Lu = 0.5 ppm, for example.

On thin section scale, clinopyroxene cores of a bytownite tilaite from Kytlym (sample KT44) have La/Lu and Lu concentrations that are close to the garnet melting trend (Fig. 7, 14). However, the rims and the interstitial grains in this sample have decreasing La/Lu as Lu increases. These trends are opposite to the trend that one would expect during clinopyroxene crystallization (Fig. 7, 16). Clinopyroxenes from sample KT46 show an even more complex REE distribution defining two evolution trends (Fig. 16a). Along one trend the La/Lu increases from 34 to 48 along with the Lu contents (from 0.18 ppm to 0.23 ppm). This trend is broadly consistent with a path of clinopyroxene fractionation. However, it tends to be steeper than expected, which likely reflects the addition and the mixing with another melt having a high La/Lu ratio (>48). More evolved clinopyroxene rims and matrix grains built up a second trend where the La/Lu ratio decreases from 48 to 34 as Lu increases from 0.23 to 0.36 ppm (Fig. 16a). Crystallization of clinopyroxene or plagioclase, or even the cotectic crystallization of feldspartoids (plagioclase, K-Feldspar, nepheline) and clinopyroxene can not explain the observed decrease of the La/Lu ratio. The observed trend follows a mixing line of with a component having a La/Lu of 36 at a Lu content of 0.5 ppm Fig. 16a).

In Fig 7a, La/Lu versus Lu, most of different lithologies display such trends and suggest hyperbolic curve progressions. In a diagram La/Lu versus 1/Lu, these lines become linear (Fig. 14). This implies that the REE distribution in clinopyroxene from different intrusive bodies as well as on the scale on a thin section follows mixing lines. Thus, the decrease of La/Lu with increasing Lu in clinopyroxene monitors the addition of a more evolved magma with low La/Lu (C and D in Figs. 7 and 14) and it appears to be an intrinsic feature of the Uralian Alaskan-type complexes.

The observation of magma mixing at thin section scale provides an additional clue for deciphering the evolution of the gabbroic and tilaitic rocks. In some bytownite tilaites we observe in one thin section clinopyroxene cores with different compositions and different inclusion assemblages. At similar Lu concentrations (0.18 ppm) the cores of the two clinopyroxene types have different La/Lu (type1: 14.5; type 2: 6; Fig. 16b). These two clinopyroxene cores could not have crystallized at the same time, nor in the same melt. They indicate the presence of two magma compositions. The envelope of both cores has a homogeneous composition with intermediate La/Lu ratios of 9-11 but higher Lu

contents of about 0.3 ppm (Fig. 16b). This can be explained, if these parts of the clinopyroxenes crystallized from a hybrid magma derived by mixing of the parental magmas forming the two crystal cores. However, this hybrid melt did not evolve by crystallizing clinopyroxene and/or feldspar but follows a trend indicating the addition of a third, more evolved liquid, because clinopyroxene rims and grains in the matrix have higher Lu concentrations and lower La/Lu ratios. This evolved liquid would have formed clinopyroxene similar to that present in the some external gabbros (sample PE440) with La/Lu = 5.4, Lu = 0.75 ppm (D in Figs. 7 and 14).

The clinopyroxene grain from sample NT-8 (Fig. 10) also equilibrated with two chemically very different melts. The core has a relatively evolved composition with high Lu contents and La/Lu ratio but low Sr concentrations and Sr/Sr*. The envelope crystallized from a less fractionated melt having low Lu contents and La/Lu ratios but high Sr and Sr/Sr*. The two parts of the clinopyroxene are connected by zones with intermediate compositions. These variations cannot be explained by fractional crystallization. In fact, they identify the presence and monitor the mixing of two different melts.

Clinopyroxene in some Bytownite tilaites from Tilay Mountain and the external gabbros have such low LREE/HREE at a given Lu content that they do not follow the trends defined by the remaining tilaites (Fig. 14). These samples also differ in many other chemical and mineralogical characteristics, for example strong negative anomalies of Sr, Eu and the presence of orthopyroxene, as well as lower Na_2O-contents in clinopyroxene from the other tilaites and the most fractionated ultramafic rocks. They can not be simple crystallization products of the parental magmas of the ultramafic rocks. However, their petrographic and chemical fingerprints can be explained if they represent crystallization products of a hybrid magma formed by the mixing of the parental magmas of the external gabbros (B) and the Alaskan-type series (A) (Figs. 7, 15). The cores of many clinopyroxenes from Tilay Mountain lie close to the mixing line where 10-25% of Alaskan type melt (A) have been added to the Island arc tholeiitic melt to form the bytownite parental magma (Figs. 7, 14).

The chemical differences between the nepheline tilaites from Nizhnii Tagil and SW-Kytlym can be ascribed to primary differences in the composition of the parental melt

(Figs. 6, 7; Krause et al., 2007). However, the bytownite tilaites coexisting with the nepheline tilaites consistently have lower La/Lu ratios than the nepheline tilaites at similar Lu concentrations. This could be due the addition of a small amount (10-20 %) of the component B (Island arc tholeiite) to a nepheline tilaite magma (Figs. 7a and 14).

Previous studies described petrologic differences between the rocks in the western and the eastern part of the Kytlym Complex and ascribed them to the crystallization of parental melt at different depths (Savelieva et al., 1999; Pertsev et al., 2000; Savelieva et al., 2002). Our detailed study of trace elements in minerals shows that two coeval parental magmas from different sources are necessary to explain the observed petrologic and geochemical variations in the gabbroic rocks of the Uralian-Alaskan-type complexes in Nizhnii Tagil and Kytlym. In addition, the large variation of trace element concentrations observed on regional and thin section scale is predominantly caused by magma mixing processes rather than fractional crystallization processes. Thus, the parental magmas of the bytownite tilaites are hybrid melts derived by mixing of primitive alkaline and tholeiitic magmas. In turn, the evolution of these parental primary and hybrid magmas is dominated by the addition and mixing of more differentiated melts, which are fractionation products of the parental magmas themselves. These processes probably occurred in open system magma chambers. The trace element variations of the clinopyroxenes in Fig. 9 indicate a gradual and continuous change of the melt composition. This may reflect the continuous addition of new, hot melt to the chamber forming a turbulent plume (Sparks et al., 1980). This will entrain the host magma and results in complete mixing. However, a new pulse of magma entering a magma chamber may also lead to the development of a compositionally stratified magma chamber (Huppert and Sparks, 1980). The existence of such a chamber could be indicated by the clinopyroxene profile of Fig. 10, which implies that the crystal grew in at least two compositionally different magma types. Extensive crystallization of mainly mafic minerals at the base of the magma chamber may form evolved, more fractionated and lighter melts which destabilizes the stratification and can lead to overturning and mixing in the chamber. This process could explain the systematic decrease of La/Lu with increasing Lu concentrations observed in most lithologies.

4.3 Petrogenetic evolution of the Kytlym Complex

The Kytlym complex represents a composite intrusion and its petrogenesis can be comprehensively explained if one appreciates the existence of two contemporaneous magmatic plumbing systems. In the western part Alaskan-type open magma chamber systems dominate which are fed by silica undersaturated, alkaline parental melts with a high CaO/Al_2O_3 and high contents of incompatible elements. The large variation of the La/Lu ratio may monitor different degree of partial melting ranging from 2-15% of a garnet and/or spinel-bearing source. The magma chamber became episodically replenished with primitive melt but continuously crystallized olivine and clinopyroxene, eventually plagioclase and other feldspartoids to form cumulates of dunite, wehrlite, clinopyroxenite and finally nepheline tilaite. In the eastern part of the Kytlym complex, a silica saturated Al_3O_3-rich tholeiitic melt containing one order of magnitude lower concentrations of incompatible trace elements, builds up a second magmatic system giving rise to the suite of external gabbros at the same time. The Tilay Mountain area represents the interface region between both systems where variable proportions of magmas from both systems are mixed. The presence of a orthopyroxene free association of ultramafic cumulates (dunite, wehrlite and clinopyroxenite) at Tilay Mountain implies that the mixing occurs at a time when the ultramafic cumulates in the Alaskan-type magma chamber are already formed. Further to the west only a small amount of the tholeiitic magma mixed with a larger proportion of the Alaskan-type melt to form the bytownite tilaites of SW-Kytlym.

At the contact zone of both magma chamber systems parts of the existing ultramafic clinopyroxenite cumulates could have been intruded by the tholeiitic melt and could be incorporated as rafts in the tholeiitic magma chamber. This explains the occurrence of six larger and numerous smaller clinopyroxenite bodies in the orthopyroxene-rich External gabbros in the eastern part of the Kytlym complex (Serebryanka, Valentorka, and Sukhogorsk blocks; Fig 1b). High temperature plastic deformation (e.g. Efimov, 1977; Fershtater and Pushkarev, 1992; Savelieva et al., 1999; Pertsev et al., 2000; Savelieva et al., 2002) occurred at different stages of this process and overprinted locally the original geometry and lithological contacts. The proposed metasomatic (Vorobeva et al., 1962) or metamorphic (Efimov et al., 1993) origin of the Kytlym

complex cannot explain the observed variation and spatial distributions of major and trace elements in the rock-forming minerals of the mafic and ultramafic rocks.

4.4 Implications for Uralian-Alaskan-type complexes and subduction zone magmatism

Uralian-Alaskan-type complexes have been interpreted as the root zones of magmatic arcs using geochemical, petrological and structural observations (e.g. Ivanov and Shmelev, 1996; Batanova et al., 2005; Pettigrew and Hattori, 2006). The coexistence of two different magmas in Uralian-Alaskan-type complexes in the Ural Mountains raises the question whether this is a typical feature of such complexes and what are the implications for subduction zone magmatism in general?

Characteristic features of Uralian-Alaskan-type complexes worldwide are, beside the rock assemblage, structure and PGE mineralization the absence of orthopyroxene and the extensive occurrence of clinopyroxene in the ultramafic rocks. The occurrence of hornblende and occasionally phlogopite in the ultramafic rocks indicates an elevated volatile content in some parental melts.

The uniformity of the ultramafic rocks is contrasted with the wide compositional array displayed among the associated mafic rocks ranging from orthopyroxene-free gabbros in places with hornblende, nepheline and K-feldspar (e.g. Findley, 1969; Hammack et al., 1991; Kepezhinkas et al., 1993a-b) to orthopyroxene-bearing gabbros in places with quartz (e.g. Taylor and Noble, 1960; Irvine, 1967; Himmelberg et al., 1986; Batanova et al., 1992; Batanova and Astrakhantsev, 1994; Helmy and El Mahallawi, 2003) to monzogabbros and monzonites (Astrakhantsev et al., 1991; Batanova et al., 2005) and diorites (Nixon et al., 1997). Like in the Kytlym complex a variety of different mineralogical and chemical compositions are often described within the same intrusive complex and it has been proposed that not all of these mafic rocks are cogenetic with each other or not even coeval with the ultramafic rocks (e.g. Taylor and Noble, 1960; Irvine, 1967; Irvine, 1976; Batanova et al., 1992).

A variety of different compositions for the parental melt of Uralian-Alaskan-type complexes have been discussed. Proposed mafic compositions include olivine-rich

tholeiites (Murray, 1972) and sub-alkaline orthopyroxene normative basaltic magmas (Nixon et al., 1990; Kepezhinkas et al., 1993a; Tistl et al., 1994; Himmelberg and Loney, 1994). Also ultramafic compositions are suggested to represent the parental melts, for example H_2O-rich ankaramites (Irvine, 1974; Fershtater and Pushkarev, 1987; Fershtater et al., 1999; Pushkarev, 2000; Krause et al., 2007; Thakurta et al., 2008) and picrites (Batanova et al., 2005; Thakurta et al., 2008).

Recent estimates of the composition of the parental melt advocate a silica undersaturated, alkaline melt with high CaO/Al_2O_3 (>1), Mg# and LREE/HREE. In agreement with a subduction related geotectonic setting a positive anomaly for Sr and negative anomalies for the HFSE were assumed (Pushkarev, 2000; Batanova et al., 2005; Krause et al., 2007). Following experimental studies of Medard et al. (2006) the melting of amphibole bearing wehrlite at pressures of 1 Gpa, a temperature above 1190°C and a low melt fraction produces nepheline normative hydrous melts with a high MgO and a CaO/Al_2O_3 >1. Such ultra-calcic melts closely match the above described characteristics for the parental melt (Alaskan-type component A) of the ultramafic rocks and the nepheline tilaites in Nizhnii Tagil and the western part of the Kytlym complex. However the presence for garnet in the source indicated by the HREE abundances may imply slightly higher pressures. The second melt with a tholeiitic, orthopyroxene-normative composition may reflect a source with different composition and/or a deeper source region in the mantle wedge above a subduction zone at 2-4 GPa and 1200-1400°C. Gabbros with tholeiitic compositions are also known from other Uralian-Alaskan-type complexes (e.g. Himmelberg et al., 1986; Batanova et al., 1992).

In addition Medard et al. (2006) suggested that typical arc related tholeiitic melts are produced in a source in the lower part of the mantle wedge, like the ones which are parental to the orthopyroxene-bearing gabbros in the eastern part of the Uralian-Alaskan-type complexes in the UPB. These melts rise to shallower mantle levels close to the MOHO into an upper mantle of wehrlitic composition that contains some amphibole. The reaction of the melt with this mantle material would lead to the generation of ultra-calcic, nepheline normative melts that represent the parental melt of the ultramafic rocks and the nepheline tilaite.

The variety of the gabbroic rocks observed in Kytlym has also been described in similar complexes world wide. It implies that the coexistence of magmas of different origin plays an important role in the genesis of many Uralian-Alaskan-type complexes and thus in island arcs. The study of trace element variations in rock forming minerals especially clinopyroxene from other Uralian-Alaskan-type complexes world wide may unravel the importance of a bimodal mafic-ultramafic magmatism and traces the igneous processes in the root zones at destructive plate margins.

5 Conclusions

The Uralian-Alaskan-type complexes of Nizhnii Tagil and Kytlym consist of ultramafic and mafic rocks which represent cumulates formed predominantly by crystallization of olivine, clinopyroxene, spinel and feldspar. Major and trace element concentrations and ratios in clinopyroxene and petrographic features suggest that they crystallized from a series of contemporaneous magmas which represent hybrid mixing products formed by mixing of two petrologically fundamentally different parental magmas and by mixing of parental and very evolved, more fractionated magmas. Mixing process are the primary cause for the observed large variation of incompatible elements and element ratios because they define evolution paths which follow mixing lines rather than trends of fractional crystallization. Nevertheless, all the magma types, parental and hybrid ones, have negative HFSE anomalies and positive Sr and Ba anomalies, which implies that they formed in a subduction zone environment.

The existence and mixing of two different magmas can be directly observed on the scale of a thin section. Cores of clinopyroxene phenocrysts in the same sample have contrasting major and trace element abundances, for example different LREE/HREE at similar HREE concentrations, demonstrating that they are derived from two different magmas. Towards the phenocryst rims and in the matrix the clinopyroxene compositions are homogeneous indicating the mixing of both melts followed by the addition, mixing and crystallization of a third, more evolved magma. In places profiles of single phenocrysts of clinopyroxene indicate that it crystallized in different magmas which are not related by fractional crystallization but by mixing processes.

One parental magma is ultra-calcic (CaO/Al_2O_3 > 1), silica under-saturated, and has a high MgO. It has an alkaline affinity, is enriched in incompatible elements and has high and variable LREE/HREE. It is the origin of the ultramafic rocks and finally forms nepheline and K-feldspar-bearing nepheline tilaites as the most fractionated products. The large variation of for example La/Lu ratios suggest that ultramafic and mafic cumulates are derived from a series of parental melts formed by polybaric melting of garnet- and spinel-bearing mantel sources involving different degrees of partial melting ranging from about 2 to 15%. These parental melts may evolve in open magma chamber systems to form the most fractionated nepheline tilaites. Ultramafic compositions are suggested to represent the parental melts, for example H_2O-rich ankaramites (Irvine, 1974; Fershtater and Pushkarev, 1987; Fershtater et al., 1999; Pushkarev, 2000; Krause et al., 2007; Thakurta et al., 2008) and picrites (Batanova et al., 2005; Thakurta et al., 2008).

The second parental melt crystallizes a sequence of olivine gabbros, hornblende gabbros and gabbro norites in the eastern part of the Kytlym complex. It is of tholeiitic composition, silica saturated, orthopyroxene-normative and has a CaO/Al_2O_3 <1. It also is characterized by a flat REE pattern and low LREE/HREE. These mineralogical and chemical features resemble those of island arc tholeiites and volcanic rocks described from the Tagil-zone in the Ural Mountains. The major mafic lithological units, external gabbro, bytownite and nepheline tilaites represent fractionation products of either these parental melts or their mixing products.

The nepheline tilaites in Nizhnii Tagil and the south western part of the Kytlym complex represent one end member and crystallized from a melt that is parental to the ultramafic rocks in the Uralian-Alaskan-type complexes. The addition of a small fraction (10-20%) of the tholeiitic melt formed the bytownite tilaites that occur together with the nepheline tilaites. The eastern part of the Kytlym complex largely consists of gabbros that crystallized from a tholeiitic melt with a strong island arc affinity. The trace element composition in the bytownite tilaites from the Tilay Mountain region suggests that approximately 20% of Alaskan-type melt is mixed with the tholeiitic melt. Together with orthopyroxene free ultramafic rocks his area represents the contact region between two

contemporaneous magma chamber systems where melts with different degrees of fractionation are mixed.

The presence of orthopyroxene and An-rich plagioclase distinguishes nepheline and bytownite tilaites and this is consistent with the involvement of the tholeiitic parent during their evolution.

Most of the clinopyroxene cores are surrounded by successive zones and eventually rims in which the La/Lu ratio systematically decreases as Lu concentrations increase. Matrix grains have compositions which are identical to those of the phenocryst rims. The decrease of La/Lu with increasing fractionation cannot be explained by fractional crystallization of clinopyroxene and/or feldspar. Rather this variation implies the continuous addition of a fractionated liquid to a residing melt in a magma chamber. The entering melt could represent a fractionation product of the residing melt. However, in some cases large variations of the La/Lu ratios in rims and matrix grains of clinopyroxene from one thin section suggest that these fractionated melts may also be derived from different parental melts.

The Uralian Alaskan-type massifs appear to be built up by complex intrusive bodies which are formed by at least two fundamentally different, but communicating magmatic plumbing systems. In the western part of the Kytlym massif Alaskan-type open magma chamber systems dominate which are fed by silica undersaturated, ultra-calcic, alkaline parental melts forming cumulates of dunite, wehrlite, clinopyroxenite and eventually nepheline tilaite. In the eastern part of the Kytlym complex, a silica saturated Al_3O_3-rich tholeiitic melt gives rise to the suite of external gabbros at the same time. The Tilay Mountain area represents the interface region between both systems where variable proportions of magmas from both systems interact.

In the Nizhnii Tagil complex equivalent rocks to the external gabbro of the eastern part of the Kytlym complex are not exposed. However the similarity of the composition and chemical zonation of clinopyroxene in nepheline and bytownite tilaites with clinopyroxene from equivalent lithologies in south west Kytlym implies the interaction of an Alaskan-type magma chamber with magmas of Island arc tholeiitic affinity also in the Nizhnii Tagil complex.

Uralian-Alaskan-type complexes world wide have in common a large variety of gabbroic rock assemblages. This diversity could be the result of the co-existence of two magmatic systems of different heritage, and the interactions of these melts would be a typical feature for such complexes. However, Uralian-Alaskan-type complexes are relatively rare as they are only known either from a few destructive plate margins or within plate settings. This may be due to the unusual ultramafic alkaline parental magma. Such melt may only form in parts of the upper mantle with exceptional, probably wehrlitic, composition.

Acknowledgement

We thank N. Groschopf, K Herwig, B. Stoll and B. Schulz-Dobrick for assistance during the LA-ICPMS and Microprobe analyses. This study was funded by grant GK392 of the Graduiertenkolleg 'Stoffbestand und Entwicklung von Kruste und Mantel' at the University of Mainz to J. Krause. Some part of the study was supported by RFBR grant 06-05-64795a to E.V. Puschkarev

References

Andrew, A.S., Hensen, B.J., Dunlop, A.C., Agnew, P.D., 1995. Oxygen and hydrogen isotope evidence for the origin of platinum-group mineralization in Alaskan-type intrusions at Fifield, Australia. Economic Geology, 90, 1831-1840.

Astrakhantsev, O.V., Batanova, V.G., Perfilyev, A.S., 1991. Structure of the Gal'moenan dunite-clinopyroxenite-gabbro massif (Southern Koyakia). Geotectonics, 25 (2), 132-144.

Batanova, V.G., Astrakhantsev, O.V., 1992. Tectonic position and origins of the zoned mafic-ultramafic plutons in the Northern Olyutor Zone, Koryak Highlands. Geotectonics, 26 (2), 153-165.

Batanova, V.G., Astrakhantsev, O.V., 1994. Island-arc mafic-ultramafic plutonic complexes of northern Kamchatka. In: Ishiwatari, A., Malpas, J., Ishizuka, H.,

(eds.) Proceedings of the 29th International Geological Congress, Part D, Circum-Pacific-ophiolites VSP, 129-143.

Batanova, V.G., Pertsev, A.N., Kamenetsky, V.S., Ariskin, A.A., Mochalov, A.G., Sobolev, A.V., 2005. Crustal evolution of island-arc ultramafic magma: Galmoenan pyroxenites-dunite plutonic complex, Koryak Highland (Far East Russia). Journal of Petrology, 46, 1345-1366.

Bindeman, I. N., Bailey, Y. C. 1999. Trace elements in anorthite megacrysts from the Kurile island arc: A window to across-arc geochemical variations in magma compositions. Earth and Planetary Science Letters, 169, 209-226.

Bowen, N.L., 1928. The evolution of the igneous rocks. Princeton University Press, Princeton, 334pp.

Clark, T., 1980. Petrology of the Turnagain ultramafic complex, northwestern British Columbia. Canadian Journal of Earth Sciences, 17, 744-757.

Deer, W.A., Howie, R.A., Zussman, J., 1992. An introduction to the rock-forming minerals. Pearson Prentice Hall, 696pp.

Duparc, L., Tikhonowitch, M., 1920. Le platine et les gites platiniferes de l'Oural et du Monde, Geneve, 542pp.

Efimov, A.A., 1977. Hot tectonics in the hyperbasics and and gabbroides of the Urals. Geotektonika, 1, 24-42. (in Russian)

Efimov, A.A., Efimova, L.P., 1967. Kytlym platiniferous massiv. Leningrad: Nedra, 1-356 (in Russian).

Efimov, A.A., Tavrin, I.F., 1978. About genetical relation of platinum bearing dunite of the Urals and Aldan Shield. Doklady Academy of Sciences of USSR, 243 (4), 991-994. (in Russian)

Efimov, A.A., Efimova, L.P., Maegov, V.I., 1993. The tectonics of the Platinum Bearing Belt of the Urals: Composition and mechanisms of structural development. Geotectonics, 27 (3), 197-207.

Fershtater, G.B., Pushkarev, E.V., 1987. Magmatic clinopyroxenites of the Urals and their evolution. Izv. Akad. Nauk SSSR, Ser. Geol. 3, 13-23 (in Russian).

Fershtater, G.B., Pushkarev, E.V., 1992. Nepheline-bearing Tylaites in the dunite-clinopyroxenite-gabbro association of the Urals Platinum Belt. Izv. Akad. Nauk SSSR, Ser. Geol., 4, 74-84. (in Russian)

Fershtater, G.B., Bea, F., Pushkarev, E.V., Garuti, G., Montero, P., Zaccarini, F., 1999. Insight into the petrogenesis of the Urals Platinum Belt: New geochemical evidence. Geochemistry international, 37 (4), 302-319.

Findlay, D.C., 1969. Origin of the Tulameen ultramafic-gabbro complex, southern British Columbia. Canadian Journal of Earth Sciences, 6, 399-425.

Francalanci, L., Davies, G.R., Lustenhouwer, W., Tommasini, S., Mason, P.R.D., Conticelli, S., 2005. Intra-grain Sr isotope evidence for crystal recycling and multiple magma reservoirs in the recent activity of Stromboli Volcano, Southern Italy. Journal of Petrology, 46 (10), 1997-2021.

Gioncada, A., Mazzuoli, R., Milton, A.J., 2005. Magma mixing at Lipari (Aeolian Islands, Italy): Insights from textural and compositional features of phenocrysts. Journal of Volcanology and Geothermal Research, 145, 97-118.

Gittins, J., Fawcett, J.J., Brooks, C.K., Rucklidge, J.C., 1980. Intergrowths of nepheline-potassium feldspar and kalsilite-potassium feldspar: A re-examination of the 'Pseudo-Leucite Problem'. Contributions to Mineralogy and Petrology, 73, 119-126.

Guo, F., Nakamuru, E., Fan, W., Kobayoshi, K., Li, C., 2007. Generation of Palaeocene adakitic andesites by magma mixing; Yanji Area, NE China. Journal of Petrology, 48 (4), 661-692.

Hammack, J.L., Nixon, G.T., Paterson, W.P.E., Nuttal, C., 1991. Geology and noble-metal geochemistry of the Lunar Creek Alaskan-type complex, North-Central British Columbia. In: Geological fieldwork 1990: British Columbia Ministry of Energy, Mines and Petroleum resources, 1991 (1), 217-233.

Helmy, H.M., El Mahallawi, M.M., 2003. Gabbro Akarem mafic –ultramafic complex Eastern Desert, Egypt: a Late Precambrian analogue of Alaskan-type complexes. Mineralogy and Petrology, 77, 85-108.

Hidalgo, S., Monzier, M., Martin, H., Chazot, G., Eissen, J.-P., Cotten, J., 2007. Adakitic magmas in the Ecuadorian volcanic front: Petrogenesis of the Iliniza volcanic complex (Ecuador). Journal of Volcanology and Geothermal Research, 159, 366-392.

Himmelberg, R.G., Loney, R.A., 1995. Characteristics and petrogenesis of Alaskan-Type ultramafic-mafic intrusions, southeastern Alaska. US Geological Survey Professional Papers, 1564, 1-47.

Himmelberg, R.G., Loney, R.A., Craig, J.T., 1986. Petrogenesis of the ultramafic complex at the Blashke Islands, southeastern Alaska. US Geological Survey Bulletin, 1662, 1-14.

Hofmann, A.W., 1988. Chemical differentiation on the earth: The relationship between mantle, continental crust, and oceanic crust. Earth and Planetary Science Letters, 90, 297-314.

Huppert, H.E., Sparks, R.S.J., 1980. The fluid dynamics of a basaltic magma chamber replenished by influx of hot, dense ultrabasic magma. Contributions to Mineralogy and Petrology, 75, 279-289.

Ionov, D.A., Griffin, W.L., O`Reilly, S.Y., 1997. Volatile-bearing minerals and lithophile trace elements in the upper mantle. Chemical Geology, 141, 153-184.

Irvine, T.N., 1963. Origin of the ultramafic complex at Duke Island, Southeastern Alaska. Minaralogical Society of America, special paper 1, 36-45

Irvine, T.N., 1967. Zoned ultramafic complexes. In: Wylie, P.J., Ultramafic and related rocks, John Wiley, New York, 83-97.

Irvine, T.N., 1974. Petrology of the Duke Island ultramafic complex, southeastern Alaska. Geological Society of America, Memoir 138.

Irvine, T.N., 1976. Alaskan-type ultramafic-gabbro bodies in the Aiken Lake, McConnel Creek, and Toodagoone map-areas. Geological Survey of Canada. Paper 76-1A, 76–81.

Ivanov, K.S., Shmelev, V.R., 1996. The Platinum Belt of the Urals as a magmatic trace of the early paleozoic subduction zone. Transactions of the Russian Academy of Sciences / Earth Sciences, 347A (3), 396-399.

Jochum, K.P., Stoll, B., Herwig, K., Willbold, M., 2006. Improvement of in situ Pb isotope analysis by LA-ICP-MS using a 193 nm Nd:YAG laser. Journal of Analytical Atomic Spectrometry, 21, 666-675.

Jochum, K.P., Stoll, B., Herwig, K., Willbold, M., 2007. Validation of LA-ICP-MS trace element analysis of geological glasses using a new solid-state 193 nm Nd:YAG laser and matrix matched calibration. Journal of Analytical Atomic Spectrometry, 22, 112-121.

Kelemen, P.B., Hanghoj, K., Greene, A.R., 2003. One view of the geochemistry of subduction-related magmatic arcs, with an emphasis on primitive andesite and lower crust. In: Rudnick, R.L. ed. Treatise on Geochemistry vol. 3 The Crust. Elsevier, 593-659.

Kepezhinskas, P.K., Reuber, I., Tanaka, H., Miyashita, S., 1993a. Zoned calc-alkaline plutons in Northeastern Kamchatka, Russia: Implications for the crustal growth in magmatic arcs. Mineralogy and Petrology, 49, 147-174.

Kepezhinskas, P.K., Taylor, R.N., Tanaka, H., 1993b. Geochemistry of plutonic spinels from the North Kamchatka Arc: Comparisons with spinels from other tectonic settings. Mineralogical Magazine, 57, 575-589.

Kimura, J.-I., Yoshida, T., Iizumi, S., 2002. Origin of low-K intermediate lavas at Nekoma volcano, NE Honshu arc, Japan: Geochemical constraints for lower-crustal melts. Journal of Petrology, 43, 631-661.

Krause, J., Brügmann, G.E., Pushkarev, E.V., 2007. Accessory and rock forming minerals monitoring the evolution of zoned mafic–ultramafic complexes in the Central Ural Mountains. Lithos, 95, 19-42.

Levinson-Lessing, F.Y., 1920. Geochemical description ot the South-Zaozernaya district and Denezkhin Kamen' Mountain in the Northern Urals. Transactions of the St. Petersburg Society of Naturalists, 30, 1-257. (in Russian)

Masuda, Y., Nohda, S., Okamoto, K., 1976. Major and trace element geochemistry of the Nohi rhyolitic volcanic rocks, Central Japan. Journal of the Geological Society Japan, 82, 595-601.

Masuda, Y., Nishimura, S., Asayama, T., 1972. Rare-earth distributions in the Ibaragi Granitic Complex, Osaka Prefecture, Japan. Journal of the Geological Society Japan, 78, 521-530.

Maclennan, J., McKenzie, D., Grönvold, K., Shimizu, N., Eiler, J.M., Kitchen, N., 2003. Melt mixing and crystallization under Theistareykir, northeast Iceland. Geochemistry Geophysics Geosystems, 4 (11).

Malitch, K.N., 1999. Platinum-group elements in clinopyroxenite-dunite massifs of the East Siberia (geochemistry, mineralogy and genesis). St. Petersburg, VSEGEI Press, 1-296 (in Russian).

Medard, E., Schmidt, M.W., Schiano, P., Ottolini, L., 2006. Melting of amphibole-bearing wehrlites: An experimental study on the origin of ultra-calcic nepheline-normative melts. Journal of Petrology, 47 (3), 481-504.

Monjoie, P., Bussy, F., Lapierre, H., Pfeifer, H.-R., 2005. Modeling of in-situ crystallization processes in the Permian mafic layered intrusion of Mont Collon (Dent Blanche nappe, western Alps). Lithos, 83, 317-346.

Murray, C.G., 1972. Zoned ultramafic complexes of the Alaskan type: Feeder pipes of andesitic volcanoes. The Geological Society of America, Memoir 132, 313-335

Nagasawa, H., 1973. Rare-earth distribution in alkali rocks from Oki-Dogo Island, Japan. Contributions to Mineralogy and Petrology, 39, 301-308.

Nixon, G.T., Hammack, J.L., Connelly, J.N., Case, G., Paterson, W.P.E., 1990. Geology and noble metal geochemistry of the Polaris ultramafic complex, north-central British Columbia In: Geologic fieldwork 1989: British Columbia Ministry of Energy, Mines and Petroleum resources, 1988 (1), 307-404.

Nixon, G.T., Hammack, J.L., Ash, C.H., Cabri, L.J., Case, G., Connelly, J.N., Heaman, L.M., Laflamme, J.H.G., Nuttall, C., Paterson, W.P.E., Wong, R.H., 1997. Geology and platinum-group-element mineralization of Alaskan-type ultramafic–

mafic complexes in British Columbia, British Columbia Ministry of Employment and Investment, Energy and Mines Division, Bulletin, 93, 1-141.

Noble, J.A., Taylor, H.P., 1960. Correlation of the ultramafic complexes of southeastern Alaska with those of North America and the World. 21st International Geological Congress in Copenhagen 1960, Report part 13, 188-197.

Pertsev, A.N., Savelieva, G.N., Astrakhantsev, O.V., Magmatic origin of the ultramafic-mafic association of the Kytlym Massif, Platinum Belt of the Urals, 2000. Petrology, 8 (4), 370-393.

Pettigrew, N.T., Hattori, K.H., 2006. The Quetico Intrusions of Western Superior Province: Neo-Archean examples of Alaskan/Ural-type mafic-ultramafic intrusions. Precambrian Research, 149, 21-42.

Pushkarev, E.V. 2000. Petrology of the Uktus dunite-clinopyroxenite-gabbro massif (Middle Urals). Ekaterinburg. Ural Division of RAS, 296pp.

Rankenburg, K., Lassiter, J.C., Brey, G., 2004. Origin of megacrysts in volcanic rocks of the Cameroon volcanic chain – constraints on magma mixing genesis and crustal contamination. Contributions to Mineralogy and Petrology, 147, 129-144.

Salters, V.J.M., Stracke, A., 2004. Composition of the depleted mantle. Geochemistry Geophysics Geosystems, 5 (5).

Savelieva, G.N., Sharaskin, A.Y., Saveliev, A.A., Spadea, P., Pertsev, A.N., Babarina, I.I., 2002. Ophiolites and zoned mafic-ultramafic massifs of the Urals: A comparative analysis and some tectonic implications. In: Browen, D., Juhlin, C., Puchkov, V. (eds.). Mountain building in the Uralides: Pangea to the present. Geophysical Monograph, 132, 135-153.

Savelieva, G.N., Pertsev, A.N., Astrakhantsev, O.V., Denisova, E.A., Boudier, F., Bosch, D., Puchkova, A.V., 1999. Kytlym Pluton, North Urals: Structure and emplacement history. Geotectonics, 33, (2) 119-141.

Sidorov, E.G., Tolstykh, N.D., Podlipsky, M.Y., Pakhomov, I.O., 2004. Placer PGE minerals from the Filippa clinopyroxenite–dunite massif (Kamchatka). Russian Geology and Geophysics, 45 (9), 1128-1144.

Slansky, E., Johan, Z., Ohnenstetter, M., Barron, L.M., Suppl, D., 1991. Platinum mineralization in the Alaskan-type intrusive complexes near Fifield, N.S.W., Australia. part 2. Platinum-group minerals in placer deposits at Fifield. Mineralogy and Petrology, 43, 161-180.

Spadea, P., D'Antonio, M., Kosarev, A., Gorozhanina, Y., Brown, D., 2002. Arc-continent collision in the southern Urals: Petrogenetic aspects of the forearc-arc complex. In: Browen, D., Juhlin, C., Puchkov, V. (eds.). Mountainbuilding in the Uralides: Pangea to the present. Geophysical Monograph, 132, 101-134.

Sparks, R.S.J., Meyer, P., Sigurdsson, H., 1980. Density variation amongst mid-ocean ridge basalts: Implications for magma mixing and the scarcity of primitive lavas. Earth and Planetary Science Letters, 46, 419-430.

Stoll B., Jochum, K.P., Herwig, K., Amini, M., Flanz, M., Kreuzburg, B., Kuzmin, D., Willbold, M., Enzweiler, J., 2008. An automated Ir-Strip-Heater for LA-ICP-MS bulk analysis of geological samples. Geostandarts and Geoanalytical research, 32 (1), 5-26.

Taylor, H.P., Noble, J.A., 1960. Origin of the ultramafic complexes in southeastern Alaska. 21st International Geological Congress in Copenhagen 1960, Report part 13, 175-187.

Tepley, F.J., Lundstrom, C.C., Gill, J.B., Williams, R.W., 2006. U-Th-Disequilibria and the time scale of fluid transfer and andesite differentiation at Arenal Volcano, Costa Rica (1968-2003). Journal of Volcanology and Geothermal Research, 157, 147-165.

Thakurta, J., Ripley, E.M., Li, C., 2008. Geochemical constraints on the origin of sulphide mineralization in the Duke Island Complex, southeastern Alaska. Geochemistry Geophysics Geosystems, 9 (7).

Tistl, M., Burgath, K.P., Höhndorf, A., Kreuzer, H., Munoz, R., Salinas, R., 1994. Origin and emplacement of Tertiary ultramafic complexes in northwest Colombia: Evidence from geochemistry and K-Ar, Sm-Nd and Rb-Sr isotopes. Earth and Planetary Science Letters, 126, 41-59.

Vorobeva, O.A., Samoilova, N.V., Sveshinova, E.V., 1962. Gabbro-pyroxenite-dunite belt of the Middle Urals. Moscow: IGEM No 65, 1-318 (in Russian).

Wyssotzky, N., 1913. Platinum deposits of the Is and Nizhny Tagil districts in the Urals. St. Petersburg Geological Committee, New Series, 62, 1-694 (in Russian).

Yokoyama, T., Kobayashi, K., Kuritani, T., Nakamura, E., 2003. Mantle metasomatism and rapid ascent of slab components beneath island arcs: Evidence from ^{238}U-^{230}Th-^{226}Ra disequilibria of Miyakejima Volcano, Izu Arc, Japan. Journal of Geophysical Research, 108 (B7), 1-1-Ecv 1-25.

Chapter 3

Chemical composition and petrogenetic significance of spinel from Uralian-Alaskan-type Mafic-Ultramafic Complexes

Joachim Krause, Gerhard E. Brügmann and Evgeny V. Pushkarev

Abstract

Uralian-Alaskan-type mafic-ultramafic complexes are recognized as a distinct class of intrusions regarding their lithologic assemblage, mineral chemistry and petrogenetic setting. Characteristic petrologic features include the concentric zonation of a central dunite body that grades outward into wehrlite, clinopyroxenite and gabbro, the absence of orthopyroxene and often a platinum group element mineralization. In addition the presence of ferric iron-rich spinel discriminates Uralian-Alaskan-type complexes from most other mafic ultramafic rock assemblages. The studied Uralian-Alaskan-type complexes are southern part of a 900 km long NS-trending chain of similar intrusions between the Main Uralian Fault in the west and the Serov-Mauk Fault in the east.

In the present study we discuss new data on the distribution of major elements in minerals of the spinel group in rocks from Uralian-Alaskan-type complexes in the Ural Mountains, Russia. Cr-rich spinel (Cr_2O_3 = 20-53 wt.%) in dunite with interstitial clinopyroxene and in wehrlite cumulates indicate that they reacted with interstitial liquid resulting in the progressive substitution of Al_2O_2 and Cr_2O_3 by Fe_2O_3 and TiO_2. A distinct change in the spinel chemistry (dunite Cr_2O_3 = 47-53 wt.%, Al_2O_3 = 8.5-10.5 wt.%, Fe_2O_3 = 12-18 wt.%, TiO_2 = 0.4-0.7 wt.%) towards more Fe_2O_3-rich compositions monitors the onset of clinopyroxene fractionation (wehrlite Cr_2O_3 = 15-35 wt.%, Al_2O_3 = 1-8 wt.%, Fe_2O_3 = 25-55 wt.%, TiO_2 = 1-1.5 wt.%) During this process the Cr/(Cr+Al) decreases from ~0.77 to ~0.62. In more fractionated, mafic rocks the calculated initial composition of exsolved spinel traces the continuous fractionation of clinopyroxene

accompanied by decreasing Cr_2O_3 and increasing FeO and fO_2. Finally the occurrence of feldspar buffers the Al_2O_3 content (Al_2O_3 = 8-13 wt.%) in most of the spinels in mafic rocks at very low Cr_2O_3 contents (< 5 wt.%). The Cr/(Cr+Al) in spinel decreases from 0.6-0.8 in dunite and wehrlite to 0.02-0.20 in the mafic rocks.

The presence of exsolutions in spinel is restricted to grains with Cr_2O_3 < 27 wt.%. Spinel with Cr_2O_3 contents below 10 wt.% exsolved to blebs and oriented lamellas of pleonaste in magnetite with discrete phase boundaries. In spinel with higher Cr_2O_3 contents lamellas are absent and the phase boundaries between chromian magnetite and picotite are often gradual transitions with a complex geometry. Remarkably, exsolved spinel from all studied complex follow one distinct solvus line defining a temperature of 600°C. This indicates that the parental magmas were emplaced and eventually cooled at similar levels in the lithosphere, likely near the crust mantle boundary. Eventually, these 600°C hot bodies were rapidly transported into colder regions of the upper crust during a regional tectonic event, for example during the major active phase of the Main Uralian Fault.

Keywords: Exsolved spinel, Uralian-Alaskan-type complexes, X-ray mapping, fractionation, chromite.

1 Introduction

Chromian spinel has been established as an essential instrument for monitoring the evolution of mafic and, in particular, ultramafic rocks. Its composition gives important information about the degree of partial melting in the mantle or the evolution of mantle melts during their rise to the surface (e.g. Irvine, 1965; Irvine, 1967a; Hill and Roeder, 1974; Sack and Ghiorso, 1991a,b; Van der Veen and Maaskant, 1995; Barnes and Roeder, 2001). The compositional variation, even on the scale of a single thin section, reports thermodynamic parameters, such as temperature and oxygen fugacity during crystallization processes in lava flows and layered intrusions (e.g. Irvine, 1967a; Hill and Roeder, 1974; Cameron, 1975) as well as late stage magmatic equilibration with interstitial liquid (e.g. Henderson, 1975; Henderson and Wood, 1981; Roeder and Campbell, 1985; Scowen et al., 1991; Candia and Gaspar, 1997). The spinel

composition is also useful to discriminate between geotectonic settings (e.g. Irvine, 1967a; Dick and Bullen, 1984; Roeder, 1994; Cookenboo et al., 1997; Lee, 1999; Barnes and Roeder, 2001). However, the spinel composition is subjected to considerable subsolidus re-equilibration, such as diffusive mass exchange with neighbouring silicate phases as temperature decreases and post-magmatic metasomatic or metamorphic overprint (e.g. Jackson, 1969; Springer, 1974; Frost, 1975; Pinsent and Hirst, 1977; Lehmann, 1983; Kimball , 1990; Melcher et al., 1997; Mellini et al., 2005; Frost and Beard, 2007; Iyer et al., 2008). This can result in misleading interpretations concerning tectonic environment and P-T estimates (Power et al., 2000).

Uralian-Alaskan-type mafic to ultramafic complexes define a distinct class of mafic ultramafic intrusions regarding their tectonic setting, lithological association and the composition of rock forming and accessory minerals (Taylor and Noble, 1960; Noble and Taylor, 1960; Irvine, 1967b; Findlay, 1969; Yefimov, 1977; Himmelberg et al., 1986; Himmelberg and Loney, 1995; Pertsev et al., 2000; Batanova et al., 2005; Krause et al., 2007). Characteristic features of this class of intrusions include the often concentrically zoned association of dunite, wehrlite, clinopyroxenite and gabbro along with the absence of orthopyroxene in the ultramafic rocks and their setting in elongated belts along convergent margins.

Linear belts of Uralian-Alaskan-type complexes, often several hundred kilometres long have been described from the Cordillera of Alaska and British Columbia (e.g. Taylor and Noble, 1960; Irvine, 1967; Findlay, 1969; Himmelberg et al., 1986; Himmelberg and Loney, 1995), on Northern Kamchatka, Russia (e.g. Batanova and Astrakhantsev, 1992; Kepezhinskas et al., 1993a-b; Batanova et al., 2005) and in the Ural Mountains, Russia (e.g. Noble and Taylor, 1960; Yefimov, 1977; Ivanov and Shmelev, 1996; Pertsev et al., 2000; Chashchukhin et al., 2002; Savelieva et al., 2002; Krause et al., 2007). One of the characteristic features of Uralian Alaskan type complexes distinguishing them from other mafic-ultramafic associations is the chemical composition of chromium spinel, in particular its elevated Fe_2O_3-content (e.g. Noble and Taylor, 1960; Irvine, 1967b; Findlay, 1969; Taylor and Noble, 1969; Himmelberg et al., 1986; Himmelberg and Loney, 1995; Chashchukhin et al., 2002; Krause et al., 2007). This feature has been ascribed either to high total iron contents in the parental melt (Taylor and Noble, 1969),

distinctive fractionation processes (Findlay, 1969; Krause et al., 2007) or an elevated oxygen fugacity (Himmelberg and Loney, 1995; Chashchukhin et al., 2002).

In the $(Mg,Fe^{2+})_{1+x}(Cr,Al,Fe^{3+})_{2-2x}(Ti)_xO_4$ solid solution series several miscibility gaps over a wide range of temperatures have been documented by experimental data and thermodynamic calculations (e.g. Ghiorso and Sack, 1991; Sack and Ghiorso, 1991a,b and references therein). Miscibility gaps exist at magmatic temperatures in the $(Fe,Mg)_2TiO_4$ – $(Fe,Mg)Al_2O_4$, and at subsolidus conditions in the $MgFe_2O_4$ – Mg_2TiO_4, the $FeCr_2O_4$ – Fe_3O_4, the $(Fe,Mg)Al_2O_4$ – $(Fe,Mg)Cr_2O_4$ and the $(Fe,Mg)Fe_2O_4$ – $(Fe,Mg)Al_2O_4$-series.

For the Ti-poor spinels (TiO_2 < 9 wt.%) in the studied Uralian-Alaskan-type complexes the latter between the magnetite and the picotite-$spinel_{ss}$ series is of particular interest (e.g. Turnock and Eugster, 1962; Ghiorso and Sack, 1991; Sack and Ghiorso, 1991a, b). Exsolution of spinel is also described in greenschist to amphibolite facies metamorphic rocks (e.g. Evans and Frost, 1975; Loferski and Lipin, 1983; Eales et al., 1988; Ozawa, 1988; Burkhard, 1993; Van der Veen and Maaskant, 1995; Candia and Gaspar, 1997).

However, despite its omnipresence in magmatic rocks only a few occurrences of exsolved spinel have been described (Muir and Naldrett, 1973; Jan et al., 1992; Pushkarev et al., 1999; Garuti et al., 2003; Tamura and Arai, 2005; Krause et al., 2007; Ahmed et al., 2008). The present study focuses on new data about the distribution of major elements in minerals of the spinel group in ultramafic and mafic rocks from Uralian-Alaskan-type complexes in the Ural Mountains, Russia and their petrogenetic implications. The distribution of major components in Cr-rich spinel from dunite and wehrlite cumulates indicate a reaction of primitive magmatic spinel with interstitial liquid resulting in the replacement of Al_2O_2 and Cr_2O_3 by Fe_2O_3 and TiO_2. The onset of clinopyroxene fractionation is monitored by a distinct change in the spinel chemistry towards more Fe_2O_3-rich compositions. The calculated initial composition of exsolved spinel in the more evolved mafic rocks traces the continuous fractionation of clinopyroxene accompanied by decreasing Cr_2O_3 and increasing Fe_2O_3, FeO and fO_2. Finally the Al_2O_3 content in spinel in the mafic rocks at very low Cr_2O_3 contents is buffered by feldspar. The occurrence of exsolved spinel in various lithologies of the

three studied complexes indicates slow cooling of the host cumulates from igneous temperatures down to about 600°C. This suggests that magma chambers were formed and cooled close to the MOHO and ultimately these bodies were emplaced into the upper crust during a regional tectonic event, probably a movement along the Main Uralian Fault.

Below, the term spinel will be applied for all minerals of the spinel group $(Mg,Mn,Co,Zn,Fe^{2+})_{1+x}(V,Cr,Al,Fe^{3+})_{2-2x}(Ti)_xO_4$. If applicable, we will use more precise terms like chromian spinel or chromian magnetite.

2 Samples and Analytical Methods

2.1 Sample description

In the Ural Mountains 15 Uralian-Alaskan-type mafic-ultramafic complexes form a 900 km long linear belt along the 60-th meridian (Fig. 1a). Due to the occurrence of economic platinum placer deposits associated with these complexes this chain is known as the “Ural platinum belt” (UPB). The UPB is situated in the western section of the Tagil-Magnitogorsk zone between two N-S trending fault zones, the Main Uralian Fault in the west and the Serov-Mauk Fault in the east (Fig. 1a).

The samples for the present study were collected from the Uralian-Alaskan-type complexes of Nizhnii Tagil, Sevtley Bor and Kytlym (Fig. 1). The Nizhnii Tagil complex predominantly consists of dunite, which is overlain by clinopyroxenites with, in places, a few meters of wehrlite at the contact. Gabbroic rocks occur only in some small lens shaped bodies in the northern part and at the south-eastern rim of the complex (Fig. 1d; Chashukhin et al., 2002; Savelieva et al., 2002).

The Svetley Bor complex consists of a dunite core that is surrounded by a rim of clinopyroxenite (Fig. 1c). The clinopyroxenite locally contains hornblendites where clinopyroxene is replaced by hornblende. Gabbroic rocks are not exposed in the Svetley Bor complex (e.g. Garuti et al., 1997).

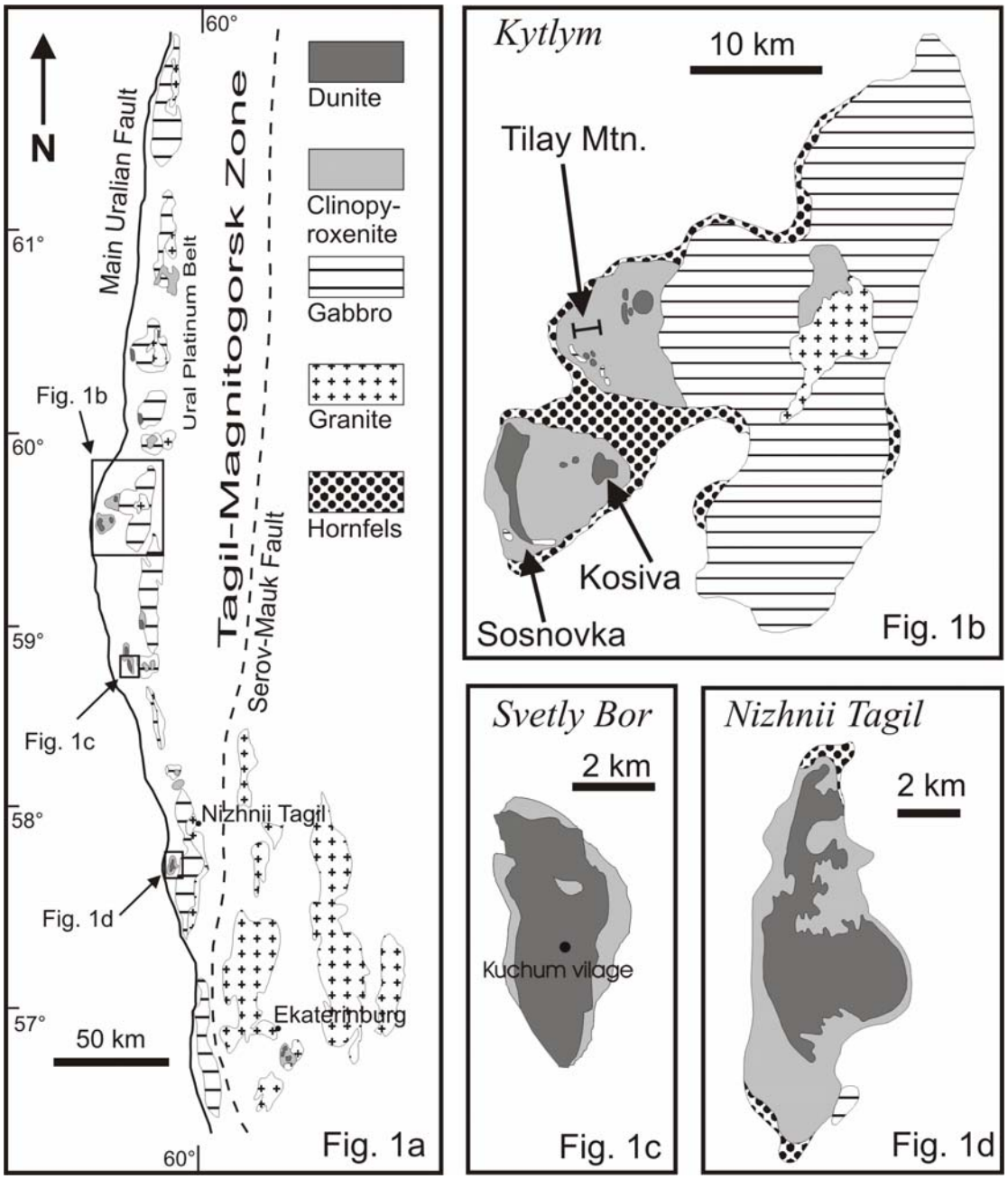

Fig. 1: Regional geology of the Ural platinum belt (a) and of the studied Uralian-Alaskan type complexes of Kytlym, Svetley Bor and Nizhnii Tagil (b-d); Modified after Chashukhin et al. (2002) and Garuti et al. (1997).

In the western part of the Kytlym complex a number of dunite bodies (Sosnovka, Kosiva Mountain, and Tilay Mountain) are surrounded by clinopyroxenite (Fig. 1b). Several smaller and at least two larger gabbroic massifs are also present (Garuti et al., 1997; Savelieva et al., 1999; Savelieva et al., 2002; Chashukhin et al., 2002). In places a tectonically induced interleafing between different lithologies can be observed. The

mafic and ultramafic rocks in SW part of the Kytlym complex (Sosnovka and Kosiva Mountain) are in composition similar to those of Nizhnii Tagil and Svetley Bor and thought to be formed from alkaline silica undersaturated parental melts (Krause et al., 2007; Chapter 2). The eastern part of the Kytlym complex consists of different gabbros and gabbro norites with minor amounts of ultramafic and granitic rocks. They are interpreted to be derived from a tholeiitic melt (Chapter 2). The Tilay Mountain area represents a transition zone between the two magmatic systems where melts from both sources were mixed (Chapter 2).

A detailed lithological and mineralogical description of the studied ultramafic rocks has been given in Krause et al. (2007). The dunites consist of coarse grained olivine, medium to fine grained mostly euhedral chromian spinel and interstitial clinopyroxene. Inclusions of spinel in olivine are small and scarce. The degree of serpentinization varies between 10 and 60 percent. In the wehrlite layers of coarse grained hypidiomorphic olivine alternate with clinopyroxene rich layers. Spinel occurs as hypidiomorphic to idiomorphic grains or as inclusion in silicates. Clinopyroxenite with an equigranular to porphyric texture is made up of coarse- to medium-grained hypidiomorphic clinopyroxene with a matrix of fine grained olivine, amphibole and hypidiomorphic to xenomorphic spinel. Spinel also forms idiomorphic inclusions in clinopyroxene. Hornblendite forms veins and dykes in the dunites at Kosiva Mountain in Southwest Kytlym (Fig. 1b) and dykes and larger bodies within the clinopyroxenites of the Svetley Bor complex. Spinel is present here as hypidiomorphic to idiomorphic interstitial grains or as idiomorphic grains enclosed in the silicate phases.

Tilaites were first described by Dupark and Tikhonowitch (1920) from the Tilay Mountain area in the eastern part of the Kytlym complex (Fig. 1b). They are coarse grained rocks which often show a porphyric texture and contain mainly clinopyroxene, less feldspar and a significant amount of olivine. Tilaites can be interpreted as feldspar-bearing clinopyroxenite. Based on their different mineralogical and chemical composition three groups of tilaites have been distinguished (Chapter 2). Nepheline Tilaites represent the most fractionated products of the melt that initially formed the ultramafic cumulates. Beside coarse grained clinopyroxene phenocrysts they contain olivine, clinopyroxene, phlogopite, hornblende, intermediate plagioclase$_{An28-48}$, K-feldspar, nepheline and

xenomorphic to hypidiomorphic spinel in the matrix. Idiomorphic spinel is enclosed in olivine and clinopyroxene. Nepheline tilaites occur in Nizhnii Tagil and to the southwest of the Kytlym complex.

Bytownite tilaite shares many mineralogical and textural features with the nepheline tilaite, but it is devoid of nepheline and K-feldspar, has plagioclase with a higher An content (An = 68-87) and contains rare orthopyroxene. Such tilaites occur together with nepheline tilaites, but due to the different composition of silicate minerals the bytownite tilaites from Tilay Mountain are recognized as a separate group (Chapter 2).

2.2 Determination of major elements in spinel and ilmenite

Thirty eight polished thin sections 30 or 150 µm thick were used for the microprobe measurements. Spinel and ilmenite were analysed with the Jeol JXA 8200 microprobe of the Max-Planck-Institute for Chemistry and the Jeol JXA 8900RL microprobe at the Institute of Geosciences of the University of Mainz. We used natural minerals and oxides (Si, Ti, Al, Fe, Mg, Mn, Cr and Zn) and pure element standards (V, Co) for calibration. The oxide minerals were measured with five WDS spectrometers at 20 kV acceleration voltage, a probe current of 12 or 20 nA and either a focussed beam or a beam diameter of 2 µm.

2.3 Determination of the major element distribution in spinel by element mapping

Element maps of 30 exsolved and 17 homogeneous spinels were obtained with the Jeol JXA 8900RL microprobe at the Institute of Geosciences of the University of Mainz at 15 or 20 kV and 12-20 nA with a focussed electron beam. Chromium, Mn, Al, Mg and Ti were measured with WDS spectrometers at counting times between 100 and 200 ms, Fe, Ca and Si with an EDS spectrometer and in addition the BSE image was recorded. The step size varied between 0.2 and 2 µm.

3 Results

The large number of analysis from 38 samples (1461 of exsolved spinel, 252 of homogeneous chromian spinel, 206 of recalculated exsolved spinel and 46 ilmenite grains) permits only the presentation of selected analyses in Tables 1-6. The entire data set can be found in the electronic attachment. In addition, the published dataset from Krause et al. (2007) on ultramafic rocks has been used in this study.

3.1 Textural observations among the spinel phases

Homogeneous chromian spinel is present in all dunite and wehrlite and in some of the clinopyroxenite samples (NT13, KT39, KT5/290, KT52) except the ones from Tilay Mountain (Kytlym), where some of the dunites host exsolved spinel. It occurs as idiomorphic to hypidiomorphic grains devoid of an optical zonation. Many grains show veins filled with serpentine and magnetite. In samples with intensive serpentinization chromite is sheared under brittle conditions. In places, magnetite forms small interstitial xenomorphic grains and also a narrow discontinuous rim around chromite. In wehrlite the larger spinel grains up to 2 mm tend to be hypidiomorphic or even xenomorphic. Small idiomorphic spinel up to 200 µm can be found enclosed in olivine or clinopyroxene.

Exsolved spinel occurs in dunite at Tilay Mountain (Kytlym) and in clinopyroxenite of all sampled massifs. Exsolved spinel is also present in nearly all sampled tilaites and gabbros. It forms single grains and aggregates of xenomorphic to hypidiomorphic grains in the matrix and idiomorphic to hypidiomorphic inclusions in pyroxene and olivine. The size of the spinel inclusions of up to 200 µm is in general one order of magnitude smaller than that of matrix grains in the same sample.

Three exsolution textures of Fe-rich and Al-rich spinel exsolutions can be observed. The first type A is present in all studied samples having exsolved spinel regardless of the textural position, the chemical composition and the grain size of spinel. One Al-rich spinel phase forms irregular bleb-like textures, predominantly near the rim of individual spinel grains or along cracks (Fig. 2). In some cases they might be related to sub grain boundaries. The other phase forms the matrix around these blebs. The contacts

between both phases are always sharp, have a simple, strait geometry and are well defined by a strong contrast in the reflected light (Fig. 2). Similar textures have been shown by Krause et al. (2007, Fig. 10a therein).

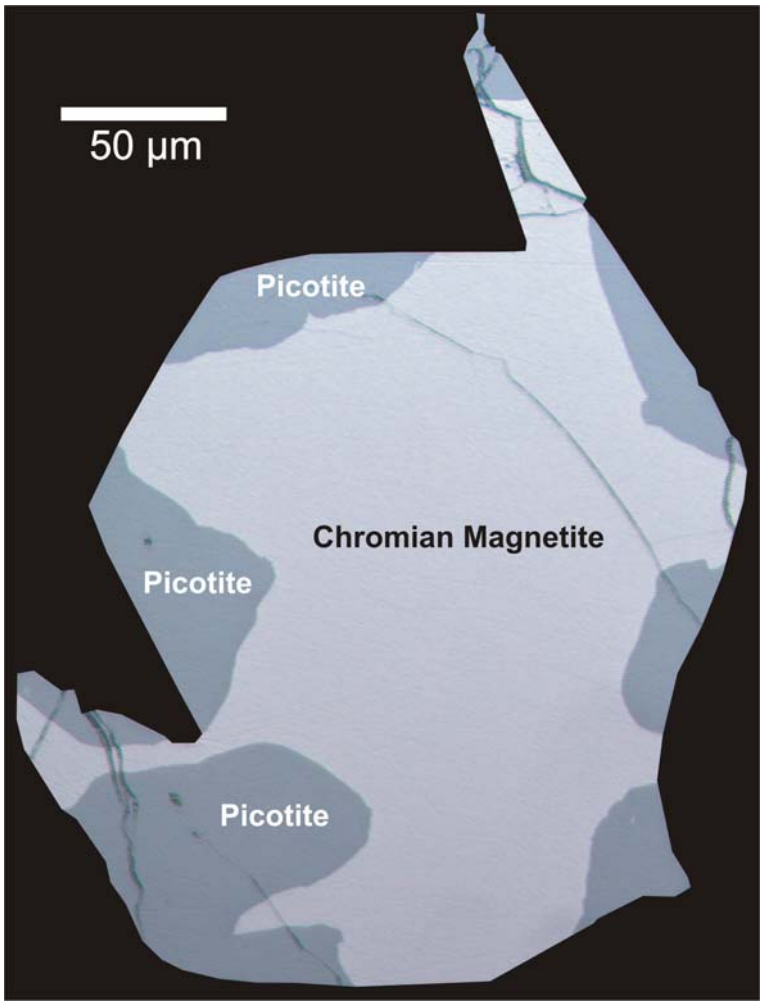

Fig. 2: Reflected light image of exsolution type A in spinel with blebs of picotite at the rim and chromian magnetite in the centre. (Sample KT35, Hornblendite vein in dunite).

The second texture type B is limited to spinel with a low Cr content (Cr_2O_3 < 10 wt.%), and occurs in gabbros, tilaites and some clinopyroxenite samples (KT43, KT5-290, KT5-370, KT5-440, KT5-610). It consists of lamellas oriented parallel to the (110) planes which commonly form a network-like texture defined by the appearance of two perpendicular orientations (Fig. 3a). These lamellas have lengths of ten to several hundred micrometers at a typical width of less than two micrometers. This prevented a precise chemical analysis with the electron microprobe in most of the cases.

Interestingly, the lamellas always consist of an Al-rich spinel in a matrix of Fe-rich spinel. In general the lamellas are absent in the direct vicinity of type A exsolutions (Figs. 3 a, c) indicating that the type A exsolutions were formed prior to the lamellas. In a few cases lamellas are in a direct contact with type A exsolutions implying a cogenetic relationship (Fig. 3b).

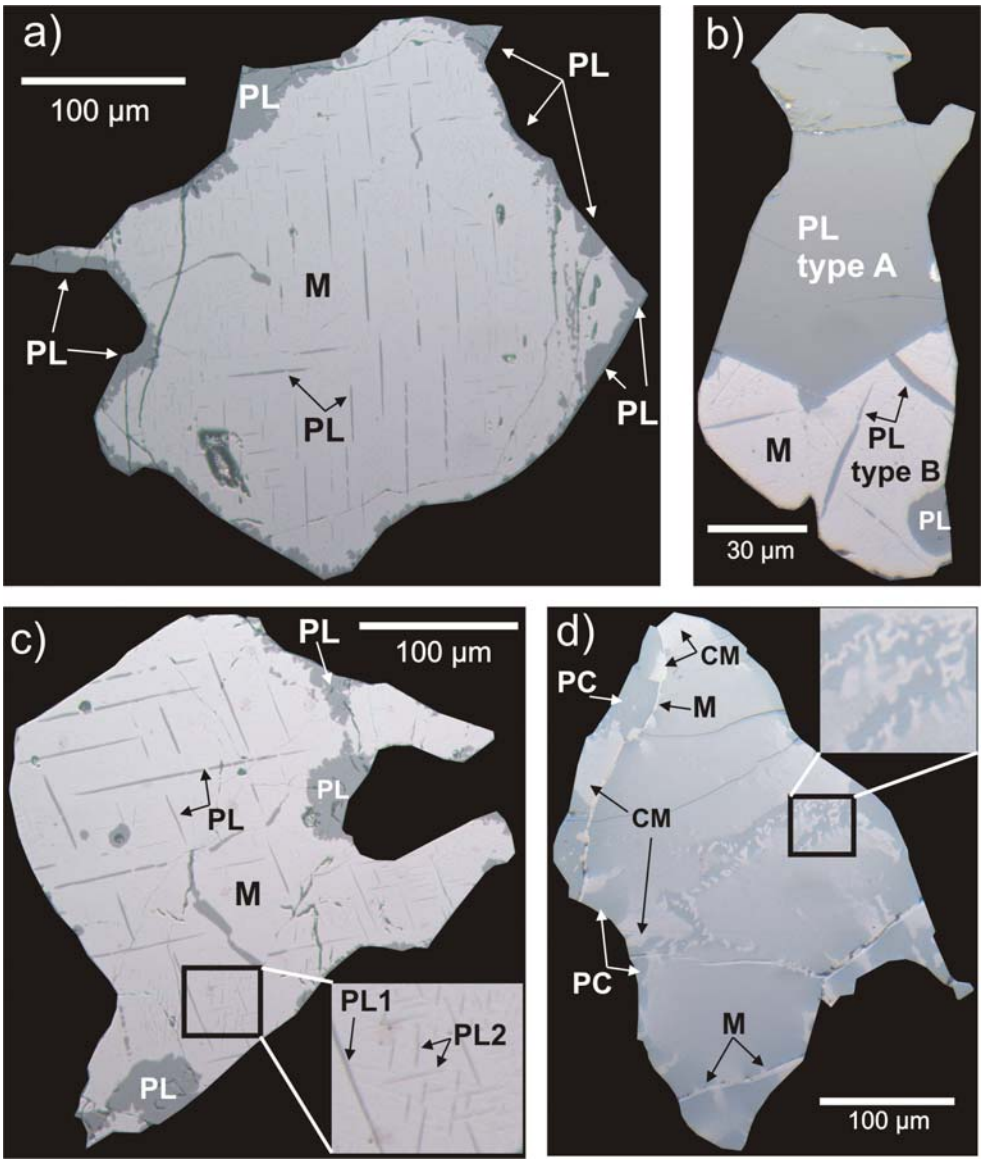

Fig. 3: Reflected light images of exsolution textures in spinel. PL = pleonaste, M = magnetite, PC = picotite, CM = chromian magnetite. (a) Lamellar exsolutions type B in the core and blebs of pleonaste in a matrix of magnetite (NT9b). (b) Direct connection of a lamellar exsolution (type A) and a bleb (type B) of similar composition (NT8). (c) Second generation of fine, lamellar exsolutions Pl2 forming an angle of 30° with the first generation Pl1 (KT46). (d) Irregular exsolution (type C) concentrated along cracks and grain boundaries (KT328).

In places a second set of very fine lamellas of Al-rich spinel is present. These lamellas are much smaller and either parallel to the lamellas of the first set or are offset with an angle of ca. 30° (Fig. 3c). The two sets of lamellas have no direct contact and they are separated by a precipitate free zone. According to their textural position and the presence of a precipitate free zone, lamellas of the second set are interpreted to represent a second, younger generation relative to the larger lamellas of the first set.

The exsolution texture type C is restricted to spinels with a significant Cr content (Cr_2O_3 = 15 wt.% to 35 wt.%) and is found in dunite, hornblendite and in one case in a bytownite tilaite (KT324). This texture has an irregular geometry and predominantly occurs in larger spinel grains (more than 50µm diameter, Fig. 3d), whereas smaller grains in the same samples mostly show A-type textures. Contacts between the two exsolving phases are commonly diffuse and irregular (insert Fig. 3d). But several grains especially in the dunite show also sharp boundaries between both phases with a type A-like texture as an end member. Under the microscope with reflected light the brighter Fe-rich phase seems to be concentrated at grain boundaries and along healed cracks (Fig. 3d). Remarkably, these spinels often show areas which seem to be unaffected by any exsolution process and have preserved the original composition.

Spinels in tilaites, gabbros and hornblendite frequently are intergrown with ilmenite. It forms one prismatic grain that is often entirely enclosed in spinel. In a few spinels from Nepheline tilaites X-ray maps confirm the presence of several very narrow, elongated prismatic ilmenite grains.

3.2 Chemical composition of spinel

3.2.1 Composition of homogeneous spinels

The chemical and petrographic features of homogenous spinels from the complexes of Nizhnii Tagil, Svetley Bor and Kytlym have been described by Krause et al. (2007). The present study provides additional data especially from dunite in the eastern part of the Kytlym complex (Tilay Mountain) and describes in addition some detailed profiles across chromite grains in samples from Nizhnii Tagil and the south-western part of the Kytlym Complex.

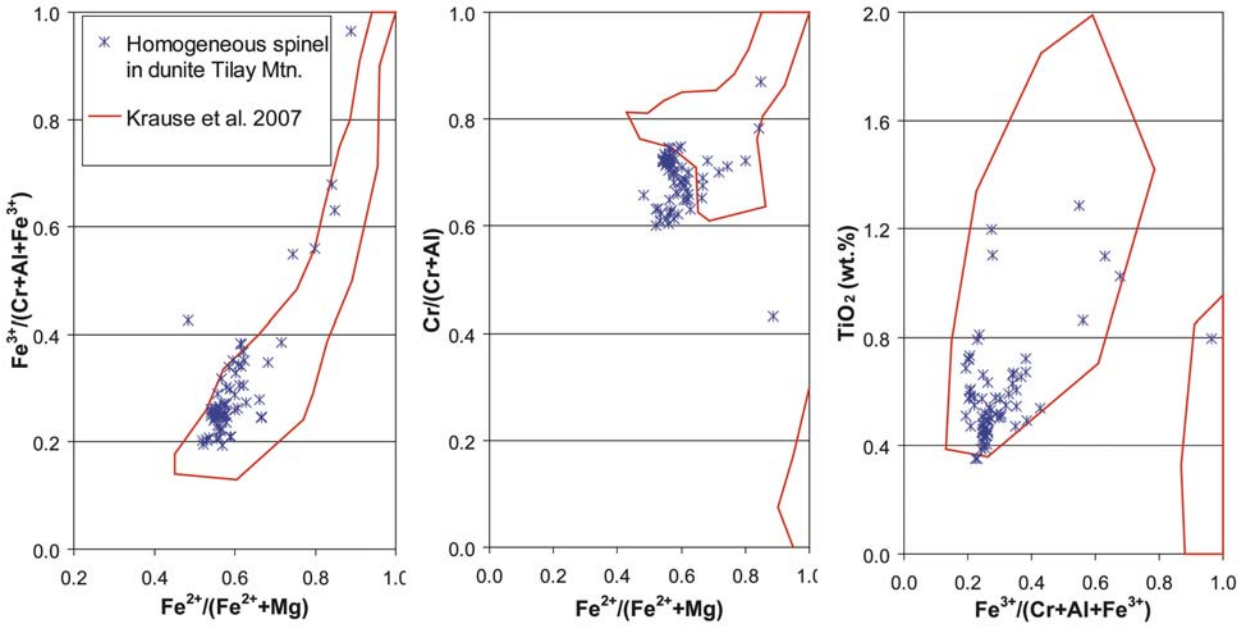

Fig. 4: Variation of $Fe^{2+}/(Fe^{2+}+Mg)$, $Fe^{3+}/(Cr+Al+Fe^{3+})$, $Cr/(Cr+Al)$ and TiO_2 in homogeneous spinel in dunite from Tilay Mountain (Kytlym). For comparison, the compositional fields of homogeneous spinel in dunite from all complexes are shown (from Krause et al., 2007).

Spinels in dunites from Tilay Mountain are in some samples homogeneous (KT310 and KT311), but display exsolution textures in others (KT328, KT330, KT332 see below). The homogeneous spinels from Tilay Mountain are in composition similar to those described from the other dunite bodies (Fig. 4; Krause et al., 2007). They are slightly more evolved than most of the spinels in dunites from Nizhnii Tagil, Svetley Bor and south west Kytlym covering the low end of the TiO_2, Cr_2O_3, Fe_2O_3, $Fe^{2+}/(Mg+Fe^{2+})$, $Cr/(Cr+Al)$ and $Fe^{3+}/(Al+Cr+Fe^{3+})$ variations (Fig. 4, Tab. 1).

Tab. 1: Composition of selected homogeneous spinels in dunite from Tilay Mountain, Kytlym. C = core, R = rim, FeO_m = all iron measured as FeO, FeO_{calc} and Fe_2O_{3calc} are calculated assuming stoichiometry, b.d. = below limit of detection.

Sample	KT310-101	KT310-105	KT310-119	KT310-121	KT310-133	KT311-14	KT311-17	KT311-29	KT311-34	KT311-64
Poaition	R	C	C	C	R	R	C	R	R	C
SiO_2 (wt.%)	b.d.	b.d.	0.03	0.01	0.12	0.05	0.02	0.02	0.07	0.04
TiO_2	0.67	0.48	0.35	0.44	0.80	1.03	0.47	0.49	1.29	0.73
Al_2O_3	10.14	10.72	9.72	10.53	0.88	3.11	13.69	8.88	5.92	15.86
FeO_m	45.27	37.86	35.94	38.33	86.83	69.70	36.19	50.58	59.82	35.60
MnO	0.43	0.37	0.37	0.35	0.20	0.31	0.46	0.48	0.36	0.40
MgO	7.73	8.61	8.73	8.93	1.98	2.88	8.27	5.39	4.79	9.29
Cr_2O_3	32.98	40.30	42.97	40.52	1.00	16.74	39.48	30.93	21.66	37.45
NiO	0.17	0.13	0.09	0.11	0.33	0.45	0.16	0.21	0.44	0.16
V_2O_3	0.11	0.05	0.03	0.07	0.07	0.08	0.12	0.05	0.12	0.11
ZnO	0.14	0.17	0.22	0.17	0.02	0.16	0.22	0.34	0.07	0.16
CoO	0.07	0.12	0.09	0.06	0.06	0.08	0.06	0.08	0.09	0.04
Total	97.73	98.86	98.56	99.56	92.29	94.59	99.14	97.49	94.70	99.86
Cr/(Cr+Al)	0.69	0.72	0.75	0.72	0.43	0.78	0.66	0.70	0.71	0.61
$Fe^{3+}/(Cr+Al+Fe^{3+})$	0.34	0.25	0.23	0.26	0.96	0.68	0.21	0.39	0.55	0.21
$Fe^{2+}/(Mg+Fe^{2+})$	0.61	0.57	0.56	0.56	0.89	0.84	0.59	0.72	0.74	0.55
FeO_{calc}	21.44	20.24	19.67	20.02	27.95	27.21	21.20	24.31	24.88	20.57
Fe_2O_{3calc}	26.49	19.58	18.08	20.35	65.43	47.22	16.65	29.19	38.83	16.70

X-ray maps and detailed profiles of idiomorphic chromites (200-800 µm in diameter) in dunite samples from Nizhnii Tagil (NT7) and SW-Kytlym (KT40) show a weak but continuous chemical zoning parallel to the grain boundary indicated by an increase of Fe, Mn and Al and a decrease of Cr and Mg contents from core to rim (Fig. 5a). Little or no zonation is observed for Ti, Ni, V and Co (Tab. 2). In the Al_2O_3 vs. Cr_2O_3 diagram a negative correlation is visible for analyses taken from chromite with a symmetric Cr zonation as both rims have lower Cr_2O_3 but higher Al_2O_3 contents (Fig. 5a). The Cr/(Cr+Al) decreases from the core (~0.778) towards the rim on both sides (~0.755), while the Fe^{3+} increases from 0.3 a.p.f.u. in the core to 0.36 a.p.f.u. at the rim (Fig. 5a). These variations are expected if the chromite crystallizes from a continuously evolving melt.

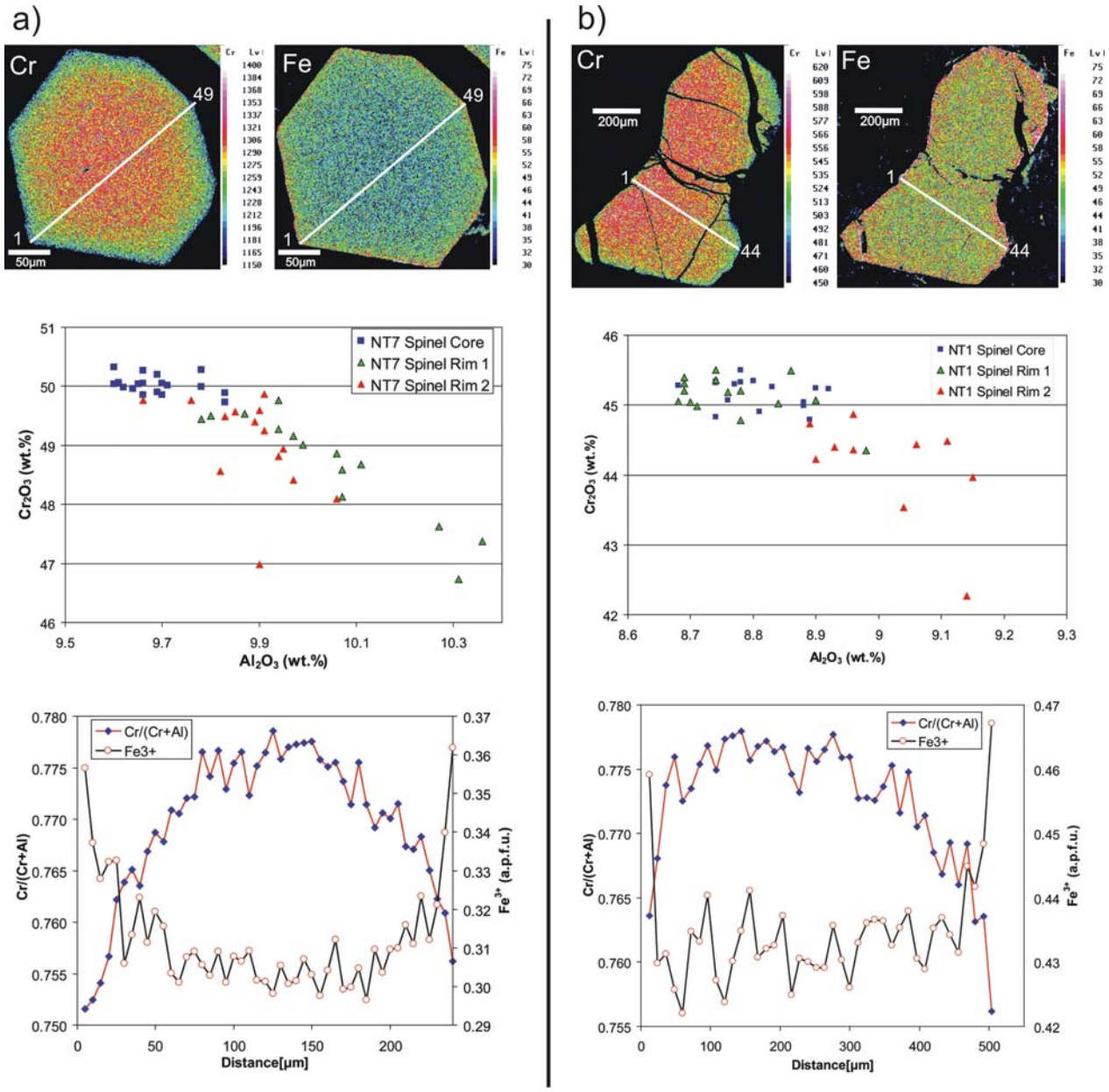

Fig. 5: Compositional variation and spatial distribution of major elements and Cr/(Cr+Al) in homogeneous spinel in dunite. White lines in the element distribution maps indicate the position of the profiles of the microprobe analyses. Rim1 and Rim2 refer to the analyses near both ends of the profile. (a) Symmetric distribution of Cr, Fe_{tot}, Fe^{3+} and Cr/(Cr+Al) in chromite from a dunite containing no interstitial clinopyroxene (NT7). (b) Asymmetric distribution of Cr, Fe_{tot}, Fe^{3+} and Cr/(Cr+Al) in spinel in dunite containing interstitial clinopyroxene (NT1).

In many grains, however, the zonation of Cr is different in that it is asymmetric and crosscutting the zonation patterns of the other elements that are parallel to the grain boundary. In these cases Cr increases from one side of the grain towards the other (Fig. 5b). Such grains have a broad plateau (defined by core and left rim in Fig. 5b) which is

characterized by high and constant Cr contents. But at the same time Al_2O_3 decreases 8.9 to 8.7 wt., Fig. 5b). There is also a negative correlation of Al_2O_3 and Cr_2O_3 at high Al_2O_3 contents (>8.9 wt.%; Fig. 5b), like that observed in the symmetric grains, implying that these parts in the grain reflect the crystallization from a melt. Cr/(Cr+Al) decreases from the core (~0.778) towards one side of the grain (0.764) but remains constant towards the other side ignoring the analysis of the outermost rims (Fig. 5b, Tab. 2). Within the same profile the Fe^{3+} is variable in the core (0.42 – 0.44 a.p.f.u.) and increases towards the rim on both sides (0.47 a.p.f.u.). A systematic analysis of this sample shows several grains with similar zonation patterns. It is thus unlikely, that this kind of zonation can be attributed to the position of the section plane. This distribution is a primary feature, because in the X-ray element maps we cannot see any evidence for a redistribution of major elements related to the cracks filled with serpentine and pure magnetite (Fig. 5b).

Tab. 2: Composition along profiles across zoned spinel in dunite with and without interstitial clinopyroxene from Nizhnii Tagil. Du = Dunite, FeO_m = all iron measured as FeO, FeO_{calc} and Fe_2O_{3calc} are calculated assuming stoichiometry, b.d. = below limit of detection.

Sample	NT7 6-1	NT7 6-8	NT7 6-15	NT7 6-18	NT7 6-24	NT7 6-31	NT7 6-34	NT7 6-36	NT7 6-44	NT7 6-49
Lithology	Du - Cpx	Du - Cpx	Du - Cpx	Du - Cpx	Du - Cpx	Du - Cpx	Du - Cpx	Du - Cpx	Du - Cpx	Du - Cpx
Position	Rim1	Rim1	Rim1	Core	Core	Core	Core	Rim 2	Rim 2	Rim 2
Distance (µm)	0	35	70	85	115	150	165	175	215	240
SiO_2 (wt.%)	0.06	0.06	b.d.	0.03	0.01	0.01	0.03	0.01	0.01	0.04
TiO_2	0.60	0.53	0.52	0.46	0.43	0.44	0.45	0.44	0.52	0.54
Al_2O_3	9.41	10.06	9.80	9.78	9.78	9.60	9.71	9.91	9.94	9.78
FeO_m	35.78	30.75	29.38	29.14	29.11	28.79	29.15	28.80	30.07	33.38
MnO	0.54	0.38	0.47	0.45	0.38	0.39	0.49	0.37	0.49	0.50
MgO	7.18	9.51	10.12	10.20	10.30	10.32	10.46	10.28	9.58	8.00
Cr_2O_3	44.44	48.86	49.50	49.99	50.28	50.04	50.02	49.87	48.81	45.24
NiO	0.10	0.08	0.06	0.07	0.09	0.07	0.08	0.09	0.11	0.08
V_2O_3	0.03	0.05	0.05	0.06	0.06	0.04	0.04	0.02	0.03	0.04
ZnO	0.20	0.17	0.16	0.19	0.15	0.16	0.16	0.19	0.19	0.20
CoO	0.11	0.06	0.07	0.05	0.04	0.06	0.03	0.07	0.08	0.08
Total	98.50	100.57	100.16	100.44	100.67	99.93	100.65	100.16	99.90	97.91
Cr/(Cr+Al)	0.760	0.765	0.772	0.774	0.775	0.778	0.776	0.771	0.767	0.756
$Fe^{3+}/(Cr+Al+Fe^{3+})$	0.199	0.159	0.156	0.153	0.153	0.153	0.158	0.152	0.158	0.184
$Fe^{2+}/(Mg+Fe^{2+})$	0.633	0.533	0.502	0.499	0.496	0.492	0.487	0.494	0.524	0.592
FeO_{calc}	15.29	12.68	12.45	12.29	12.28	12.24	12.71	12.14	12.51	14.14
Fe_2O_{3calc}	22.02	19.34	18.18	18.08	18.06	17.78	17.71	17.88	18.81	20.66

Tab. 2: (cont.)

Sample	NT1 12-1	NT1 12-8	NT1 12-17	NT1 12-20	NT1 12-25	NT1 12-29	NT1 12-33	NT1 12-36	NT1 12-40	NT1 12-43
Lithology	Du +Cpx	Du +Cpx	Du +Cpx	Du +Cpx	Du +Cpx	Du +Cpx	Du +Cpx	Du +Cpx	Du +Cpx	Du +Cpx
Position	Rim 1	Rim 1	Rim 1	Core	Core	Core	Core	Rim 2	Rim 2	Rim 2
Distance (µm)	0	84	192	228	288	336	384	420	468	504
SiO_2 (wt.%)	0.05	0.05	b.d.	b.d.	0.03	0.01	0.04	b.d.	b.d.	0.04
TiO_2	0.76	0.55	0.55	0.58	0.54	0.55	0.59	0.64	0.57	0.61
Al_2O_3	4.51	8.78	8.70	8.90	8.78	8.88	8.74	8.96	8.90	9.14
FeO_m	47.75	35.42	34.69	34.49	34.86	35.08	35.77	35.79	36.53	37.85
MnO	1.06	0.39	0.44	0.43	0.39	0.45	0.40	0.43	0.38	0.52
MgO	4.18	8.87	9.12	9.42	9.14	9.13	8.73	8.57	8.32	7.67
Cr_2O_3	38.16	45.20	45.04	45.24	45.33	44.99	44.83	44.36	44.23	42.27
NiO	0.20	0.12	0.09	0.08	0.09	0.11	0.11	0.10	0.10	0.07
V_2O_3	0.03	0.05	0.03	0.04	0.04	0.03	0.08	0.04	0.04	0.05
ZnO	0.26	0.20	0.15	0.19	0.16	0.15	0.19	0.19	0.24	0.18
CoO	0.07	0.06	0.08	0.07	0.06	0.05	0.08	0.07	0.04	0.09
Total	97.57	98.93	98.42	99.21	98.43	98.59	98.50	98.28	97.74	97.18
Cr/(Cr+Al)	0.850	0.775	0.776	0.773	0.776	0.773	0.775	0.769	0.769	0.756
$Fe^{3+}/(Cr+Al+Fe^{3+})$	0.349	0.220	0.220	0.219	0.218	0.221	0.223	0.221	0.226	0.237
$Fe^{2+}/(Mg+Fe^{2+})$	0.770	0.557	0.542	0.531	0.544	0.544	0.564	0.570	0.582	0.610
FeO_{calc}	25.28	17.26	17.14	17.20	17.14	17.40	17.41	17.25	17.63	18.29
Fe_2O_{3calc}	25.00	19.89	19.27	19.01	19.44	19.42	20.10	20.27	20.67	21.39

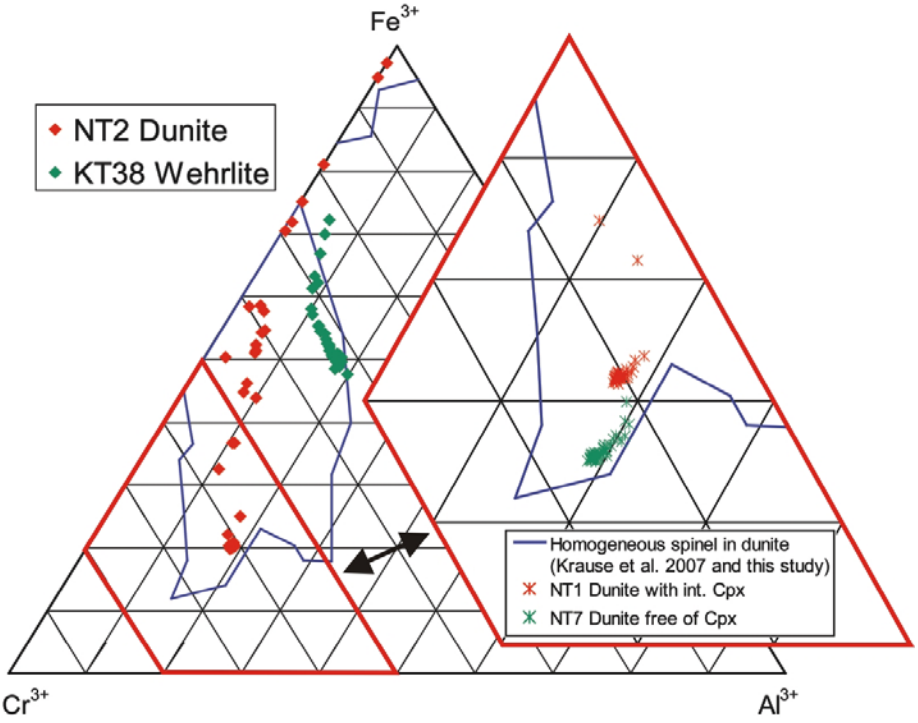

Fig. 6: Distribution of the trivalent cations in the homogeneous spinel shown in Figs. 5 and 7. The spinel in clinopyroxene-bearing lithologies has similar or lower Al_2O_3, but higher Fe_2O_3 contents than that in clinopyroxene-free dunites. Data for compositional variation in homogeneous spinel in dunite from all Uralian complexes are from Krause et al. (2007).

In sample NT1 the Cr-rich side of the spinel grain with the asymmetric zoning can be found near (within a few mm) interstitial xenomorphic clinopyroxene, which is interpreted to have been crystallized from interstitial melt (Krause et al., 2007; Chapter 2). In the trivalent cations diagram, the clinopyroxene-free dunite with a symmetric distribution of Cr_2O_3 forms a trend of decreasing Cr_2O_3 at increasing Al_2O_3 and Fe_2O_3 reflecting the crystallization of the chromite from an olivine crystallizing melt (Fig. 6). The trend for the chromite from the clinopyroxene-bearing dunite with an asymmetric zonation in Cr_2O_3 shows the enrichment of Fe_2O_3 at the expense of Cr_2O_3, but no increase in Al_2O_3 (Fig. 6).

In sample NT2 some chromite grains show a distinctly different element distribution. In contrast to the previously described spinels Cr/(Cr+Al) and Fe^{3+} variations are positively correlated across the entire grain (Fig. 7a, Tab. 3) The idiomorphic grain has a core with an irregular shape which is in composition similar to the previously described chromites (Cr/(Cr+Al) = 0.76-0.77; Fe^{3+} = 0.39-0.41 a.p.f.u.; Fig. 7a). This core is surrounded by a rim of ferritchromite (Cr/(Cr+Al) = 0.83-0.88; Fe^{3+} = 0.64-1.13 a.p.f.u.) in composition similar to the outermost rims of the above described chromites. Small Ni-sulphide inclusions are present within this zone and at the contact to the core. The contact between the ferritchromit and the chromite core is sharp and the concentration of many elements change more than 50% within a distance of less then 5 µm (Fig. 7a). The zone of ferritchromit is encircled with a discontinuous rim of magnetite (Fe^{3+} > 1.4 a.p.f.u.; Fig. 7a). In the Al_2O_3 vs. Cr_2O_3 diagram the core shows a small variation in Al_2O_3 at constant Cr_2O_3. In the ferritchromit zone Al_2O_3 rapidly decreases from about 8 to about 1 wt.%, whereas at the same time Cr_2O_3 decreases just by a factor of 2.5, from 42 to about 15-20 wt. % (Fig. 7a). The decrease in Cr_2O_3 and Al_2O_3 is balanced by an increase in Fe_2O_3 and MgO is simultaneously replaced by FeO (Tab. 3). In the trivalent cations diagram this variation defines the trend of Fe^{3+}-enrichment on the expense of Cr^{3+} and Al^{3+} (Fig.6) and this trend has also been described for homogeneous, disseminated chromite in dunites (Krause et al., 2007).

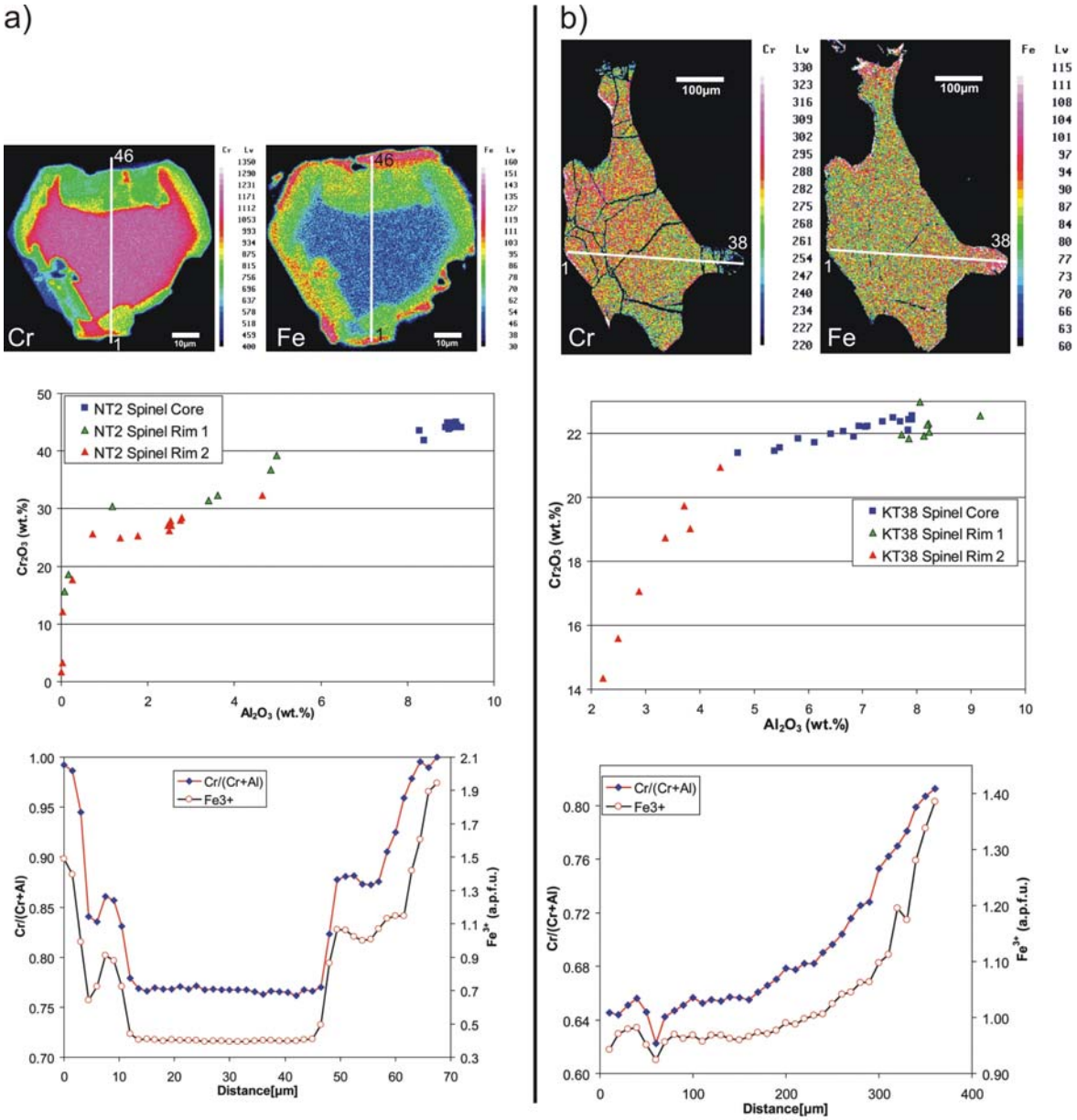

Fig. 7: Compositional variation and spatial distribution of major elements and Cr/(Cr+Al) of homogeneous spinel. (a) Resorbed core of chromite overgrown with chromian magnetite and magnetite (dunite NT2). (b) Xenomorphic grain with asymmetric distribution of Fe, Cr and Al (wehrlite KT38).

Spinel in wehrlite from the SW-Kytlym (KT38) has in general lower Cr_2O_3 and MgO at higher Fe_2O_3 and FeO contents than those in dunites (Fig. 7b, Tab. 3). The investigated grains have an inhomogeneous asymmetric chemical zonation in all major elements with Fe_2O_3 and FeO replacing Al_2O_3, Cr_2O_3 and MgO respectively (Fig. 7b).

Tab. 3: Composition along profiles across zoned spinel in dunite (NT2) and wehrlite (KT38). NT = Nizhnii Tagil, SW-KT = southwest Kytlym FeO_m = all iron measured as FeO, FeO_{calc} and Fe_2O_{3calc} are calculated assuming stoichiometry, b.d. = below limit of detection.

Sample	NT2 13-1	NT2 13-3	NT2 13-7	NT2 13-9	NT2 13-16	NT2 13-23	NT2 13-31	NT2 13-33	NT2 13-39	NT2 13-44
Locality	NT	NT	NT	NT	NT	NT	NT	NT	NT	NT
Position	Rim 1	Rim 1	Rim 1	Core	Core	Core	Core	Rim 2	Rim 2	Rim 2
Distance (µm)	0	3	9	12	22.5	33	45	48	57	64.5
SiO_2 (wt.%)	0.24	0.12	0.09	0.07	0.06	0.11	0.10	0.15	0.87	0.31
TiO_2	0.28	0.53	0.57	0.44	0.52	0.44	0.50	0.63	0.71	0.22
Al_2O_3	0.08	1.19	3.62	8.27	9.06	9.11	8.96	4.64	2.50	0.04
FeO_m	70.03	56.82	54.00	38.09	36.37	36.09	37.30	54.34	59.62	76.62
MnO	0.70	1.28	0.64	0.72	0.53	0.53	0.59	0.65	0.86	0.45
MgO	2.74	2.35	4.00	6.05	6.96	6.82	6.22	4.42	3.28	1.25
Cr_2O_3	15.66	30.40	32.30	43.51	44.70	44.78	43.80	32.26	26.17	12.09
NiO	0.17	0.14	0.15	0.03	0.12	0.06	0.06	0.12	0.08	0.19
V_2O_3	0.02	0.03	b.d.	0.03	0.02	0.01	0.07	0.01	0.05	0.04
ZnO	0.11	0.20	0.20	0.22	0.22	0.24	0.25	0.16	0.17	0.07
CoO	0.06	0.12	0.11	0.14	0.09	0.08	0.08	0.09	0.13	0.09
Total	90.11	93.23	95.76	97.56	98.65	98.31	97.92	97.50	94.62	91.49
Cr/(Cr+Al)	0.993	0.945	0.857	0.779	0.768	0.767	0.766	0.823	0.875	0.995
$Fe^{3+}/(Cr+Al+Fe^{3+})$	0.752	0.504	0.447	0.222	0.204	0.200	0.208	0.439	0.547	0.810
$Fe^{2+}/(Mg+Fe^{2+})$	0.835	0.861	0.779	0.681	0.642	0.647	0.676	0.763	0.814	0.925
FeO_{calc}	50.32	34.39	32.05	16.73	15.65	15.32	15.75	32.23	37.86	54.38
Fe_2O_{3calc}	24.75	25.87	25.17	23.03	22.28	22.31	23.13	25.34	25.56	27.69

Sample	KT38 18-1	KT38 18-4	KT38 18-8	KT38 18-11	KT38 18-19	KT38 18-25	KT38 18-30	KT38 18-32	KT38 18-35	KT38 18-37
Locality	SW-KT	SW-KT	SW-KT	SW-KT	SW-KT	SW-KT	SW-KT	SW-KT	SW-KT	SW-KT
Position	Rim 1	Rim 1	Rim 1	Core	Core	Core	Core	Rim 2	Rim 2	Rim 2
Distance (µm)	0	30	70	100	180	240	290	310	340	360
SiO_2 (wt.%)	0.05	0.03	0.02	0.01	0.03	0.01	0.05	0.03	0.01	0.05
TiO_2	1.10	1.16	1.16	1.27	1.27	1.34	1.32	1.40	1.38	1.28
Al_2O_3	8.06	7.85	8.23	7.81	7.56	6.64	5.38	4.38	2.88	2.22
FeO_m	58.56	60.17	58.95	59.73	60.09	61.12	62.43	64.21	69.52	71.87
MnO	0.54	0.37	0.51	0.54	0.42	0.43	0.48	0.52	0.37	0.34
MgO	3.48	3.44	3.69	3.59	3.53	3.28	2.95	2.67	2.20	1.98
Cr_2O_3	22.97	21.83	22.05	22.25	22.48	22.07	21.45	20.93	17.07	14.34
NiO	0.16	0.20	0.17	0.19	0.20	0.17	0.19	0.19	0.24	0.22
V_2O_3	0.10	0.10	0.17	0.11	0.16	0.15	0.16	0.17	0.19	0.16
ZnO	0.15	0.13	0.19	0.26	0.16	0.15	0.12	0.12	0.12	0.07
CoO	0.08	0.11	0.07	0.07	0.10	0.08	0.05	0.07	0.07	0.04
Total	95.59	98.59	98.83	99.08	98.27	98.36	97.73	98.81	97.88	96.82
Cr/(Cr+Al)	0.656	0.651	0.642	0.656	0.666	0.690	0.728	0.762	0.799	0.812
$Fe^{3+}/(Cr+Al+Fe^{3+})$	0.486	0.507	0.496	0.503	0.504	0.524	0.554	0.581	0.669	0.722
$Fe^{2+}/(Mg+Fe^{2+})$	0.815	0.818	0.804	0.810	0.815	0.826	0.841	0.856	0.880	0.890
FeO_{calc}	34.77	36.23	35.45	36.02	36.07	37.03	38.48	40.05	45.43	48.26
Fe_2O_{3calc}	27.27	27.57	27.06	27.32	27.64	27.80	27.81	28.17	28.64	28.44

In the xenomorphic grain of Fig. 7b Cr/(Cr+Al), Fe^{3+} and $Fe^{2+}/(Mg+Fe^{2+})$ increase from one side (Cr/(Cr+Al) = 0.64, Fe^{3+} = 0.95 a.p.f.u., $Fe^{2+}/(Mg+Fe^{2+})$ = 0.8) to the other (Cr/(Cr+Al) = 0.81, Fe^{3+} = 1.35 a.p.f.u., $Fe^{2+}/(Mg+Fe^{2+})$ = 0.89; Fig. 7b, Tab. 3). The Al_2O_3 vs. Cr_2O_3 diagram shows at relatively constant Cr_2O_3 contents a quick decrease of Al_3O_3; but starting at an Al_3O_3 content of about 4.5 wt.%, Cr also decreases strongly (Fig. 7b). This is accompanied by a rapid increase in Fe_2O_3 (Figs. 6, 7b).

3.2.2. Composition of exsolved spinels

The exsolved spinels cover a wide compositional array ranging from pleonaste to picotite and chromian magnetite to almost pure magnetite. Representative analyses from the studied Uralian-Alaskan-type complexes can be found in table 4. In general, it is apparent that the lower the Cr_2O_3-content of the initial spinel is, the larger is the chemical difference of the two exsolved spinel phases. The Fe-rich phase has high contents of TiO_2 (up to 8.1 wt.%) and V_2O_3 (up to 1.6 wt.%), low contents of MgO (up to 6.9 wt.%) and ZnO (up to 0.17 wt.%). The coexisting Al-rich phase has higher MgO up to 20.9 wt.% and ZnO up to 3.7 wt.%. For other components like Cr_2O_3, NiO, MnO and CoO there is no obvious systematic difference between these phases (Tab. 4).

In diagrams showing $Fe^{2+}/(Mg+Fe^{2+})$ vs. Cr/(Cr+Al) or $Fe^{3+}/(Cr+Al+Fe^{3+})$ vs. TiO_2 the composition of the exsolved spinel in ultramafic rocks is shifted towards lower Cr/(Al+Cr) and higher TiO_2-contents relative to the field of homogeneous spinel in dunite (Fig. 8a-c). In the $Fe^{2+}/(Mg+Fe^{2+})$ vs. $Fe^{3+}/(Cr+Al+Fe^{3+})$ diagram most of the exsolved spinels in ultramafic rocks plot in the compositional field defined by homogeneous, disseminated spinels from dunites (Fig. 8a; Krause et al., 2007). Pleonaste with less than 33 wt. % FeO_{tot} in some clinopyroxenites and in the mafic rocks extends this trend towards lower values (Fig. 8a, d). Spinels in hornblendite are exsolved into picotite (Cr/(Cr+Al) = 0.18-0.38, $Fe^{2+}/(Mg+Fe^{2+})$ = 0.34-0.60, $Fe^{3+}/(Al+Cr+Fe^{3+})$ = 0.06-0.22, TiO_2 = 0.2-1.0 wt.%) and chromian magnetite (Cr/(Cr+Al) = 0.58-1.0, $Fe^{2+}/(Mg+Fe^{2+})$ = 0.75-0.91, $Fe^{3+}/(Al+Cr+Fe^{3+})$ = 0.42-0.7, TiO_2 = 2.9-8.1 wt.%; Figs. 8a-c).

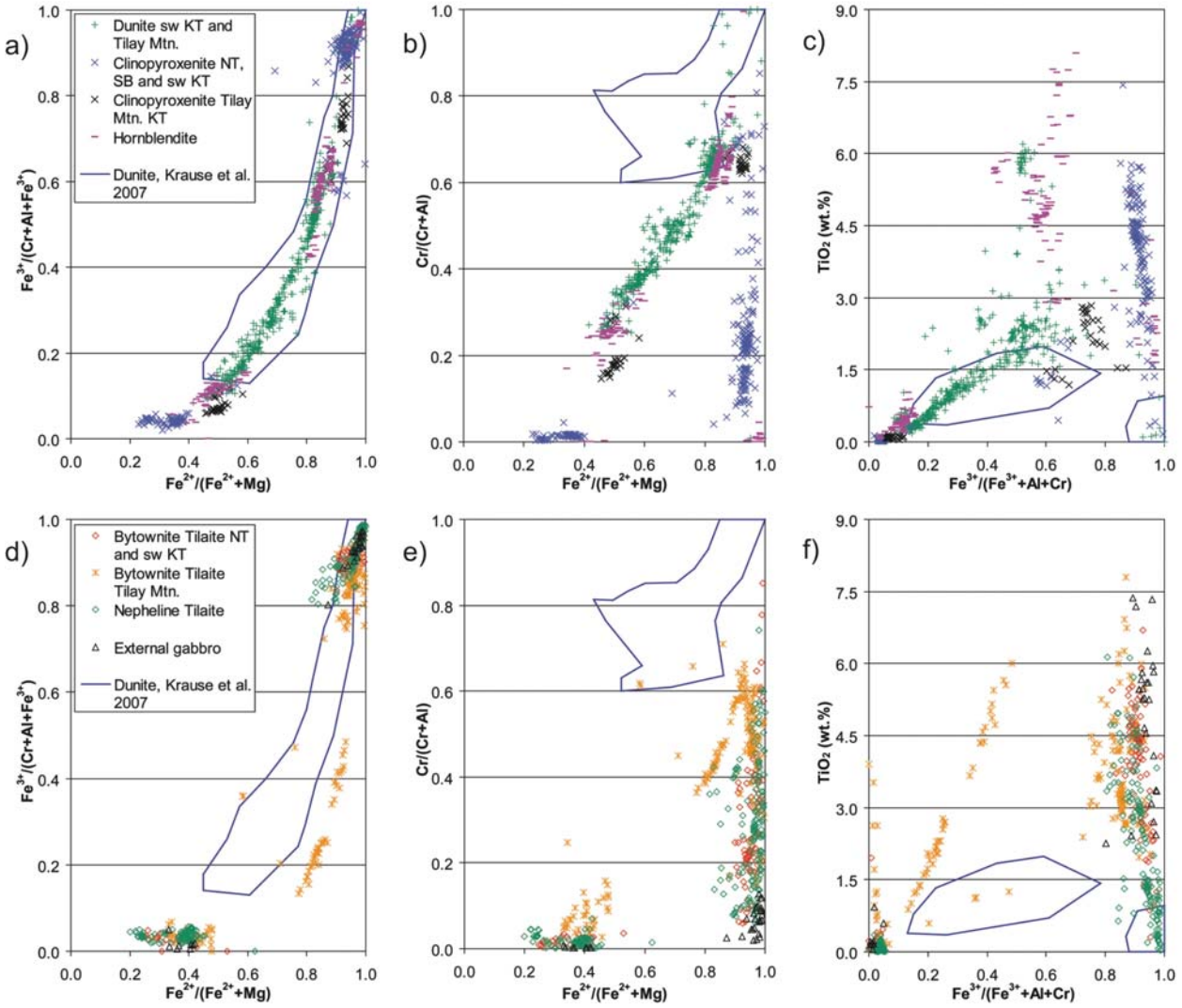

Fig. 8: Variation of $Fe^{2+}/(Fe^{2+}+Mg)$, $Fe^{3+}/(Cr+Al+Fe^{3+})$, Cr/(Cr+Al) and TiO_2 in exsolved spinel from Uralian-Alaskan-type complexes. Data for compositional variation in homogeneous spinel in dunite from all Uralian complexes are from Krause et al. (2007). (a-c) Spinel in the ultramafic rocks, follows the trends in the ultramafic rocks for $Fe^{2+}/(Fe^{2+}+Mg)$ and $Fe^{3+}/(Cr+Al+Fe^{3+})$ having lower Cr/(Cr+Al) and elevated TiO_2-contents if compared to homogeneous spinel. (d-e) Spinel in the mafic rocks has higher $Fe^{2+}/(Fe^{2+}+Mg)$ at a given $Fe^{3+}/(Cr+Al+Fe^{3+})$ and Cr/(Cr+Al) and elevated TiO_2-contents, if compared to the homogeneous spinel in dunite.

Type C exsolutions with diffuse contacts between both exsolved phases is the dominant exsolution texture in dunite from the eastern part of the Kytlym complex and occurs also in hornblendite. In the dunites these spinels form a continuous compositional trend ranging from picotite (Cr/(Cr+Al) = 0.27, $Fe^{2+}/(Mg+Fe^{2+})$ = 0.45, $Fe^{3+}/(Al+Cr+Fe^{3+})$ = 0.12, TiO_2 = 0.4 wt.%) to chromian magnetite (Cr/(Cr+Al) = 0.75, $Fe^{2+}/(Mg+Fe^{2+})$ = 0.8, $Fe^{3+}/(Al+Cr+Fe^{3+})$ = 0.7, TiO_2 = 3.5 wt.%; Fig. 8a-c). In chromian magnetite with FeO_{tot}

<77 wt.% the Cr/(Al+Cr) is predominantly controlled by the Al abundance and is systematically higher in the chromian magnetite than in the coexisting pleonaste and picotite.

Tab. 4: Composition of selected exsolved spinels. NT = Nizhnii Tagil, Til KT = Tilay Mountain – Kytlym, SW-KT = southwest Kytlym, NeTil = nepheline tilaite, ByTil = bytownite tilaite, HBDu = hornblendite in dunite, Clin = Clinpyroxenite, Dun = dunite * = un-exsolved core. FeO_m = all iron measured as FeO, FeO_{calc} and Fe_2O_{3calc} are calculated assuming stoichiometry, b.d. = below limit of detection.

Sample	NT8-265	NT8-266	NT8-244	NT8-243	NT212-90	NT212-91	KT50-173	KT50-174	KT50-176	KT50-177
Locality	NT	NT	NT	NT	NT	NT	Til KT	Til KT	Til KT	Til KT
Lithology	NeTil	NeTil	NeTil	NeTil	ByTil	ByTil	ByTil	ByTil	ByTil	ByTil
SiO_2 (wt.%)	0.07	0.05	0.03	0.18	0.08	0.20	0.27	0.28	0.19	0.13
TiO_2	0.64	0.04	1.17	0.05	1.24	0.04	3.68	0.21	2.81	0.11
Al_2O_3	2.92	61.89	1.59	62.99	0.84	63.23	3.39	50.00	2.78	57.17
FeO_m	83.09	19.50	89.98	19.45	89.69	18.43	74.92	20.96	80.56	18.32
MnO	0.45	0.24	0.29	0.56	0.22	0.30	0.43	0.23	0.33	0.20
MgO	0.59	14.83	0.42	15.57	0.37	16.15	1.53	14.10	0.91	16.31
Cr_2O_3	5.78	1.74	0.85	0.98	0.45	0.50	8.08	11.17	5.46	5.84
NiO	0.10	0.11	0.09	0.13	0.08	0.13	0.27	0.16	0.19	0.18
V_2O_3	0.43	0.03	0.45	0.03	0.45	0.02	0.42	0.07	0.40	0.03
ZnO	b.d.	1.34	0.03	0.54	b.d.	0.31	0.04	1.32	0.03	1.12
CoO	0.02	0.10	0.04	0.10	0.13	0.12	0.12	0.13	0.13	0.12
Total	94.08	99.88	94.95	100.58	93.55	99.42	93.14	98.62	93.78	99.52
Cr/(Cr+Al)	0.570	0.019	0.263	0.010	0.267	0.005	0.615	0.130	0.568	0.064
$Fe^{3+}/(Cr+Al+Fe^{3+})$	0.845	0.022	0.950	0.025	0.973	0.023	0.778	0.053	0.842	0.041
$Fe^{2+}/(Mg+Fe^{2+})$	0.967	0.398	0.977	0.382	0.979	0.362	0.920	0.396	0.952	0.334
FeO_{calc}	30.97	17.51	32.03	17.14	31.61	16.34	31.53	16.45	32.08	14.60
Fe_2O_{3calc}	57.92	2.22	64.40	2.57	64.55	2.32	48.22	5.01	53.88	4.13

Sample	KT35-407	KT35-405	KT51-271	KT51-272	KT332-250AB17	KT332-250AB12*	KT332-250AB1	KT328-9	KT328-21*	KT328-20
Locality	SW-KT	SW-KT	Til KT	Til KT	Til KT	Til KT	Til KT	Til KT	Til KT	Til KT
Lithology	HBDu	HBDu	Clin	Clin	Dun	Dun	Dun	Dun	Dun	Dun
SiO_2 (wt.%)	0.09	0.03	0.09	0.05	0.05	0.02	0.03	0.14	0.02	0.02
TiO_2	4.19	0.60	2.21	0.09	1.89	1.87	0.35	2.30	2.41	0.35
Al_2O_3	4.52	32.03	3.82	46.56	7.56	8.60	29.32	4.66	6.35	30.33
FeO_m	66.77	34.87	76.20	26.11	61.51	59.20	33.65	68.82	63.47	32.67
MnO	0.54	0.38	0.33	0.21	0.48	0.47	0.33	0.42	0.50	0.32
MgO	2.52	9.01	1.27	11.25	3.53	3.83	9.68	2.93	3.27	10.06
Cr_2O_3	18.23	23.03	10.06	14.32	20.89	21.92	25.34	14.41	19.60	25.08
NiO	0.23	0.11	0.11	0.12	0.23	0.26	0.11	0.29	0.20	0.09
V_2O_3	0.34	0.16	0.33	0.03	0.18	0.19	0.09	0.26	0.23	0.09
ZnO	0.09	0.61	0.03	1.36	0.09	0.06	0.31	0.06	0.08	0.37
CoO	0.13	0.13	0.09	0.12	0.07	0.08	0.08	0.04	0.05	0.09
Total	97.66	100.96	94.55	100.23	96.48	96.49	99.29	94.32	96.19	99.47
Cr/(Cr+Al)	0.730	0.325	0.638	0.171	0.649	0.631	0.367	0.675	0.674	0.357
$Fe^{3+}/(Cr+Al+Fe^{3+})$	0.597	0.147	0.750	0.063	0.522	0.487	0.158	0.665	0.557	0.149
$Fe^{2+}/(Mg+Fe^{2+})$	0.876	0.592	0.933	0.509	0.818	0.804	0.554	0.846	0.833	0.540
FeO_{calc}	31.81	23.31	31.45	20.77	28.31	27.97	21.44	28.66	28.99	21.05
Fe_2O_{3calc}	38.85	12.85	49.74	5.93	36.90	34.71	13.57	44.63	38.32	12.92

With the exception of a few Cr_2O_3-rich grains in the bytownite tilaite from Tilay Mountain all spinels in the mafic rocks and the clinopyroxenites exsolved to magnetite and pleonaste. The pleonaste (Cr/(Cr+Al) = 0-0.07, $Fe^{2+}/(Mg+Fe^{2+})$ = 0.2-0.43, $Fe^{3+}/(Al+Cr+Fe^{3+})$ = 0-0.06, TiO_2 = 0-0.25 wt.%) coexists with magnetite (Cr/(Cr+Al) = 0.05-0.85, $Fe^{2+}/(Mg+Fe^{2+})$ = 0.82-0.99, $Fe^{3+}/(Al+Cr+Fe^{3+})$ = 0.8-0.99, TiO_2 = 0-6.9 wt.%; Fig. 8). Due to the low contents of Cr_2O_3 and Al_2O_3 in some magnetites with (FeO_{tot} >77 wt.%) the Cr/(Al+Cr) is highly variable because small concentration changes have large effects on the ratio (Figs. 8b, e).

Magnetite exsolved from spinels in the external gabbros in the eastern part of the Kytlym complex have low (Cr/Cr+Al) and high $Fe^{2+}/(Mg+Fe^{2+})$, $Fe^{3+}/(Al+Cr+Fe^{3+})$ and TiO_2-contents if compared to the spinels from the other mafic rocks (Fig. 8d-f).

In the triangular plot of the trivalent cations the exsolved spinels plot along a curved line between the Fe_2O_3 and the Al_2O_3-corner (Fig. 9). Spinels with a high Cr_2O_3 content, predominantly from dunite and hornblendite, form a continuous trend that ranges from the Cr_2O_3-poor end of the compositional field defined by the homogeneous spinels towards the Al_2O_3 and Fe_2O_3 corners. Spinel exsolved from Cr_2O_3-poor precursors in clinopyroxenite tilaite and gabbro continue this trend almost reaching the pure end member compositions. Remarkably, spinels from all complexes lie along the same line, which represents the solvus curve for spinel coexisting with olivine Fo_{80} at about 600°C (Fig 9) calculated by Sack and Ghiorso (1991a, b). The deviation of the measured data from the calculated solvus curves can be attributed to the equilibration of spinel with olivine having Fo contents above 80, especially in the ultramafic rocks. Olivine with Fo up to 95 has been reported from the ultramafic rocks (Krause et al., 2007). In addition the significant Ti-content (up to 0.22 a.p.f.u.) requires the charge balance ($Ti^{4+} + M^{2+} \leftrightarrow M^{3+} + M^{3+}$) and might also explain the mismatch between our data and the solvus curves calculated by Sack and Ghiorso (1991b).

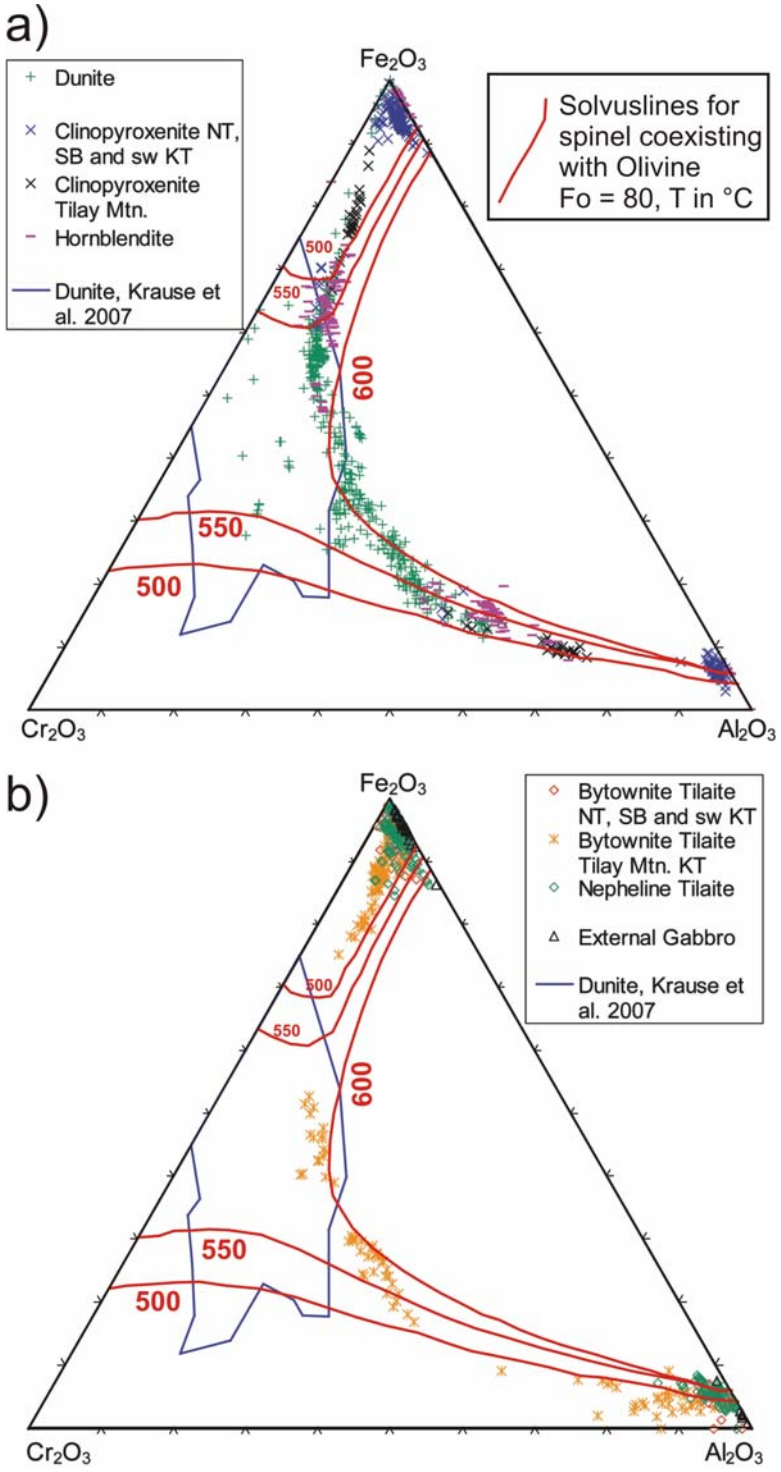

Fig. 9: Variation of the trivalent cations in exsolved spinel from ultramafic rocks a) and mafic rocks b). Solvus curves (red) calculated for spinels coexisting with olivine (Fo 80) are taken from Sack and Ghiorso (1991b). The compositions of all spinels lie close along a solvus line suggesting an equilibration at about 600°C. Data for compositional variation in homogeneous spinel in dunite from all Uralian complexes are from Krause et al. (2007).

3.2.3 Element distribution in exsolved spinels

Representative cross-sections of the spinel chemistry across the phase boundaries of coexisting spinels for the three types of exsolution are shown in Figs. 10 and 11.

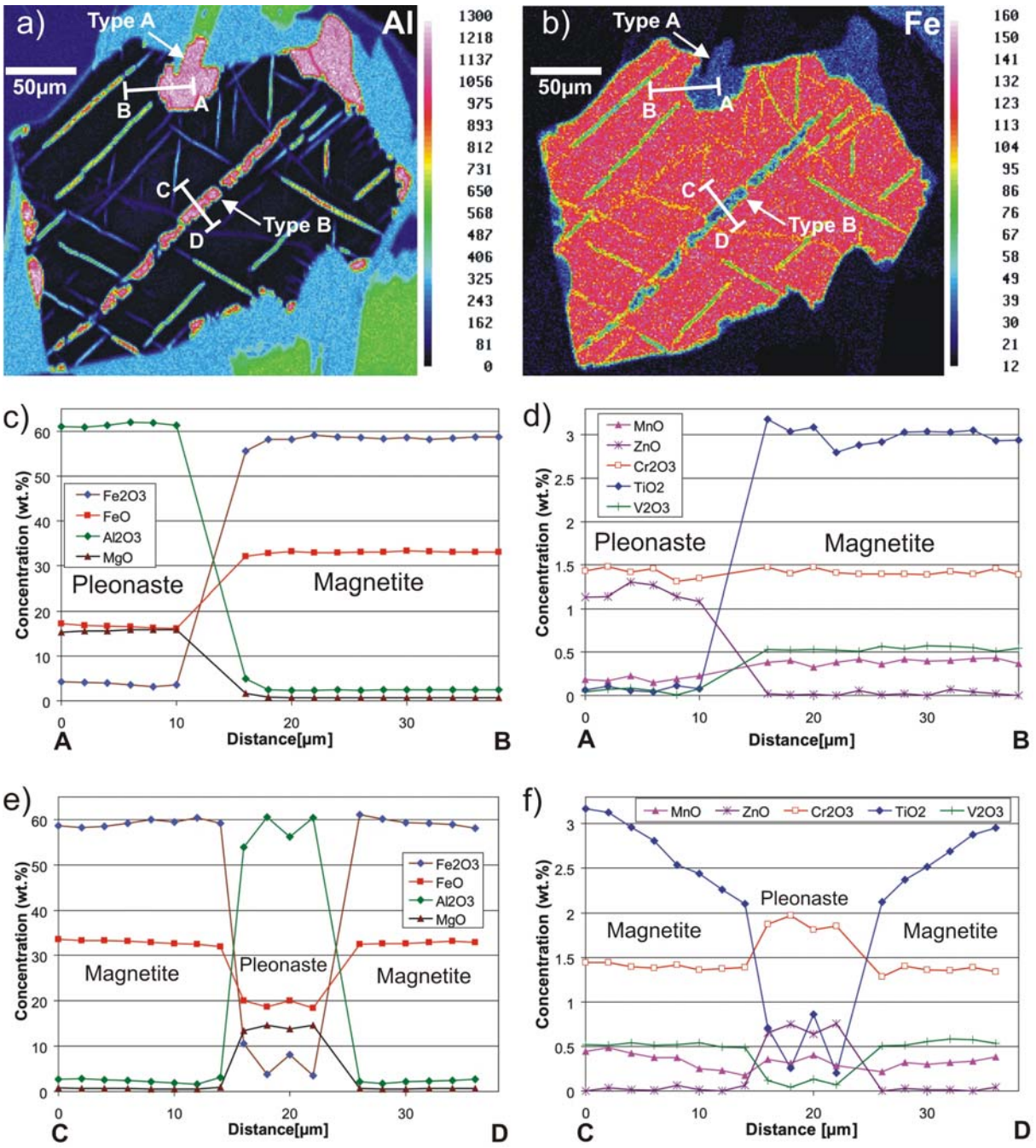

Fig. 10: Variation of minor and major components across types A and B of exsolution textures. (a, b) Element distribution maps of Al and Fe. (c, d) Bleb-like exsolution type A (PE910), (e, f) wide, lamellar exsolution, type B (PE910). Note the presence of both exsolution textures within one grain and their similar chemical composition.

The first cross-section (A-B) runs across a bleb-like exsolution texture of type A in a spinel which is enclosed together with biotite in the core of a clinopyroxene phenocryst from a nepheline tilaite from Kytlym (sample PE910; Fig. 10a, b). The second cross-section (C-D) runs across a lamellar exsolution (type B) within the same exsolved spinel grain (Fig. 10a, b). The chemical composition of the pleonaste forming the lamella is similar to the pleonaste in the bleb (Figs. 10c-f). The phase boundaries between magnetite and pleonaste are very narrow in both cases (>5µm). They are defined by a sharp contrast in the concentration of major and minor elements, for example FeO, Fe_2O_3, TiO_2, V_2O_5 and MnO decrease, while Al_2O_3, MgO, and ZnO increase from the magnetite to the pleonaste (Figs. 10c-f). Interestingly Cr_2O_3, likewise CoO, does not change much, by less than 0.5 wt.% (Figs. 10d, f). On both sides of the phase boundaries a very small chemical gradient is visible, e.g. a slight increase of Al_2O_3 and TiO_2 contents in the magnetite and a slight decrease of FeO and Fe_2O_3 with increasing MgO in the pleonaste of the bleb-like exsolution.

A profile (E-F) typical for all spinels showing the type-C exsolution texture in a dunite from Tilay Mountain, Kytlym (KT332) is shown in figure 11. At about 5 µm close to the rim of the grain the distinct phase boundary between picotite and chromian magnetite is visible with an obvious chemical contrast similar to that described in the previous profiles (Fig. 11c, d). Starting just behind the phase boundary Fe_2O_3, FeO and TiO_2 decrease, while Al_2O_3, Cr_2O_3, MgO, and ZnO increase. These trends become accelerated between 30 and 38 µm and eventually reach a picotite composition similar to that of the left side. The different slopes for the diverse elements may indicate specific diffusion velocities during the exsolution process. The area with intermediate compositions, for example Al and Fe in Figs. 11a, b can be interpreted to represent a remnant of the initial spinel that was not completely exsolved.

In agreement with the profiles of Figs. 10 and 11, X-ray element maps of spinel in the tilaites and clinopyroxenites show sharp phase boundaries between magnetite and pleonaste (Figs. 10 a, b and 11a, b).

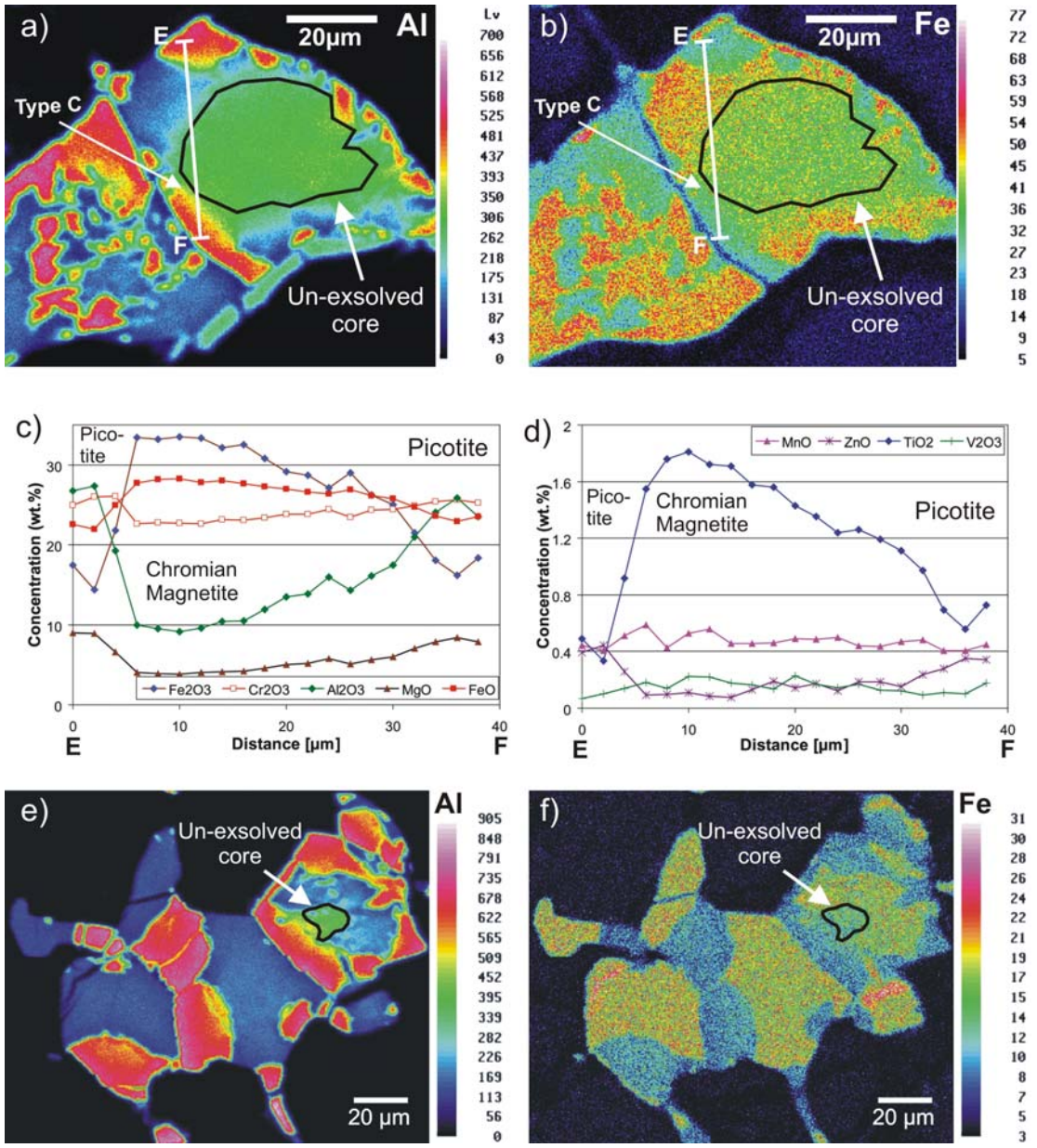

Fig. 11: Variation of minor and major components across type C exsolution textures. (a, b) Element distribution maps of Al and Fe. (c, d) Concentration profiles across exsolution type C with sharp chemical contrast on one and a gradual change in composition at the other side (KT332). (e, f) Element distribution maps of Al and Fe of an aggregate of several spinel grains from the same sample demonstrates the complex geometry of type C exsolutions. Note the presence of discrete as well as gradual boundaries between the two phases and the unexsolved core outlined in black.

Spinels from dunite and hornblendite with type-C exsolution textures have sharp contacts between the exsolved picotite and chromian magnetite, but in the core of the chromian magnetite often a phase with intermediate composition regarding all major elements can be observed (Fig. 11). This phase is interpreted to represent very closely

the composition of the unexsolved, primary spinel. In the often 5-20 µm wide transition zone between the chromian magnetite and the core the composition changes gradually (Fig. 11). None of the spinels mapped with the microprobe in the mafic and ultramafic rocks shows a significant redistribution of major elements neither between the two exsolved spinel phases nor between spinel and silicate phases in the matrix (Figs. 11 and 12). Exceptions are Ti and Cr showing some late redistribution if ilmenite exsolves from spinel (Fig. 12). Few grains in the dunite samples KT328-KT332 have cracks filled with pure magnetite which crosscut the exsolution textures. They are interpreted to be related to retrograde processes e.g. serpentinization of the surrounding olivine or the decomposition of clinopyroxene (Iyer et al., 2008) or to a late stage reequilibration with an water rich oxidizing environment (Mellini et al., 2005).

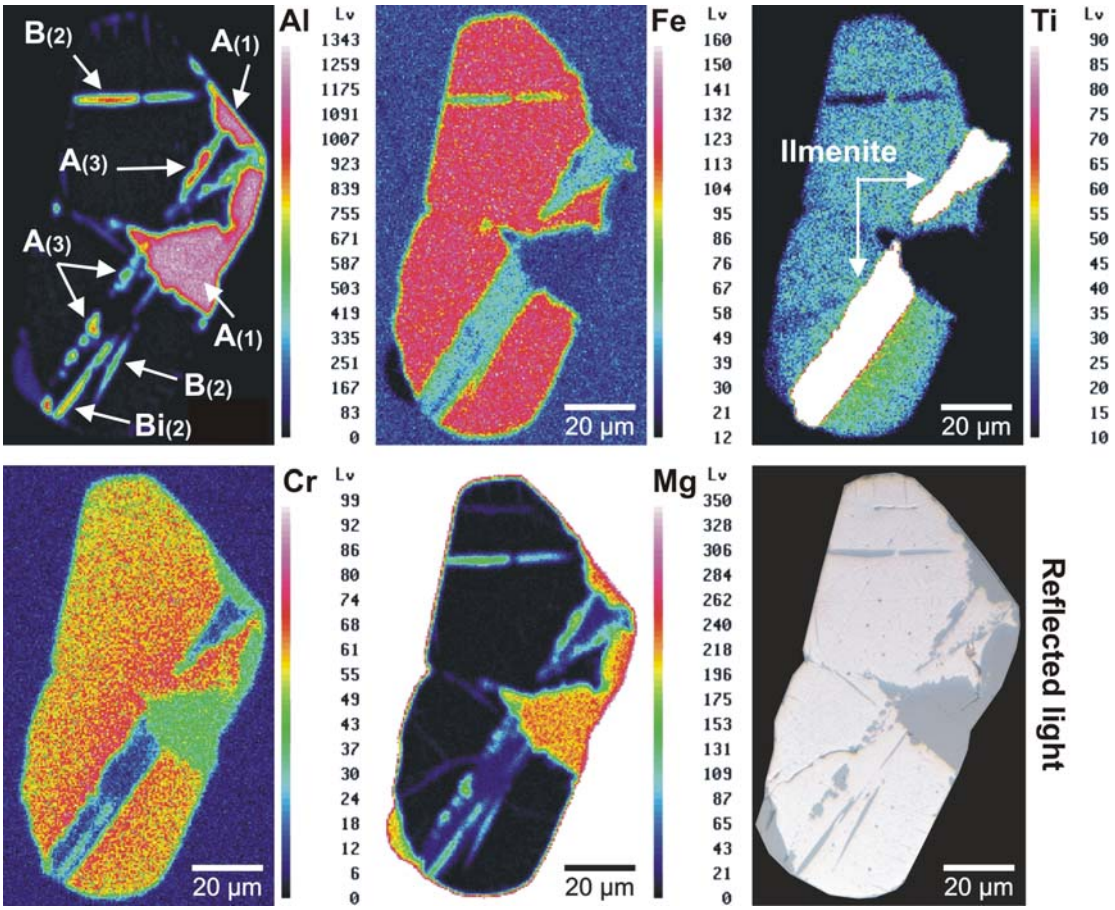

Fig. 12: Element distribution maps for Al, Fe, Ti, Cr and Mg and the reflected light image of exsolved spinel enclosed in olivine from nepheline tilaite, Nizhnii Tagil (NT8). Note the presence of Al-rich exsolutions of the type A at the rim towards the surrounding olivine $A_{(1)}$ and at the boundary of ilmenite with magnetite $A_{(3)}$. Exsolutions of the type B are present outside $B_{(2)}$ and inside $Bi_{(2)}$ of a lamella of ilmenite. Numbers in brackets denote the order of their formation (for details see text).

3.2.4 Estimation of area fractions in exsolved spinels and their initial composition

X-ray element maps are prepared in order to understand the spatial distribution of major elements and with the purpose of estimating the spinel composition prior to its exsolution. Two different approaches were applied to calculate the total area and area fractions of the different spinel phases in 206 exsolved spinel grains (Tab. 5). For 27 grains X-ray Element maps for Fe and Al were converted to gray scale maps and the matrix was removed using vector graphic software (Corel Draw®). The area fractions of spinel were then calculated using the ImageJ® software (Abramoff et al. 2004). Reflected light images of 179 spinel grains were processed in a similar way to calculate the area fractions. The reflected light images of 7 large xenomorphic spinel grains and grain assemblages with a complex texture were corrected for irregular illumination before the processing with the graphic software.

Tab. 5: Recalculated initial composition of the exsolved spinels in Tab. 4. IO = inclusion in olivine, M = interstitial, IC = Inclusion in clinopyroxene. Other abbreviations are as in Tab. 4.

Sample	NT8 265-267	NT8 242-244	NT212 90-91	KT50 173-174	KT50 176-177	KT35 401-413	KT51 271-272	KT332 Map 250	KT332 19-21
Locality	NT	NT	NT	Til KT	Til KT	SW-KT	Til KT	Til KT	Til KT
Lithology	NeTil	NeTil	ByTil	ByTil	ByTil	HB i DU	Clin	Dun	Dun
Position	IO	M	M	IC	M	M	M	M	M
Proportions of exsolved spinel	(Area%)								
Al-rich	23	9	30	14	11	48	28	37	22
unexsolved	0	0	0	0	0	0	0	36	62
Fe-rich	77	91	70	86	89	52	72	28	16
SiO_2 (wt.%)	b.d.	b.d.	0.12	0.27	0.18	b.d.	b.d.	b.d.	b.d.
TiO_2	0.50	1.07	0.88	3.19	2.50	2.47	1.61	1.13	1.00
Al_2O_3	16.61	7.24	19.54	9.91	8.89	17.69	15.97	17.77	21.19
FeO	68.33	83.49	68.33	67.38	73.56	51.50	61.96	48.06	44.82
MnO	0.40	0.32	0.24	0.40	0.32	0.46	0.30	0.43	0.41
MgO	3.89	1.82	5.10	3.29	2.64	5.63	4.11	6.36	7.02
Cr_2O_3	4.84	0.86	0.47	8.51	5.50	20.53	11.27	23.57	22.60
NiO	0.10	0.09	0.09	0.26	0.19	0.17	0.11	0.18	0.16
V_2O_3	0.33	0.42	0.32	0.37	0.36	0.25	0.25	0.14	0.14
ZnO	0.31	b.d.	0.09	0.22	0.15	0.34	0.41	0.20	0.30
CoO	b.d.	b.d.	0.12	0.12	0.13	0.13	0.10	b.d.	0.10
Total	95.43	95.47	95.31	93.91	94.43	99.24	96.16	97.96	97.78
Cr/(Cr+Al)	0.164	0.074	0.016	0.365	0.293	0.438	0.321	0.471	0.417
$Fe^{3+}/(Cr+Al+Fe^{3+})$	0.591	0.827	0.596	0.633	0.710	0.349	0.503	0.326	0.285
$Fe^{2+}/(Mg+Fe^{2+})$	0.800	0.904	0.748	0.834	0.865	0.734	0.795	0.689	0.661
FeO_{calc}	27.84	30.66	27.04	29.42	30.12	27.74	28.41	25.15	24.38
Fe_2O_{3calc}	45.00	58.71	45.90	42.18	48.28	26.40	37.28	25.46	22.72

In dunite, hornblendite and the clinopyroxenites from Tilay Mountain (central-Kytlym) the initial spinels show a positive correlation of the Cr_2O_2 content with the area fraction of the Al-rich phase (Fig. 13). Hence the Cr_2O_3 content is similar in the Al-rich and in the coexisting Fe-rich phase (Figs. 9a, 10d, f) a change in the proportions of Al- and the Fe-rich phases would have little or no influence on the Cr_2O_3 content of the recalculated spinel. The Cr_2O_3 is independent from the fraction of Al-rich spinel and reflects probably a fractionation trend with an increase of Al_2O_3 on the expense of Cr_2O_3 of spinel crystallizing from a melt together with olivine and a small amount of clinopyroxene.

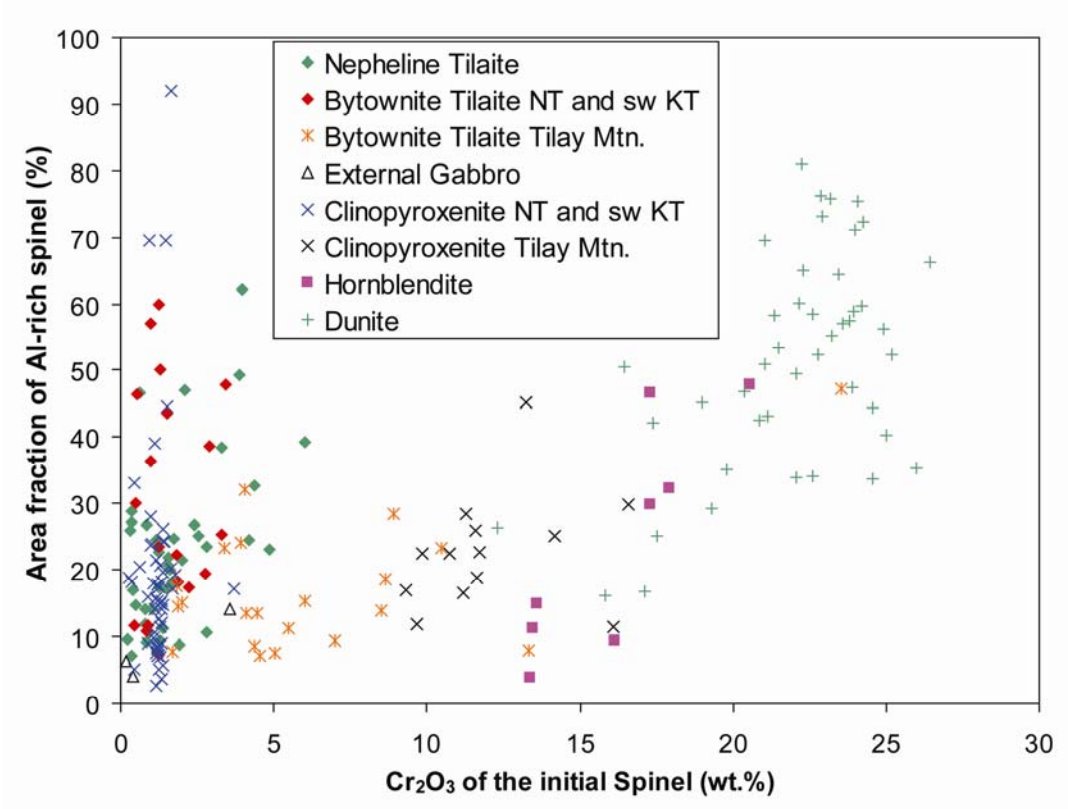

Fig. 13: Variation of the area fraction of the Al-rich phase in exsolved spinel with the recalculated Cr_2O_3 content of the spinel prior to the exsolution. Note the positive correlation of both parameters at Cr_2O_3 > 5 wt. % reflecting the fractionation of olivine and clinopyroxene in the parental melt.

Most initial spinels in clinopyroxenite, tilaite and gabbro have low Cr_2O_3 contents (Cr_2O_3 < 10 wt.%) and show a large scatter in the area fraction (3-92 %) of the Al-rich phase with the majority of the grains containing less than 30 % of this phase. Due to the coarse exsolutions in relation to the grain size of the entire spinel grain (Fig. 3b) the area estimation is strongly affected by the section level. Therefore spinels having more than

30 % of the Al-rich component and Cr_2O_3-contents below 10 wt.% are interpreted as artifacts of the section level and these data are not considered for the following discussion.

Beside its higher Al_2O_3 content, lower Cr/(Cr+Al) and slightly elevated $Fe^{2+}/(Mg+Fe^{2+})$, the calculated composition of spinel in hornblendite and dunite prior to the exsolution is similar to that of homogeneous spinel in dunite (Figs. 14a, c; Tab. 5). The recalculated primary spinel in clinopyroxenite and tilaite from Nizhnii Tagil and SW Kytlym and in the gabbro has lower $Fe^{2+}/(Mg+Fe^{2+})$ at a given $Fe^{3+}/(Al+Cr+Fe^{3+})$, if compared to the homogeneous spinel in dunite (Fig. 14b). In comparison with spinels from the more evolved rocks in other Alaskan-type complexes, the studied spinels have lower Fe_2O_3 and higher Al_2O_3-contents (Kepezhinskas et al., 1993a, b; Barns and Roeder, 2001; Batanova et al., 2005).

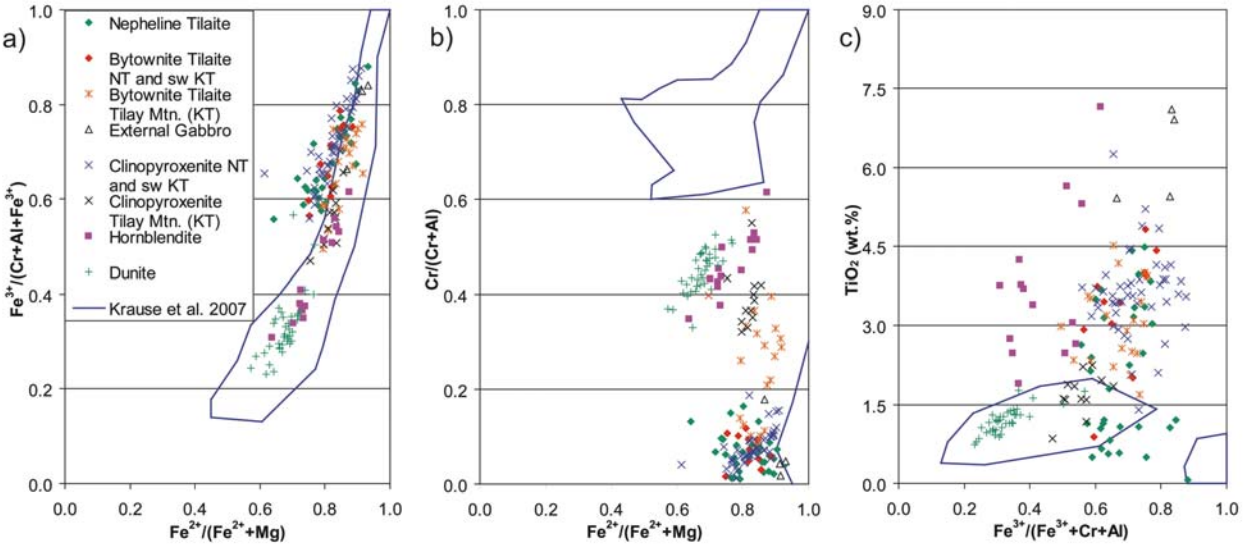

Fig. 14: Variation of $Fe^{2+}/(Fe^{2+}+Mg)$, $Fe^{3+}/(Cr+Al+Fe^{3+})$, Cr/(Cr+Al) and TiO_2 in recalculated exsolved spinel. a) $Fe^{3+}/(Cr+Al+Fe^{3+})$ vs. $Fe^{2+}/(Fe^{2+}+Mg)$, b) Cr/(Cr+Al) vs. $Fe^{2+}/(Fe^{2+}+Mg)$. Note the similar variation of $Fe^{2+}/(Fe^{2+}+Mg)$ and $Fe^{3+}/(Cr+Al+Fe^{3+})$ and the lower Cr/(Cr+Al) an higher TiO_2, if compared with the homogeneous spinel in dunite. Data for the compositional variation in homogeneous spinel in dunite from all Uralian complexes are from Krause et al. (2007).

Elevated TiO_2 (>2 wt.%) and the low Cr_2O_3 contents (<5 wt.%) in most calculated initial spinels from the more evolved rocks also indicate a higher degree of fractionation in their parental melt, if compared with homogeneous spinel in the dunite (TiO_2 = 0.15-1.95 wt.%, Cr_2O_3 >27 wt.%; Fig. 14c; Tab. 5; Krause et al., 2007). Interestingly the spinel

from nepheline tilaite enclosed in olivine and clinopyroxene has systematically higher Cr_2O_3 and lower $Fe^{2+}/(Mg+Fe^{2+})$, $Fe^{3+}/(Al+Cr+Fe^{3+})$ and Fe_2O_3, if compared to interstitial spinel (Fig. 15a).

Recalculated spinel compositions in clinopyroxenite and bytownite tilaite from Tilay Mountain (E-Kytlym) indicate higher Cr_2O_3 contents (clinopyroxenite 9.3-16.6 wt.%, bytownite tilaite 1.7-13.3 wt.%) if compared to equivalent rocks from the other localities (Fig. 15b, Tab. 5). Similar to the observation in nepheline tilaites, spinel in bytownite tilaite from Tilay Mountain enclosed in clinopyroxene tend to have higher Cr_2O_3 contents than the interstitial grains (Fig. 15b).

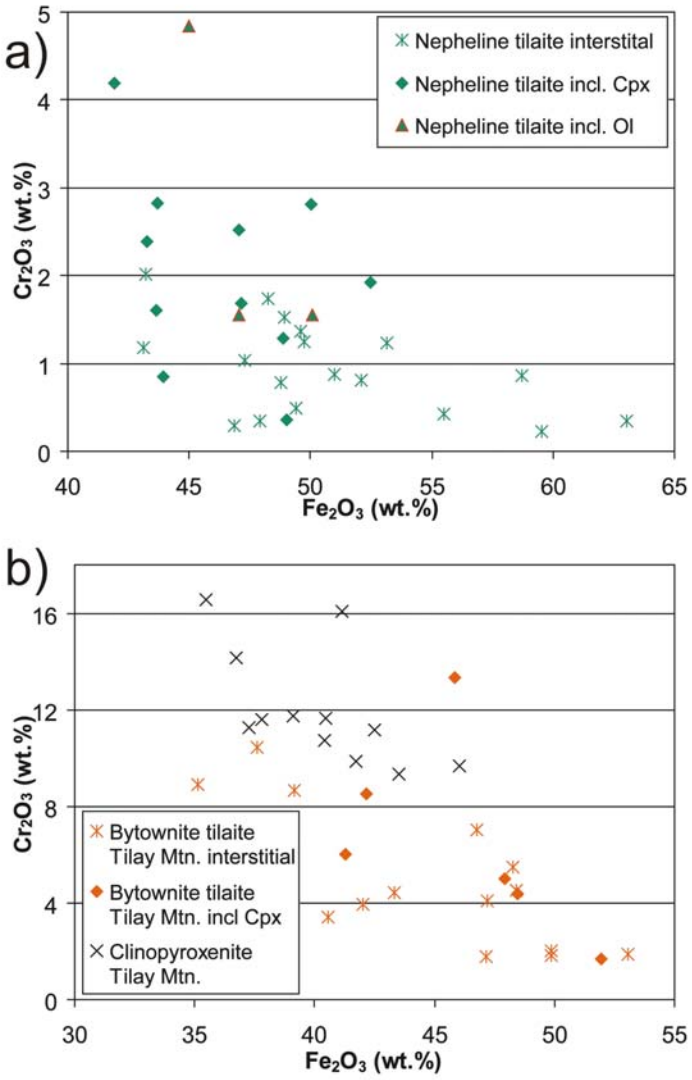

Fig. 15: Variation of Fe_2O_3 and Cr_2O_2 in recalculated exsolved spinel in interstitial pore spaces and included in clinopyroxene and olivine (a) nepheline tilaite Nizhnii Tagil and SW Kytlym, (b) Bytownite tilaite from Tilay Mountain (Kytlym).

3.3 Chemical composition of ilmenite

Representative analyses of ilmenite are given in Tab. 6. Ilmenite forms prismatic to needle-like grains enclosed in spinel from hornblendite, tilaite and gabbro. Separate grains of ilmenite could not be found. At the grain boundary to the spinel often recurs blebs of Al-rich spinel (Fig. 12). The chemical composition of the ilmenite depends on the lithology (Tab. 6). For example ilmenite in bytownite tilaite has low contents in MnO (1.1-2.4 wt.%) and high contents in MgO (1.8-4.6 wt.%), whereas ilmenite in nepheline tilaite has high MnO (4-7.1 wt.%) and low MgO (1.2-2.7 wt.%) and that in hornblendite has intermediate contents (MnO: 3.0-4.7 wt.%; MgO: 0.3-2 wt.%). The observed ilmenite composition is similar to compositions reported for ilmenite from convergent margin settings, in gabbroic rocks of the Uktus Uralian-Alaskan-type complex and in ultramafic rocks from the Uralian-Alaskan-type complex of Kachkanar, Urals (Pushkarev et al., 1999). According to Jang and Naslund (2003) and Scoon and Eales (2002), ilmenite from layered intrusions like Bushveld and Skaergaard has much lower MnO contents (0.4-1.2 wt.%) at similar MgO.

Tab. 6: Composition of selected ilmenites. SB = Svetley Bor, NT = Nizhnii Tagil, TM, KT = Tilay Mountain – Kytlym, SWKT = southwest Kytlym, E-KT = east Kytlym. NeTil = nepheline tilaite, ByTil = bytownite tilaite, HB = hornblendite, Ext. GB = external gabbro, b.d. = below limit of detection.

Sample	SB30-251	NT8-260	NT9-331-18	KT44-251	NT213-57-14	KT321-74-30	KT322-106	KT324-121	KT325-260	KT53-232	PE440-52
Locality	SB	NT	NT	SWKT	NT	TM, KT	TM, KT	TM, KT	TM, KT	E-KT Ext	E-KT
Lithology	HB	Ne Til	Ne Til	By Til	By Til	By Til	By Til	By Til	By Til	GB	Ext GB
TiO_2 (wt.%)	51.36	52.68	52.84	51.74	52.72	53.01	52.77	54.81	53.58	53.26	52.22
Al_2O_3	0.05	0.67	0.21	1.71	0.07	0.17	0.06	0.06	0.03	0.03	0.04
FeO	43.95	40.34	38.56	40.20	43.46	41.01	45.72	39.45	43.21	42.44	45.82
MnO	3.47	3.99	6.77	1.78	2.17	1.13	1.82	2.42	1.22	1.04	1.81
MgO	1.14	2.72	2.34	4.44	1.94	3.86	0.98	4.42	2.33	3.61	b.d.
Cr_2O_3	b.d.	0.16	0.09	0.62	0.11	0.31	0.14	0.21	0.06	b.d.	b.d.
NiO	b.d.	b.d.	b.d.	b.d.	b.d.	b.d.	b.d.	0.03	b.d.	b.d.	0.04
V_2O_3	b.d.	b.d.	b.d.	b.d.	0.03	b.d.	0.02	b.d.	b.d.	b.d.	b.d.
ZnO	0.05	0.03	b.d.	0.04	0.05	0.03	0.01	0.02	0.02	b.d.	b.d.
CoO	0.09	0.04	b.d.	0.05	0.03	0.04	0.08	0.08	0.08	0.08	b.d.
Total	100.11	100.63	100.80	100.58	100.58	99.56	101.60	101.48	100.52	100.45	99.93

4 Discussion

4.1 Evolution of spinel and ilmenite exsolutions: Implications from petrographic observations and thermodynamic considerations

4.1.1 Formation of spinel exsolutions

Lamellar inclusions oriented along well defined planes of a crystal lattice, such as our type B texture, are classical examples for exsolution textures. They are well known from e.g. orthopyroxene in clinopyroxene and vice versa, perthite and antiperthite in alkalifeldspar (Putnis, 1992), hematite-ilmenite, (Haggerty, 1991). The roundish shape of type-A texture is unusual for solid state exsolution, but nevertheless described from spinels (e.g. Haggerty, 1991; Garuti et al., 2003; Krause et al., 2007; Ahmed et al., 2008). We believe that texture A also is the result of an exsolution process, where two spinels exsolved at subsolidus conditions from a homogeneous precursor. They are not the result of a high stress overprint, where during shearing due to dynamic recrystallization the initially lamella structure breaks down into a fine-grained globular structure. They do not reflect globular structures formed during low temperature alteration, because there is no significant late stage remobilization of major elements during the interaction with the surrounding silicate matrix, including serpentine. Lamellar and bleb-like textures have similar chemical compositions regardless whether they represent Al-rich or Fe-rich phases, and regardless of their textural position (Fig. 10). They are similar in composition and texture to spinels which have been interpreted as exsolutions (e.g. Evans and Frost, 1975; Loferski and Lipin, 1983; Eales et al., 1988; Tamura and Arai, 2005; Ahmed et al., 2008).

Spinel textures similar to types A and B found in rocks from the Alaskan-type complexes in the Ural Mountains have also been observed in metamorphic rocks (e.g. Evans and Frost, 1975; Loferski and Lipin, 1983; Eales et al., 1988; Ozawa, 1988; Burkhard, 1993; Van der Veen and Maaskant, 1995; Candia and Gaspar, 1997). In igneous rocks coexisting Al-rich and Fe-rich spinels are known from the Giant Nickel Mine in British Columbia (Muir and Naldrett, 1973), the Chilas mafic-ultramafic complex, Pakistan (Jan et al., 1992), the Iwanai-dake peridotite, Japan (Tamura and Arai, 2005) and from Alaskan-type complexes in Egypt (Ahmed et al., 2008) and the Ural Mountains (Pushkarev et al., 1999; Garuti et al., 2003; Krause et al., 2007). In all these cases the

coexistence of two spinel phases has been attributed to a break-down process either induced by subsolidus cooling/reheating (e.g. Loferski and Lipin, 1983; Eales et al., 1988; Ozawa, 1988; Jan et al., 1992; Burkhard, 1993; Garuti et al., 2003; Tamura and Arai, 2005; Ahmed et al., 2008), subsolidus re-equilibration with silicate phases or reactions with coexisting liquid (e.g. Muir and Naldrett, 1973; Evans and Frost, 1975; Van der Veen and Maaskant, 1995; Candia and Gaspar, 1997). These studies also report that depending on the composition of the spinel prior to exsolution an Al-rich host and a Fe-rich guest or a Fe-rich host and an Al-rich guest spinel is formed. This is also observed in the present study.

Spinodal decomposition and nucleation and growth are proposed as potential mechanisms for the exsolution of ulvöspinel and magnetite from a solid solution (Price, 1980; Harrison and Putnis, 1999). Price (1980) assumed a nucleation and growth mechanism along grain boundaries and lattice defects for forming coarse exsolutions similar to types A and C. The framework of lamellar exsolutions of type B could have been initially formed by spinodal decomposition and subsequent coarsening.

The chemical composition namely the Cr_2O_3-content seems to control the geometry of the exsolution textures. Lamellar exsolutions (Type B) are restricted to spinels with a Cr_2O_3-content below 10 wt.%, which have initial compositions relatively far from the solvus curve at 600°C (Fig. 9). Exsolution textures of type C have been found only in spinels with Cr_2O_3 contents above 15 wt.% prior to the exsolution. The appearance of texture type A seems not to be controlled by a particular chemical composition of the initial spinel.

The thermodynamic stability of the spinel solid solution in the system $(Mg, Fe^{2+})(Al,Cr,Fe^{3+})_2O_4$ as a function of temperature, oxygen fugacity and the composition of coexisting olivine has been studied by Sack and Ghiorso (1991a,b). These thermodynamic models estimate solvus curves in the trivalent cation plot for a given temperature and forsterite content of coexisting olivine. All exsolved spinels from the Ural mountains, regardless of the lithology and provenance of the sample, plot along a single solvus curve which indicates a temperature of about 600°C, given a coexisting olivine with Fo=80 (Fig. 9). Exsolved spinels with similar compositions are observed in metamorphosed mafic-ultramafic rocks (e.g. Loferski and Lipin, 1983) where the

metamorphic peak temperatures are estimated to be close to 600°C. In addition similar spinel compositions from the Chilas ultramafic complex, Pakistan are supposed to be equilibrated at 600°C (e.g. Jan et al., 1992). According to Sack and Ghiorso (1991a, b), at a given forsterite content in the coexisting olivine the geometry of the solvus curve is strongly dependent on temperature. Already at slightly lower temperatures of 550°C the solvus curve opens up towards Cr_2O_3- rich spinels and reaches the Cr_2O_3-Fe_2O_3-apex in the plot of the trivalent cations (Fig. 9). Compositions of exsolved spinels fitting such a solvus line (<600°C) have not been observed in our study in the Cr_2O_3-rich part of Fig. 9. Indeed the low Cr_2O_3 part of the field of homogeneous spinels from ultramafic rocks borders and confines the 600°C solvus line. This implies slow cooling of the magma body after its solidification and a final equilibration of spinel at 600°C.

According to Turnock and Eugster (1962) and Ghiorso and Sack (1991) the exsolution process starts at about 850-900°C for Cr_2O_3-free spinels with Al_2O_3/Fe_2O_3 close to 1 (Turnock and Eugster, 1962; Ghiorso and Sack, 1991). In spinels with lower or higher Al_2O_3/Fe_2O_3 and/or higher Cr_2O_3- contents the exsolution begins at lower temperatures. Most spinels in clinopyroxenite, tilaite and gabbro are Cr_2O_3-poor and lie close to the Al_2O_3-Fe_2O_3-apex in the plot of the trivalent cations (Fig. 9b). According to their Al_2O_3/Fe_2O_3, their exsolution started between 900 and 750°C. The immiscibility gap increases during cooling from this apex towards the center of the diagram. Therefore, the Cr-poor spinel exsolves first during cooling and their different exsolution textures reflect the complete cooling history of the host body. Spinel with low Cr_2O_3 content has exsolutions of type A (blebs) and B (two generations of oriented lamellas; Fig. 3c). Textural observations (Figs. 2, 3 and 10a, b) indicate that the blebs formed early during the exsolution process, i.e. at the highest temperatures. At this time the miscibility gap is small and a magnetite with a relatively high Al_2O_3 content and a pleonaste with a significant Fe_2O_3 content are the two exsolving phases. Further cooling enlarges the miscibility gap, forces a continuous re-equilibration of the initial exsolution generation and eventually induces the formation of almost pure magnetite and pleonaste. The excess Al_2O_3 component in magnetite forms crystallographically oriented lamellas of pleonaste. At the same time the FeO, Fe_2O_3 and TiO_2 in the early picotite blebs are redistributed and diffuse into the adjacent magnetite forming pleonaste. This also explains the similar composition of blebs and lamellas within the same grain (Fig. 10). A

second generation of lamellas is in places present and separated by a precipitate free zone from the lamellas of the first generation. The preservation of two generations presumably reflects the slower diffusion at decreasing temperatures preventing complete re-equilibration between the blebs or the lamellas of the first generation and the surrounding magnetite. A decrease of the FeO and Fe_2O_3 contents in some pleonaste blebs immediately at the phase boundary with magnetite and the increase of these element concentrations in the magnetite immediately at the phase boundary are visible in some profiles (Fig. 10e, f). Together with the increase of Al_2O_3 in some pleonaste at the phase boundary to magnetite (Fig. 10c, d) this can be interpreted as the very last resurrection of diffusion, which is related to the exsolution process.

The occurrence of exsolution type C is restricted to Cr_2O_3-rich spinels with an initial composition close to the solvus curve at 600°C. This exsolution started the latest, i.e. at the lowest temperature (Fig. 9b). Some large spinels in the dunites show a transition between type A and C as well as unexsolved areas (Figs. 3d, 11). The exsolutions of type C can thus be interpreted to represent an early state of type A development, but due to the low diffusion rate at the low temperature not all spinel grains could generate the final equilibrium texture.

4.1.2 Formation of ilmenite exsolutions

Ilmenite lamellae and spinel exsolutions occur together in one grain in the most fractionated rocks - hornblendites, tilaites and gabbros (Fig. 12) They are well known from other igneous mafic rocks (e.g. Muir and Naldrett, 1973; Morse, 1980; Eales et al., 1988; Speczik et al., 1988; Lindsley, 1991; Haggerty, 1991; Lattard, 1995; Pushkarev et al., 1999; Lattard et al., 2005; Pang et al., 2008). Experimental studies suggest a very low solubility of ilmenite in magnetite at temperatures below 800°C (e.g. Lindsley, 1963; Taylor, 1964). Accordingly the observed ilmenite lamellae are interpreted as exsolutions of ilmenite and magnetite from a Ti-rich spinel. The genetic interpretation of the ilmenite lamellas as products of an exsolution process that might be related to an increase in the oxygen fugacity is also supported by the absence of ilmenite as a discrete phase in the studied samples.

Textural observations suggest that ilmenite exsolved after the formation of bleb and lamellae textures ($A_{(1)}$ and $B_{(2)}$ in Fig. 12) in the spinel, because the strait contact between the ilmenite lamella and the magnetite is interrupted by a picotite-bleb ($A_{(1)}$ in Fig. 12). In addition the ilmenite encloses an Al_2O_3-rich spinel lamella ($Bi_{(2)}$ in Fig. 12). As ilmenite should not exsolve such spinels this lamellae must have existed before the formation of ilmenite. This suggests that the TiO_2- content in the primary magmatic spinel is too low to allow the crystallization of ilmenite. As discussed above the blebs are in general interpreted to be the first exsolution product. The exsolution of the primary spinel during cooling probably produced a magnetite which was Ti-rich enough to trigger ilmenite exsolution. The Al_2O_3–rich bleb shaped spinel grains at the rim of ilmenite ($A_{(3)}$ in Fig. 12) probably represent a new generation of Al-rich spinel formed during the ilmenite exsolution. It formed due to the access of Al_2O_3 available after the breakdown of the Ti-spinel, which cannot be accommodated by the Ti-oxide.

In order to exsolve the Ti-rich phase an increase of the oxygen fugacity and/or a decrease of the temperature is required (Buddington and Lindsley, 1964; Morse, 1980; Eales et al., 1988; Speczik et al., 1988; Pang et al., 2008). Buddington and Lindsley 1964 stated that the intergrowths of ilmenite and magnetite formed by oxidation of magnetite-ulvöspinel solid solution do not represent exsolutions sensu stricto, because this is not a closed system. The term oxidation exsolution was proposed for magnetite-ilmenite intergrowths formed as the result of an oxidation of a magnetite ulvöspinel solid solution (Lindsley, 1991; Haggerty, 1991; Lattard, 1995; Lattard et al., 2005).

In our samples low TiO_2-magnetite coexists with ilmenite with a low magnetite component. This is consistent with our petrographic observation, because it also indicates that the ilmenite exsolution did not occur during spinel crystallization but at temperatures below the solidus (e.g. Ghiorso and Sack, 1991b, Sauerzapf et al., 2008). The thermal equilibration of spinel at about 600°C should result in a re-equilibration of ilmenite and spinel at temperatures below the original exsolution and at elevated oxygen fugacity. Temperature estimates of coexisting ilmenite and magnetite using the ILMAT-geo-thermometer of Lepage (2003) range from 370 to 615°C and are thus lower than calculations based on the spinel solvus. However, recently new experiments performed by Sauerzapf et al. (2008) show that the uncertainty in this temperature range is large

especially for phases with significant contents in Al_2O_3, MgO, MnO and Cr_2O_3 > 6 wt.% as in our samples.

In summary we suggest the following sequence of formation of the oxide phases:

1) Crystallization of homogeneous spinel (spinel 1) together with silicate phases from a mafic-ultramafic melt starting with chromite in the dunites, picotite in the wehrlites and eventually Cr-Ti-bearing magnetite in clinopyroxenite and mafic rocks.
2) Exsolution of an Al- and a Fe-rich spinel from Cr_2O_3-poor spinel 1 in tilaite, clinopyroxenite and gabbro when the temperature falls below 900°C. Formation of the first exsolutions of Fe-rich pleonaste blebs in a matrix of Al-rich Ti-magnetite that probably move towards existing lattice defects or grain boundaries.
3) With further cooling more and more Cr_2O_3- rich spinels in some dunites and hornblendites get exsolved to form picotite blebs in a matrix of chromian magnetite. Under the same conditions the earlier exsolved phases in the spinels from mafic rocks and clinopyroxenite become unstable and Fe and Ti in the pleonaste blebs diffuse into the Ti-magnetite matrix and excess Al from the magnetite forms one or two generations of pleonaste lamellas in the magnetite.
4) Exsolution of ilmenite and magnetite from the Ti-magnetite as a reaction to increasing oxygen fugacity and decreasing temperature in hornblendite and the mafic rocks (oxidation exsolution according to Lindsley, 1991; Haggerty, 1991). Formation of a second generation of small pleonaste blebs at the interface between ilmenite and magnetite (Fig. 12).

4.2 Spinel: a monitor of the evolution of mafic and ultramafic rocks from Uralian-Alaskan-type complexes

4.2.1 Chemical evolution of spinel in ultramafic cumulates

Based on major and trace elements in clinopyroxene, the characteristic lithological association of dunite, wehrlite, clinopyroxenite, and nepheline tilaite in Nizhnii Tagil, Svetley Bor and southwest Kytlym is the result of a complex interplay of igneous

processes like the mixing of magmas of different sources and evolution state and variable degrees of partial melting and fractional crystallization and replenishment in open magma chamber systems (Krause et al., 2007; Chapter 2).

The idiomorphic chromites in dunite with a concentric chemical zonation show a negative correlation of Al_2O_3 with Cr_2O_3 and a decreasing Cr/(Cr+Al) from the core towards the rim accompanied by a small increase of Fe_2O_3 (Fig. 5a, b). The most primitive, Cr-richest spinels in dunite samples from all Uralian complexes also show a negative correlation in the Al_2O_3 vs. Cr_2O_3 (Fig. 16a). This trend is well known from spinels in ocean island basalts, basalt from back arc basins, MORB, and boninites (Barnes and Roeder, 2001), where Al_2O_3 systematically increases at decreasing Cr_2O_3 and Fe_2O_3 remains rather constant (Fig. 16b). According to Irvine, (1967a) this variation reflects the fractionation of spinel and olivine from a mafic-ultramafic melt. The systematically higher Fe_2O_3- contents of the spinels in Uralian-Alaskan-type complexes, if compared with spinel from other basaltic rocks, reflect an elevated oxygen fugacity in their parental melts (Fig. 16b).

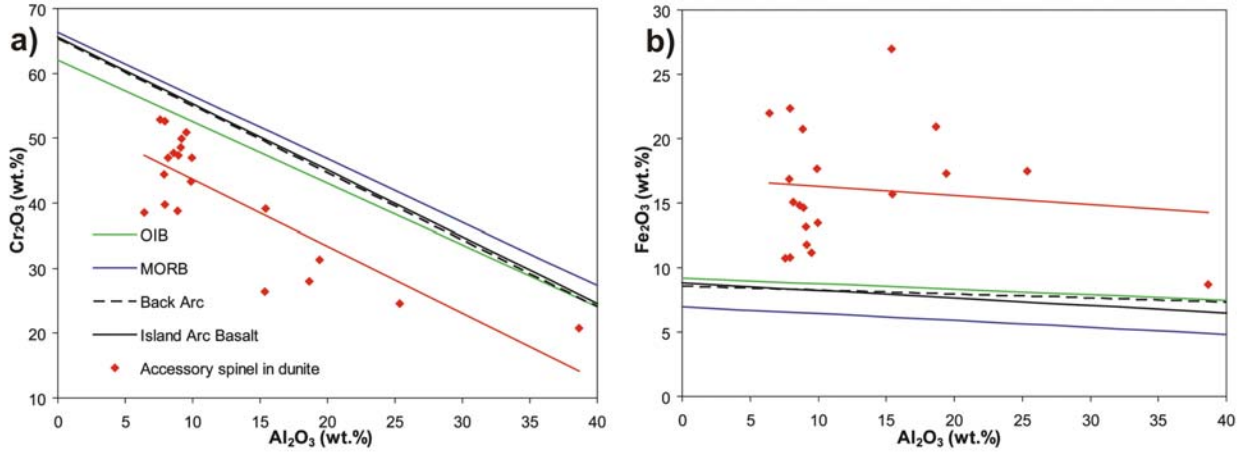

Fig. 16: Variation of Al_2O_3 vs. a) Cr_2O_3 and b) Fe_2O_3 in homogeneous spinels with the highest Cr_2O_3- content of each dunite sample. The calculated red trend line runs parallel to the fractionation trends known from spinel in other tectonic settings (data from Barnes and Roeder, 2001). The elevated Fe_2O_3 contents in the studied samples indicate a higher oxygen fugacity in the parental melt.

Interestingly, the Uralian samples display a considerable variation of the Cr_2O_3 content at low Al_2O_3 contents between 5 and 10 wt.%. Compared with the basaltic samples, they follow a trend of lower Cr_2O_3 at a given Al_2O_3 content (Fig. 16a). The low Al_2O_3 content

reflects a primitive parental magma composition, as indicated by the sole crystallization of olivine and spinel, and because no plagioclase is at the liquidus (Krause et al., 2007). However, this does not explain the lower Cr_2O_3 content. One explanation could be the fractionation of other mafic Al_2O_3 and Cr_2O_3-bearing phases such as clinopyroxene. Since clinopyroxene is present in dunite only as small, interstitial grains probably representing an interstitial liquid, it had no influence on the composition of the cores of the most primitive, early crystallizing spinels. Besides temperature, pressure and composition of the melt, partitioning of Cr into spinel also depends on the availability of Fe^{3+}, which in turn is controlled by the oxygen fugacity of the melt (Hill and Roeder, 1974; Cameron, 1975). The competition with higher contents of Fe^{3+} would lead to lower Cr contents in the spinel. Thus, the lower Cr_2O_3 content in spinel from the most primitive cumulates in combination with an elevated Fe_2O_3 content suggests that the parental magmas were more oxidized than common upper mantle derived melts. In addition, the large variation of Cr_2O_3 and Fe_2O_3 at a given Al_2O_3 content implies that there were significant differences in the oxidation states among the parental and their derivative melts forming the Alaskan-type complexes (Fig. 16). This has also been inferred by Chashchukhin et al. 2002 studying chromite in dunite and chromitite from Uralain-Alaskan-type complexes of Kytlym, Nizhnii Tagil and Uktus in the Ural Mountains. The redox state in dunite and chromitite was determined to vary between 1.9 and 3 logarithmic units above the FMQ buffer.

In wehrlite cumulates, where clinopyroxene is on the liquidus together with olivine, spinel has similar or slightly lower contents in Al_2O_3, at considerably lower Cr_2O_3 and higher contents in ferric iron, if compared to chromite in the dunites (Fig. 7). Homogeneous spinel in clinopyroxenites (Krause et al., 2007) and recalculated initial compositions of exsolved spinel in clinopyroxenite from Nizhnii Tagil and SW-Kytlym indicate a further decrease of Cr_2O_3 and Al_2O_3 at increasing Fe_2O_3 contents (Fig. 17). The decreasing Cr_2O_3 content in spinel is consistent with decreasing Mg/(Mg+Fe) in coexisting olivine and clinopyroxene (Krause et al., 2007) and hence indicates the fractionation of the parental melt. This is also consistent with increasing Fe_2O_3 and TiO_2 contents in spinel (Figs. 14, 17; Tab. 5) in the course of the fractionation. However, one would also expect an increase of the Al_2O_3-content in the parental melt. Clinopyroxene shows a continuous increase of Al_2O_3 with fractionation, from 0.4 wt.% in dunite up to 5.5 wt.% in

clinopyroxenites (Krause et al., 2007; Chapter 2). But, such an increase of Al_2O_3 is not reflected in the spinel composition.

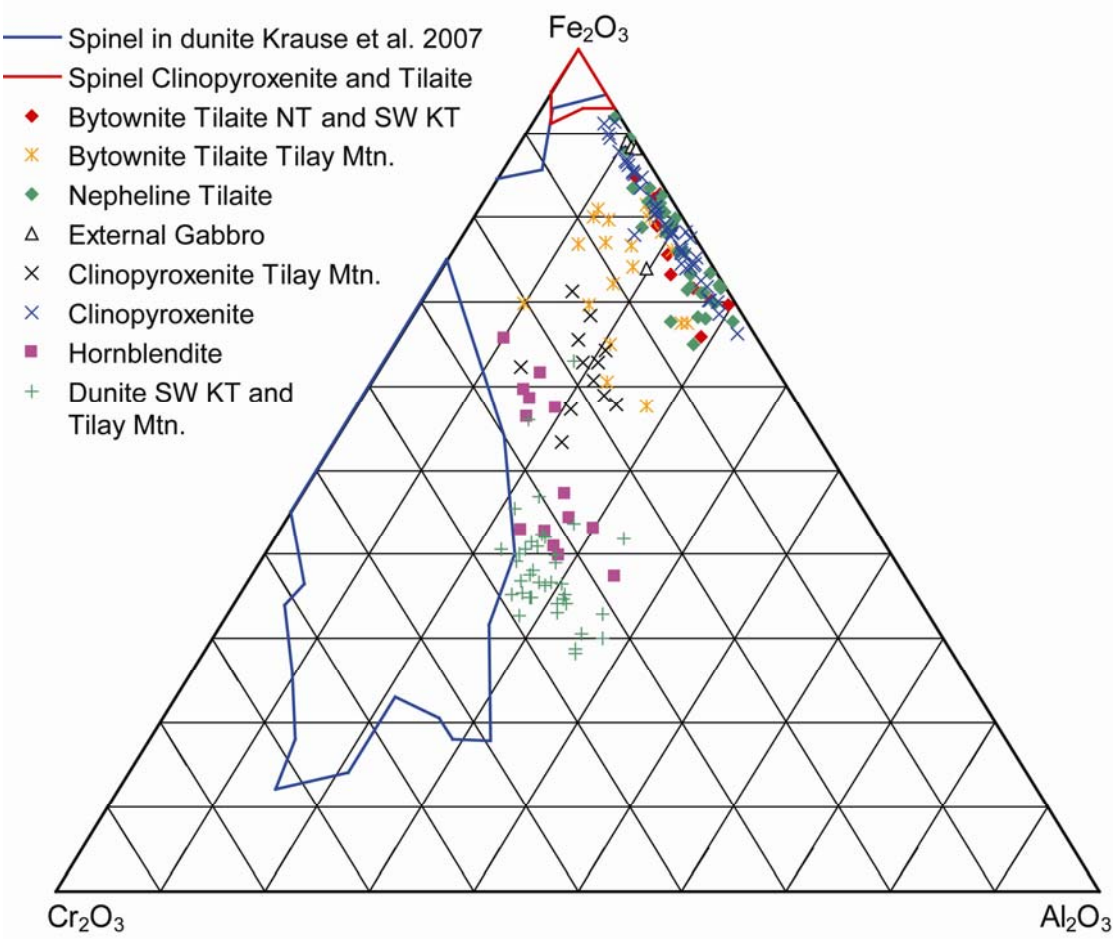

Fig. 17: Variation of the trivalent cations in recalculated exsolved spinel. Cr_2O_3 and Al_2O_3 decrease in the course of fractionation from dunite to clinopyroxenite and tilaite. Data for compositional variation in homogeneous spinel in dunite from all Uralian complexes are from Krause et al. (2007).

The decrease of the Al_2O_3 content as clinopyroxene starts to crystallize has also been observed in experimental studies (e.g. Irvine, 1967; Hill and Roeder, 1974). One explanation for the constant or decreasing Al_2O_3 content in spinel with advanced fractionation could be the competition of spinel and clinopyroxene for Al_2O_3. Clinopyroxene in wehrlite contains between 0.9 and 2.9 wt.% Al_2O_3. Mass balance consideration imply that due to the large clinopyroxene-spinel mass ratio a large amount of Al_2O_3 in the melt partitions into clinopyroxene, and the Al_2O_3 content in spinel in wehrlite cannot increase. The enhanced decrease of the Al_2O_3 content in spinel from

clinopyroxenites could be related to the excessive fractionation of clinopyroxene with even higher Al_2O_3 contents (1.5 – 5.5 wt.%). In addition estimations on the composition of the parental melt of Uralian-Alaskan-type complexes suggest relatively low Al_2O_3 contents of 8.2-10.7 wt.% Al_2O_3 (Irvine, 1973; Pushkarev, 2000; Batanova et al., 2005; Thakurta et al, 2008), if compared to other arc-related mafic melts (e.g. Kelemen et al., 2003).

On the other hand, the low Al_2O_3- but high Fe_2O_3-content in spinel could reflect the enhanced competition between Fe^{3+} and Al^{3+} when the oxygen fugacity of the melt increases. According to Hill and Roeder (1974) an elevated oxidation state is necessary to prevent chromian spinel from getting resorbed and replaced by a rim of chromian magnetite when clinopyroxene appears on the liquidus. In the investigated samples resorbed chromite is rarely observed (Fig. 7a) and the vast majority of homogeneous spinels do not show resorption. Together with the characteristically high content of ferric iron in the chromite from dunite (Krause et al., 2007), this indicates an initially elevated oxidation state in the parental melt of the ultramafic rocks that further increased in the course of the fractionation. This could be the result of prolonged crystallization of olivine and clinopyroxene which removes preferentially Fe^{2+}, whereby causing an increase of the Fe^{3+} proportion. This process implies a closed system evolution of the magma with regard to the oxygen fugacity.

The chemical composition of chromian spinels in dunite describes a second trend that is defined by chromite with a non concentric distribution of Cr and Fe, where Al_2O_3 decreases with decreasing Cr_2O_3 and increasing Fe_2O_3 contents (Figs. 5, 7). This trend reflects the enrichment of ferric iron in spinel on the expense of initially Al_2O_3 and subsequently also Cr_2O_3 (Figs. 5-7). It is a characteristic feature of spinels from Alaskan-type complexes world wide (e.g. Barnes and Roeder, 2001; Krause et al., 2007) and also known from ankaramitic and alkaline arc magmas and layered intrusions (Barnes and Roeder, 2001).

Metasomatic (e.g. Mellini et al., 2005; Frost and Beard, 2007; Iyer et al., 2008) or metamorphic overprint (e.g. Springer, 1974; Frost, 1975; Pinsent and Hirst, 1977; Kimball, 1990) may cause an enrichment of ferric iron in spinel. However, the distribution of major elements in the maps and profiles of chromites does not indicate any influence

of serpentinization or other metasomatic processes (Figs. 5, 7, 11). A substantial metamorphic overprint at upper greenschist to amphibolite facies conditions is not known for the Alaskan-type complexes in the Ural Mountains neither supported by our petrographic observations.

Igneous processes explaining the enrichment of ferric iron include oxidation of the parental melt during crystallization (Hill and Roeder, 1974; Cameron, 1975) or equilibration of chromite with interstitial liquid (e.g. Henderson, 1975; Henderson and Wood, 1981; Roeder and Campbell, 1985; Scowen et al., 1991; Candia and Gaspar, 1997). The fast equilibration of spinel, including the Ti^{4+}, Al^{3+} and Fe^{3+} components, with interstitial liquid has been demonstrated in the Kilauea Iki lava lake on Hawaii, even if the spinel is enclosed in olivine (Scowen et al., 1991).

The non-symmetrical Cr_2O_3 distribution occurs if spinel is closely associated with interstitial clinopyroxene (for example in sample NT2; Fig. 7a), whereas in samples devoid of clinopyroxene chromite only displays the magmatic fractionation trend of concentric zoning discussed above (for example sample NT7; Fig. 5a). We therefore favor the idea that this kind of distribution of the trivalent cations is caused by the reaction of spinel with interstitial liquid. However, a local subsolidus re-equilibration of spinel with the interstitial clinopyroxene during the cooling of the cumulate pile is a viable alternative. Crystallization of clinopyroxene from interstitial liquid is supported by its texture and by their extensive enrichment in trace elements, such as REE, on the scale of a thin section (Krause et al., 2007).

Like in the dunites containing interstitial clinopyroxene the non concentric chemical distribution of the major elements in chromites from the wehrlite KT38 indicates the reaction with interstitial liquid and clinopyroxene (Fig. 6). Spinel in clinopyroxenite is either homogenous (almost pure magnetite, Krause et al., 2007) or exsolved at subsolidus conditions to magnetite and picotite, hereby loosing an eventually preexisting chemical zonation.

Irvine (1967a) and Hill and Roeder (1974) suggested that chromite which initially crystallized together with olivine can be resorbed by a reaction with the melt and clinopyroxene when clinopyroxene starts to crystallize. The sample NT2 contains about two percent interstitial clinopyroxene. Thus, the irregular shape of the core of a chromite

grain from this sample (Fig. 7a) can be explained by resorption of an early crystallized chromite during its reaction with clinopyroxene-saturated liquid in the pore space. Subsequently, the core has been overgrown with ferritchromit (Fig. 7a).

4.2.2 Chemical evolution of spinel in mafic cumulates

In the plot of the trivalent cations the recalculated spinels are shifted with increasing fractionation from Cr-rich towards Fe^{3+}-rich compositions (Fig. 17). In the tilaites and gabbros feldspar is an additional interstitial and liquidus phase. The compositions of recalculated spinels in the tilaites from Nizhnii Tagil and SW-Kytlym and in the external gabbros overlap in composition with the clinopyroxenites from the same areas (Figs. 14 and 17). In particular the Al_2O_3/Fe_2O_3 remain relatively constant in the course of fractionation indicating that the Al_2O_3 content of spinel in these rocks is buffered by the cotectic crystallization of feldspar and clinopyroxene.

Systematic higher $Fe^{2+}/(Mg+Fe^{2+})$, $Fe^{3+}/(Al+Cr+Fe^{3+})$ and Fe_2O_3 and lower Cr_2O_3 is observed in disseminated spinel from the nepheline tilaites and in the bytownite tilaite from Tilay Mountain, if compared to compositions of spinel enclosed in cumulus clinopyroxene and olivine (Fig. 15, Tab. 5). This can either reflect a fractionation trend, reaction with interstitial melt (Scowen et al.,1991), a subsolidus re-equilibration with silicate phases (Henderson and Wood, 1981), or a retrograde alteration process (e.g. Mellini et al., 2005; Frost and Beard, 2007; Iyer et al., 2008).

Scowen et al. (1991) demonstrated that spinel enclosed in olivine can re-equilibrate with interstitial liquid by volume diffusion of Cr^{3+} and Al^{3+} from interstitial liquid to the spinel and of Ti^{4+} and Fe^{3+} in the opposite direction. The olivine has low Al_2O_3, Cr_2O_3 and TiO_2 contents close to or below the EMPA detection limit (Krause et al., 2007). A subsolidus redistribution of these elements between olivine and enclosed spinel can be therefore excluded. Within the same sample spinel enclosed in clinopyroxene and olivine share the same composition. A systematic mapping of the large clinopyroxene phenocrysts enclosing exsolved spinels did not indicate any significant redistribution of major elements within the clinopyroxene nor between clinopyroxene and spinel at near solidus and subsolidus conditions (Fig. 12; Chapter 2). The compositional variation in Al_2O_3,

Cr_2O_3 and TiO_2 of recalculated spinels enclosed in olivine and clinopyroxene is therefore interpreted to predominantly monitor the fractionation of the parental melt.

Spinel in clinopyroxenite and tilaite from the Tilay Mountain area (E-Kytlym) has significantly higher Cr_2O_3 contents than spinel from similar lithologies in Nizhnii Tagil and southwest Kytlym (Fig. 17). The Tilay Mountain area lies at the interface of two fundamentally different magmatic plumbing systems (Chapter 2). In the west cumulates are dominantly derived from an alkaline ultramafic parental magma, whereas the eastern gabbros stem from a tholeiitic parent. The cumulates in the Tilay Mountain area are interpreted to represent crystallization products from hybrid magmas, which originated from mixing alkaline and tholeiitic parental liquids (Chapter 2). This process could explain the different spinel compositions in clinopyroxene and tilaites from the different areas. It is probably also reflected in the higher Al_2O_3 and lower Cr_2O_3 contents of chromite in the dunites from Tilay Mountain (Fig. 4), if compared to chromite from dunites in Nizhnii Tagil and southwest Kytlym (Krause et al., 2007). A similar overprint and reaction of early cumulates with melts injected in the magma chamber is also described from Uralian-Alaskan-type complexes in the Kamchatka Arc (Kepezhinskas et al., 1993a).

5 Conclusions: Petrogenetic implications for the evolution of the Uralian-Alaskan-type complexes

The discussion above demonstrates that the spinel composition traces the petrogenetic processes that form the Uralian-Alaskan-type complexes in the Ural Mountains. The early fractionation of olivine and spinel is monitored by an increase of Al_2O_3 on the expense of Cr_2O_3 in concentrically zoned chromian spinel (Fig. 18). The equilibration of these early chromian spinels with interstitial liquid, which now also crystallizes clinopyroxene, leads to an increase of Fe_2O_3 and a decrease of first Al_2O_3 and successively Cr_2O_3 in spinel (RCI-trends in Fig. 18). The irregular geometry of the distribution of major elements in such spinels indicates that only parts of the grain were in equilibrium with the interstitial liquid presumably at an increasing oxygen fugacity. The chemical variation in these spinels is similar to the trend ascribed to ocean-floor

metamorphism of spinel in ultramafic rocks (Iyer et al., 2008). Thus, a detailed knowledge of the spatial distribution of major elements in spinel and coexisting phases is necessary for applying spinel as indicator for petrogenetic processes or to constrain the geotectonic setting in order to avoid misleading interpretations. Almost pure magnetite fills cracks that crosscut the exsolution textures in chromite in dunite and forms in places narrow rims around these grains. Its formation is related to a late alteration process, presumably the serpentinization of olivine (Fig. 18).

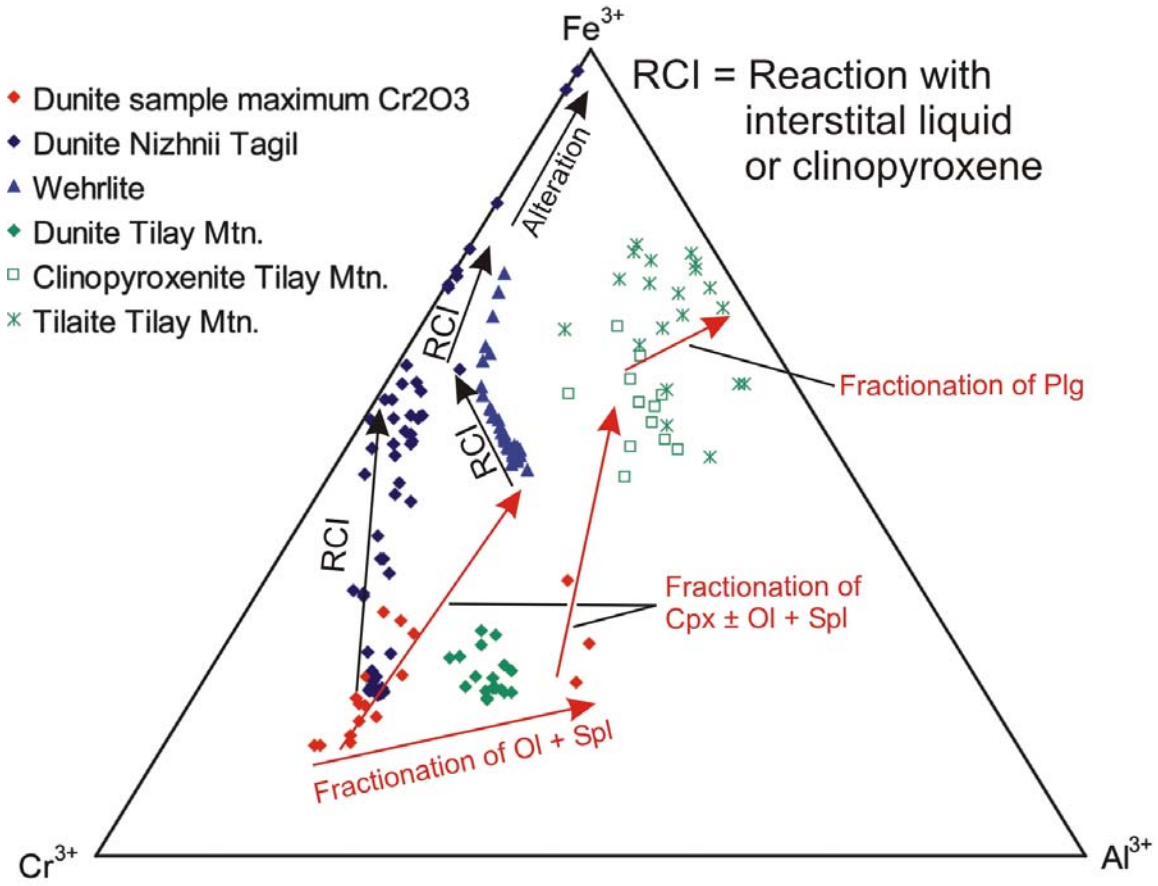

Fig. 18: Trivalent cation plot for selected samples summarizing the evolution of spinel compositions during fractionation processes within and among different lithologies (in red) and re-equilibration processes with interstitial liquid or at sub solidus conditions (RCI in black).

The elevated Fe_2O_3 at low Cr_2O_3 and Al_2O_3 contents in spinel from wehrlite and subsequently formed clinopyroxenite cumulates reflect the competing partitioning of Cr_2O_3 and Al_2O_3 from the melt into clinopyroxene and spinel. It could also indicate closed system fractionation causing an increase in the oxygen fugacity (Figs. 5, 7). The onset of the crystallization of feldspar in the tilaites and gabbros buffers Al_2O_3 at

relatively low levels whereas Cr_2O_3 contents continue to decrease to almost Cr_2O_3-free spinels (Fig. 18).

At temperatures below 900°C and Cr_2O_3 contents below 27 wt.% chromian spinel exsolves two new spinel phases. The exsolution into an Al-rich and a Fe-Ti-rich phase resulted in three different textures indicating nucleation and growth of bleb textures followed by two generations of oriented lamellas in Cr-poor spinels that probably reflect spinodal decomposition. The chemical composition also controls the texture of the exsolutions. Lamellar exsolutions (type B) are confined to spinels with Cr_2O_3-contents below 10 wt.% whereas exsolutions with diffuse and irregular contacts of both phases (type C) are restricted to spinels with Cr_2O_3 contents above 15 wt.%. Bleb-like exsolution textures (type A) occur in all exsolved spinels despite of their chemical composition. The Ti-magnetite component of exsolved spinel in hornblendite, tilaite and gabbro got further exsolved into ilmenite and magnetite. This represents the latest increment of equilibration of the oxide phases and indicates further increasing oxygen fugacities at decreasing temperatures after the exsolution of the two spinel phases. Their formation is accompanied by the formation of a second generation of blebs of Al-rich spinel at the phase boundary between ilmenite and magnetite.

In the trivalent cation plot all exsolved spinels closely match the solvus curve indicating equilibrium temperatures with olivine of Fo = 80 of 600°C. We consider this temperature to be close to the temperature of the host rocks in which the parental magmas of the Uralian-Alaskan-type complexes formed magma chambers. They gave rise to the different lithologies of dunite, wehrlite, clinopyroxenite, tilaite and gabbro cumulates. The depth of the crust-mantle boundary could correspond to the 600°C isotherm above a subduction zone (Tatsumi, 1989; Furukawa, 1993) and the contrast in density and rheology at this boundary would facilitate the emplacement of mantle-derived melts. This scenario would presume a tectonic environment of a continental or oceanic volcanic arc as proposed for Uralian-Alaskan-type complexes by earlier studies (e.g. Ivanov and Shmelev, 1996; Batanova et al., 2005; Krause et al., 2007). Fragments of migmatized crustal rocks indicate an intensive contact metamorphic overprint at the direct contact between intrusions and host rocks. Unfortunately, a detailed study of the contact

relations is obscured by a late stage tectonic overprint and a continuous contact aureole is not preserved.

The similarity of the exsolution temperatures among the different complexes over a distance of several hundred kilometres implies a regional tectonic event that terminated the exsolution process. This event is potentially associated with the final emplacement of the Uralian-Alaskan-type complexes within the Tagil Magnitogorsk-Zone. Exhumation along regional tectonic structures (e.g. the Main Uralian Fault or the Serov Mauk Fault, (Fig. 1a) transported the complexes into cold upper crustal levels, which stopped the re-equilibration process.

References

Abramoff, M.D., Magelhaes, P.J., Ram, S.J., 2004. Image Processing with ImageJ. Biophotonics International, 11 (7), 36-42.

Ahmed, A.H., Helmy, H.M., Arai, S., Yoshikawa, M., 2008. Magmatic unmixing in spinel from late Precambrian concentrically-zoned mafic-ultramafic intrusions, Eastern Desert, Egypt. Lithos in press. Doi:10.1016/j.lithos.2007.11.009.

Barnes, S.J., Roeder, P.L., 2001. The range of spinel compositions in terrestrial mafic and ultramafic rocks. Journal of Petrology, 42 (12), 2279-2302.

Batanova, V.G., Astrakhantsev, O.V., 1992. Tectonic position and origins of the zoned mafic-ultramafic plutons in the Northern Olyutor Zone, Koryak Highlands. Geotectonics, 26 (2), 153-165.

Batanova, V.G., Pertsev, A.N., Kamenetsky, V.S., Ariskin, A.A., Mochalov, A.G., Sobolev, A.V., 2005. Crustal evolution of island-arc ultramafic magma: Galmoenan pyroxenites-dunite plutonic complex, Koryak Highland (Far East Russia). Journal of Petrology, 46, 1345-1366.

Burkhard, D.J.M., 1993. Accessory chromium spinels: Their coexsistence and alteration in serpentinites. Geochimica et Cosmochimica Acta, 57, 1297-1306.

Candia , M.A.F., Gaspar, J.C., 1997. Chromian spinels in metamorphosed ultramafic rocks from Mangabal I and II complexes, Gioás, Brazil. Mineralogy and Petrology, 60, 27-40.

Cameron, E.N., 1975. Postcumulus and subsolidus equilibration of chromite and coexisting silicates in the Eastern Bushveld Complex. Geochimika et Cosmochimica Acta, 39, 1021-1033.

Chashchukhin, I.S., Votyakov, S.L., Pushkarev, E.V., Anikina, E., 2002. Oxithermobarometry of ultramafic rocks from the Ural Platinum Belt. Geochemistry International, 40 (8), 762-778.

Cookenboo, H.O., Bustin, R.M., Wilks, K.R., 1997. Detrial chromian spinel compositions used to reconstruct the tectonic setting or provenance: Implications for orogeny in the Canadian Cordillera. Journal of Sedimentary Research, 67 (1), 116-123.

Dick, H.J.B., Bullen, T., 1984. Chromian spinel as a petrogenetic indicator in abyssal and alpine-type peridotites and spatially associated lavas: Contributions to Mineralogy and Petrology, 86, 54-76.

Duparc, L., Tikhonowitch, M., 1920. Le platine et les gites platiniferes de l'Oural et du Monde, Geneve, 1-542.

Eales, H.V., Wilson, A.H., Reynolds, I.M., 1988. Complex unmixed spinels in layered intrusions within an obducted ophiolite in the Natal-Namaqua mobile belt. Mineralium Deposita, 23, 150-157.

Evans, B.W., Frost, B.R., 1975. Chrome-spinel in progressive metamorphism- a preliminary analysis. Geochimica et Cosmochimica Acta, 39, 959-972.

Findlay, D.C., 1969. Origin of the Tulameen ultramafic-gabbro complex, southern British Columbia. Canadian Journal of Earth Sciences, 6, 399-425.

Frost, R.B., 1975. Contact metamorphism of serpentinite, chloritic and blackwall and rodingite at Paddy-Go-Easy Pass, Central Cascades, Washington. Journal of Petrology, 16 (2), 272-313.

Frost, R.B., Beard, J.S., 2007. On silica activity and serpintinization. Journal of Petrology, 48 (7), 1351-1368.

Furukawa, Y., 1993. Magmatic processes under arcs and formation of the volcanic front. Journal of Gephysical Research, 98 (B5), 8309-8319.

Garuti, G., Pushkarev, E.V., Zaccarini, F., Cabella, R., Anikina, E., 2003. Chromite composition and platinum-group mineral assemblage in the Uktus Uralian-Alaskan-type complex (Central Urals, Russia). Mineralium Deposita, 38, 312-326.

Garuti, G., Fershtater, G., Bea, F., Montero, P., Pushkarev, E.V., Zaccarini, F., 1997. Platinum-group elements as petrological indicators in mafic-ultramafic intrusions of the central and southern Urals: preliminary results. Tectonophysics, 276, 181-194.

Ghiorso, M.S., Sack, R.O., 1991a. Thermochemistry of the oxide minerals. In: Lindsley (ed.). Oxide minerals petrogenetic and magnetic significance, Reviews in Mineralogy, 25, 221-302.

Ghiorso, M.S., Sack, R.O., 1991b. Fe-Ti oxide geothermometry: Thermodynamic formulation and the estimation of intensive variables in silicic magmas. Contributions to Mineralogy and Petrology, 108, 485-510.

Haggerty, S.E., 1991. Oxide textures – A mini-atlas. In: Lindsley (ed.). Oxide minerals petrogenetic and magnetic significance, Reviews in Mineralogy, 25, 129-220.

Harrison, R.J., Putnis, A., 1999. The magnetic properties and crystal chemistry of oxide spinel solid solutions. Surveys in Geophysics, 19, 461-520.

Henderson, P., 1975. Reaction trends shown by chrome-spinels of the Rhum layered Intrusion, Geochimica et Cosmochimika Acta, 39, 1035-1044.

Henderson, P., Wood, R.J., 1981. Reaction relationships of chrome-spinels in igneous rocks – further evidence from the layered intrusion of Rhum and Mull, Inner Hebrides, Scotland. Contributions to Mineralogy and Petrology, 78, 225–229.

Hill, B., Roeder, P., 1974. The crystallization of spinel from basaltic liquid as a function of oxygen fugacity. Journal of Geology, 82, 709-729.

Himmelberg, R.G., Loney, R.A., 1995. Characteristics and petrogenesis of Alaskan-Type ultramafic-mafic intrusions, southeastern Alaska. US Geological Survey Professional Papers, 1564, 1-47.

Himmelberg, R.G., Loney, R.A., Craig, J.T., 1986. Petrogenesis of the ultramafic complex at the Blashke Islands, southeastern Alaska. US Geological Survey Bulletin, 1662, 1-14.

Irvine, N.T., 1965. Chromian spinel as a petrogenetic indicator part 1. Theory. Canadian Journal of Earth Sciences, 2, 648-672.

Irvine, N.T., 1967a. Chromian spinel as a petrogenetic indicator part 2. Petrologic applications. Canadian Journal of Earth Sciences, 4, 71-103.

Irvine, T.N., 1967b. Zoned ultramafic complexes. In: Wylie, P.J., Ultramafic and related rocks, John Wiley, New York, 83-97.

Irvine, T.N., 1973. Bridget Cove volcanics, Juneau Area, Alaska: Possible parental magma of Alaskan-type ultramafic complexes. Carnegie Institution Washington Yearbook, 72, 478-491.

Ivanov, K.S., Shmelev, V.R., 1996. The Platinum Belt of the Urals as a magmatic trace of the early paleozoic subduction zone. Transactions of the Russian Academy of Sciences / Earth Sciences, 347A (3), 396-399.

Iyer, K., Austrheim, H., John, T,, Jamtveit, J.T., 2008. Serpentinization of the oceanic lithosphere and some geochemical consequences: Constraints from the Leka Ophiolite Complex, Norway. Chemical Geology, 249, 66-90.

Jackson, E.D., 1969. Chemical variation in coexisting chromite and olivine in chromitite zones of the Stillwater Complex. In: Wilson, H.D.B., (ed) Magmatic ore deposits a symposium, Economic Geology, Monograph 4, 41-71.

Jan, M.Q., Khan, M.A., Windley, B.F., 1992. Exsolution in Al-Cr-Fe^{3+}-rich spinels from the Chilas mafic-ultramafic complex, Pakistan. American Mineralogist, 77, 1074-1079.

Jang, Y., D., Naslund, H.D., 2003. Major and trace element variation in ilmenite in the Skaergaard Intrusion: petrologic implications. Chemical Geology 193, 109-125.

Kelemen, P.B., Hanghoj, K., Greene, A.R., 2003. One view of the geochemistry of subduction-related magmatic arcs, with an emphasis on primitive andesite and lower crust. In: Rudnick, R.L. ed. Treatise on Geochemistry vol. 3 The Crust. Elsevier, 593-659.

Kepezhinskas, P.K., Reuber, I., Tanaka, H., Miyashita, S., 1993a. Zoned calc-alkaline plutons in Northeastern Kamchatka, Russia: Implications for the crustal growth in magmatic arcs. Mineralogy and Petrology, 49, 147-174.

Kepezhinskas, P.K., Taylor, R.N., Tanaka, H., 1993b. Geochemistry of plutonic spinels from the North Kamchatka Arc: Comparisons with spinels from other tectonic settings. Mineralogical Magazine, 57, 575-589.

Kimball, K.L., 1990. Effects of hydrothermal alteration on the composition of chromian spinels. Contributions to Mineralogy and Petrology, 105, 337-346.

Krause, J., Brügmann, G.E., Pushkarev, E.V., 2007. Accessory and rock forming minerals monitoring the evolution of zoned mafic–ultramafic complexes in the Central Ural Mountains. Lithos, 95, 19-42.

Lattard, D., 1995. Experimental evidence for the exsolution of ilmenite from titaniferous spinel. American Mineralogist, 80, 968-981.

Lattard, D., Sauerzapf, U., Käsemann, M., 2005. New calibration data for the Fe-Ti oxide thermo-oxybarometers from experiments in the Fe-Ti-O system at 1 bar, 1000-1300°C and a large range of Oxygen fugacities. Contributions to Mineralogy and Petrology, 149, 735-754.

Lee, Y.L., 1999. Geotectonic significance of detrial chromian spinel: a review. Geosciences Journal, 3 (1), 23-29.

Lehmann, J., 1983. Diffusion between olivine and spinel: application to geothermometry. Earth and Planetary Science Letters, 64, 123-138.

Lepage, L.D., 2003. ILMAT: an Excel worksheet for ilmenite-magnetite geothermomety and geobarometry. Computers and Geosciences, 29, 673-678.

Lindsley, D.H. 1991. Experimental studies of oxide minerals. In: Lindsley (ed.). Oxide minerals petrogenetic and magnetic significance, Reviews in Mineralogy, 25, 69-106.

Loferski, P.J., Lipin, B.R., 1983. Exsolution in metamorphosed chromite from the Red Lodge district, Montana. American Mineralogist, 68, 777-789.

Melcher, F., Grum, W., Simon, G., Thalhammer, T., Stumpfl, E., 1997. Petrogenesis of the ophiolitic giant chromitite deposits of Kempirsai, Kazahkstan: a study of solid and fluid inclusions in chromite. Journal of Petrology, 40 (10), 1419-1458.

Mellini, M., Rumori, C., Viti, C., 2004. Hydrothermally reset magmatic spinels in retrograde serpentinites: formation of “ferritchromit” rims and chlorite aureoles. Contributions to Mineralogy and Petrology, 149, 266-275.

Morse, S.A., 1980. Kiglapait Mineralogy II: Fe-Ti oxide minerals and the activities of oxygen and silica. Journal of Petrology, 21 (4), 685-719.

Muir, J.E., Naldrett, A.J., 1973. A natural occurrence of two-phase chromium-bearing spinels. Canadian Mineralogist, 11, 930-939.

Noble, J.A., Taylor, H.P., 1960. Correlation of the ultramafic complexes of southeastern Alaska with those of North America and the World. 21st International Geological Congress in Copenhagen 1960, Report part 13, 188-197.

Ozawa, K., 1988. Ultramafic tectonite of the Miyamori ophiolitic complex in the Kitakami Mountains, Northeast Japan: hydrous upper mantle in an island arc. Contributions to Mineralogy and Petrology, 99, 159-175.

Pang, K.-N., Zhou, M.-F., Lindsley, D., Zhao, D., Malpas, J., 2008. Origin of Fe-Ti oxide ores in mafic intrusions: Evidence from the Panzhihua Intrusion, SW China. Journal of Petrology, 49 (2), 295-313.

Pertsev, A.N., Savelieva, G.N., Astrakhantsev, O.V., Magmatic origin of the ultramafic-mafic association of the Kytlym Massif, Platinum Belt of the Urals, 2000. Petrology, 8 (4), 370-393.

Pinsent , R.H., Hirst, D.M., 1977. The metamorphism of the Blue River ultramafic body, Cassiar, British Columbia, Canada. Journal of Petrology, 18, (4), 567-594.

Power, M.R., Pirrie, D., Andersen, J.C.Ø., Wheeler, P.D., 2000. Testing the validity of chrome spinel chemistry as a provenance and petrogenetic indicator. Geology, 28 (11), 1027-1030.

Price, G.D., 1980. Exsolution microstructures in titanomagnetites and their magnetic significance. Physice of the Earth and planetary Interiors, 23, 2-12.

Pushkarev, E.V., Anikina, Ye.V., Garuti, G., Zaccarini, F., Cabella, R., 1999. Geikielite (Mg-ilmenite) in association with Cr-spinel and platinoids from the Uktus massif dunite, Middle Urals: genetic implications. Dokl Earth Sciences, 369A (9), 1220–1223.

Pushkarev, E.V. 2000. Petrology of the Uktus dunite-clinopyroxenite-gabbro massif (Middle Urals). Ekaterinburg. Ural Division of RAS, 296pp.

Putnis, A., 1992. Introduction to mineral sciences. Cambridge University Press, 457pp.

Roeder, P.L., 1994. Chromite: From the fiery rain of chondrules to the Kilauea Iki lava lake. The Canadian Mineralogist, 32, 729-746.

Roeder, P.L., Campbell, I.H., 1985. The effect of postcumulus reaction and composition of chrome-spinels from the Jimberlana Intrusion. Journal of Petrology, 26 (3), 763-786.

Sack, R.O., Ghiorso, M.S., 1991a. Chromite as a petrogenetic indicator. In: Lindsley (ed.). Oxide minerals petrogenetic and magnetic significance. Reviews in Mineralogy, 25, 323-353.

Sack, R.O., Ghiorso, M.S., 1991b. Chromian spinel as petrogenetic indicators: Thermodynamics and petrological applications. American Mineralogist, 76, 827-847.

Sauerzapf, U., Lattard, D., Burchard, M., Engelmann, R., 2008. The titanomagnetite-ilmenite equilibrium: New experimental data and thermo-oxybarometric application to the crystallization of basic to intermediate rocks. Journal of Petrology, 49 (6), 1161-1185.

Scoon, R.N., Eales, H.V., 2002. Unusual Fe-Ti-Cr spinels from discordant bodies of iron-rich ultramafic pegmatite at the Amandelbult Platinum mine, northwestern Bushveld Complex. Mineralogical Magzine, 66 (6), 857-879.

Scowen, P.A.H., Roeder, P.L., Helz, R.T., 1991. Reequilibration of chromite within Kilauea Iki lava lake, Hawaii. Contributions to Mineralogy and Petrology, 107, 8-20.

Savelieva, G.N., Sharaskin, A.Y., Saveliev, A.A., Spadea, P., Pertsev, A.N., Babarina, I.I., 2002. Ophiolites and zoned mafic-ultramafic massifs of the Urals: A

comparative analysis and some tectonic implications. In: Browen, D., Juhlin, C., Puchkov, V. (eds.). Mountain building in the Uralides: Pangea to the present. Geophysical Monograph, 132, 135-153.

Savelieva, G.N., Pertsev, A.N., Astrakhantsev, O.V., Denisova, E.A., Boudier, F., Bosch, D., Puchkova, A.V., 1999. Kytlym pluton, north Urals: Structure and emplacement history. Geotectonics, 33 (2), 119-142.

Speczik, S., Wiszniewska, J., Diedel, R., 1988. Minerals, exsolution features and geochemistry of Fe-Ti ores of the Suwalki District (North-East Poland). Mineralium Deposita, 23, 200-210.

Springer, R.K., 1974. Contact metamorphosed ultramafic rocks in the Western Sierra Nevada Foothills, California. Journal of Petrology, 15 (1), 160-195.

Tamura, A., Arai, S., 2005. Unmixed spinel in chromitite from the Iwanai-Dake peridotite complex, Hokkaido, Japan: A reaction between peridotite and highly oxidized magma in the mantle wedge. American Mineralogist, 90, 473-480.

Tatsumi, Y., 1989. Migration of fluid phases and genesis of basalt in subduction zones. Journal of Geophysical Research, 94 (B4), 4697-4707.

Taylor, H.P., Noble, J.A., 1969. Origin of magnetite in the zoned ultramafic complexes of Southeastern Alaska. In: Wilson, H.D.B. (ed.) Magmatic ore deposits 209-230.

Taylor, H.P., Noble, J.A., 1960. Origin of the ultramafic complexes in southeastern Alaska. 21st International Geological Congress in Copenhagen 1960, Report part 13, 175-187.

Thakurta, J., Ripley, E.M., Li, C., 2008. Geochemical constraints on the origin of sulphide mineralization in the Duke Island Complex, southeastern Alaska. Geochemistry Geophysics Geosystems, 9 (7).

Turnock, A.C., Eugster, H.P., 1962. Fe-Al Oxides: Phase relationships below 1000°C. Journal of Petrology, 3 (3), 533-565.

Van der Veen, A.H., Maaskant, P., 1995. Chromian spinel mineralogy of the Staré Ransko gabbro-peridotite, Czech Republic, and its implications for sulfide mineralization. Mineralium Deposita, 30, 397-407.

Yefimov, A.A., 1977. Hot tectonics in the hyperbasics and and gabbroides of the Urals. Geotektonika, 1, 24-42. (in Russian)

Appendix

Excel files of the tables 1-1 to 3-6 can be found as supplementary data.

Chapter 1:
Table 1-1 Whole rock
Table 1-2 Olivine
Table 1-3 Spinel
Table 1-4 Clinopyroxene

Chapter 2:
Table 2-1 Whole rock
Table 2-2 Clinopyroxene
Table 2-3 Olivine
Table 2-4 Feldspar and nepheline
Table 2-5 Partition coefficients

Chapter 3:
Table 3-1 Spinel dunite Tilay Mtn
Table 3-2 Zoned spinel dunite
Table 3-3 Zoned spinel dunite_wehrlite
Table 3-4 Exsolved spinel
Table 3-5 Recalculated exsolved spinel
Table 3-6 Ilmenite